Ultrastructural Evaluation of Pathological and Acutely Injured Mammalian Corneas

A Thesis Submitted to Cardiff University for the Degree of Doctorate of Philosophy

School of Optometry and Vision Sciences

2012

Erin P. Dooley MSc

Dedication

This thesis is dedicated to my grandfather John W. Dooley Esq. who taught me how to observe the world, love nature and to question everything; and to my grandmother Josephine M. Gondek for her unconditional love and support and who gave me the belief that I can achieve anything.

You were both taken away too soon, but your spirit lives on in all of the lives you have touched.

Acknowledgements

I would like to thank my supervisors Professor Keith M. Meek and Professor Andrew J. Quantock for all of their help, support, and unending patience throughout my PhD.

I would also like to thank Dr. Christina Kamma-Lorger, Dr. Craig Boote, and Professor Phil Stephens for their help and supervision of my individual projects.

I would like to thank Dr. Sally Hayes, Dr. Gill Smith, Dr. Rob Young, Dr. Lee Gonzalez, and Dr. Tariq Alhamad for all of their technical and research support.

I would like to thank Dr. Jacek Pijanka for helping me over the last few hurdles and for helping me to see the forest through the trees when things got tough.

I would like to thank the 'Biophysics Girls' (Dr. Barbara Palka, Dr. Leona Ho, Francis Jones, Elena Koudouna, and Sian Morgan) for all of their support and the good times we had. You are like my sisters.

Finally, I would like to thank my family for being there and believing in me.

Abstract

Ultrastructural Evaluation of Pathological and Acutely Injured Mammalian Corneas

It is estimated that there are millions of corneal operations performed annually in the United Kingdom and United States following pathology and/or acute injury. Equally, millions elect to have corneal refractive surgery to remedy visual disorders such has myopia, prespreopia, astigamatism and associated keratoconus. Following all of these procedures, there is a risk of complications from scar formation, cell loss, and corneal oedema which may adversely affect the surgical outcome and resulting best vision. Through research into how the cornea heals, it is hoped that these factors could be better understood and ultimately used to increase patient satisfaction. The projects are outlined as followed:

1) Using X-ray scattering techniques to investigate the role of Pax 6 on the collagen ultra-structure of murine corneas

2) Oral mucosal fibroblasts as a novel wound healing treatment of LASIK injured ovine cornea

3) Using X-ray scattering techniques to investigate the ultra-structural changes of a 12 year post-operative penetrating keratoplasty for keratoconous

4) Using small angle X-ray scattering techniques to investigate limbal collagen ultra-structure of keratoconic and normal human tissue

In this wound healing study, a range of different pathological and acutely injured mammalian corneas (human, sheep, and mouse) were evaluated using a range of quantitative techniques. These techniques encompass small and wide angle X-ray scattering, mechanical analysis, immunofluorescence, spectrophotometry, and cell/organ culture model. We feel that investigating various species and disorders has provided a more comprehensive and broad overview of the various maladies which can occur during the wound healing process.

General Index

List of Figures

Chapter One:

Chapter Two:

Chapter Three:

Chapter Four:

Chapter Five:

Chapter Six:

List of Tables

1.1 Cornea structure and function

The cornea is the transparent outer covering of the eye which provides protection, structural integrity, biomechanical strength, and a clear 'window' which allows light into the ocular chamber thus enabling vision. The cornea and lens are the only mammalian tissue which evolved to be functionally transparent (Christens-Barry et al.,1996). In order to retain its transparent qualities, the cornea has an avascular structure with a high number of unmyelinated nerves (Snell and Lamp, 1997).

The superficial cornea has limited regenerative properties which assist in preventing damage from acute injury, invasion of foreign bodies, noxious environmental toxins, and pathogens. The biomechanical properties of this renewal process are assisted by blinking and tear film production which aides in the delivery of nutrients, whilst also removing and transporting dead cells and waste products. These processes also contribute to the appearance of a smooth corneal epithelium (Panan-Langston, 2007).

The renewal process within the cornea is due to the balance between epithelial cell proliferation, apoptosis, differentiation of stem cells, and other forms of natural cell death (e.g. programmed cell death and senescence) (Glaso et al.,1993). It should be noted, however, that not all of the cornea's anatomical structures are capable of total or partial regeneration *in vivo*. Following injury, most superficial wounds result in either scar formation or permanent damage leading to a loss of best vision (Stocum, 2006). This will be discussed later in the chapter.

The mammalian cornea serves two main functions. These are:

1) Maintenance of transparency (to enable vision and refract light)
2) Biomechanical strength and structural integrity (protection)

The transparent and protective qualities of the cornea are rooted in its ability to exist in a homeostatic state which includes the ability to partially regenerate itself, maintain appropriate hydration levels, and retain its general shape and structure (whilst maintaining flexibility). Flexibility is important as the eye is continuously undergoing accommodative changes and minute fluctuation movements from a regular ocular

pulse (Perkins, 1985). Any major changes to the shape of the eye (whether congenital or acquired) will result in a refractive error and ultimate loss of best vision through myopia, presbyopia, or corneal astigmatism (Koomen et al., 1949).

Later in this introductory chapter, the biophysical properties of both corneal transparency and biomechanics will be discussed in further detail.

1.2 The five layers of the cornea

The cornea is comprised of five distinct layers. The human cornea is approximately 0.5 mm thick at the centre and slightly increases in thickness towards the periphery (Franco et al., 1985). The eye and cornea are often mistakenly referred to as being a homologous orbital structure, however in reality the cornea sits anteriorly on the eye with a progressively smooth elevated topography.

The thickness of the cornea differs to different magnitudes between left and right eyes, individuals, and species. The thickness of the cornea is also dependent on the hydration of the tissue (Hedbys and Mishima, 1966). The morphology of the cornea also differs between species (Gelatt,2006). These differences will be addressed in the individual experimental chapters.

The five layers of the cornea from anterior to posterior are:

1) Epithelium: comprised of six to seven layers of nucleated cells of varying phenotype. The epithelium is capable of regeneration through a supply of differentiated stem cells.
2) Bowman's membrane: a layer comprised of various types of laminar collagen. The epithelial cells adhere to this collagen layer.
3) Stroma: makes up the bulk of the cornea's thickness. The stroma is made primarily of strictly ordered Type I collagen in alternating stacked layers. The stroma also contains a supply of keratocytes (corneal fibroblasts) which produce extra-cellular matrix components.
4) Descemet's membrane: a collagen rich lamellar layer. The collagen layer

allows for the adherence of cells.

5) Endothelium: comprised of one layer of flattened phenotypically hexagonal mitochondria-rich cells. These cells regulate fluid transport within the cornea
(Figure 1.1).

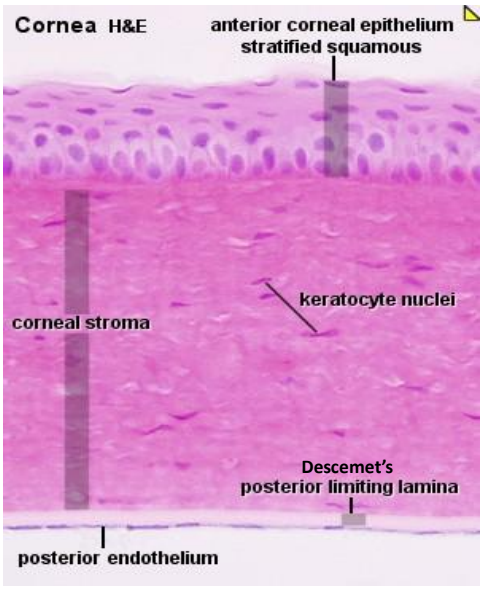

Figure 1.1 H&E stained human cornea demonstrating the layers. All five layers are evident along with their respective proportions. (www.lab.anhb.uwa.edu.au May 2009)

Each of these layers plays a specific role in maintaining corneal health and homeostasis. Each layer also plays a specific role in the wound healing and regenerative process of the cornea. For these reasons, the specific composition and function of each layer will be discussed in greater detail.

1.2.1 The Epithelium

As previously noted, the epithelium is the most anterior layer of the cornea. The epithelium in itself is comprised of cells with three distinct phenotypes which are distributed in approximately six layers. In the deepest layer, the cells are columnar in appearance. Above this layer are two to three layers of three-dimensional polygonal shaped cells. The most anterior layer consists of squamous epithelial cells which contain flattened nuclei and tight cell-to-cell junctional organisation. These cells are laid out in two to three layers (Mannis and Hollande, 2002) (Figure 1.2).

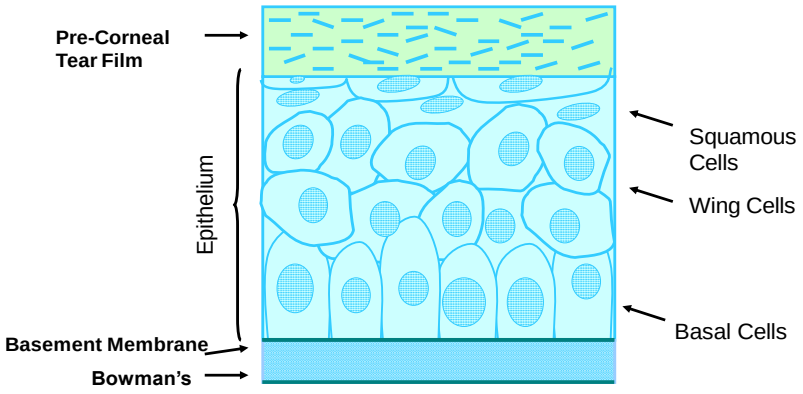

Figure 1.2: Schematic of the tear film, corneal epithelium and Bowman's layer. After Butterworth-Heinemann 2009

The desmosomes between the gap junctions permit the cells to send biochemical signals between each other through chemical signal channels (connexin) in the event of an injury, cell death, or the presence of external pathogens (Figure 1.3). This allows the cells to act as a 'community' acting together against any threats with the ultimate aim to maintain homeostasis. There are also very strong apoptotic (programmed cell death) responses by these epithelial cells as evidenced by the presence of chromatin c (Long 1998). Programmed cell death (PCD) allows for a balance between cell death and re-epithelisation so the healthy epithelium can maintain its structure. PCD also protects neighbouring cells from succumbing to infection or threat if there is an injury in the vicinity. This process also provides a limited degree of regeneration of the anterior ocular structure which contributes to its smooth appearance (Pfister, 1975).

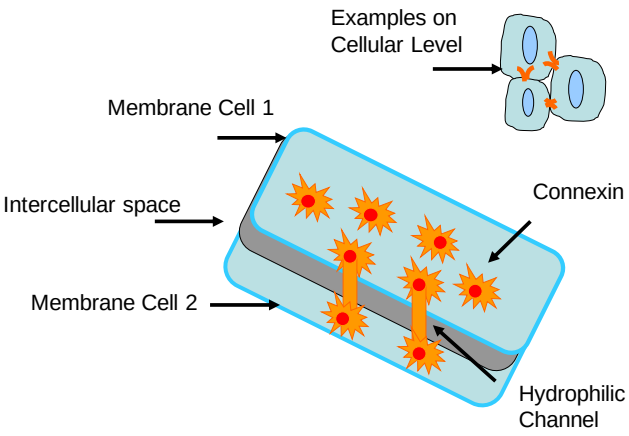

Figure 1.3: Schematic demonstrating the gap junctions between cells which allow them to communicate both maintaining homeostasis and during times of stress, injury, or danger

1.2.2 Bowman's Layer

The Bowman's layer is an acellular layer of laminar collagen which separates the epithelium and the stroma. The primary functions of the Bowman's are to adhere the epithelium and act as a barrier between the two layers (thereby separating and maintaining the unique environments in homeostasis) (Forrester et al., 1996). The layer is approximately 10-12 um in depth and is comprised of strong laminar collagen fibres of types I, III, V, VII, XII, and XVI collagen (Nakayasu et al., 1986).

The Type VII collagen especially provides support for cell adhesion and anchorage. The Bowman's layer also provides a degree of structural integrity to the cornea and damage to this layer (especially from surgical incision) may adversely affect the bio-mechanical strength and shape of the cornea. This damage could ultimately result in changes in refraction and loss of best vision (Feder and Rapuano, 2006). In humans, Bowman's layer also acts as an anchorage structure for the anterior portion of the stromal lamellae (Morishige et al., 2007).

Bowman's layer also plays a key role in regulating stromal wound healing. Following the wounding of the cornea, somatic cells at the basal cell layer differentiate and proliferate. This post-wounding differentiation is mediated through the Bowman's layer. There is a reaction between the cytokines produced following wound healing and the strong adhesions between the layer and the epithelial cells adhering. The epithelial cells adhere their lamelipodia and filopodia projections through the activation of actin filaments (Gurtner et al., 2008).

1.2.3 The Stroma

The stroma is the thickest layer of the cornea. The stroma is an avascular structure and is relatively acellular with only roughly 10% of its bulk somatic keratocytes (corneal fibroblasts). The body of the stroma consists of flat layers of mainly Type I and Type V collagen superimposed on top of each other in lamellar sheets (Figure 1.4). In the healthy human cornea there are roughly 200 sheets each approximately 1-2 um in thickness. The lamellae sheets themselves comprise collagen fibrils with a diameter of around 36 nm. The thickness of the stroma gradually increases from the centre out to the periphery. The stroma also contains a network of hydrophilic proteoglycans and glycosaminoglycans which surround the fibrils. It is thought that these matrix structures help to regulate the fluid content of the stoma and maintain the strict spacing of collagen fibrils which is vital for corneal transparency (Freegard, 1997; Freund et al., 1996).

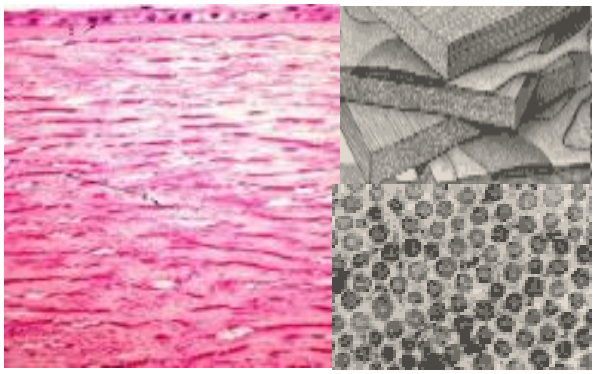

Figure 1.4: Left is an H&E stained image of a human cornea demonstrating the lamellar sheets of collagen. Right is a representation of lamella sheets (above) and individual collagen fibrils (below) Images mission for vision.org accessed April 2010

The diameter and spacing of collagen, proteoglycan content, number of collagen layers in the lamellae and the orientation of the collagen layers differ between humans and other species; these differences will be discussed in more detail in the individual chapters. The morphological characteristics of the stroma also differ between healthy and diseased individuals. These differences will also be addressed in a later chapter.

1.2.4 Descemet's Membrane

This layer is a form of Type IV collagen rich membrane which separates the stroma from the most posterior corneal layer (endothelium) (Snell and Lamp 1997). This membrane is also acellular and comprised of mainly laminar collagen (differentiating itself from the collagen in the stroma) and provides a platform for the endothelial cells and posterior stroma to adhere to. The Descemet's also provides a level of structural integrity to the eye. It also plays a key role in maintaining the fluid regulation as damage to this membrane could lead to a loss of endothelial cells (Hull, 1984).

1.2.5 The Endothelium

The endothelial layer of the cornea comprises a single layer of mitochondria-rich, flattened hexagonal cells which are attached to Descemet's membrane. It is thought that the underside of the cells is coated with a thick substance which affects the surface tension of the cells allowing them to remain hydrated. The cells are suspended in the G1 phase so do not undergo mitosis in the adult animal. This means that the endothelium does not have regenerative powers and once it is injured or diseased the integrity of the tissue is compromised (Tada, 1987). It should, however be noted that in culture conditions the cells are able to divide, so there are biochemical signals which prevent division *in vivo* (John, 2010).

The hexagonal junctions between the endothelial cells allow them to present a tight membrane which is able to regulate the transfer of ocular fluid between the stroma and the eye chamber (i.e. aqueous humours). This is vital for maintaining the correct interoccular pressure and the hydration of the cornea (Melamed et al., 1980). Changes in the corneal hydration may lead to oedema which in turn may lead to a reduction in transparency. Swelling of the corneal lamellae can also lead to the formation of corneal lakes. These lakes can cause abnormal scattering of light. On the fibril level, the increase in hydration can lead to an increase in spacing between fibrils and hence abnormal light scattering (Farrell and McCally, 1973).

There are a number of congenital and acquired diseases and disorders which can adversely affect this hydration balance including Fuch's dystrophy which ultimately results in the clouding of the cornea and loss of best vision. The endothelium can also be damaged due to acute injury or even surgical procedures or vision treatments. During refractive surgery, if the incision is made too close to the endothelial bed, swelling and loss of best vision may occur. This is also true for UV and Riboflavin cross-linking treatment in thin corneas where the UV rays may damage these delicate cells (Hafezi et al., 2009).

Following cornea transplant surgery including penetrating keratoplasty (PK), the loss of endothelial cells through damage can lead to the abnormal swelling of the implant. There is a basic requirement of roughly half of the normal adult endothelial cell count to maintain clarity of the cornea, any less than this can lead to swelling and loss of transparency (Farrell and McCally, 1976). For this reason, more recent surgical procedures retain the patient's own endothelium whenever possible to give the implant the best chance for survival and a return close to homeostasis. There are also changes which can occur to the endothelial cell density with advancing age due to a decrease in mitochondrial activity (Sanchis-Gimeno et al., 2005).

1.3 The Limbus

On the anterior periphery of the sclera and corneal interface (at the anterior epithelium), the annular limbus is located (Figure 1.5). This structure is generally believed to house adult epistem cells (which differentiate into epithelial cells and are key to corneal regeneration). These cells are thought to be produced in the vascular-rich limbus and are stored in specialised niches where the local environment maintains the epistem cell state. In some animals and individuals with a higher level of eye pigmentation (melanocytes), the limbus is visible as a pigmented ring around the cornea/sclera join. In individuals with fair or non-pigmented eyes, the limbus is visually indistinguishable from the adjoining sclera and transparent cornea (Daniels et al., 2001).

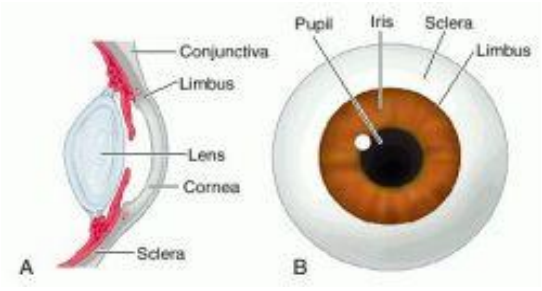

C 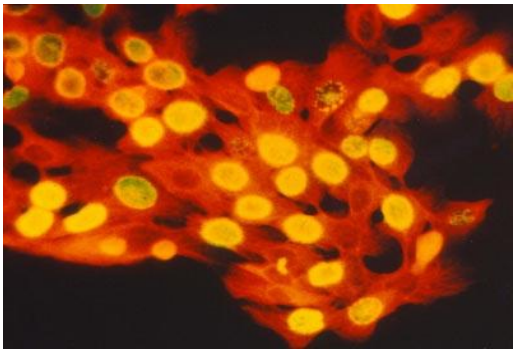

Figure 1.5 Images A and B: the location of the limbus and its relative position in the eye. Image copyright : Dorland's Medical Dictionary 2007. Image C: limbal epithelial stem cells cultured on human amniotic membrane. (http://www.med.nyu.edu/sun/research/index.html) accessed 2012

In the early 1970's, Davanger and Evensen were the first to propose that the limbal area contained stem cells which are directly involved in the regenerative process (Davanger and Evensen, 1971). They discovered that when the corneal epithelium of heavily pigmented eyes was wounded, the epithelial cells (which also contain pigment) would migrate from the limbus to the central cornea. They ascertained that the genesis of these cells would be the long thin channels which they observed radiating from the corneal epithelium into the limbus (Davanger and Evensen, 1971) (Figure 1.6). Other groups have identified what are believed to be limbal stem cells through Brdu and cell cycling.

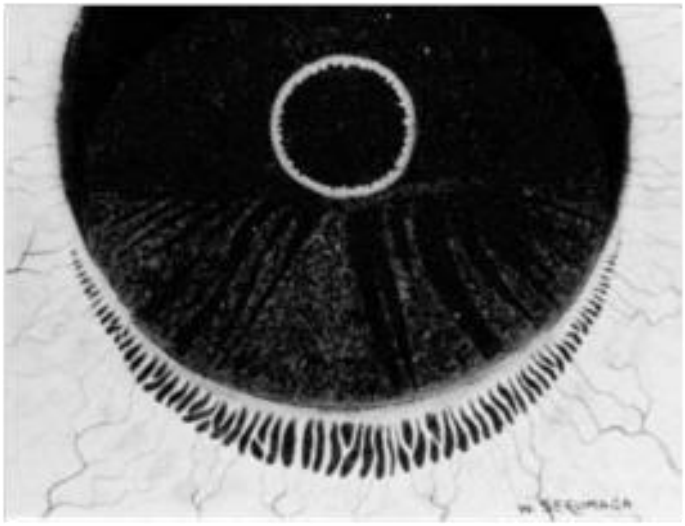

Figure 1.6: Illustration demonstrating the Palisades of Vogt in an individual with darker pigmentation of the eyes. (Davanger and Evensen, 1971)

The channels are known as the Palisades of Vogt and are comprised of a network of blood vessels, laminar membrane, 'pegs' of stromal tissue and Bowman's collagen. The channels were previously described in human and animal anatomical texts as early as the mid 19th century, however their role was not known (Townsend, 1988).

More recent research using immunohistochemistry and fluorescent cell labelling have almost conclusively proven that within the channels lay a phenotype of progenitor cell. It has also been discovered that as the limbal cells have a stem/progenitor phenotype and they do not contain connexins and gap junctions. As the cells eventually differentiate into adult epithelium, the phenotypes then change to include both connexin and gap junctions. The presence of connexins in the cells from null to positive is an indicator of the 'stem-ness' of the cell maturing into an adult epithelial phenotype, thus almost conclusively proving the origin of the cells (Chen et al., 2006).

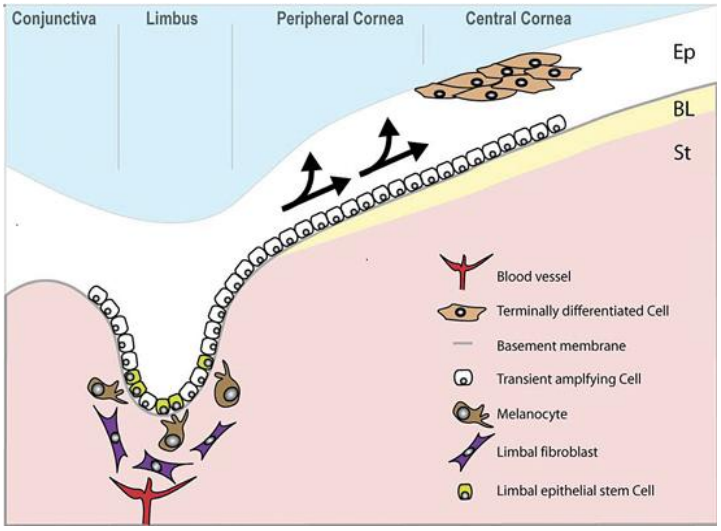

Figure 1.7: Limbal epithelial cells of the cornea and how they differentiate and are transported through the cornea. Secker and Daniels et al. www.stembook.org accessed 2011

Like other stem cells in the body, the limbal cells are stored in specialised stem cell niches or 'buds' (Figure 1.7). The niches are thought to provide the cells with a biochemically controlled environment which allows the cells to maintain a state of un-differentiated homeostasis until they are exposed to the necessary growth factors which ultimately lead to differentiation (Dua et al., 2000). The stem cells are thought to be bone-marrow derived cells which are able to access a rich blood supply at the vascular plexus . Research suggests that the stem cells migrate towards the centre region of the cornea in a centripetal or spiral pattern (Mannis and Hollande 2001).

In order to maintain a healthy stem cell supply, when one cell divides there always remains a 'daughter' population which is created and maintained. The other cell then differentiates into either a transient amplifying cell or a fully differentiated cell (e.g. adult corneal epithelium) (Daniels et al., 2001). Damage to the limbal region, whether through acute injury, pathology, or congenital defect, may lead to a decreased wound healing response and subsequent visual impairment. Wound healing experiments have discovered that the eye always healed to some extent as long as a significant part of undamaged limbus remained intact (Gurtner et al., 2008;Mannis and Holland, 2001).

1.4 Stromal Collagen

In order to understand the morphology and function of the stroma on a gross level, it is important to understand the individual components and how they interact on a biochemical level. The key component making up the bulk of the cornea stroma is collagen (mainly Type I) (Jakobiec, 1983). Collagen is a protein which forms connective tissue throughout the body. The collagen molecule (tropo-collagen) has a high degree of tensile strength and is comprised of long protein chains (alpha-chains) in a triple helix. There is a unique amino acid sequence required for the formation of a triple helix with glycine every third amino acid and a high proportion of proline and hydroxyproline repeats (Jakobiec, 1983).

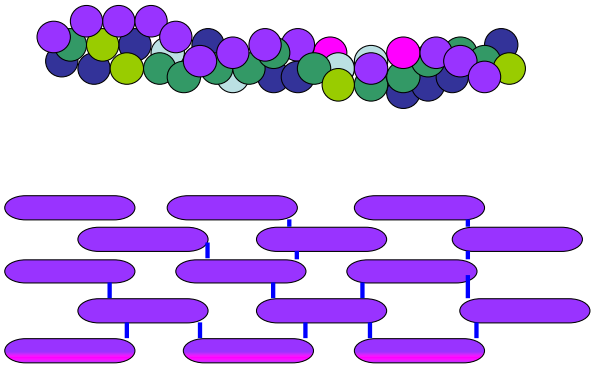

Figure 1.8: Above a schematic of tropocolagen made of three alpha chains (purple, blue, and green). Below schematic of how collagen molecules are cross-linked (blue bars) and assemble into larger structures.

From these individual collagen molecules, a wider network is created through covalent cross-linking. During the cross-linking process, strong covalent bonds are created between the individual collagen molecules to create strength and produce a more structurally robust structure in the form of fibrils. An increase in the incidence of collagen cross-linking has been associated with natural aging and exposure to exogenic factors (e.g. ultra violet light exposure) (Eyre et al.,1984). More recent research has indicated that cross-linking may occur not only between the collagen molecules but also within the collagen molecules making them less elastic. Damage can occur to weaken these covalent bonds and compromise the structural integrity of the tissue. These include free radical damage (Chase et al.,1991).

The collagen fibrils which are formed are arranged in a short range order. This order is vital for the transparency of the cornea. In the normal human, the individual fibrils are approximately 30-45 nm in diameter with a spacing of 65-66 nm between the fibrils depending on the species and if there are any pathologies present (Meek et al., 1993). Studies have indicated that there may be differences which are age related in the normal human (Daxer et al., 1998) and vary greatly between normal and pathological models including Fuchs (Gottsch et al., 2005). There are also believed to be differences in the spacing and diameter of the collagen dependent on the corneal region (Boote et al., 2003).

The exact orientation of the collagen fibrils is presently not fully understood, however data from electron microscopy and x-ray scattering studies have indicated that the spacing is regular and in a short range order (i.e. a set relationship between neighbouring fibrils) however the order is lost between more distant fibrils (Hart and Farrell,1969).

The cross-linked collagen bundles (fibrils) are bound together and obliquely oriented to form strong flat lamellar sheets. In the human stroma there are approximately 200 sheets which are stacked perpendicularly so that the direction of the collagen fibrils is alternated throughout the depth of the stroma (Cox et al., 1970). The collagen sheets are supported by an extracellular matrix (ECM) which originates from the products produced by the keratocytes which are scattered throughout the structure. The orientation of this lamellar collagen directly contributes to the biomechanical properties, strength, and protection of the cornea (Meek et al., 1987).

1.5 Stromal Fibroblasts

The stromal keratocytes (also known as fibroblasts) originate from neural crest cells during embryological development (Funderburgh et al., 2005). The cells are flattened and transparent and are scattered throughout the bulk of the stroma (Figure 1.9). The cells are flattened and elongated so they present a small size in the direction of the light path through the cornea.; the overall size of the cells is 7-8 um long. The cells' transparent properties allow for the cornea to remain transparent without cell

interference through scattering. The primary role of these cells is to produce ECM components and produce Type I and Type V collagen during development. In the adult, the cells are activated during the wound healing process to create Type I collagen and matrix to quickly repair and close the wound. The phenotype of the fibroblasts (and the matrix components produced) in the wound healing process differs from the quiescent keratocytes (Wilson et al., 2000).

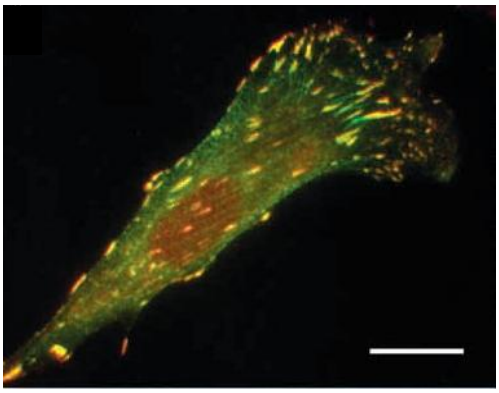

Figure 1.9: Corneal fibroblasts Bar 20 mm Petroll et al ., 2003

Following corneal injury (and the subsequent exposure to inflammation agents and growth factors), the fibroblasts are activated into producing collagen and ECM components which are rapidly and locally dispatched to close the wound and protect from the invasion of external pathogens. This leads to an excess of un-modelled collagen and the formation of a scar which normally lacks the transparency of the native tissue (Fini, 1999). It is also thought that during the wound healing process, the phenotype of the fibroblast changes on a nuclear level becoming more reflective. The reflective fibroblasts scatter light and are thought to lead to a 'haze' in vision (Fagerholm et al., 1994).

Like other avascular tissues (e.g. the cartilage of the knee and other joints), the lack of a direct blood supply for transport can result in the fibroblasts having a limited degree of motility (Vemuganti et al., 2004). Without a regular blood supply, cells are not easily removed following necrosis or apoptosis. This can result in detritus material remaining in the tissue following cell death. It is thought that the remains of the activated fibroblasts in intercellular space may lead to abnormal scattering of light (Behndig et al., 2011). This is currently up for debate in the scientific community with

some believing the cells transform back into the original phenotype. As the proliferation, necrosis, and apoptosis of keratocyte cells are presently poorly understood there is currently no consensus as to what happens to cells during the process of activation through cell death.

1.6 Stromal Nerve Supply

The cornea has a rich nerve supply. The nerves of the cornea are un-myelated (unsheathed) to allow them to retain their transparency and maximise on sensation which is vital to protecting the eye (Muller et al., 2003). Following damage to the eye (either accidental or through intentional surgical wounding) there is an immediate loss of nerve supply when the nerves are severed. The nerve sensation gradually returns with the onset of the wound healing process, however it is thought that the nerves never fully recover and return to homeostasis. It is thought that following some refractive surgical procedures (e.g. LASIK), Bowman's layer loses approximately 80% of the initial nerve supply with only roughly 60% of function returning after several years (Wilson et al 1998) (Figure 1.10).

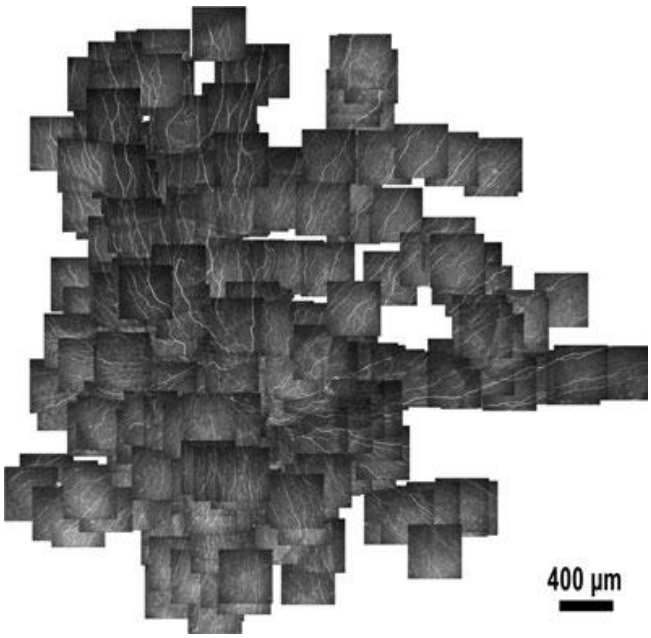

Figure 1.10: A montage of 301scanning in vivo microscopy images depicting the architecture of the normal corneal sub-basal nerve plexus (Linda Mueller)

The nerve supply to the eyes is important as it facilitates the blink and tear reactions.

The nerves are also thought to aid in the communication between the stroma and the corneal epithelium. With damage to the nerves, a patient's eyes may not be sensitive enough to detect a foreign body or promote the natural blink/tear reactions. A reduction in the normal reaction and the possible knock-on effect in the composition of tears (clinically known as dry eye syndrome) could result following corneal nerve injury. This damage can eventually impact on other corneal processes including the regeneration of the epithelium and general ocular homeostasis (Moilanen et al. 2008).

The nerves of the cornea are also important as the super sensitive nerves readily transmit pain and injury. Following surgery, the damage to the nerves and subsequent pain can greatly affect the patient. Post operative pain is one of the main complaints from patients who have undergone full surface ablation procedures such as PRK, LASEK, and corneal cross-linking procedures (Gabler et al., 2002).

1.7 Proteoglycans and Glycosaminoglycans

1.7.1 Glycosaminoglycans

Glycosaminoglycans (GAGs) are carbohydrate structures which are polysaccharides and are comprised of repeated disaccharide units. GAGs are produced by the stromal keratocytes in addition to collagen and other matrix proteins. GAGs are extremely hydrophilic in nature and can retain water, acting as 'cushions' to provide flexibility and absorb mechanical load and impact. They also play a key role in fluid retention and regulation (Forrester et al 1996).

The GAG's retain fluid and maintain homeostasis of hydration levels in the cornea; this level of homeostasis aids in the strict spacing between the collagen fibres. Any abnormalities of the GAG's and their fluid retention will have a direct impact on the amount, location, and layout of the collagen. This will in turn have an impact on the transparent qualities of the cornea (Saika et al., 1999).

Corneal GAGs include in the normal healthy cornea:

- Keratan sulphate

- Hyaluronan
- Chondroitin 4,6, sulphate
- Dermatan sulphate
- Heparin (trace)

(After Hollande et al., 2005)

Of all of the GAGs found in the cornea, the most plentiful is keratan sulphate. KS is mainly found in the cornea and cartilage. KS is a form of sulphated GAG (Pintar, 1978). It is the most abundant in the cornea making up 65% of the GAG's present (Holland, 2005). KS is comprised of disacharride repeats of *N* -acetylglucosamine and galactose, a GAG which interacts with the surface of cells along with the extracellular matrix (ECM) (Mehmet et al., 1986).

1.7.2 Proteoglycans

In the cornea, these GAGs (with the exception of hyluronic acid) can assemble and link to core proteins forming proteoglycans (Hollande, 2005). The individual GAG chains assemble and branch off the core protein like bristles on a brush (figure 1.11) (Forrester et al., 1996).

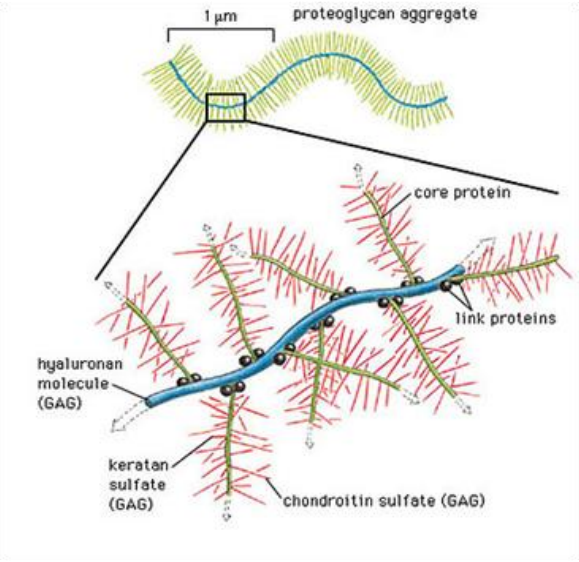

Figure 1.11: Schematic illustration of a proteoglycan aggregate and its assembly (www.Rejuvinate.com accessed 2011)

To date, there has not been a conclusive answer as to how the corneal collagen is spaced, however recent studies have indicated that long and short chains of proteoglycans may hold the answer (Hassell et al. 1983; Parfitt et al 2009). There are a number of combinations in which the GAGs and core proteins can assemble and the subsequent products regulate a range of functions in the cornea. The table below is adapted from Hollande 2005 (Table 1.1).

Core Protein	**GAG**	**Function in Cornea**
Lumican	Keratan Sulphate	Lumican and keratan maintain fibril spacing and prevent fusion
Keratocan	Keratan Sulphate	Maintaining Corneal Shape
Mimecan	Keratan Sulphate	Fibril Organisation
Decorin	Chondroitin Sulphate or Dermatan Sulphate	Make up the bulk of corneal GAGs and play a role in wound repair

Table 1.1: The functions and compositions of Corneal PGs. After Hollade 2005

As KS is the most abundant GAG present in the cornea, when it is assembled as a proteoglycan it plays a major role in corneal homeostasis. KS interacts with the surface of cells and the extracellular matrix (ECM) (Meier and Hay, 1974). There are believed to be several variations of the KS proteoglyan groups. The main functions of this group are thought to be maintaining the order and spacing of the stromal collagen during fibrilogenesis (Iozzo et al., 2000). Within this keratan sulphate group, there are different proteoglycan assemblages including the core proteins keratocan, lumican, and mimecan. Decorin is a related PG which binds to sulphated sites of chondroitin and dermatan (Snell and Lamp, 1997).

Keratocan is a leucine-rich proteoglycan. Knock out murine models have demonstrated that a lack of Keratocan may result in cornea plana. It is interesting, however, that some studies have noted that transparency continues to be maintained (Kao and Liu, 2002). This suggests that KERA plays a role in the structural integrity and biomechanical strength of the cornea but not the spacing between the corneal collagen fibrils (Kao and Liu, 2002). It is also believed that keratocan is regulated by lumican (Carlson et al., 2005).

Mimecan knockout murine models have also demonstrated abnormalities in the organisation of collagen fibrils. The changes associated with a mimecan deficiency tend to demonstrate a disorganisation of the collagen which results in a direct impact on the loss of transparency (Chakravarti, 2000). Lumican is expressed by stromal keratocytes (although it may also be present in epithelial cells during wound healing). Knock-out studies of lumican demonstrate loss of transparency which mimics the outcome of the mimecan studies (Saika et al 1999).

1.7.3 Chondrotion/Dermatan Sulphate

Chrondrotin Dermatan Sulphate (CS-DS) is mainly found in skin and other connective tissues and is a key component of the extra cellular matrix (ECM). It makes up approximately 40% of the remaining corneal PGs (Funderburgh, 1998). Decorin is the main DS proteoglycan in the cornea and comprises a leucine-rich protein core along with a GAG chain. Decorin is associated with the maintenance of corneal structure and biomechanical strength (Scott and Stockwell, 2006). It is believed that these proteoglycans work in conjunction with one another in order to maintain homeostasis in the cornea allowing it to maintain both its biomechanical strength and its transparent properties (Saika et al., 1999).

Recently, researchers from Cardiff University (Parfitt et al., 2010) developed a modelling technique to better understand the location and orientation of proteoglycans in the murine eye. Using a 3-D electron tomography in a tilt series, the group was able to create a three-dimensional reconstruction of the mouse cornea which clearly demonstrated the role that PG's play in maintaining corneal architecture (namely fibril spacing and diameter) (Figure 1.12). It is hoped that this model could be

applied to other species (along with pathological variants) to better understand the roles of proteoglycans in their interaction with collagen.

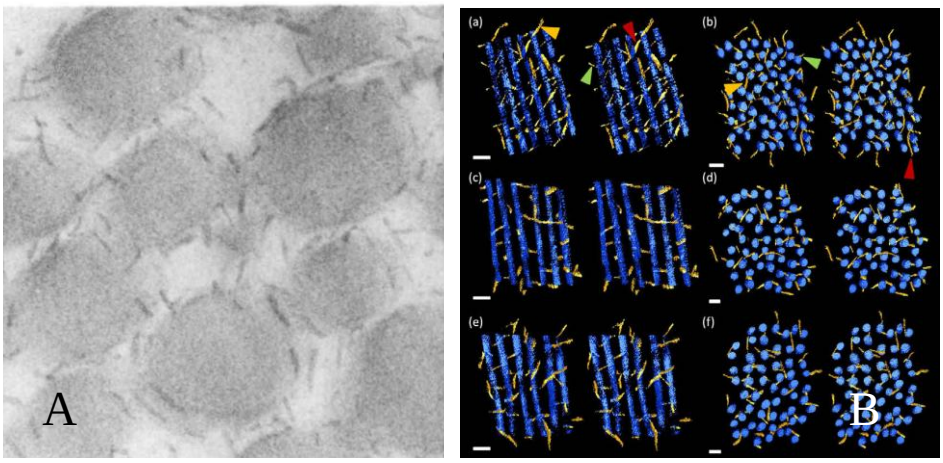

Figure 1.12 : A)TEM image of round collagen fibrils separated by darker proteogolycan chains Young et al *J (1985)* B) 3D reconstruction of collagen–proteoglycan interactions in the mouse corneal stroma by electron tomography Parfitt et al 2010

1.8 Corneal Ultrastructure

The unique ultra-structural properties of the normal corneal stroma give rise to its transparency and biomechanical strength. This is due to the organisation of the corneal collagen on both the inter-fibril and molecular level. Transmission Electron Microscopy (TEM), X-ray scattering, Second Harmonic Generation Microscopy (SHG) and histological analysis have all provided insight into the structure of the cornea and have led to a better understanding of how the cornea functions. Understanding the physiology of the cornea is vital for the treatment of diseases, injury, and disorder.

1.8.1 Collagen Organisation on the Fibril Level

Earlier in the chapter, the nature of Type I and Type V corneal collagen were discussed. The fibrils are spaced uniformly in a ‘short range’ packing order (Hart and Farrell 1969). The average diameter and spacing of the fibrils increase in size from

the sclera, through the limbus and through the central corneal region (Boote et al., 2003). This increase in fibril diameter is thought to provide additional biomechanical strength to the cornea.

Other collagen types are present in the corneal stroma (including Types VI and V) along with proteoglycans which are hypothesised to regulate the diameter and spacing of the fibrils (Birk et al., 1986; Parfitt et al., 2010).

On the lamellar level, there are also changes in the properties of collagen across the cornea. Wide angle X-ray scattering has been instrumental in determining the organisation and distribution of corneal collagen. This organisation differs from species to species, slightly from individual to individual, and even between eyes (Boote et al., 2005). There are differences between healthy individual eyes and the diseased / congenital defective. On the whole, however, there are morphological features which result in the biomechanical strength of the cornea.

1.8.2 Collagen Organisation of the Human Cornea

The ultrastructure of the human cornea has been extensively researched as findings directly impact the success of clinical treatments. The organisation of corneal collagen presents a number of key characteristics.

- The organisation of central collagen
- The collagen annulus
- The organisation of collagen at the cornea/limbus
- The organisation of collagen at the limbal/sclera
- The organisation of collagen in relation to ocular muscle

Wide angle X-ray scatter analysis has revealed that the collagen in the central portion of the cornea (along the visual axis) presents a preferential alignment of collagen along horizontal and vertical meridians (Meek et al., 1987; Fratzl and Daxer, 1997; Agamohammadzadeh et al., 2004). The collagen appears ordered and the fibrils are

thinner than those in the more peripheral tissue. Radiating out from the centre of the eye, the collagen appears to be stacked in a less 'crossed' manner until the outer boundary of the corneal/sclera join where there appears to be little to no crossing of the fibres (Boote et al. 2006). There are differences in collagen organisation between individual left and right eyes. There are always slight differences between collagen at the fibrillar level, but the most marked differences are between the orientation of the supporting / reinforcing fibres. The fibres are arranged in a "mirror" image to each other with left and right eyes distinct (1.13 A and B).

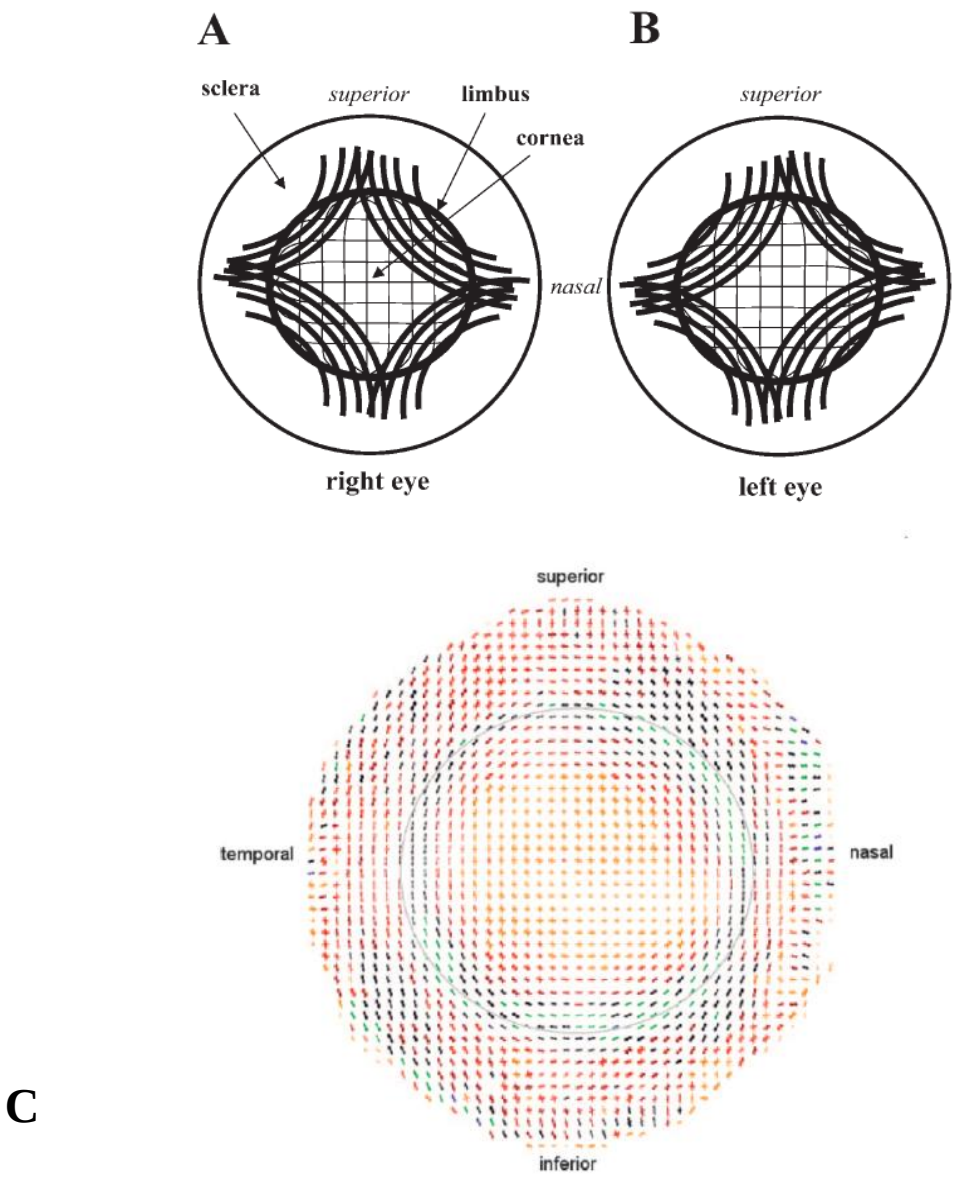

Figure 1.13: Images A and B demonstrate the long collagen bundles. The image C demonstrates an x-ray scattering-derived map of the cornea with the limbus circled. Note the crossed collagen in the centre of the eye (Boote et al. 2006) .

The annulus is a ‘ring’ of collagen which is found along the periphery of the cornea. It consists of collagen which has a preferential collagen alignment of horizontal collagen at the top and bottom of the cornea, vertical collagen along the nasal and temporal sides, and angled collagen joining the four sections. The “ring” is on average 2 mm wide in the human cornea and is thought to provide support for the curved part of the cornea. In corneal biomechanics, it is thought that the annulus acts as a supporting band giving the cornea its curvature and raised topography (Newton and Meek, 1998; Meek and Boote, 2009). Not all animal species have a collagen annulus and certain diseases and disorders appear to cause an absence of annulus. This will be discussed in further detail in Chapter 3.

The join where the cornea and the limbus meet contains a different collagen morphology and organisation from the neighbouring tissue. Along the limbal/sclera there is a change in the collagen type and orientation. The most notable difference is that the collagen loses transparency at the sclera and becomes an opaque white (due to the collagen organisation found in the sclera) . The spacing between the collagen fibrils is through to increase and the alignment of the collagen becomes more ordered resembling the Type I collagen of rat-tail tendons (Quantock et al., 1988). There have been a number of histological studies on the sclera, however there have been few x-ray scatter studies. It is thought that there is a change in the direction of collagen along the border and the interface between the limbus and sclera (Newton and Meek, 1998). This interface area is thought to be biomechanically weaker than the rest of the tissue (Aghamohammadzadeh et al., 2004).

There are also thought to be four distinct anchor points where reinforcing bands of collagen attach creating the ‘diamond’ morphology around the cornea (Figure 1.3 A and B). These fibres are thought to keep the cornea under tension (Boote et al., 2006). It has been postulated that breeching these fibres during ocular surgery could lead to complications; in a clinical setting, it may be important that incisions are made outside these anchor points (Boote et al., 2006).

There are also changes in thickness and the organisation of collagen on the gross level. Wide angle X-ray scattering has demonstrated that the central portion of the cornea is thinner than surrounding tissue and the thickness increases going out towards the periphery (Boote et al., 2006). The percentage of aligned collagen has also been established to increase closer to the periphery. It is thought that the thicker peripheral collagen supports the anterior portion of the eye (e.g. as seen in the annulus) (Meek and Boote, 2009).

In addition to the collagen fibril changes across the cornea from region to region, the collagen fibrils differ in depth from anterior through to posterior (Freund et al.,1995). Femtosecond Laser Technology has been used to precisely and accurately divide human cornea into anterior, mid, and posterior sections (Abahussin et al., 2009). These sections were then individually analysed using wide angle X-ray scattering. It was discovered that in the mid and posterior sections of the cornea the collagen lamellae were orientated along the equatorial and meridional axis towards the sclera and rectus muscle attachments. The collagen in the anterior section of the cornea was not seen to run in any preferred orientation but was more isotropic in nature (Abahussin et al., 2009).

1.9 Corneal Transparency

Understanding the transparent properties of the cornea is important for clinical purposes (figure 1.14). The swelling of the cornea following injury or pathology (inflammation) has been observed to be one of the main factors which have a negative impact on the transparent properties. Patients who suffer from dry eye syndrome (DES), diabetes and glaucoma have also been observed to have an effect on the thickness (and therefore the transmittance) of the cornea. In addition, the wounds following corneal injury (or surgery) can lead to changes to the hydration, thickness and resulting transparency of the cornea (Cinton et al., 1978).

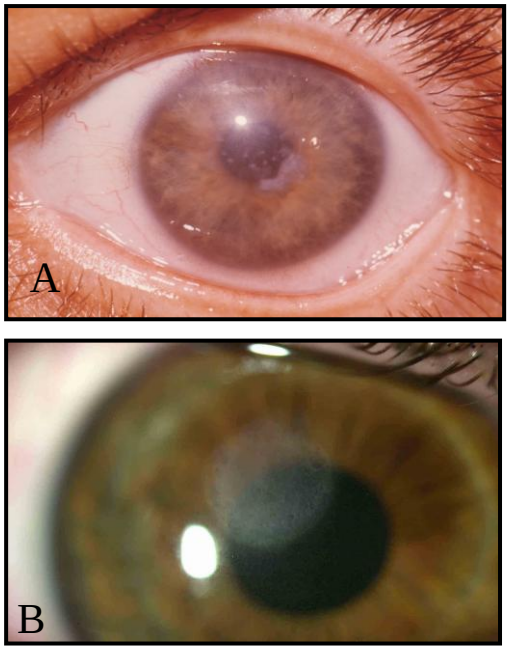

Figure 1.14: A) Macular corneal dystrophy which results in a loss of corneal transparency (University of Arizona 2011) B) Loss of transparency following the formation of a scar from a contact lens ulcer (Andrew Gasson, 2011).

Earlier in this introductory chapter, some reasons postulated to explain the transparent properties of the cornea were touched upon including mention of congenital disorders and pathologies. Over the last hundred years, there have been a number of models put forward for the explanation of corneal transparency, however there is currently no firm agreement as to how exactly it is achieved (Meek, Leonard et al 2003).

Maurice (1957) hypothesised that the fibrils of the cornea could be ordered in a strict lattice structure with equal spacing between each fibril. He noted that when a small amount of swelling was introduced, the cornea increased in opacity. Maurice surmised that if such minor fluctuations in hydration occurred that there would be a knock-on effect for fibril spacing and this would be enough to entirely change the way light was scattered (Maurice, 1957; Potts, 1962).

This model contained some slight discrepancies raised based on TEM electron micrograph evidence. The images of corneal collagen did not show a strict crystalline structure with uniform spacing of fibrils. There appeared to be some order to the

collagen but not the strict 'crystalline' structure which would scatter light following Bragg's law. It was initially thought that this discrepancy was an artefact due to the heavy processing which occurs during electron microscopy. It was thought that the processing had caused damage to the tissue and matrix thus altering the collagen arrangement. Some felt that this was not the case and the problem was later addressed by Hart and Farrell (1969).

Hart and Farrell (1969) developed a radial distribution function based on their analysis of electron micrographs. The radial distribution function calculates the likelihood of finding two 'scattering centres' a set distance apart. From this information the degree by which there will be constructive or destructive interference could be calculated. This radial distribution function differed from the strict ordering which would be found in a lattice, and more closely resembled that found in a "liquid crystal" or a 'quasi-lattice' with a regular and random structure. Whilst the findings differed in part from Maurice's ideas, they were able to reconcile this with what would later be known as the 'short range order' theory. As long as the distances between and arrangement of neighbouring fibrils were such that there was destructive interference of scattered light, then it does not matter if the overall structure is not a perfect crystalline lattice (Hart and Farrell 1969).

There are a number of other factors that contribute to the physical properties of corneal transparency including the size, hydration and general morphology of the cornea (differing across species and pathological status) and the general stromal structure. The refractive index and the orientation/spacing of the stromal components (including collagen, keratocytes, and proteoglycans) and proper hydration levels play a role in maintaining corneal transparency (Freund et al., 1991).

In spite of these hurdles, there is an overall agreement that there are a set of factors which govern the overall transparency of the cornea:

1) The number and density of the collagen fibrils in a given area
2) The diameter of the collagen fibrils
3) The spacing between the collagen fibrils
4) The refractive indexes between the collagen and surrounding ECM, ocular

fluid and keratocytes

5) The thickness of the cornea (including swelling and dehydration)
6) The thickness of the cornea through its central depth

As there is believed to be a set of proposed criteria governing why the cornea is transparent then a resulting lack of transparency (and associated lack of light scattering) would also be governed by a set series of qualifiers.

Meek et al., 2003 have noted these to be:

1) Any alteration or destructive change in the order of the fibril spacing
2) Any increase in the diameters of the fibrils
3) Any increase in the density of the fibrils
4) Any increase in the spacing between the fibrils
5) Any increase in the refractive indexes of either the fibrils, proteoglycans, ECM or fluid components
6) An increase in the overall thickness of the cornea (which and occur with a change in corneal thickness from swelling)
7) Any cellular changes with may occur (e.g. following wound healing or cell loss through apoptosis). (Meek et al., 2003)

1.10 General Wound Healing Response in Mammals

The complex biochemical process of wound healing is vital to the survival and return to homeostasis in the organism. Following an injury, a series of biological processes are initiated to clean and close the wound and prevent foreign invasion. The main mechanism for this is the activation of fibroblasts which produce large quantities of fibrotic tissues which close the wound and form a scar (Gurtner et al., 2008).

Once the wound is closed, the scar tends to remain as a non-functioning mass. The tensile strength of the scar is a fraction of the original tissue (the disordered laying down of tissue which differs from the native tissue) and the tissue never completely heals to its prior state. In organs such as the eye, the fibrotic build up would compromise the transmission of light and cause visual disturbances (Girgis et al.,

2007).

From an evolutionary stand point, the process for the quick and efficient closure of wounds through scar formation is effective and (when successfully completed) the organism can return to activities with minimal disturbance. It has been noted that no matter the injury type or the location of the wound, the healing response is similar across the organism.

This natural response occurs in distinct stages.

1) Inflammatory stage
2) Granulation and re-epithelialisation stage
3) Proliferative stage of ECM and remodelling
4) Wound contraction
5) Collagen proliferation and tissue remodelling

(Fagerholm, 2000)

Immediately after injury, the inflammation stage begins. The integrity of the organ has been breached so it is necessary to prevent the further loss of blood (in a system which undergoes angiogenesis) and fluids and to prevent the invasion of foreign bodies into the system. The inflammatory and immune processes are activated (along with the coagulation process in vascular tissue) and biochemical signals are sent to prevent infection, promote localised apoptosis, and temporarily close the wound, generally with a fibrous clot (Garg and Longaker, 2000).

Following the temporary closure of the wound, fibroblasts begin to lay down collagen and ECM components to permanently seal the wound. This leads to the formation of scar tissue. Scar tissue differs from native tissue as the collagen and ECM components are not laid down in the strict formation of native tissue. This leads to a mass of tissue which differs in phenotype and mechanical properties (Garg and Longaker, 2000). Over time, the scar tissue is slowly re-modelled through matrix metalloproteinases (MMPs) and other collagenases. The remodelling of the scar tissue includes a reduction of inflammation and a return to a phenotype more closely

related to native tissue.

This thesis will look at two distinct areas of corneal wound healing. These are:

a) The wound healing response of the epithelium
b) The wound healing response of the stroma

Whilst there are other regions of the cornea which have an impact on the cornea's ability to heal (e.g. direct damage to the limbal region and the endothelium), this thesis is focused on epithelial and mid-depth stromal wounds which would not directly impact on the functioning of either the limbus or the endothelium. There is however related clinical and research studies which suggest that endothelial wounding post-refractive surgery is a very rare complication (Azar and Koch, 2002).

1.10.1 The Epithelial Response in Wound Healing

The epithelial response is the first response in a series of corneal wound healing processes. As the most anterior layer of the cornea, the epithelium, is the first tissue to be damaged during surgical wounding. PRK scrape-type injuries directly involve the initial ablation of the epithelium (either manual scrape, by brush, by laser or followed by application of alcohol) before the underlying stroma is exposed and the tissue is remodelled (Enoch, 1997).

The healing of the epithelium occurs in distinct stages:

An inflammatory stage following initial injury and necrosis of cells

- Intracellular cell matter is abruptly released into the extracellular space
- This leads to the initiation of the apoptotic response by neighbouring cells resulting in the release of caspase zymogens or activation of Fas-Ligand cell receptors
- The release of pro-inflammatory interleukins (namely IL-1, IL-6 and IL-8) which mediate the wound healing process

- The release of growth factors including TGF-β, Hepatocyte growth factor (HGF), Platelet-derived growth factors (PDGF), Tumour necrosis factors, and Epidermal growth factor (EGF) which transform and activate cells

A latent phase where changes occur at the wound edge

- wound edge retraction
- migration of cells to the wound edge
- a change in epithelial cell phenotype from flattened desmosomal to more rounded
- a thinning of the epithelium at the wound edge
- the synthesis of actin filaments and an increase of superficial fibronectin, fibrin and fibrinogen

Migration phase

- Lamellopodia and filopodia form
- Actin filaments begin cell migration
- An increase in cell volume to cover larger surfaces
- Proliferation of cells in the limbal area which migrate towards the wound through a centripetal pattern

The complete re-epithelisation of the wound

- The wound is covered by one to two layers of cells
- New basement membrane is developed
- Lamellopodia and filopodia cell anchoring increases
- Cessation of the release of growth factors and cytokines

(Fagerholm, 2000)

The initial stages of this wound healing process occur immediately following wound healing. The complete closure of the wound occurs up to 48-72 hours following the

initial wounding. The complete healing of the wound occurs once the basement membrane is reformed and all cell to cell interactions are established. Until complete healing occurs, there remains a fluctuation in the vision of the patient (Lu et al., 2001).

1.10.2 The Stromal Response in Wound Healing

Following the damage to the epithelium, there is surgical wounding to the Bowman's and the underlying stroma. The wound healing response of the stromal layer differs greatly from the epithelium. The stromal layer is relatively cellular when compared to other corneal structures. Following initial wounding, stromal keratocytes undergo apoptosis roughly 50 to 200 µm below the wound area (Wilson et al., 2001). It is believed that this is Fas-L mediated apoptosis (Kamma-Lorger et al., 2008).

These cells are repopulated several days after surgery but are no longer in a quiescent state. The cells have been transformed (by the growth factors and interlukens released by the epithelium) into activated fibroblasts. Phenotypic changes which occur during this stage include a flattening of the cells, a darkening of the cell nuclei, and a decrease in crystalline proteins. The main function of these activated fibroblasts is to synthesise collagen, proteoglycan components (including hyaluronan) and ECM components to restore the Bowman's membrane and the stromal tissue. Activated fibroblasts are believed to cause a number of visual disturbances experienced postoperatively. These disturbances include haze, halos, and starbursts. It has been clinically documented that these complications improve over time (generally six months to a year) (Wu et al., 1999).

As mentioned earlier, there is currently a debate as to what happens to these activated fibroblasts following the repair of the tissue. The three hypotheses are:

1) The cells apoptose over time and are replaced with new somatic cells derived through the mitosis of neighbouring keratocytes
2) The cells revert to native form over time, cease in production of smooth muscle actin, and regain their original phenotypes
3) The cells apoptose over time and are replaced with new keratocytes derived

from bone marrow derived stem cells or latent limbal progenitor cells

Corneal Wound Healing Table

Epithelial Injury Following Wounding/Surgery 
Keratocyte Apoptosis (immediately adjacent to the wound region) 
Growth Factor and Cytokines Produced by Lacrimal Glands 
Epithelium Healing Through Mitosis and Migration of Cells 
Inflammatory Cell Proliferation (Transported by Tears) 
Keratocytes Undergo Mitosis and Migration 
Keratocytes Transform to Fibroblasts and then Myofibroblasts 
Collagen and GAGs Production by Transformed Fibroblasts 
Release of MMPs and Collagenases from Transformed Fibroblasts 
Transformation Back Into Keratocytes? 
Migration of the Epithelium Continues 
Return of Epithelium and Stroma to Homeostasis 

Table 1.2: Corneal Wound Healing Cascade Adapted from (Wilson et al. 2001)

1.10.3 Proteoglycans in Wound Healing

Proteoglycans have been flagged as key to the normal embryological morphogenesis of the cornea and vital for maintaining homeostasis in the adult animal. When this homeostasis is breeched (e.g. following injury or surgery) their roles change to prevent further damage or invasion of foreign bodies.

Immediately following wounding, there is immediate localised cell death and matrix damage due to direct injury. If the injury is superficial, the epithelial cells rapidly proliferate and heal the injury. If the wounds are deeper or more complex (resulting in keratocyte death), it is thought that the proteoglycans along the injury are activated by a change in the environment from the aqueous humour and tears and may swell to help close the wounds. The narrower the wound, the more likely there is for cell to cell interactions and the rebuilding of matrix (Hollande, 2005).

In early research, it was noted that there was a decrease in KS proteoglyans but an increase in the dermatan sulphate proteoglycans following wound healing. DS is more associated with a high presence in connective tissue and skin. Some studies did not find an up-regulation of the KS proteoglycans until nearly four months after wounding. It is thought that the disruptions to the PGs cause a change in the matrix and could contribute to the decrease in light transmission during wound healing (Funderburgh, 1998).

This strict organisation can be altered following injury or pathology either through a disorganisation of new collagen fibrils (laid down during the wound healing/scar formation process) or through a disruption in the fluid homeostasis in the cornea (which inevitably leads to oedema) (Connon and Meek, 2004). Electron micrographs of scar tissue demonstrate an alteration in corneal spacing causing it to become more irregular. Over time, the cornea's matrix re-models to a more normal appearance.

1.11 Injury/Surgery

As the eye is generally exposed to the outside environment, there is a high risk that the eye may undergo accidental injury. In addition to unintentional injury, surgery is

intentional injury to the eye for future benefits. Both surgical and accidental injury to the cornea can lead to compromises to the transparency and bio-mechanical functions.

1.11.1 Incision

Incisions can occur due to general injury or can be inflicted as a part of a surgical procedure. LASIK, PRK, Penetrating Keratoplasty (PK), Descemet's Stripping Endothelial Keratoplasty (DSEK) and a range of other procedures use surgical blades, trephines, and lasers to make incisions into the cornea. This raises a number of issues relating to wound healing.

Although the surface area of an incision is generally smaller than a burn or an abrasion, the depth of the wound is often greater. This means that the Bowman's layer and collagen lamella are disrupted. The depth of the wound may also damage the endothelium. As mentioned earlier in the introduction, damage to the endothelium can lead to swelling of the cornea and may be irreparable.

The overall bio-mechanics of the cornea could also be affected with an incision. Earlier in this chapter the organisation of corneal collagen was discussed, specifically that some of the collagen is believed to be situated in a 'diamond' like orientation with longer collagen bundles spanning the cornea from top to mid-line. When an incision is made which may cut the tension in this collagen band, the mechanics of the cornea may be compromised.

1.11.2 Corneal Transplant Procedure

There are two different donor-based corneal transplant procedures which are currently preformed by surgeons. The first is a lamellar keratoplasty which involves a replacement of the anterior portion of the donor cornea leaving the patient's own Descemet's and endothelium intact. This is a relatively newer procedure which has a high success rate due to presence of the original tissue which remains. The graft is then attached using either a localised or a running stitch.

1.11.3 Penetrating Keratoplasty

The more traditional standard surgical procedure for corneal transplant is penetrating keratoplasty. The procedure involves a full-depth tissue replacement where a trephine is used to remove a 'button' of tissue from the central portion of the cornea. The trephine is usually 8mm -9 mm in diameter. A more recent variation on the trephine has been the development of laser trephination which can be performed in a 'free form' manner. Like in other forms of corneal surgery, the use of the laser allows for a more precise cut which is free from the irregularities which may be caused by a mechanical method (Schmitz et al., 2006).

Whether it is a standard or laser trephine, the same procedure is performed on the donor cornea. The harvested tissue is then aligned using forceps and stitched either with localised stitches or (more recently) a running stitch to maintain the same amount of tension around the circumference of the wound. The patient is then given steroids for a period of several months.

Following the procedure, there are complications which can arise which include the development of astigmatism (which may require corrective lenses). The cornea does not always stabilise, so the degree of astigmatism may also change over time. It has been noted that within the first few months the vision fluctuates the most (Melki, et al., 2001). Care must be taken through the life-time of the implant to avoid dehiscence of the graft through eye trauma (Binderet al., 2005).

This procedure has a slightly higher rate of rejection than the more recent lamellar keratoplasty with 11% to 18% rejection with bilateral implants presenting a higher rejection rate (Kirkness et al., 1990). In most patients, the graft lasts on average 10 to 15 years although there are individual cases where the graft has lasted longer. The general consensus is that wound healing appears to near completion after six months to a year (Kirkness et al., 1990). *In vivo* observations of the integrated tissue have demonstrated collagen lamellae which run parallel to the original tissue however the donor tissue appears to retain its original phenotype.

There are other variations on the penetrating keratoplasty procedure including a partial limbal graft. Earlier in this chapter, the role of the limbus and limbal stem cells in wound healing has been discussed. In these surgeries, part of a donor limbus is also implanted to improve the healing of the wound along the graft margin.

1.12 Refractive Surgery

1.12.1 Types of Refractive Surgery

Refractive surgery is a form of eye surgery where the cornea is reshaped (either through scraping, chemically, or more commonly with a laser) to improve the refractive powerof the eye to reduce or eliminate the patient's need for glasses. The first refractive eye surgical procedures were performed as early as the mid-nineteenth century, with more modern procedures (including radial incisions of the cornea) developed in the mid-twentieth century. More recently, keratomileusis (or corneal shaping) procedures have been used including LASIK (laser in-situ keratomileusis), PRK (Photorefractive Keratectomy), and LASEK (laser sub-epithelium keratomileusis) (Gimbel and Penna, 2004).

It has been estimated that over 17 million patients worldwide have undergone some form of refractive surgery with estimates of 700,000 to 1.5m per year in the United States alone (Spectrum consulting 2005). In 2006, the United States consumer group Visionwatch reported that 70% of patients surveyed were satisfied with their post-operative results three to four months following surgery (Visionwatch.org accessed 2010).

Whilst refractive surgeries have an overall high level of patient satisfaction, there continue to be a significant number of patients for which surgery has not been entirely successful. These patients report visual disturbances (sometimes years post-operatively) and in many cases need to return to wearing corrective lenses.

The following is a brief summary of each of the main refractive surgical procedures and common complications:

1.12.2 PRK

Photorefractive keratectomy was the first commonly performed procedure using an excimer laser to ablate the corneal tissue by exciting and breaking down biochemical bonds. The excimer laser is a 'cold' laser as it does not burn the corneal tissue (Moilanen and Vesalymoa, 2003).

During PRK the epithelium is removed from the surgical region and the stroma is shaped using the laser (Figure 1.15). As the epithelium retains rapid regeneration properties, following the procedure the epithelium heals itself through a supply of limbal stem cells. The PRK procedure alters less of the cornea. This was originally thought to be the most beneficial for the patient.

With PRK, there have been a number of complications reported by patients including painful eyes (the loss of the epithelial layer is thought to increase the exposure and sensitivity of the underlying stroma), longer recovery times when compared to 'flap' procedures, dry eyes, haze and starbursts, scarring and reduced night vision.

Although PRK has traditionally been replaced by LASIK and LASEK procedures, there are a number of patients whom the surgery is still recommended for (e.g. patients with very thin corneas or who may develop ectasia). Also, patients who have occupations where the dislodging of a corneal flap or dehedisence is a danger may be referred for PRK-type surgeries (Ambrosio and Wilson, 2003).

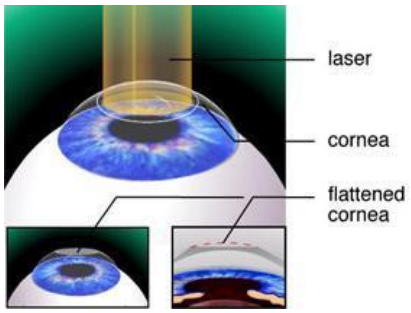

Figure 1.15 : Schematic of the PRK procedure. Following an epithelial ablation, a laser is used to remove stromal collagen (www.aucklandeye.co.nz June 09)

1.12.3 LASIK

The LASIK procedure is also performed with an excimer laser, however this procedure differs from PRK as the epithelium is not removed and discarded but the stroma is cut into a hinged flap and re-positioned over the laser ablated area following the surgery (Figure 1.16). Patients noted less pain and a faster healing time when the epithelium was conserved (Ambrosio and Wilson, 2003; Camellin et al. 2003).

The flap is created using a microkeratome (or specialist knife with an oscillating blade) or cut with a femtosecond laser. Traditionally, the flaps were created in the upper third of the stroma to preserve flap integrity (to prevent flap tears, button holes, dislocations and 'melts') and allow the remainder of the stroma to be shaped with the excimer laser (May et al., 2004).

More recently, clinicians have noted that a thinner flap created sub-Bowman's layer (using the femtoscond laser) would allow the eye to retain much of its structural integrity whilst reducing healing time and complications (Machat et al., 1998). Complications reported in traditional and sub-Bowman's LASIK include dry eyes, haze, halos, flap dislocation or loss, DLK (or particles lodged between the flap and the surface of the eye), over and under correction (Ambrosio and Wilson, 2002).

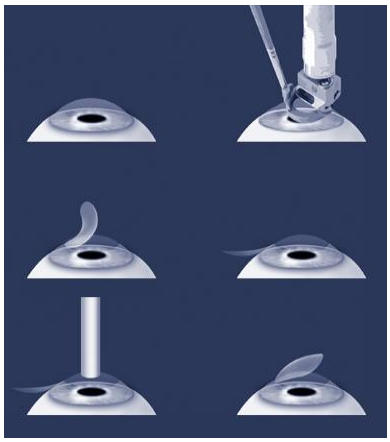

Figure 1.16: Schematic of the LASIK procedure. A microkeratome is used to surgically cut a hinged flap. As with PRK a LASER is then used to remove the anterior stroma (www.wakelasik.com June 09)

1.12.4 LASEK

LASEK is a variation of PRK where following the removal of the epithelium and laser ablation, the epithelium is replaced and a soft contact lens is inserted over the wound area as a bandage to hold the epithelium in place (Figure 1.17). Clinicians believe that the bandage affords the eye additional protection and reduces pain associated with dry eye and nerve exposure in traditional PRK. This procedure is also recommended for patients who fall in a high risk of eye injury category (such as participation in boxing and martial arts).

The complications associated with LASEK are similar to those experienced in LASIK and PRK including dry eyes, pain, scarring, and visual disturbances (including starburst, halos, and haze). Although the three surgical procedures differ, the shared complications are the result of the eye's natural wound healing process following the intentional surgical wounding (Ambriso and Wilson 2002).

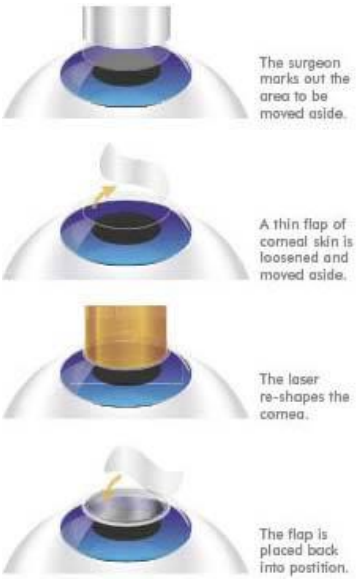

Figure **1.17**: Schematic demonstrating the LASEK procedure.
(www.wefixeyes.com) June 09

1.13 Scarless Wound Healing

With the amount of corneal injuries and surgeries, and the low supply of donor corneas, the quest for a scarless form of cornea repair is imperative. Due to the complex biochemical mechanisms which govern the healing of corneal wounds, it is difficult to isolate and determine exactly what factors need to be altered to accomplish scarless healing. It is thought that the most plausible research streams would be to either prevent the activation of the fibroblasts, or to alter the type of collagen produced to more of a foetal phenotype. The latter is thought to be accomplished by replacing the fibroblasts with cells of a more preferential healing type (Du et al., 2007).

1.14.1 Stem Cells

As discussed earlier in this chapter, stem cells have been associated with corneal wound healing and regeneration. It is thought that the limbal cells are from a bone marrow derived source. Cells have been immuno-labelled *in vivo* to demonstrate the migration of these cells over the surface of the wounded cornea. Any damage or deficiency to this cell supply will ultimately result in poor wound healing (Gurtner et al., 2008).

In 1997, Pellegrini et al first described the use of autologous limbal stem cells in the human ocular wound healing process. These cells were cultured *in vitro* and appeared an ideal treatment for patients who had undergone unilateral damage to the eyes. Other studies demonstrated the use of limbal allografts cultured *in vitro* for patients who have bilateral eye damage. Another option for patients with bilateral eye damage is the use of stem cells derived from other non-ocular tissue sources, embryological tissue, induced pluripotent stem-cells (IPS cells).

There are, however a number of drawbacks regarding the use of stem cells in ocular wound healing. The fist is that is a number of patients, the autologous cell supply is not sufficient due the disease or damage to the donor tissue. If donor cells are used, there remains the increased chance for rejection. The limbus is a highly vascular tissue which an increase in Langerhans cells and HLA_DR antigens (Danielset al., 2001).

The use of harvested stem cells from embryological sources carries with it a number of social and political considerations. There is also a limited initial supply of cells and tissue available. Liu, Jester et al (2010) have researched using human umbilical mesenchymal stem cells expanded in culture to treat murine corneal defects in lumican-deficient mice with success. The use of the umbilical cord would allow for a sound supply of 'foetal' type cells which could be used in ocular repair (Liu et al., 2010).

More recently IPS cells created from the donors own somatic cell bank are being explored, but at present the technology is young, complex, and not practical or cost effective. Du, Rho, Funderburgh et al. at the University of Pittsburgh have researched into using adipose derived stem cells (ADSC) for corneal repair due to their ability to change cell phenotype when stimulated with localised environmental factors (Du et al., 2010).

One type of cells they can differentiate into are neural crest cells which are the progenitors of the keratocyte. The group were ultimately able to discern keratocyte type properties (e.g. corneal matrix materials) in the differentiated somatic cells after exposing them to corneal environmental factors. Treatment such as this would allow the cells to be developed from a non-embryological cell source.

The group has also investigated using human stem cells injected into scarred mouse corneas resulting in a decrease in the appearance of scarring and there was a great improvement in the clarity of the cornea after three months. Critics presented a caveat that the corneal matrix of the mice differs from that of human cornea and may need further investigation. The hope for human trials regarding stem cell injections are believed to be two years away.

Another issue, regardless of stem-cell source, is the targeted application of the cells and the possibility of migrating cells leading to tumour genesis in other parts of the body. Once cells are applied to the surface, they need to remain in the appropriate target area and differentiate into the required cells for repair. In the eye, there remains the additional challenge of blink/tear mechanisms which mechanically removed superficial cells. Some groups have suggested using seeded contact lens bandages, amnionic membranes, or artificial collagen gels as delivery systems for the cells (Girolamo et al., 2009). These treatments could not only protect the cells, but be comprised of materials with growth factors which will promote cell differentiation.

Research at the University of New South Wales, Australia has focused on developing a soft contact lens which was seeded on the posterior side with autologous stem cells from limbal biopsies. The cultured cells were found to adhere to the contact lens providing a more secure environment for the cells. The preliminary results appeared positive with patients reporting visual acuity sufficient for obtaining a driving licence and the results were stable after eighteen months. The model may also be used for other cell culture types. There are, however, potential drawbacks with using a 'bandage' which involve the percentage of cells which adhere to the contact vs. the eye and disruption due to the removal (Sidhu, 2011).

1.14.2 Oral Mucosal Cells

One type of tissue which has proven wound healing and regeneration properties is the oral mucosa. The oral mucosa is the mucous membrane epithelial lining of the mouth, gums, and internal surface of the cheeks. Dental surgery has revealed that wounds to the oral mucosa heal more rapidly than ordinary somatic tissue with a limited amount of scarring. The wound healing process of the oral mucosa does not differ in the sequential stages of other tissues discussed earlier in this chapter. The differences with wound healing in the oral mucosa are based in the how the exact mechanism is activated (e.g. the phase, duration, and severity of inflammation and granulation). (Enoch et al., 2007).

It is thought that this biological response may have evolved due to the frequency of cell turn-over due to the dynamic mechanical forces on the mouth due to breathing, drinking, chewing, and the introduction of foreign bodies.

There are three distinct layers to the oral mucosa including:

1) Lining mucosa: which is comprised of stratified squamous epithelium
2) Masticatory: a more robust tissue which is comprised of keratinised stratified squamous epithelium which covers the tongue and upper and lower pallets
3) Specialised: which makes up specialised structures such as the taste buds

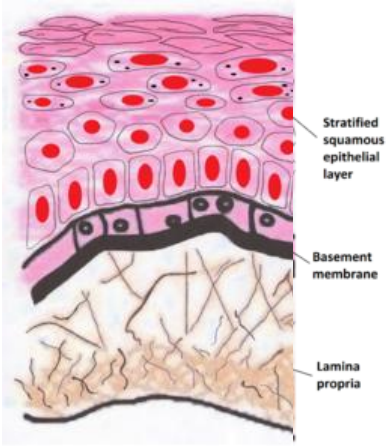

Figure 1.18: Illustration representing the organisation of oral mucosal tissue. Copyright Wiki-minor accessed January 2013

One characteristic which all three of these tissue types share is an increased capacity for wound healing and the decrease in the appearance of scars. The oral mucosa is characterised by:

- Rapid healing
- Quick turn-over necessary so cells have a high hayfick number
- Saliva rich in hyaluronan (which has been known to increase wound healing)
- Cells which have longer teleomeres (which act "younger")
- Have inflammatory response of shorter duration
- Do not have activated myofibroblasts present in the scar
- Retain 'feotal' or 'stem cell' like properties

(Wong et al., 2009; Stephens et al., 1996; Enoch et al., 2010)

Like foetal wounds, the rapid healing of the oral mucosa was originally believed to be due the moisture rich environment and the possible presence of growth factors and cytokines present in the saliva. This theory was challenged, however by animal models where skin from outside the oral cavity was transplanted and presented somatic scarring patterns. This led researchers to investigate the healing at the cellular level.

1.14.3 Oral Mucosa (Epithelium vs. Oral Fibroblasts)

Within the three types of oral mucosal tissue, there is an architecture of various cell types. It has already been established that there are stem-cell/progenitor cells which are located in niches within tissue. There are also phenotypic differences between the tissue of the epithelium and that of fibril producing fibroblasts (e.g. in the cornea the limbal derived epithelium vs. keratocytes). These cells respond to different cell to cell signals and are activated by different biochemical cascades. This would have a direct impact on how the cells interact in any repair situation (Enoch et al., 2010).

1.15.4 Oral Epithelium

The oral epithelium has played a role in ocular repair for several decades. The earliest use of the tissue was believed to be in osteo-odonto-keratoprosthesis surgery (OOKP) (Strampelli et al., 1969). The surgery involves the creation of an artificial lens using either the patient's own/donor canine tooth. The tooth is stored in the cheek cavity to maintain the blood supply whist an oral epithelial sheet is eventually used as a replacement cornea to hold the tooth in place. As the tissue belongs to the patient, there is less of a rejection risk.

Whilst this operation has been successful for a number of patients, OOKP is seen as a bit of a clinical novelty with a number of adverse side-effects. The most striking of these side-effects is the increased vascularising of the wound site. As the oral epithelial layer contains a high number of blood vessels, the graft continues to

develop and promote the blood supply which does not abate. The blood supply also makes the possibility of donor tissue more complicated (Kanayama et al., 2007).

The oral epithelium has also been used to culture cell sheets for corneal repair. Osaka University developed cultures of oral epithelial cells on temperature responsive culture surfaces with feeder cells. After two weeks they developed a confluent cell layer of three to five layers which could be removed as a sheet and transplanted onto the surface of the eye (in the preliminary studies rabbits were used). The repaired corneas retained transparency and four weeks post-operatively the implant's morphology matched that of the cornea (Kanayama et al., 2007).

The experiment was later performed on human patients who had undergone bilateral limbal stem cell deficiencies. The sheets were cultured as noted above and applied with a new suture-less technology. Initial results were positive with the "cornea" retaining transparency without marked vascularisation to the wound site. Unfortunately, there was a slow increased in vascularisation to the border of the wound after sixteen months (however it was noted that the central cornea was not adversely affected).

1.14.5 a-SMA and Oral Mucosal Fibroblasts

In the general wound healing section, the role of a-SMA in the wound healing process was outlined. The expression of a-SMA is an indication of the activation of the fibroblast into the myofibroblast phenotype. The myofibroblasts phenotype is somewhere suspended between a smooth muscle cell and the original fibroblast phenotype . The myofibroblast cells are motile and have contractile properties. Myofibroblast cells are present in cutaneous wounds (granular tissue) and in some scarring disorders of the internal organs. Myofibroblasts are associated with scar formation (Shannon et al., 2005).

Immunostaining for a-SMA along the wound edge have indicated the presence of cells with these contractile filaments from around 72 hours to one week. It is thought that the cells are activated upstream by inflammatory agents such as TGFB-1 and Interleukin-1 and take some time to transform. This has been seen in the cornea

where along LASIK type wounds activated cell have been found along the flap edges where the cells are activated. This is in contrast to oral mucosal cells which have demonstrably lower level expression in oral wounds (Shannon et al., 2005).

It has been noted that the oral mucosal cells are highly motile and swiftly re-populate the wound, however the cells move due to tractional mechanical forces and not through the contraction of a-SMA microfibrils. Whilst the contractile properties are beneficial for swiftly closing a wound, the remainder of differentiated myofibroblasts which remain in the corneal wound may contribute to scar formation. As there is no general consensus whether keratocyte fibroblast cells de-differentiate into the quiescent state, undergo apoptosis, or remain activated with a-SMA properties for the weeks to months following the wound healing process, the myofibroblasts may contribute the factors associated with postoperative corneal haze (Shannon et al., 2005).

1.15 Keratoconus

As we age, the eye undergoes changes which in some people result in a loss of best vision. It is not clearly understood if these changes are genetic or due to environmental factors. The most common of these are the development of myopia (generally at puberty) and presbyopia (generally associated with advanced age). There are also changes which occur to the shape of the cornea which can affect vision know as astigmatism. There is a condition which has been associated with extreme astigmatism known as keratoconus (Colin et al., 2000).

Figure 1.19: Illustration representing fully progressed keratoconus compared to a normal cornea. The smooth topography of the normal cornea is replaced by steepened cone. This has an adverse effect on best vision. Image UIC Department of Ophthalmology 2011

Keratoconus (KC) is a generally non-inflammatory disorder (albeit it presents as an inflammatory disease) characterised by a progressive thinning of the cornea resulting in a change in corneal shape and ectasia. As previously noted, a healthy cornea is curved in a dome whereas, in patients presenting KC, the cornea begins to steepen ultimately resembling a cone (figure 1.18). The disorder does not present any abnormal vascular changes or cellular infiltrations.

The disorder progresses with age and in the later stages there are further complications such as corneal scar formation (from ill fitting lenses, contact lens ulcers, and rubbing from the eyelid). Another advanced development is the onset of small tears in Bowman's layer resulting in ruptures of the blood vessels and the formation of a Fleisher's ring due to the changing biomechanics of the cornea (Bron 1988).

1.16 Difference in Corneal Structure Across Mammalian Species

The corneal morphology outlined in this introductory chapter was that of the human cornea. In this thesis, a number of animal corneas are used, the corneas of which differ on a number of structural and compositional points. It should be noted,

however that many of the processes the mammalian eye undergoes (e.g. embryological developmental stages, wound healing, immune and apoptotic responses, and regeneration ability) are generally evolutionarily conserved and seen across a number of individual species.

1.16.1 Murine

The cornea of the mouse has been extensively researched. Murine tissue is easily obtained and the rapid developmental life span of the mouse is short compared to other species. This allows for traits to be followed across many generations. There is also the advantage of selective breeding and genetic manipulation which allows for the creation and study of 'knock out' gene models and transgenic mutations.

The most obvious difference between the human and mouse cornea is the size. The healthy mouse cornea is approximately 2.5 to 3.5 mm in diameter. The thickness of the murine cornea has been estimated using OCT to be rougly 90.8 um thick (Xiangtianet al., 2007). It is also estimated that in a healthy non-dry eye mouse, almost half (48 um) of the total corneal thickness is epithelium. The Bowman's layer is thought to be about 0.7 um in thickness with the stroma at 20-30 um. The Descemet's and endothelial layer comprise the remaining bulk (Haysashi et al., 2002).

Electron microscopy and X-ray scattering techniques have revealed that the collagen in the central mouse cornea differs from the human cornea. The mouse does not normally have the significant amount of orthogonal preferentially aligned collagen found in the centre of the human eye (Sheppard et al.,2010). Nearer the periphery, however, there are similarities to the human eye including the presence of a collagen annulus (Quantock et al., 2003). Due to these differences in collagen organisation the mouse model is not always ideal as a comparator with the human model.

The proteoglycan (PG) composition, role, and function of the murine eye has been researched in depth. The benefits of using transgenic and other mutation models have allowed PG knockout models to be created with a focus on KS and CS/DS. The GAG and proteoglycan composition of the mouse cornea differs from the human cornea due to the overall size (surface area) and thickness of the cornea.

Despite the differences between the human and the mouse cornea, it has been firmly established that the mouse model serves as an invaluable tool for understanding human corneal conditions. There are a number of genetic and pathological conditions seen in mice which can be directly related to human disorders and diseases. Ramaesh et al. (2003) confirmed that heterozygous Pax 6 deficient mice (Pax6 +/-) present similar phenotypic changes as seen in human disorders such as aniridia-related keratopathy which is caused by a lack of Pax 6 expression. This particular pathology will be discussed in detail in Chapter three.

1.16.2 Ovine

The overall size of the ovine cornea is roughly one and a half to twice the size of the human cornea. The thickness of the cornea is similar to humans with a range of 0.5 - 0.7 mm. Reichard et al., 2010noted in their comparative anatomical study of the corneas from several different species that the sheep demonstrated a very clear and distinct Bowman's layer. They also found the epithelium of the sheep to be similar to that of humans. The main similarity was that the sheep epithelium is also comprised of three distinct layers of cells.

The similarities in size and composition to the human cornea makes the sheep eye a good in vitro cell and tissue culture model for wound healing experiments.

1.16.3 Bovine

The bovine eye is approximately three to four times the circumference of the human eye. The thickness of the cornea has been estimated at between 0.8 -0.9 mm. It is generally thought that the bovine eye lacks a distinct Bowman's layer, however some studies have noted a thin acellular layer of laminar Type IV collagen between the stroma and epithelium . The classification of this layer as a traditional Bowman's is up for debate. The collagen found in stroma of the bovine cornea is roughly 89% Type I with the remainder Type III and Type V. The Type III collagen is located in the anterior cornea closer to the 'Bowman's' (Lee and Davidson, 1984).

Unlike in humans, the eyes of cattle species are characterised by a thicker central cornea which gradually decreases in thickness as it approaches the conjunctiva (Feng et al., 2003). It is for this reason that in transparency studies the sheep cornea is used as it more closely mimics the human corneal morphology.

Kamma-Lorger et al. (2009) mapped the collagen orientation of the uninjured bovine cornea using wide angle X-ray scattering techniques and discovered that the preferred orientation of collagen was orientated in a superior/inferior direction. This collagen morphology was also noted by Hayes et al., 2007. Whilst the orientation of the collagen differs from the human cornea, where structural collagen changes are compared in certain more evolutionarly conserved scenarios (e.g. following wound healing) the bovine model is appropriate for use.

1.17 Research Aims

In this wound healing study, a range of different pathological and acutely injured mammalian corneas (human, sheep, and mouse) were evaluated using a range of quantitative techniques. These techniques encompass small and wide angle X-ray scattering, histological analysis, immunofluroescence, confocal microscopy and second harmonic imaging, spectrophotometry, UV/Riboflavin cross-linking and cell/organ culture model.

The aims of this thesis are:

5) To use X-ray scattering techniques to investigate the role of Pax 6 on the ultrastructure of murine corneas

6) To investigate the use of oral mucosal fibroblasts in corneal wound healing treatment of LASIK injured ovine corneas

7) To use X-ray scattering techniques to investigate the healing response in a 12-year post-operative penetrating keratoplasty for keratoconous

8) To use small-angle X-ray scattering to investigate limbal collagen ultrastructure of keratoconic and normal human tissue

Through research into how the cornea heals, it is hoped that the process of scar formation and remodelling on the ultrastructural level could be better understood and ultimately used to improve corneal biomechanics and transparency with a return to homeostasis. Applied to a patient model, reducing scar formation can lead to an increase in best vision and a reduced reliance on organ donation (Cinton et al., 1978).

The investigation of various species and disorders will lead to a more comprehensive and broad overview of the various maladies which can occur during the wound healing process.

Chapter 2: General Methods

2.1 Introduction

A number of different *in vitro* techniques were used to quantify the transparency and biomechanical properties the corneas analysed. Due to the variety of tissue types studied, there was, in some cases, a very specific methodology for analysis; the more specific methodologies will be addressed in the individual results chapters (Chapters 3-6). In addition to these specific methodologies, there were general methodologies which could be applicable to more than one research chapter. These more general methods will be discussed and the relevant protocols described in this chapter.

2.2 Organ Culture

In vitro organ cultures are important for optimising research protocols before tests on animal and human models. In corneal research, *in vitro* organ culture models have been used to analyse wound healing time and the efficacy of various treatments (Cameron et al., 1974). Although the organ culture model works as in the artificial environment, the cornea is able to function much as it would *in vivo*. The fluid regulating pumps of the endothelium are able to function for over four weeks if the cornea is in a controlled environment (Sperling, 1979). The continued operation of the endothelium supports other functions of the cornea such as epithelial cell proliferation, stromal fibroblast activation, the replenishing of ECM components, and general wound healing (Summerlin et al. 1973).

There are, however, some drawbacks to organ culture; not all of the eye's function (e.g. the hydrodynamics of tear flow or the blink mechanism) can be replicated. The type of organ culture model used also affects the success of the experiment. Models where the tissue was submerged fully in the media caused damage to the epithelium and swelling of the tissue. These models differ greatly from the natural environment of the cornea, as the cornea is exposed to the external environment in a fluid/air interface. It was found that a model with an air/media interface was the best for wound healing (Richards et al., 1991) and future corneal wound healing models evolved based on this premise (Foreman et al., 1996).

Despite these drawbacks, the benefits of the organ culture model makes it a useful tool for understanding wound healing and transparency in enucleated corneas (Foreman et al., 1996).

2.2.1 Organ Culture Protocol

The protocol that was used for this experiment was followed as described by Forman et al., 1996. The ultimate aim was to create a fluid/air interface model for observing corneal wound healing. Ovine eyes were obtained from a local abattoir within hours of death and were transported to the laboratory on ice. The corneas were visually checked for any signs of damage or prior scarring. The eyes with clear corneas were selected for experimentation.

Excess muscle and tendon were removed from the eyes using surgical scissors and the eyes were placed in a clean 500 ml beaker. The eyes were then covered in 25% Betadine iodine solution (diluted in dH_2O) (Meda, Sweden) to disinfect for a maximum period of five minutes (leaving the iodine solution on the eyes for any longer would be toxic to the tissue).

A class II tissue culture cabinet was prepared by spraying with 70% ethanol and wiping with sterile towel. The beaker containing the eyes/Betadine solution was sprayed with 70% ethanol and introduced to the cabinet. The eyes were then transferred to another 500 ml beaker filled with autoclaved PBS (Sigma, UK). The remaining Betadine solution was returned to the container for re-use.

A sterile work surface was prepared within the cabinet by saturating disposable towels in 70% ethanol. Each eye was removed from the PBS and trephine or LASIK-type wounded depending on the experiment. This will be addressed in more detail in the individual project chapters. Unwounded samples acted as controls in the trephine wounds and untreated flaps were used as controls in the LASIK-type wounding experiments. The eyes were removed from PBS and surgically injured with either a 5mm trephine (Swann Morton, Sheffield, UK) or a microkeratome (Hansatome Bausch and Lomb, Germany). Both instruments were used to create a wound in the centre of the cornea. Care was taken to wound the cornea to mid-stromal depth and not fully penetrate the entire structure. The 5mm disc was removed using a sterile

scalper blade and forceps. Both wounded and control corneas were excised from the eyes using surgical scissors. Care was also taken to include approximately 4-5 mm of the adjacent sclera.

2.2.2 Creating the Gel Support

A preparation of gelatine/agar support solution (see appendix II) was melted in a microwave on medium power for two minutes until liquid. The plastic lids of six specimen vials were soaked in 70% ethanol and inverted in the hood to evaporate the excess alcohol. These lids would act as a support for the enucleated corneas. Once the alcohol had evaporated, the extracted corneas were placed in each lid epithelium side down.

Using a sterile pipette, the cooled support solution was dropped into each cornea until level with the limbal ring. The solution was then left to set to room temperature. Once the gel support was set, each of the lids was inverted into a sterile Petri dish. 12 ml of Trowles™ (Invitrogen, UK) media mix (see appendix II) was added to each dish so that the limbal ring was covered by the media.

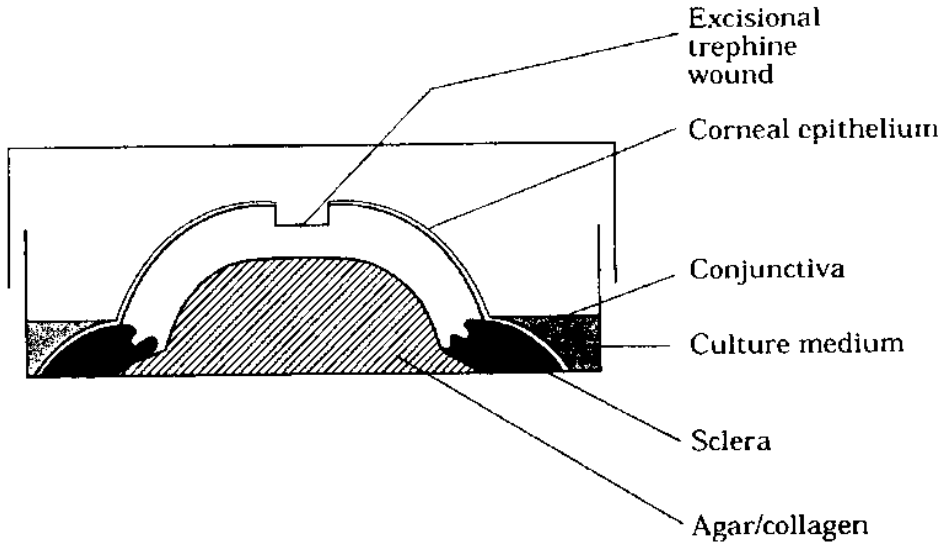

Figure 2.1 : Organ Culture Model of Sheep Cornea demonstrating the air/fluid interface. (Foreman et al. 1996)

The dishes were then transferred to a culture cabinet to incubate at the required culture time points (note Chapter 4). Several drops of media mix were added to each

eye twice daily to keep the eyes moist and prevent bacterial/fungal infection. The culture medium was replaced with fresh media on the fifth and tenth day of culture.

2.3 X-Ray Scattering

When X-rays are passed through a crystalline structure a scatter pattern is produced with areas of both high and low intensity. The pattern produced is based upon Bragg's scattering principles. Bragg's law is the fundamental law of crystallography (X-ray diffraction). Crystal lattices can be inorganic structures such as minerals or organic structures such as tissues and proteins. Each material has a unique structural composition. When X-rays are passed through a crystal lattice, a reflective interference pattern is produced with different peaks of intensity (Figure 2.2 B). These intensity patterns can be captured by a detector (e.g. camera) and provide information regarding the composition of the material.

The Bragg Equation is:

$$n\lambda = 2d \sin\theta$$

n is an integer referred to as the *order* of diffraction.

d is the distance between the crystal lattice planes

λ is the wavelength of X-ray beam incident to the crystal planes

θ is the Bragg angle

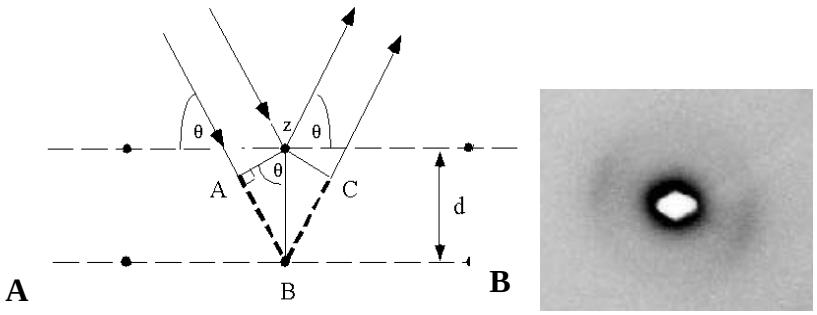

Figure 2.2. Braggs law. **A** The difference in path length (ABC) between the incident and reflected waves is equal to an integral number of wavelengths (nλ). From geometry, ABC=2dsinθ. (www.serc.carleton.edu accessed 2011) **B** X-ray scatter pattern from mouse cornea.

There are two main points to note concerning Braggs scattering

1) The angle of incidence of the wave = the angle of reflection = 2 × scattering angle
2) The difference in path length is equal to an integer number of wavelengths

(Phillips, 1946).

From Bragg's law we can see that there is an inverse relationship between the spacing d and the scattering angle 2θ, larger spacings scatter at smaller angles and vice versa. X-rays can be scattered at either a high (wide) or low (small) angle. In the cornea, equatorial diffraction (i.e. diffraction perpendicular to the collagen fibril axis) arises from the regular packing of the collagen fibrils (small angle) or the molecules within them (wide angle). Wide-angle X-ray scatter provides information regarding the molecular arrangement of corneal collagen, its distribution, and orientation. It can also be used to measure the total amount of scatter (based on the thickness/hydration of the sample), which can give information about the amount of collagen in the path of the X-ray beam. Small-angle X-ray scatter (typically 0.1 - 10°) provides information on the spacing and diameter of the individual collagen fibrils. The wide angle pattern consist primarily of a single reflection at about 1.6nm arising from the packing of collagen molecules within fibrils. The small angle pattern comprises an interference function (Bragg reflections) arising from the relative positions of the collagen fibrils, multiplied by a fibril transform (representing the scatter expected from an isolated fibril). Fibrils are approximated to cylinders, so the fibril transform takes the form of a Bessel function.

2.3.1 Generating X-ray Beams

A synchrotron (Figure 2.3) is an apparatus which accelerates electrons to near the speed of light The electrons are passed into storage rings containing magnets which force them into a circular path. The electrons are deflected by these magnets and emit high intensity radiation at all wavelengths, including X-rays.

Figure 2.3: Arial photograph of Diamond Light Source Synchrotron, Didcot UK. (http://www.diamond.ac.uk/)

This light is more intense than conventional X-rays which were previously used in X-ray scatter studies. The power generated combined with the small wavelength of the radiation allows X-ray scatter patterns from the cornea to be collected with very short exposure times (seconds), thereby minimising specimen damage. The non-destructive nature of the synchrotron is also beneficial as the specimen does not require pre-processing which occurs with other ultrastructural analysis techniques such as electron microscopy.

2.3.2 Synchrotron Stations

Radiating from the main storage ring, are a series of individual beam lines or 'stations' (Figure 2.4). Two specific stations at the Diamond synchrotron are specialised for small or wide angle X-ray scatter. There are general hardware requirements including a mechanised stage on which to situate the sample, a camera/detector, and a lead beam stop which is situated between the sample and the detector. The stop prevents damage to the detector from the full intensity of the beam.

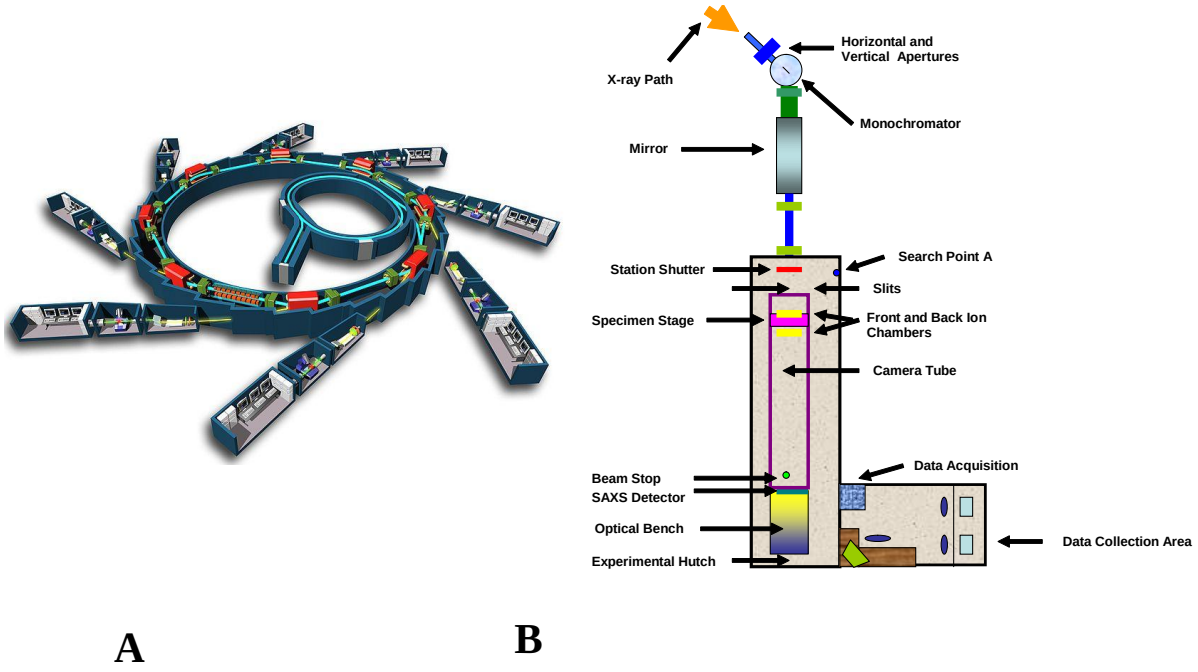

Figure 2.4: Representations of individual stations and how they are orientated along the synchrotron. A) Copyright © Chaix & Morel et associés B) Adapted from Meek and Quantock, 2001

2.4 Small Angle X-ray Scattering

For the small angle X-ray scattering analysis, two different synchrotron stations (one at the Diamond synchrotron, Oxford, UK and the other at the ESRF synchrotron, Grenoble, France) were used. The cornea and scleral rim of the left eye of a keratoconic individual who had undergone penetrating keratoplasty for the condition 12 years previously will be discussed in depth in Chapters 5 and 6 was analysed at station I22 at Diamond. The microfocus beam in station ID13 at the ESRF was used to evaluate the pair matched keratoconic cornea (right eye) of the PK sample at a finer resolution. Both beam-lines operate under similar conditions and any experimental differences will be addressed in the experimental chapters.

2.4.1 I22 Set-up

The high intensity X-ray beam at I22 had dimensions of 0.2 x 0.2 mm. The detector camera was a high overall throughput (HOT) SAXS detector which produced digital images of the scatter pattern. The detector camera distance was set to 5m to collect the

small angle x-ray scatter signal. Between the sample stage and the detector was a lead beam-stop centrally positioned on a piece of mylar to eliminate X-ray damage whilst on the detector.

2.4.2 Treatment of Samples

The corneas were all enucleated for the experiments and frozen at -80°C. Care was taken to retain a sclera rim around the cornea to maintain the structure and for orientation purposes. There was a range of tissue storage techniques used for each sample which will be addressed in the individual chapters. The mounting of the tissue in the chamber was the same for all samples. This was done using a piece of cling film large enough to cover the cornea. The film was weighed on a digital balance to obtain a weight which would later be subtracted from the final weight. The cornea was then wrapped in the cling film to prevent dehydration of the sample, and both the cornea and cling film were then weighed to determine the hydrated weight of the cornea.

The sample was placed in a custom made air tight Perspex and mylar chamber (figure 2.5) used to hold the specimen in place on the beam line.

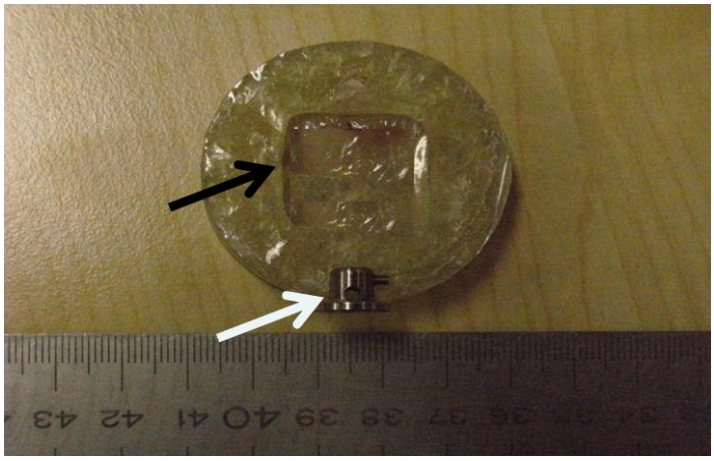

Figure 2.5: Air-tight Perspex and mylar specimen chamber. Black arrow indicates window where the specimen is placed. The white arrow indicates magnet used to attach the holder to the stage.

2.4.4 Situation on the Beam

The sample was orientated so that the beam would first pass through the anterior surface of the cornea. Using the microscope/viewer, the mechanised stage was positioned so that the cornea was centralised in the view. An approximate exposure time was programmed (based on previous experience) and a sample image was collected. This was to ensure that the signal was strong enough for future analysis and processing. It was also necessary to determine that the apparatus was properly aligned and there were no unnecessary vibrations or complications. It was determined that an exposure time of 10 seconds was appropriate for the sample.

Once the exposure time was determined, an area large enough to cover the sample was mapped out (Figure 2.6). Images were taken at 0.5 mm or 0.25 mm steps (depending on the sample) and the corneas were scanned. Each step correlates to an X-ray scatter image produced.

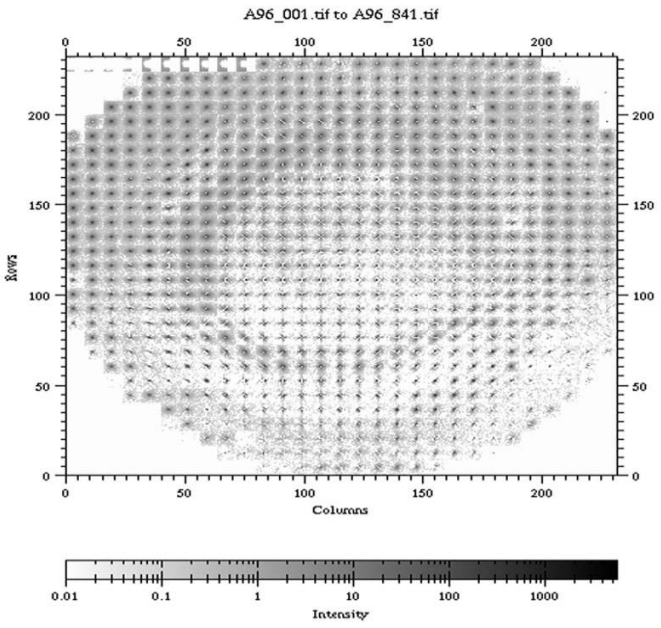

Figure 2.6: Example of image collage of individual x-ray files produced by individual files in a 29 x 29 file grid.

When the scan was completed, the sample was removed from the cell, weighed in the clingfilm (Dow Corning, UK) on the same balance to ensure consistency of results, and placed in fresh Optisol^{TM} solution (Chiron Ophthalmics, Irvine, California). The cornea was again transported at 4^0 C and on the following day, transferred in 4% paraformaldehde (PFA). This was to prepare the sample for future wide angle scatter.

2.4.5 Calibration of the Beam Line

In this experiment, intact type I rat tail tendon collagen was used to calibrate the beam line. Hydrated rat tail tendon has a known D periodicity (67nm) which can be used to normalise the data collected. A meridonal peak is produced by the rat tail collagen (Figure 2.7); this peak moves position based upon the specimen/detector distance so is different in each experiment.

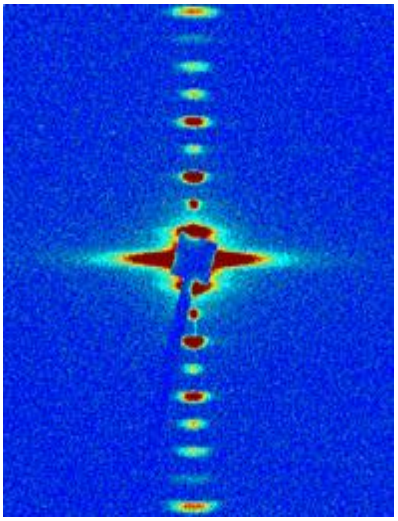

Figure 2.7: Image of SAXS scattering of rat tail tendon. Siam Photon Laboratory, 2012

2.4.5 Data Analysis

BSL file formats save the individual images as a series of frames within one large file. Using Fit2D analysis programme (ESRF, Grenoble, France) the files were opened and individual frames were accessed. Using a macro, the individual frames were converted into .tif file format. These files were then montaged in Fit2D to create a 29 row x 29 column series. The image produced (e.g. Figure 2.6) was a representation of the raw data which the detector collected.

2.4.6 Transformation of the Data

Using this map to choose a sample file, a .tif file of high intensity (near the centre of the cornea) was opened in Fit2D image viewer. The image that was produced in Fit2D was 512 pixels across. The data signal presented a diffuse signal along the vertical. A sample transect was taken from this file to ensure that the signal was properly represented.

The rat tail tendon file was then converted to a .tif file in Fit2D as above. Using a ruler tool, two points on either side of the vertical data signal were marked out to create an area where a vertical transect could be extrapolated. These co-ordinates were entered into a macro which removes these transects for each file and saves the data as a .chi file. This stage of the image process both reduces the size of the file and isolates the necessary data signal. Once the parameters for the rat tail tendon were determined, the macro was used to remove the transect from all of the files. These files were transformed into .chi files.

2.4.6 Folding the Data

To improve the signal-to-noise ratio, the data from both sides of the symmetrical diffraction pattern was folded over upon itself and averaged. The rat tail tendon file was opened using Microsoft Excel and the intensity of the signal was plotted against the position of the file. Two clear peaks were produced. The positions along the x axis of the first peaks on either side of the y axis were measured. These positions were

added together and then the sum was divided by two. This figure represented the central point of the two data sets indicating where the data should be folded.

To test this folding point, the data was manually divided at the half way point in Microsoft Excel and re-plotted. The two peaks matched and were overlaid upon each other. Once the folding point was established, a macro (include macro at end) was used to fold the .chi files and convert them into .XLS files. The macro also re-allocated the data so that the position (R) was in column 1 and the total intensity of the folded data (I) was in column 3.

2.4.7 Statistica

Using Statistica (StatSoft, UK), a macro was run which converted the .XLS files into .sta worksheets and allowed for the superfluous background scatter to be removed. The background was estimated by converting the data signal into a logarithmic graph (figure 2.8A). With the data in a Log format, a linear horizontal transect could be placed beneath the data to remove the background signal (figure 2.8B). Six points were chosen along the base of the data in order to fit the transect. Care was taken not to cut off any of the data signal. Once the background had been determined, each file intensity value was multiplied by the radial position within the pattern to account for the fact that the pattern was being sampled rather than truly integrated, and the background was subtracted (Figure 2.9).

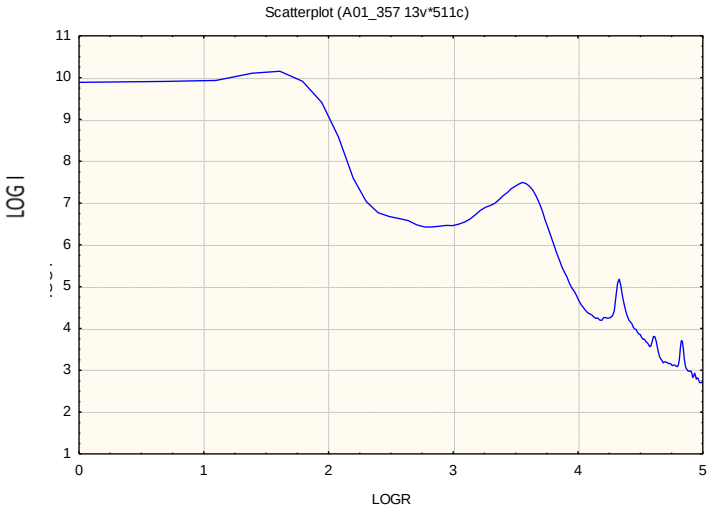

A

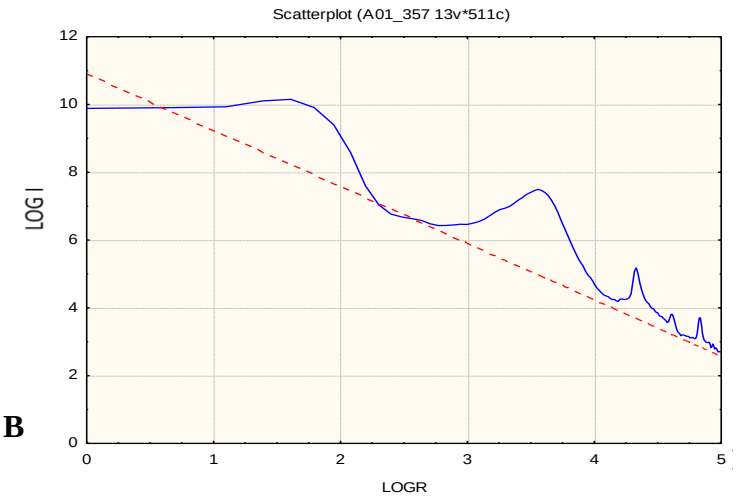

B

Figure 2.8 : (A) Log of the intensity (I) vs the Log of the Position (R). Presenting the data in a Log fashion allows a linear background to be removed from the signal (B). Six points are chosen beneath the data signal, a transect is fitted (red dotted line) and the signal (blue line) is isolated.

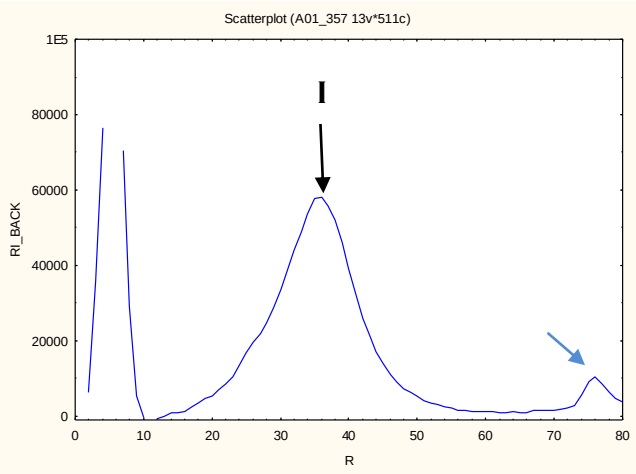

Figure 2.9: Background-subtracted integrated intensity (RI_Back) vs Position (R). The interference (I) peak is indicated by a black arrow. Blue arrow indicates the diameter transform.

2.4.8 Determining the Collagen Peaks

There are two peaks that arise from the spacing of the collagen fibrils and the diameter of the fibrils (respectively). Once the locations of the two peaks were identified, the data was opened in a scatter plot where RI-Back (the integrated intensity minus the background) was plotted against R (position) and analysis of the interference function was carried out (figure 2.9). The position, width at half-height, and the highest point of the interference peak were measured in Statistica using the point tool. The results were then entered in an Excel spread sheet at the corresponding file number. This data was recorded in pixels.

The fibril transform was then measured (again in pixels). A Bessel function was fitted to the second peak. The height of the Bessel function peak was determined together with the central point. This procedure was carried out for each file and the data were entered into a Microsoft Excel spread sheet.

2.4.9 Degree of Disorder: Width at Half the Height

The shape of an X-ray scattering peak is influenced by the degree of disorder of the structures that give rise to the peak, the broader the peak, the higher degree of

disorder. So whilst the overall position of the peak may appear normal, the width of the peak may be affected, indicating that the size or spacing being measured is, on average, unchanged, but the order is affected. The width of the peak at half of the peak's height is thus a useful relative measure of the degree of disorder. In the present investigation, the width at half height of the interference function peak was recorded as described above, and used to investigate changes in the amount of disorder in the spacing of collagen fibrils (Figure 2.10).

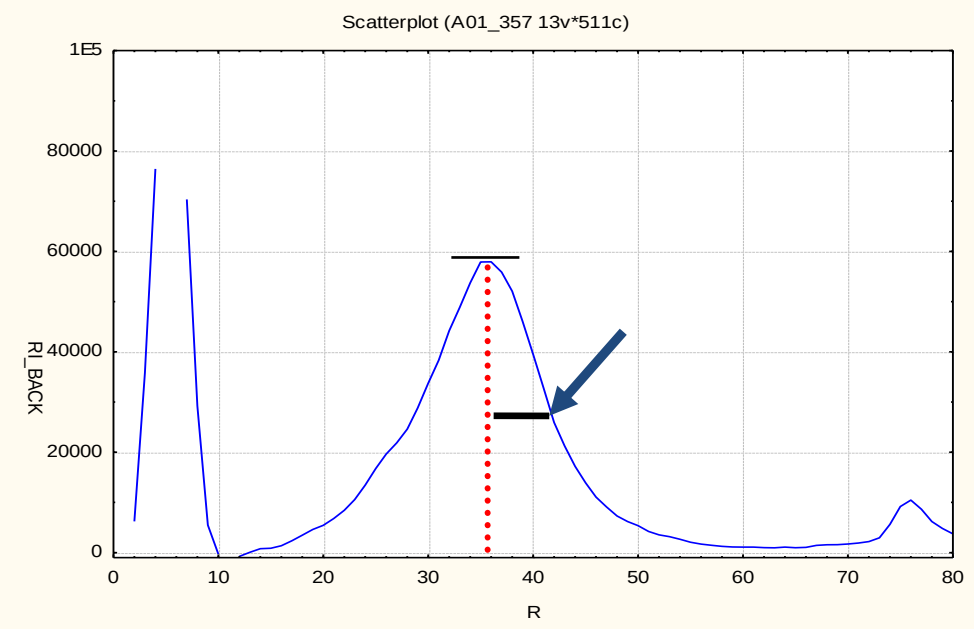

Figure 2.10: RI_Back vs R to maximise the signal. From this, the degree of disorder of the spacing can be determined based on the position in pixels at half of the height. This can provide information for the height of the peak vs the width. The less steep the peak the more disordered the spacings.

2.4.10 Conversion of Pixels into Nanometres

The distances between collagen fibrils (and their diameters), are measured in nanometres. The data which is analysed in the above stages was carried out in pixels. The pixel measurements therefore had to be converted into nanometers. This was done using two mathematical equations (for the spacing and diameter).

2.4.11 Calculation of Fibril Diameter and Spacing in Nanometeres

The position of the 1st subsidiary maximum of the X-ray pattern (i.e. the fibril transform Bessel function) is related to the fibril diameter d (2r):

$$\mathbf{2r = 5.14/\pi Q}$$

(Vainshtein and Urmakher, 1966)

where

d = 2r = the fibril diameter (r = radius)

Q = reciprocal space position of the first subsidiary maximum (nm^{-1})

Q is calculated using the calibrant (in this case rat tail tendon) as follows:

$$\mathbf{Q = \frac{1^{st}\ subsidiary\ maximum\ position\ (Bessel\ position\ in\ pixels)}{1^{st}\ order\ meridional\ peak\ position\ of\ the\ calibrant\ (pixels)\ x\ D\text{-}spacing\ of\ calb.\ (nm)}}$$

A similar equation was used to convert the position of the interference peak (in pixels).

$$\mathbf{Q = \frac{Position\ of\ interference\ peak,\ I\ (in\ pixels)}{1^{st}\ order\ meridional\ peak\ position\ of\ the\ calibrant\ (pixels)\ x\ D\text{-}spacing\ of\ calb.\ (nm)}}$$

Q was converted into nanometres by taking the reciprocal.

2.4.14 Conversion of Bragg's spacing to Actual Spacing

Another conversion performed was to convert the Bragg spacings (as indicated above) into actual spacing. The Bragg spacing assumes an ordered crystal structure; the short range order of the cornea is more representative of a liquid/crystal where the fibrils demonstrate a degree of order but are not a strict crystal. As discussed previously, when calculating scatter in an ordered crystal, the Bragg equation can be used. Worthington and Inouye (1985) proposed that the Bragg spacings should be multiplied by a factor of 1.12 to demonstrate the increased distance between fibrils in

a liquid crystal. The final Bragg spacing of the interference function would therefore be multiplied by 1.12 to determine the actual nearest neighbour spacing.

2.4.15 Creation of Plots and Maps

Using Microsoft Excel, scatter plots were created of cross sections of the cornea. These were created for the entire cornea from superior to inferior. MS Excel surface maps were also created using a grid to demonstrate the entire area of the sample.

2.5 Wide Angle X-ray Scatter Techniques

Wide angle x-ray scattering was used to determine the arrangement and orientation of the collagen in the stroma. In these experiments, the x-ray beam was passed along a direction parallel to the visual axis (Figure 2.11) so the resulting patterns were generated by the total collagen in the path of the x-ray beam. For the wide angle experiments, the samples were analysed at Diamond Light Source station I02 (Didcot, UK) and station 13 at the ESRF in Grenoble, France.

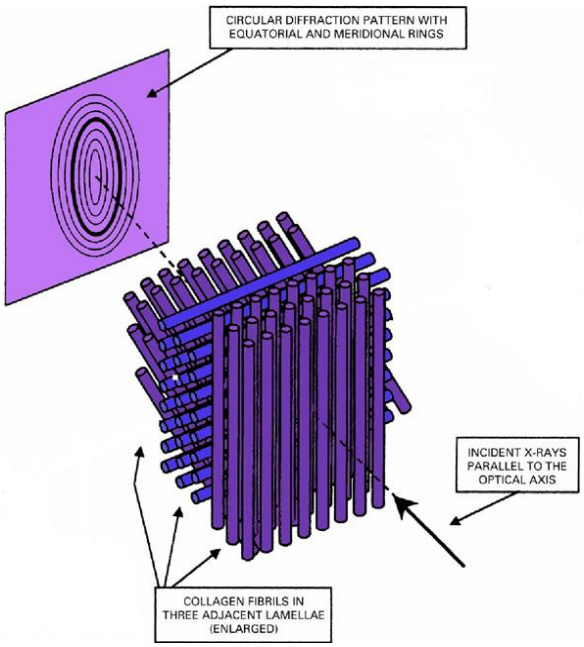

Figure 2.11: X-rays pass through corneal collagen lamellae orientated in different directions . If there is an equal number of fibrils parallel to the optical axis, the resulting in an X-ray pattern will be a series of concentric circles (after Meek and Quantock, 2000).

The intensity of the scatter pattern produced during XRD is proportional to the amount of collagen present in the part of the sample through which the beam travels, provided the water content within each collagen fibril remains constant. In this experiment it was assumed that a higher intensity reading relates to a greater amount of collagen (Daxer and Fratzl, 1997; Newton and Meek, 1998).

2.5.1 Preparation of the Sample

Following the small angle scatter, the samples were stored in 4% PFA at 4^0C. The storage in PFA has been known to improve the quality of the scatter pattern through preservation of the corneal shape and it is thought intermolecular spacings (unpublished data). The sample was removed from the PFA and wrapped in clingfilm (Dow Corning, UK).

The sample and the clingfilm were weighed on a digital balance and the sample was placed in the air-tight Perspex and mylar chamber so that the anterior of the cornea was facing down. The chamber was placed on the mechanised stage, and the sample was centrally positioned. A test image was taken to determine the optimum exposure time. Once the exposure time was set, the chamber and stage were positioned for x and y co-ordinates for scanning at 0.25mm frame intervals.

2.5.2 Analysis

A grid was created in Microsoft Excel based on the file series. This was used to manage the files and map out the x-ray scan area. The image files (.img) were first transformed into .tiff files using image processing programme Fit2D (ESRF, Grenoble, France.) and a macro which isolates the scatter pattern. A montage of the .tif images was not possible as there were 4500+ files. The .tif files were transferred on a hard drive to Optimas^{TM} (Mayer Instruments, Houston) to extrapolate the intensity data.

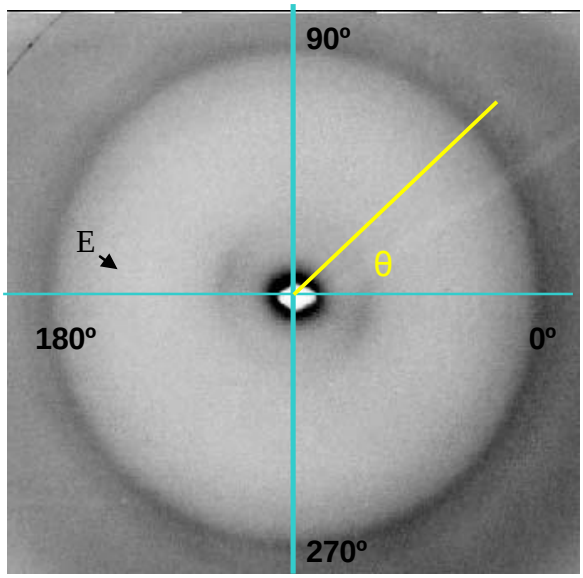

Figure 2.12: Representation of the annular integration method performed using Optimas. A radial integration is performed at each angle θ between 0 and 360 degrees. The radial background is subtracted and the area under the equatorial peak E is integrated. This intensity, I, is then plotted as a function of θ (Figure 2.12)

The wide angle patterns were used to quantify the angular distribution of the lamellae within the cornea. In terms of the analysis, this meant analysing the distribution of scatter intensity as a function of angle around the reflection (the pattern was calibrated using powdered calcite). This was done as follows:

The wide angle x-ray scatter data was analysed using a radial integration method as outlined by Daxer and Fratzl (1997) and Meek and Boote (2009). Using Optimas™ image analysis software, the scatter intensity was measured along a radius from the centre of the pattern (figure 2.12), the radial background was subtracted and the area under the equatorial peak was integrated to produce a value for the x-ray scatter (I) from collagen for that particular angle. This was repeated for angles between zero and 360 degrees so that a plot of scatter intensity against angle could be produced (figure 2.13 B)

2.5.3 Removal of the Isotropic Scatter

The total scatter pattern produced includes both the preferentially aligned and isotropic scatter. A macro was used to isolate the preferentially aligned collagen. The points which were chosen for either side of the intensity file were entered into the

macro. The macro removed the isotropic scatter, but also normalised the data (by dividing the data by the multiplication product of the beam frequency by the exposure time) and extrapolated the total collagen, aligned collagen, and percentage aligned collagen data signals.

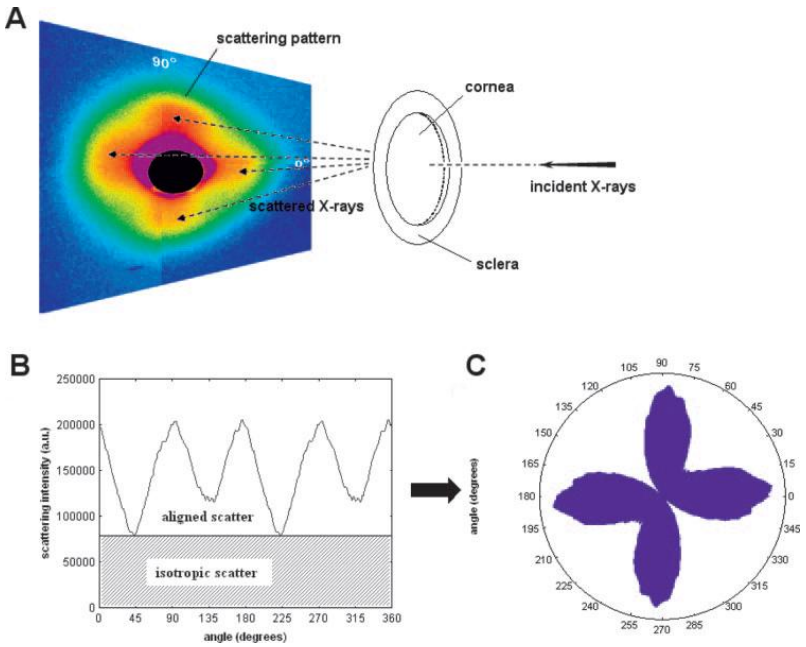

Figure 2.13: Analysis method for Wide-angle x-ray scattering. **A**) an x-ray pattern is created through passing an incident x-ray beam through the cornea. **B**) Preferentially aligned collagen is isolated from the general isotropic scatter. **C**) The aligned collagen is converted to an angle of distribution and represented in polar plots. (Boote et al., 2006)

2.5.4 Creation of Orientation Plots

The normalised intensity patterns were then entered as a spreadsheet in Statistica. The data was transformed so that the columns across were representative of individual files and the rows down were representative of 256 rotational degree points. A macro was used to convert the data signal into a rotational data plot (or polar plot) indicating both the intensity of the signal (colourmetrically) and the alignment of the collagen based on the position of the plot. The intensity levels programmed into the macro were based upon the data range minimum and maxima as set intervals (figure 2.21 C).

2.5.5 Mapping of the Polar Plots

The individual polar plots produced in Statistica were then collaged in a Microsoft Excel spreadsheet to create a map of the entire area. This map was based upon the grid created from the original data. A screen shot of the Excel map was captured and then copied into Adobe Photoshop. Images were saved as JPEG files and assembled in Microsoft Publisher.

2.5.6 Creating Surface Maps

Surface maps of the total collagen, aligned collagen, and percentage aligned collagen were created using Microsoft Excel. These maps were again based on the file grid created earlier in the analysis process.

2.5.7 Cross Sections of Data

Cross sections of data were plotted using line graphs in Microsoft Excel

2. 6 Oral Mucosal Preliminary Data: Optimisation of Protocol

Before the experiment for evaluation of oral mucosal fibroblasts as a novel treatment for LASIK flaps (Chapter 4), a short series of preliminary experiments were performed to test the efficacy of both utilising oral mucosal cells in an organ culture model and optimising the research technique.

2.6.1 Cell Passage and Organ Culture

The cells used in the preliminary experiment were obtained from Cardiff School of Dentistry and were from the established cell line of patient # 4. All human cells were treated under the governing rules of the Human Tissue Authority. The cells were passaged and treated as outlined later on in the main experiment chapter Chapter 4. The cells were applied to LASIK-type and trephine wounded sheep corneas which were prepared as outlined later in Chapter 4. The trephine wounds were created with

a 5mm trephine (Swann Morton, Sheffield, UK) in the centre of the cornea. Care was taken to wound the cornea to approximately mid stromal depth and not fully penetrate the entire structure. The 5mm disc was removed using a sterile scalper blade and forceps to emulate a corneal ablation.

The organ culture model used was from Forman et al., 1996 as outlined earlier in this general methods chapter. The corneas were cultured at one and two week time-points. The preliminary experimental model differed from the final methodology in the use of the dextran solution. In the original experiment, the corneas appeared to be swollen following the organ culture however was untreated. In the final experiment, these difficulties were overcome by using a dextran solution.

2.6.2 Immunohistochemistry

Together with others, the author published results relating to flap strength following various treatments including corneal cross linking and corneal keratocyte application in LASIK flaps (Mi et al., 2011). A part of the experimental aims was to determine the number of a-sma activated fibroblast present in each of the flap beds and along the wound margins; the results are addressed in detail in Chapter 4. For the published paper, we optimised a protocol for evaluating the presence of a-sma in LASIK-type flaps. The final results are published in Mi et al 2010 (attached in Annex VI) and the protocol was later used to evaluate the presence of a-sma in cells in Chapter 4.

2.6.3 Preparation of Corneas for Histology

Corneas (cultured and control) were rinsed in PBS (Sigma, UK). The corneas were then cut along the median using a fresh razor blade. Care was taken to place the cornea epithelium side down to prevent damage to the endothelium.
The two halves of cornea were placed in wells which were fashioned out of aluminium foil. The tissue was orientated in a vertical position so that the incision was at the base of the well. The wells were then filled with OCT compound (Sigma, UK) and transferred to the -80°C freezer to set until solid. Once frozen, the samples were removed from the foil casing and transferred to the cryostat for sectioning.

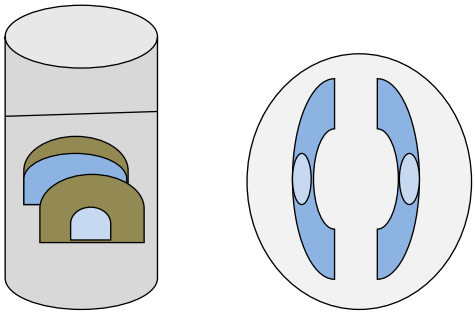

Figure 2.14: Above Image is a schematic of the orientation of the corneas in OCT. Right Image is orientation of corneas in the block for cryostat sectioning.

The tissue was initially trimmed using 30 µm section/steps. Once the wound bed in the sample was visible, 10 µm sections were obtained from cross sections of the cornea that extended from limbus to limbus. The sections were transferred to Histabond™ adhesive slides and labelled. The slides were then left to air dry at room temperature for 24 hours.

The slides were transferred to a chamber and immersed in the cooled acetone for 10 minutes at 4^{o}C to remove the OCT and fix the samples. Following the wash, the slides were immersed in haematoxylin for three minutes, rinsed in cool running water until the water ran clear, and then stained in eosin for 1minute. The slides were then washed again to remove excess stain. The slides were blotted dry using a paper towel with care taken not to disturb the tissue sample. The samples were then covered in one drop of Hydromount (National Diagnostics, UK) mounting media and covered with coverslips. The slides were left in a fume hood to dry overnight. The slides were imaged using a Leica (Leica, Germany) microscope and a 550/w colour processer camera. The images were processed using Leica Q Win version 3. Images were taken at 10x and 20x magnification.

2.6.4 Immunohistochemistry Protocol a-sma Optimisation

In order to determine the optimal antibody staining protocol, there were several attempts undertaken. For these tests, we used a zero hour wounded cornea culture (as a control) and a two week wounded cultured cornea as test samples. It has been

established in the literature that at the zero time point, the expression of α-sma would be isolated to cells located in the limbal area, but would not be detected at the incision site or throughout the tissue as fibroblast cells would not be activated at this timepoint (Mi et al., 2011). At the two week time point, the wound healing process would have activated fibroblasts along the incision edge. In these samples α-sma signal would be detected both at the wound site and along the limbus.

Through identifying the presence of a signal in the limbus, the true presence of α-sma in the fibroblasts as indicators of post-wound healing transformation could be confirmed. The activated cells were then counted and statistical analysis (in the form of cell counts) was undertaken.

2.6.5 Initial Slide Preparation

All of the slides were prepared in the same manner before the antibody staining. This is outlined below:

Full thickness cultured bovine cornea samples were preserved in OCT (Sigma, UK) and frozen at -80°C. The samples were sectioned in 10µm sections using a Cryostat (Leica, Germany) and the individual sections were mounted on Histabond™ adhesive slides. The slides were left on the bench overnight to dry at room temperature.
The following day, the slides were submerged in cooled acetone and left at 4°C for 10 minutes. The slides were then removed from acetone and dried on the bench for 20 minutes. Once the acetone evaporated, the slides were washed in PBS for ten minutes to remove the residue of the dissolved OCT. A wax pap marking pen (Sigma, UK) was used to draw around the samples to create a hydrophobic barrier to contain the anti-body treatment.

2.6.6 Protocol One

A preparation of goat serum (Sigma, UK) in PBS (Sigma, UK) (1:4 concentration) was pipetted onto each sample and left for 20 minutes. 3 µl of Sigma α-sma mouse monoclonal antibody was added to a 600 µl solution of PBS in 0.2% BSA (.01 g BSA

to 5ml PBS) each specimen was treated with 100µl of the antibody. The slides were covered and left to incubate overnight at 4°C.

The following day, the slides were washed in PBS (3x wash at 5 minutes per wash). The secondary antibody (Alexa Fluro, Invitrogen, UK) was prepared by adding 1µl of antibody per mil of PBS (1:1000 concentration). To this, 3µl of prepared Hoechst solution (1 mg per mil concentration) was added to the antibody preparation. Each specimen was treated with 100 µl of the solution.

The slides were covered in foil and left to incubate at room temperature for 1.5 hours. After this time, the slides were washed with PBS (3x wash at 5 minutes per wash). The slides were then mounted using Hydromout and glass coverslips. The mounted slides were covered in foil and stored at 4°C. Slides were imaged using a Leica 6000 fluorescent microscope. 3 sections were mounted on each slide and 10 slides were imaged for an n=3 at each time-point. Counts were taken at 40 x magnification feilds.

2.6.6 (a) Method Refinement Results: Protocol One

Both the background signal and a-sma signal were too high. Both the targeted cells and surrounding tissue appeared to be indiscriminately stained. A further block of the cell signal was required. The protocol was altered to further block the specimens by adding additional BSA to the secondary antibody. It was believed that this would increase more targeted staining.

2.6.7 Protocol Two

The goat serum blocking time and primary antibody protocol remained the same. The secondary antibody protocol was changed (as noted above). The secondary antibody and Hoechst were added to PBS/.2% BSA solution instead of plain PBS. The incubation time of the secondary antibody was increased to 2 hours at room temperature.

2.6.7(a) Method Refinement Results: Protocol Two

The signal from the cells was too weak. It was difficult to fully detect the cells. The blocking of the signal had to be increased from the first protocol, yet decreased from the second. It was decided that in the next protocol the PBS/.2% BSA solution in the secondary antibody would be removed and the original PBS would be used. To compensate the goat serum time would be increased.

2.6.8 Protocol Three

As it remained necessary to increase the blocking time, the goat serum block was changed to 30 minutes. The PBS/.2% BSA was only used with the primary antibody. The secondary antibody incubation time remained at 2 hours at room temperature.

2.6.8 (a) Method Refinement Results: Protocol Three

The results from the third protocol were nearly ideal. There was a good contrast between the background noise and the cells themselves. Cells were clearly detected along the limbus and beneath the wound edge (of the two week samples). At the time of this experiment, a further test was undertaken to ensure that the signal was at an optimal level, the procedure was completed one more time using a 40 minute goat serum block.

2.6.9 Protocol Four

The forty minute goat serum block with a 2 hour secondary antibody incubation period produced the best results in terms of cell signal and contrast. It was decided that this would be the optimal protocol for the detection of a-sma.

2.6.9 (a) Final Preparation (Protocol Four)

A preparation of goat serum in PBS (1:4 concentrations) was pipetted onto each sample and left for 40 minutes.

3 µl of Sigma a-sma mouse monoclonal antibody was added to a 600 µl solution of PBS in 0.2% BSA (.01 g BSA to 5ml PBS) each specimen was treated with 100µl of the antibody. The slides were covered and left to incubate overnight at 4°C.
The following day, the slides were washed in PBS (3x wash at 5 minutes per wash). The secondary antibody (Alexa Fluro) was prepared by adding 1µl per mil of PBS (1:1000 concentration). To this the Hoestch solution (1 mg per ml concentration) was added. Each specimen was treated with 100 µl of the solution. The slides were covered in foil and left to incubate at room temperature for two hours.

After this time, the slides were washed with PBS (Sigma, UK) (3x wash at 5 minutes per wash). The slides were then mounted using Hydromout® (National Diagnostics) and glass cover-slips. The slides were covered in foil to prevent the signal diminishing in the light and stored at 4°C. The cells were imaged using a Leica 6000 fluorescent microscope (Leica, Germany).

2.6.10 Cell Counting Technique

The slides were imaged at 40x magnification. A Perspex overlay cut to the size of the computer screen. A grid of 1 inch x 1 inch square was drawn on the Perspex sheet using a permanent marker pen. The overlay was then placed over the screen and attached with cellophane tape. The total number of cells was counted for the entire field of view. This was based upon the blue Hoecht signal stain of the nucleus. Next, the cells which demonstrated the green fluorescent signal of the α-sma were then counted. For each slide, five fields of view were imaged along the wound margin and the results were averaged each sample type/time point was represented by three individual slides.

2.6.10 (a) Statically Analysis of Cells

The percentage of activated cells was calculated using the average cell counts:

Total a-sma signal/Total number of cells

The percentages of activated cells were then compared for each sample at individual time points. Student's t test and F test were performed in Excel comparing samples.

2.6.11 OCT vs Wax Imbedding

A common difficulty with immunohistochemistry is the excessive staining of the background. Ideally, the antibodies should target specific structures, but in some instances a high level of ambient background staining occurs. The histological preparation method plays a role in the amount of antibody which is bound to the structure and the amount of background staining. It is thought that OCT causes an increase in background stain when used with the a-sma antibody. In the final experiment, histological analysis was performed with wax imbedding techniques to produce the best results.

For the oral mucosal experiment (Chapter 4) it was decided that the corneas would be wax imbedded. The protocol for this will be discussed in the individual chapter.

The Use of X-Ray Scattering to Determine Collagen Organisation in Pax Mutant Microphthalmic Mouse Corneas

3.1 Introduction:

Microphthalmia and anophthalmia are conditions where the eyes and orbits are underdeveloped or entirely absent. These disorders are present in a number of species, however, the eyes are not always affected bilaterally. Individuals with the disorder present a varying range of symptoms including reduced eye size and in some cases microcornea. These disorders are distressing for the patient as they affect both the appearance and the functionally of the eyes. Research into these disorders may lead to a better understanding of the conditions with the aim of improving the quality of life of those afflicted (Gallin, 2002).

3.1.2 Embryogenesis of the Mouse Eye

In order to understand the developmental changes which occur in the diseased models, it is necessary to understand normal pre and post-natal mouse ocular development. The gestation period of the mouse is approximately 19-21 days. The ocular development of the mouse is thought to start from about E9 and continue into the postnatal period. The development is thought to occur in seven distinct stages:

1) Contact is made between the optic vesicle and surface ectoderm and there is initial development of the retinal disc.
2) The optic vesicle invaginates and the lens pit begins to develop
3) RPE and inner retinal layer form. There is also further lens development
4) Lens and neural retina develop
5) Cornea, optic nerve and lids appear with a defined anterior chamber
6) Eyelids join together and the optic cup begins to close
7) Final layers of the neural retina develop along with iris folds and ciliary bodies

(as indicated by Pei and Rhodin, 2005)

After birth, the anterior eye continues to develop through full maturity (at around one month or 28 days). The collagen organisation and orientation of the cornea continues to change during this period. At birth the eyes remain closed up until day 10 -12, during which time the corneas continue to develop namely through the reorganisation of collagen through development of the collagen circum-corneal annulus. The corneas are originally flattened, but by 10 – 12 days after eye opening the early signs of a collagen annulus begins to develop. This ultimately changes the curvature of the cornea. There is also thought to be a change in corneal thickness which is caused not by the volume of collagen changing but the redistribution of the collagen (Sheppard et al., 2010).

3.1.3 Anophthalmia / Microphthalmia

As touched on in the general introduction, anophthalmia is a congenital disorder which involves the lack of development of the eye's orbit or ocular tissue. In some cases, small traces of ocular tissue are present when imaged with MRI. These remains of tissue and ocular organs are not functional. The disorder is rare and is thought to affect 1 in 10,000 births. There have been less conservative estimates which put the rate 10 x higher, but these may be based on the presence of non-functional tissue (British Anophthalmia., 2011). The condition is often (but not always) bilateral. It is thought that the condition is caused by an under-differentiation of neural crest tissue during embryogenesis (Kirby, 1984).

Microphthalmia is closely related to anophthalmia and is also a developmental disorder of the ocular tissue. In some clinical situations, the conditions are used inter-changeably however there are distinct differences between the two disorders. In microphthalmia the ocular tissue (and in most cases the orbits) is entirely present however is reduced in size (British Anophthalmia**,** 2011). One possible cause for this reduction in size could be due to the general foetal development of the organ or as a result of a fissure where the sclera meets the cornea. In these cases, there is a decrease in IOP which reduces the biomechanical forces on the eye during development. This results in the development of a smaller orbit (Hero et al., 1991).

In the mouse, the fusion of the ocular chamber is completed between E11-E13. It is during this time period that symptoms of microphthalmia occur (Hero et al., 1991).

The more common manifestation of the disorder presents as a thicker retina with a reduced ocular chamber. As the eye develops, the retina takes up space from the ocular chamber causing the entire globe to shrink. This puts additional biomechanical pressures on the anterior cornea resulting in a micro-cornea with a flattened appearance. The degree of incidence for microphthalmia is similar to that of anophthalmia (where it is sometimes used interchangeably as Small Eye Syndrome). The disorder is often but not always bilateral (Dora et al., 2006).

3.1.4 Complex Small Eye Syndrome

There are cases where, in addition to the general size of the eye, there are other complications that can occur. These can occur either independently or bilaterally and in any combination. The more common conditions are:

1) Absence of irises or ciliary bodies
2) Clouding of the cornea
3) Clouding of the lenses
4) Optic cysts
5) Absence of optic nerves
6) Reduction of the retina
7) Reduction of the size ocular chamber
8) Various other coloboma

(as indicated by Davis et al., 2003)

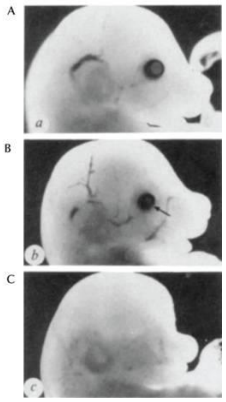

Figure 3.1: Ocular development in A) normal B) Pax 6 +/- (Sey) and C) Pax 6 -/- embryological mice. B demonstrates the small eye phenotype whilst the homozyogous Pax null embryo failed to develop eyes and nasal features. Halder et al 1995

3.1.5 Genetic Influences on Ocular Development

The exact causes for anophthalmia and microphthalmia are not known at present. It is believed that the disorders are due to under-expression of genes which are key in embryological cranial development. Gene families such as Pax and Sox are currently being studied to determine their roles in the disorders. These genes are evolutionarily conserved and are activated early on in development (Ashery-Padan and Gruss, 2001). The genes programme everything from the bilateral arms to cranial facial features. The cells which make up the ocular tissue are differentiated from the neural crest cells programmed into activation by these regulatory gene groups. In this way the Pax and Sox genes operate both autonomously and non-autonomously on tissues and systems (Friedman, 1998).

In addition to Pax and Sox, Microphthalmic-Associated Transcription Factor (MITF) has also been associated with the disorder (however this is a gene is activated upstream) (Plangue et al., 2001). When the gene fails to activate, the sclera and choroid of the optical cup fails to join and a fissure is created. This fissure allows the humour to seep out of the ocular chamber reducing the overall pressure. Without the biomechanical force from within the cornea, the overall size of the orbit is decreased. This is thought to result in a different disorder from the Pax and Sox derived Small Eye Syndromes (Muller, 1951).

3.1.6 Sox 2

The Sox 2 gene is thought to act as a gate in neural development which allows the neural crest cells to remain un-differentiated. This means that through the developmental cycle the cells are able to remain pluripotent. Sox 2 deficiencies are known to affect the brain, general motor skills, underdevelopment of the upper portion of the alimentary and respiratory canals, and ocular development. In Sox 2-dependent microphthalmia, the genetic defect is autosomal dominant and in heterozygous individuals the symptoms of small eye and columba are known to occur (Fantes et al., 2003).

3.1.7 Pax 6

Pax 6 is a very evolutionarily conserved gene which is instrumental in cranial/ocular development in most species. Like Sox 2, Pax 6 is instrumental in the development of the cranium, ocular structures, and the upper limbs. In embryological development, the normal activation of the Pax gene codes for symmetrical bilateral development of these structures. Also like the Sox 2 gene, it is thought that Pax 6 is instrumental in differentiation and migration of oral progenitor cells in the cranium (Hever et al., 2006).

Individuals who are Pax 6 null (Pax 6 -/-) fail to develop brain structures, and are still born. Heterzygous individuals (Pax 6 +/-) are missing one copy of the Pax 6 gene. The individuals with the heterozygous phenotype are born viable, however present a number of congenital abnormalities. The abnormalities are not always bilateral and can occur individually or alongside each other. The disorders associated with a decrease in Pax 6 include:

1) Absent iris
2) Anophthalmia/Microphthalmia
3) Neurological difficulties
4) Absent ciliary bodies
5) Clouded lens
6) Congenial cataracts

7) Craniofacial defects
8) Later onset corneal dystrophy

(as indicated by Hanson et al.,1993; Friedman, 1998)

Small eye (*sey*) mice which have been bred with the heterozygous Pax 6 knock-out (sey) have been instrumental in understanding the affect that the gene has on ocular development (Ramaesh, et al., 2003). In the *sey* mouse, there are a number of morphological changes which mirror Pax 6 deficiencies in humans. In the Pax 6 (sey) mice, the orbits form, however the iris and ciliary bodies fail to form and fuse with the lens. There also tends to be an underdevelopment of the nasal pit. As in humans, these changes are not always present or bilateral. It should be noted that the sey mutation is not thought to be related to other anophthalmic disorders associated with coloboma which is differently coded (Hogan et al., 2008). There is also a decrease in wound healing in Pax 6 reduced eyes (Dora et al., 2006).

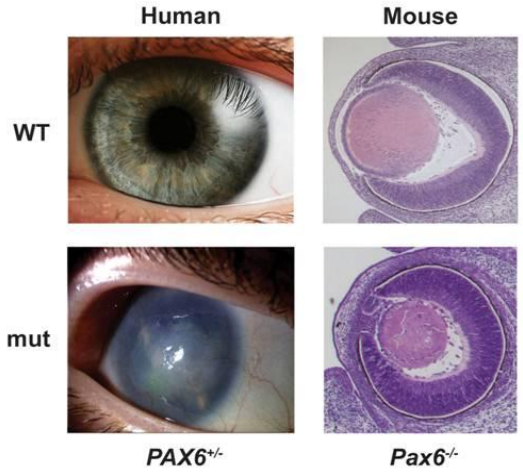

Figure 3.2: Pax 6 phenotypes for normal and heterozygous phenotypes across species. In the human the condition sometimes presents with the condition anirida and a lack of corneal transparency. In the mouse a common occurrence is a reduced anterior chamber, thickening of the retina and aberrations to both the corneal and retinal epithelium. Copyright University of South Wales

3.1.8 Increased Levels of Pax 6

In addition to the changes which can occur with a decreased expression of Pax 6, there are morphological changes which can occur with an increased expression. To better understand this, PAX77+ mice have been engineered using five to fourteen

additional copies of the human Pax gene. As the Pax 6 gene is evolutionarily conserved, copies of the gene from one species can be inserted into others to form a trans-gene model (Schedl et al., 1996; Manuel et al., 2008).

The PAX77+ mice have been found to present a number of conditions similar to a decrease in Pax 6. There is an incidence of microphthalmia, reduction in ocular chamber and a decrease in wound healing. There are also conditions which are unique to the over-expression of Pax including microcornea (a reduction in the size and steepness of the cornea), cystic irises which are often fused to the lens. There is also a high degree of congenital cataract and anterior segment disorders which can occur (Manuel et al., 2008).

Dora et al. 2006 extensively studied both the sey Pax 6 heterozygous mouse and PAX77+ model. They compiled a chart comparing the phenotypic traits which the group found to be representative of the two population groups they studied. It should be noted that some of the traits the group found differ from other studies and human clinical data (noted with *).

Condition	**Pax 6 +/- (Heterozygous)**	**PAX77+**
Microphthalmia	Yes	Yes
Reduction of Cell Layers in the Corneal Epithelium	Yes	Yes
Reduced Epithelial Thickness	Yes	No
Reduced Stromal Thickness	Yes (in some cases)	No
Absent Irises	Yes	No
Cataract *	No	Yes
Thickened Irises	No	Yes
Absence of Ciliary Bodies *	Yes	No
Decreased K12 Expression	Yes	Yes
Corneal Opacity	Yes	No
Decreased Wound Healing	Yes	Yes
Wound Healing Improved by EGF	Yes	No
Microcornea	No	Yes

Table 3.1: Differences between Pax 6 +/- and Pax77+ eyes adapted from Dora et al 2006.

3.1.9 PAX77+ Microcornea

As noted earlier, where Pax 6 +/- can present an opaque cornea, the microcornea produced during PAX77+ development is a thin transparent cornea with an abnormal radius of curvature. It is thought that one cause for the disorder may be an excessive growth of the optic cup (Garner and Klintworth, 2008) and is associated with the differentiation of the neural crest cells (which as previously noted are Pax dependent) (Funderburgh et al., 2005).

3.1.10 Pax 6 and Corneal Thickness

The overall epithelium thickness in the Pax 6 +/- cornea is reduced when compared to normal tissue. The overall thickness of the PAX77+ epithelium has been found to be normal in appearance despite a reduction in the epithelial layers present. The presence of the goblet cells in the Pax 6+/- individuals may be related to the decreased levels in Pax 6 and the neural crest development (this is also related to the absence of the iris). The PAX77+ eyes are not affected in this way as there was an absence of goblet cells **(**Ramaesh et al., 2009**,** Dora et al., 2006).

Ramaesh et al., 2009 studied the stromal morphology in Pax 6+/- and found that the stroma appeared to be thickened, irregular, and hyper-cellular in the embryological development. In the adult there was found to be a less smooth appearance to the corneal surface and the epithelium was compromised. There were also remnants of lens tissue in the epithelium. The overall thickness was increased in the central cornea and the lamellar arrangement was highly disordered when compared to native tissue. Some of the corneas were vascularised or had infiltrates of other tissue (e.g. lens tissue as mentioned above) (Dora et al., 2006).

In the PAX77+ stroma, there was found to be no clear difference in the thickness of the tissue between the trans-gene and wild-type (Dora et al., 2009). This, however, differs from other studies (e.g. chick) where the corneas were seen to be thicker and flatter than normal corneas (Manuel et al., 2008).

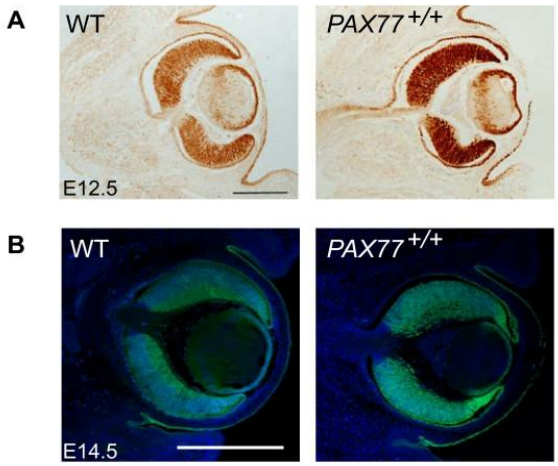

Figure 3.3: Examples of Pax77+ and wild type eyes at E 12.5 and E14.5 Image A darkened area Pax 6 expression Image B green fluorescence Pax 6 (Manuel et al. 2007)

3.1.11 Pax 6 and Corneal Keratocytes

Funderburgh et al. (2005) found that some corneal keratocytes contain trace amounts of Pax 6. It is thought that, as the cells differentiate from neural crest cells, the gene continues to be expressed in some adult tissue in small quantities. The presence of Pax 6 in ocular structures had been previously established with traces present in the retina (to a higher degree) and corneal epithelium (to a lesser degree). Pax 6, however, is generally down regulated in other ocular tissues. It was also discovered that cultured keratocytes lack the markers for Pax 6 which are evident in stromal keratocytes *in situ* (Funderburgh et al., 2005). This may be due to environmental factors (i.e. interaction with the ECM) or due to the Pax 6 being lost with each sub sequential passage.

It was also noted that Pax 6 was expressed in higher levels in the developed corneas of the PAX77+ eyes (Dora et al., 2006) due to the base level over-expression. This may have an impact on the collagen production in those geneotypes. The changes which have been found to occur in both mouse and chick PAX77+ corneas do not happen initially in development like Pax 6 +/- mutations. They have been noted from around E12-E14 so happen later in embryological development (Manuel et al., 2008). This, however, means that the continued expression of Pax may adversely affect

tissues later in the life of the animal (for example causing retinal degeneration) (Manuel et al., 2008).

When the fibroblasts are activated in wound healing (both *in vivo* and *in vitro*) the adult keratocytes fail to produce the normal transparent ECM components instead the collagen and components produced is of a different phenotype (Funderburgh et al., 2005). The scar is then remodelled with collagenases and matrix metalloproteinases (MMPs) 2 and 9 which are normally secreted by the epithelium, but dependent on the depth and location of the wound the tissue may never return to physiological state. It has been discovered that Pax 6 +/- corneas have a down regulation in MMP 9 which would directly impact on the wound healing process (Ramesh et al., 2006), this may be due to the adverse changes found in the knock-out epithelium (Ramesh et al., 2006).

Previous studies indicated that Pax 6 +/- keratocytes undergo a high level of apoptosis during wound healing. This would be a possible explanation for a lack of collagen which is necessary for wound closure (Wilson et al., 1996). It has also been hypothesised that the high level of cell death may activate neighbouring cells sending chemical signals and turning them into scar producing myofibroblasts (Ramesh et al., 2006).

There is also the possibility that there is a decrease in the initial number of stromal progenitor cells in the Pax 6 +/- (Ramesh et al., 2006). These data possibly conflict with other studies which found that there was an abnormal amount of initial keratocyte proliferation in the Pax 6 +/- stroma. Even though there is a high level of apoptosis, it is relative to the total amount of the cells present (Ramesh et al., 2006).

3.1.12 PAX and Corneal Biomechanics

During embryological morphogenesis, the expression of Pax 6 gradually decreases with development. At birth, the highest amount of Pax 6 expression is found in the retina and gradually decreases through the more anterior ocular structures until there is just a trace amount in the cornea (evident in the keratocytes). With an increase in

Pax 6 expression, the retina thickens and the ocular chamber decreases in size. This is thought to be one of the main outcomes of microcornea (Sohajda et al., 2006).

When the eyes open (approximately D 10-12 in mice after birth), there is thought to be a stimulus of the cornea driving it towards maturity (Norman et al, 2004). There is thought to be a high level of cell proliferation in all three cell layers immediately before eye opening which is abruptly arrested afterwards. It is thought that a number of genes are activated which activate the expression of proteins associated with the production and maintenance of the tear film (Zieske et al., 2004). It has been suggested that the act of eye opening also drives the re-organisation of the collagen into forming the collagen annulus which is vital for maintain corneal biomechanics (Sheppard et al., 2010).

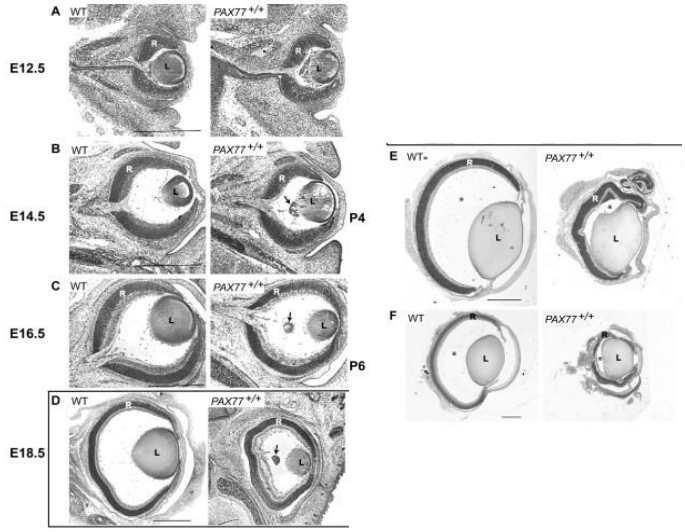

Figure 3.4: Examples of Pax77+ and wild type eyes through developmental stages. Note how the eyes are similar until E14 when the Pax77+ eye begins to degenerate (Manuel et al. 2007)

3.2 Investigative Aims

The mechanisms behind microphthalmia in Pax mutations are not currently understood. Although both types of mutation result in similar phenotypic changes, the genetic mechanisms between the two are different and it is not know whether the same pathways are involved or activated.

It was previously thought that a reason for the development of microcornea may be due to underperforming keratocytes/fibroblasts which do not produce adequate amounts of stromal collagen. Prior studies of the CBA77+ mutants did not uncover any difference in the thickness between mutant and normal corneal stromas. It was also thought that any possible differences in thickness may be isolated to the periphery of the cornea in the radial and tangential plane, but this was not confirmed with TEM analysis (Dora et al, 2008).

The orientation of stromal collagen within the plane of the cornea has been established to be a key factor in maintaining corneal structure and biomechanical strength. This collagen orientation differs between animal species and between native and pathological individuals. In this study, therefore, I have used x-ray scattering to examine the differences that occur in Pax 6 +/- and Pax77+ murine mutants. Following the TEM analysis, it was thought that the X-ray scattering techniques could be used to determine the amount, distribution, and orientation of the stromal collagen within the mutant samples and shed further light on the biological processes occurring with a Pax mutation.

3.3 Methods

3.3.1 Wildtype Controls

Eyes of eight wild type albino mice were obtained from Cardiff University School of Biosciences (CBA strain). The mice were humanely destroyed using gas according to the Association of Research in Vision Sciences (ARVO) regulations for the use of animals in research. The eyes were removed intact using a pair of forceps, divided into two groups depending on the preservation method (i.e. frozen or fixed in 4% paraformaldehyde-PFA. The superior/anterior were marked using a suture and left and right eyes from the same individuals were labelled.

The corneas were dissected out under a microscope using a scalpel and micro-scissors. The removed corneas were then wrapped in fresh cling-film (Dow Corning, UK) and transferred to a -80^{o}C chest freezer for rapid freezing. The eyes in PFA were

transferred to a 4^{o}C refrigerator for 24 hours. They were then dissected out as above. The corneas were transferred into eppendorf tubes filled with fresh PFA and returned to refrigeration.

It should be noted that difficulties were experienced extracting the corneas without causing damage due to pulling or stretching. In the end it was decided to remove the corneas through a coronal incision and then removing the iris in a separate step. It should also be noted that the eyes stored in PFA resulted in a more exact cut that gave better results in the X-ray experiment.

3.3.2 Pax Mutant Eyes

PAX77+ (bred on a CBA wildtype strain) and Pax 6+/- (referred to in the literature as Pax 6 *Sey*) mice were supplied by the University of Edinburgh Genes and Development Group. The corneas were dissected out as above and preserved in individual epindorffs filled with 4% PFA solution. The superior/anterior was marked using a suture and left and right eyes from the same individuals were labelled.

The corneas obtained were from both male and female small eye and "wildtype" (i.e. genetic background of a mutation but not expressing the phenotype). As indicated in the table below, the mice were culled on average at around seven months in age. Eyes were rejected on the following grounds:

- Loss of suture
- Distorted, torn, folded or damaged corneas
- Fused iridies which could not be removed from the cornea with forceps (this would interfere with the collagen signal). NB not all Pax mutants demonstrated the fused iridies phenotype.

3.3.3 Eyes Chosen for the Wide Angle X-ray Scatter Analysis

Below is a table of the eyes which were chosen for experimentation.

Pax77+	**Sex**	**Phenotype**	**Age in Weeks**
552L	male	small eye	24 weeks
552R	male	small eye	24 weeks
566L	male	small eye	18 weeks
567L	male	large eye	18 weeks
551R	male	small eye	24 weeks
Pax 6+/-			
785L	female	large eye	20 weeks
783L	female	large eye	20 weeks
786L	female	small eye	20 weeks
781L	female	small eye	20 weeks
789R	male	small eye	18 weeks
784L	female	small eye	20 weeks
784R	female	small eye	20 weeks

Table 3.2: List of Pax 6+/- and Pax77+ corneas scanned in the first part of the experiment. All of the mice were at full maturity.

3.3.4 X-Ray Scattering

The eyes were evaluated for wide angle X-ray scatter analysis at station ID13 at the European Synchrotron Radiation Facility (ESRF) in Grenoble France. The samples were wrapped in clingfilm to prevent dehydration and slippage within the cells during data collection. The samples in clingfilm were placed in a purpose built Perspex and mylar chamber and was orientated on the beam using a translational stage.The beam intensity was 199 mA and the exposure time was 3 seconds. The samples were analysed in two separate sessions. The first samples analysed were the Cardiff University wild type CBA corneas. Both the frozen and PFA preserved samples were analysed for comparison and optimisation of the technique.

During a second visit to the synchrotron, the genetically modified samples were analysed.

It was necessary to repeat some of the wide angle analysis, as only one PAX77+ wildtype cornea was suitable for the scanning in the first experiment. In the second experiment, the following eyes were scanned.

Pax77+	Sex	Phenotype	Age in Weeks
605L	male	large eye	31 weeks
606L	male	large eye	31 weeks
613L	male	small eye	24 weeks
614L	male	small eye	24 weeks

Table 3.3: List of Pax77+ corneas scanned in the second part of the experiment. All of the mice were at full maturity, as with the first group, but were on average culled at an older time-point.

3.3.5 Analysing the Data

The methodology for wide angle x-ray scatter analysis was outlined in the general methods chapter (Chapter 2). The data collected at the ESRF was initially analysed using Fit2D (ESRF, Grenoble, France) programming software in a UNIX environment. The image files were then analysed using Optimas™ v6.1 (Media Cybernetics) and MS Excel in Windows XP environment to isolate the background information and noise from the desired collagen signal. A macro was run using the data from the Optimas™ files to determine the total, aligned, and percentage aligned (beta) collagen amounts. This data was transferred to Excel to create surface maps demonstrating the signal in increasing intensities.

Once the background signal was removed the files were then transferred to Statistica™ to create polar plots based on the intensity and orientation of the collagen signal. The polar plots were then imaged using Microsoft Excel to create collagen orientation maps (Meek and Boote, 2009).

3.4 Results

3.4.1 Optimising the technique

The frozen Cardiff University wildtype samples which were initially analysed appeared swollen and the x-ray scatter obtained was very weak. The corneas also appeared to be distorted and damaged. This could be a result of the dissection process.

The PFA embedded samples were easier to dissect and in their analysis demonstrated a good radial scatter pattern with a limited degree of corneal distortion. It was decided that all future analysis would be performed on the PFA preserved eyes. However, the two subsequent studies were performed as an initial study (Study 1) and follow up study (Study 2)

3.4.2 Study 1: Pax 6 +/- and Pax77+ Small Eye Phenotype

a. Overall differences

There appeared to be no difference between male and female eyes studied. There were slight differences between left and right eyes, however the phenotypic changes which occur are not always bilateral *in vivo* so this should be expected.
The difference in the size between the mutant eyes and CBA wildtype eyes was small but significant.

b. Collagen amount

There was a statistically significant and proportional decrease in the amount of total scattering found in Pax77+ (Figure 3.5 B) and Pax 6 +/- (Figure 3.5C) corneal stroma when compared to the native CBA wildtype eyes (Figure 3.5 A). The amount of

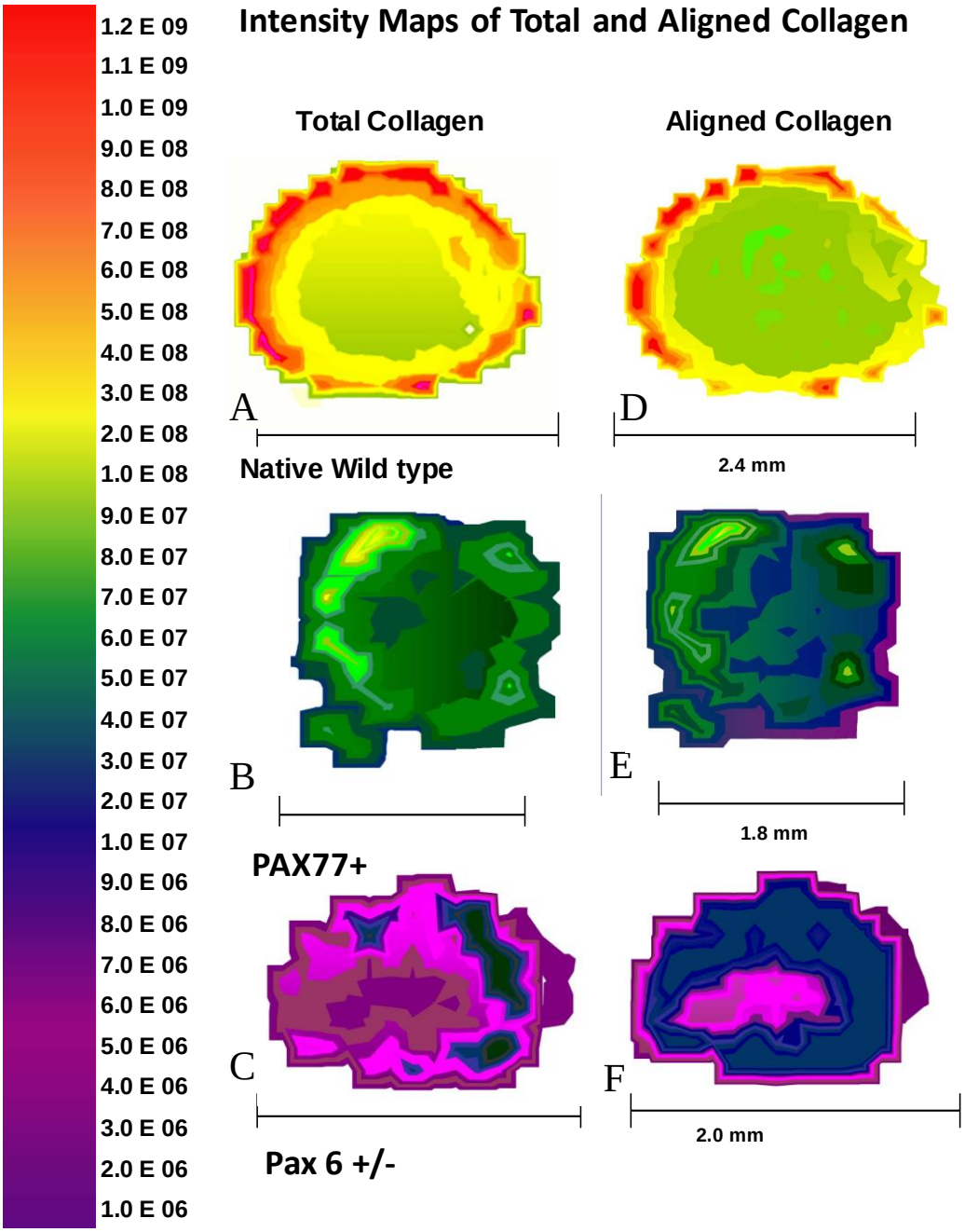

Figure 3.5: Intensity maps of total and aligned collagen for wildtype (A and D), PAX77+ (B and E) and Pax 6+/- (C and F). The total collagen scatter in the wildtype cornea (A) was nearly 10 x greater than in the PAX77+ (B) and 100 x greater than in the Pax 6+/- sample. The wildtype aligned collagen map (D) demonstrated an annulus of highly aligned collagen where the PAX77+ (E) did not demonstrate an annulus. The Pax 6+/- eye did demonstrate a higher degree of aligned collagen circumferentially however the region appeared thickened and abnormal. Scale bar is measured in Arbitrary Units (AU)

scatter appeared to decrease approximately 10 fold in the Pax77+ and 100 fold in the Pax 6 +/-. This trend was representative of all of the samples analysed.

The preferentially aligned collagen in the CBA wildtype mouse (Figures 3.5 D) demonstrated no distinct differences in the distribution when compared to total collagen. The periphery of the cornea demonstrated a broken ring of highly aligned collagen which was not evident in the central cornea, but was similar to the total collagen results. The preferentially aligned collagen of the Pax77+ (Figure 3.5 E) and Pax 6 +/- (Figure 3.5 F) small eye corneas showed considerably less aligned scatter centrally, probably due to central corneal thinning. This differs from the distribution of aligned collagen in the human cornea which demonstrates a central region of lower alignment in a diamond shape supported by highly aligned bands of collagen (Boote et al., 2006).

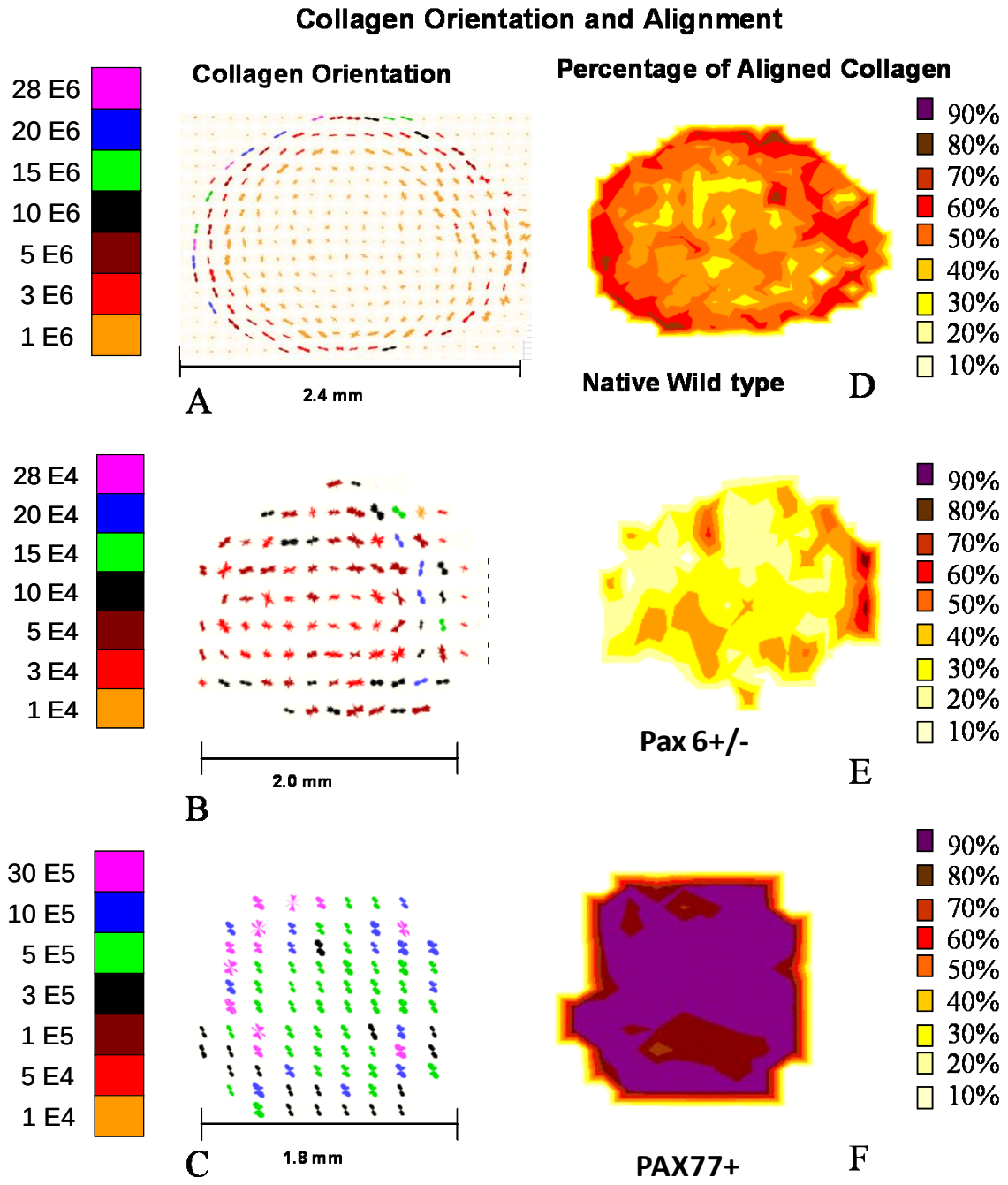

Figure 3.6: Collagen orientation and percentage collagen alignment for wildtype (A and D), small eye Pax 6+/- (B and E) and small eye Pax77+ (C and F). The CBA wildtype mouse (A) demonstrates a clear collagen annulus whereas the Pax 6+/- (B) demonstrates a more incomplete annulus. The Pax77+ (C) demonstrates a partial annulus with highly aligned collagen in the oblique direction. The percentage alignment of the wildtype cornea (D) demonstrates evenly distributed collagen around 40 to 60%. The Pax 6+/- cornea (E) demonstrated a lower degree of collagen alignment (20-40%) with the Pax77+ (F) demonstrating a very high degree of alignment (70-90%). Colours in left hand plots represent scale down factors used increasing from orange to pink in arbitrary units (AU).

c. Collagen organisation

In the normal mouse cornea, collagen lamellae are arranged in a "circular" fashion except at the centre of the cornea (Figure 3. 6 A). On average, about 60% of the lamellae contribute to this regular pattern (Figure 3.6 D), the rest being randomly orientated. The organisation of collagen in the Pax 6+/- mutant is randomised throughout the cornea, with, on average, only about 30% showing any preferred orientation (Figure 3.6 B) but with no discernable pattern except near one edge (Figure 3. 6 E). This lack of a distinct pattern was seen in all the Pax 6 +/- mutant corneas analysed.

The Pax77+ corneas had about 90% of the lamellae preferentially aligned in a uni-lateral oblique direction (Figure 3.6 C). There was no evidence of the circular annulus arrangement found at the corneal periphery of every other animal species (Figure 3.6 F). This uni-directional oblique trend was observed consistently in all of the Pax 77+ samples analysed at this age-point. This suggests that there is a mechanical aligning force on the cornea during growth and development.

3.4.3 Study 1: Pax 6 +/- and Pax77+ Large Eye Phenotype

In addition to the Pax 6 +/- and Pax 77+ small eye mutants, a single Pax77+ large eye specimen and several Pax 6 +/- large eye specimens of the same mutations were analysed. In many respects these resembled the CBA wildtype corneas, although some did have congenital cataracts. The Edinburgh group classified these large eye phenotypes as Pax 6+/- or 'Pax 77+ "wildtype" to indicate that the Pax small eye mutation (Pax 6+/-) and the Pax 77+ transgene have been bread into the CBA genetic strain even though they are not showing the microphthalmic phenotype. In this thesis they will be referred to as Pax 6+/- large eye and the Pax77+ large eye respectively.

The overall sizes of all the mutant large eye samples were greater than the microphthalmic corneas; however in the Pax77+ mice the difference was nominal. The most noticeable size difference was observed between the Pax 6+/- small eye mouse (Figure 3.7B) and the Pax 6+/- large eye mouse (Figure 3.7 A) where the eye is several hundred microns larger. However, this result may not be statistically

significant due to individual variation or an artefact from the dissection process; therefore further samples would need to be analysed.

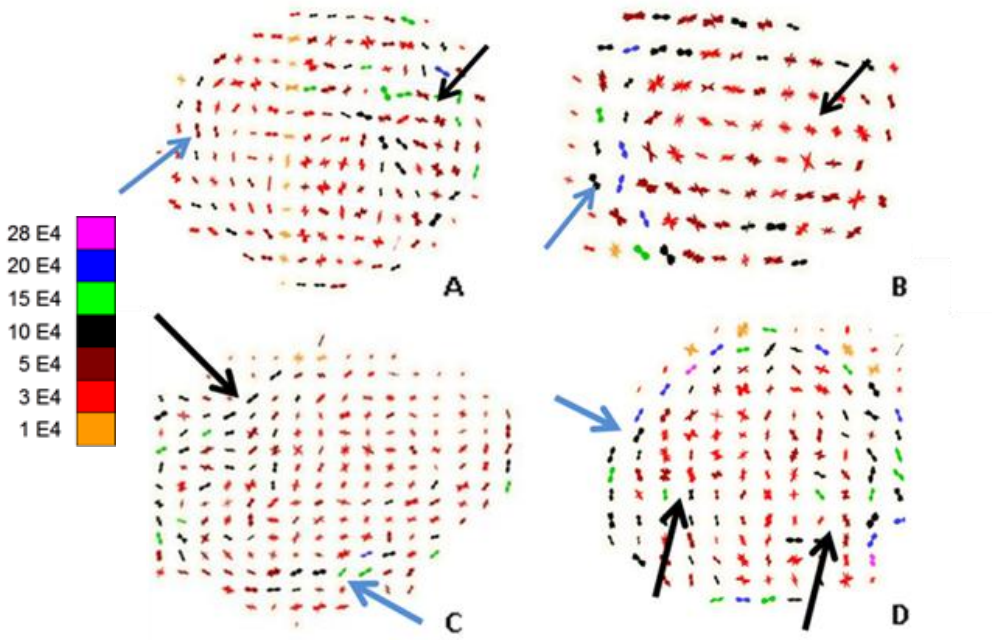

Figure 3.7 : Polar plots of small eye Pax 6+/- (A and B) and large eye Pax 6+/- (C and D). Blue arrows indicate the annular limbus. Black arrows indicate areas of collagen disorder. In the small eye, the limbus appears to be partial and underdeveloped. This is similar to the findings of Sheppard et al 2010 (Figure 3.14) of the developing mouse cornea. In the large eyes, the limbus is more evident but the collagen is more disordered than the CBA wildtype corneas. Scale down factors increase from orange to pink in arbitrary units (AU).

3.4.4 The Development of the Collagen Annulus

In both the Pax 6 +/- and Pax77+ large eye corneas there was present a rudimentary annulus where the collagen alignment was roughly circular/tangential. This annulus was either entirely absent or in localised regions in the small eye samples. Figure 3.7 A and 3.7 B show small eye Pax 6+/- individuals demonstrating that the annulus is not completely formed. Figure 3.7 C and 3.7 D show that large eye Pax 6+/- individuals demonstrate more of a complete annulus. The region around the apparently developing annulus (3.7 A and 3.7 B) appears to be highly disordered.

Figure 3.8 A,B,C are from the small eye Pax77+ individuals. The annulus is either absent or in parts. Figure 3.8 D indicates the Pax77+ large eye phenotype which also demonstrates the suggestion of an annular ring. The annular ring in the larger eye

samples was confirmed with the alignment surface maps which will be discussed later in the chapter.

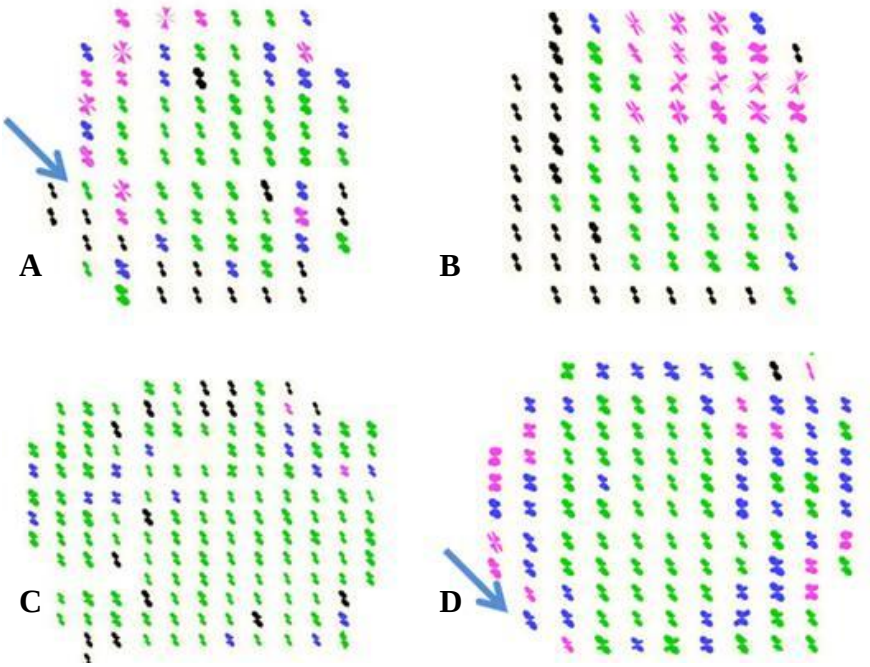

Figure 3.8 : Polar plots of small eye Pax 77+ (A ,B,C) and large eye Pax77+ (D). Blue arrows indicate the suggestion of an annular limbus. In B the region with pink plots represents ciliary tissue fused to the cornea. In all of the samples the predominant direction of the collagen was oblique. Colours represent the scale down factors, applied increasing from green, black, blue to pink in arbitrary units (AU).

The overall collagen organisation of the Pax 77+ corneas demonstrated obliquely arranged collagen which was very ordered in all of the samples observed (both large and small eye). Figure 3.8 A through C indicate the small eye phenotype whilst Figure 3.8 D indicates the large eye Pax 77+ .

3.4.7 Study 2: Differences Between Pax77+ Corneas

In the initial study, only one large phenotype eye was available for analysis from the Pax77+ genotype. It was necessary to collect more data to better understand if the high degree of collagen alignment was due to the general increase in Pax expression or was based on the actual phenotype of having larger or smaller eyes (e.g. the smaller eye could possibly due to extra strain on the smaller corneas). A second experiment was therefore performed to include two more Pax77+ large eyes. Inevitably, as they were from the same batch, these mice were older (see Table 3.3)

a. Collagen amount

Figure 3.9 shows the total and aligned collagen maps for the Pax77+ small eye and large eye phenotypes compared with the CBA control. The results confirm the trend of decreasing collagen scatter when compared to the Cardiff University CBA wildtype (Figure 3.9 A). The preferentially aligned collagen observed in the Pax77+ large eye demonstrated a more aligned collagen ring which resembles an annulus (Figure 3.9 H). This is similar to the Cardiff CBA wildtype (Figure 3.9 B) but differs from the Pax77+ small eyes (E) which only demonstrated a trace of an annulus.

The figure also shows the percentage of preferentially aligned collagen. The percentage of aligned collagen in the small eyes was on average greater than the percentage of aligned collagen in the large eyes (Fig 3.9 F and I). The differences were not as marked as in the first set of corneas. There also remained areas of very high collagen alignment along the periphery in the large eye phenotype, however overall it resembled the control with a more even distribution of alignment from central cornea to periphery.

The small eyes resembled the earlier study (Study 1) where the collagen was more aligned in the centre of the cornea. The percentage alignment in the small eye 3.9 F appeared to be more homogenous with localised areas of higher alignment.

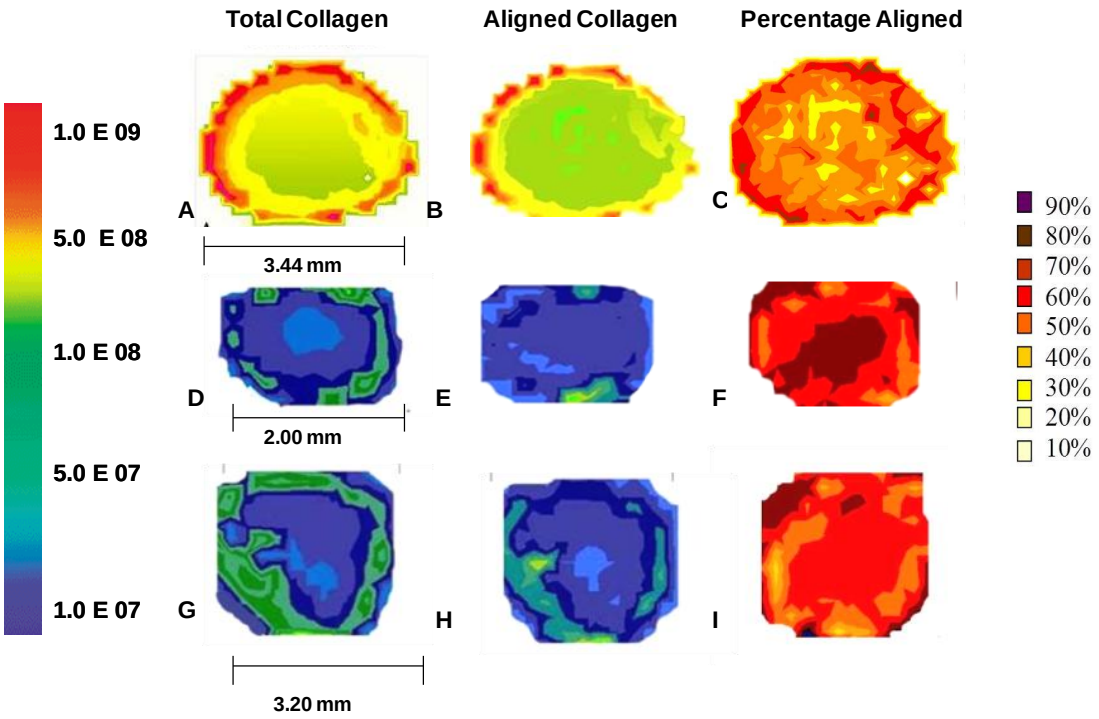

Figure 3.9: Comparison of total, aligned, and percentage aligned collagen in CBA wildtype (A - C), small eye Pax77+ Study 2 (D - F), larger Pax77+ eye Study 2 (G - I). An increase in total collagen is visible around the periphery in both the small and large Pax 77+ eyes. Collagen scatter (key on left) in arbitrary units (AU).

b. Collagen organisation

Figure 3.10 shows the collagen orientation in the small and large Pax77+ corneas. The collagen organisation in both of the Pax77+ corneas (3.10 B and C) displays orthogonality in the central region with a clear collagen annulus (most noted in the large eye samples figure 3.10 C). This arrangement is very different from that in the CBA wildtype (figure 3.10 A) and also differs from the arrangement seen in the small and large Pax77+ eyes in Study 1. It appears to be a transitional developmental step between the two extremes.

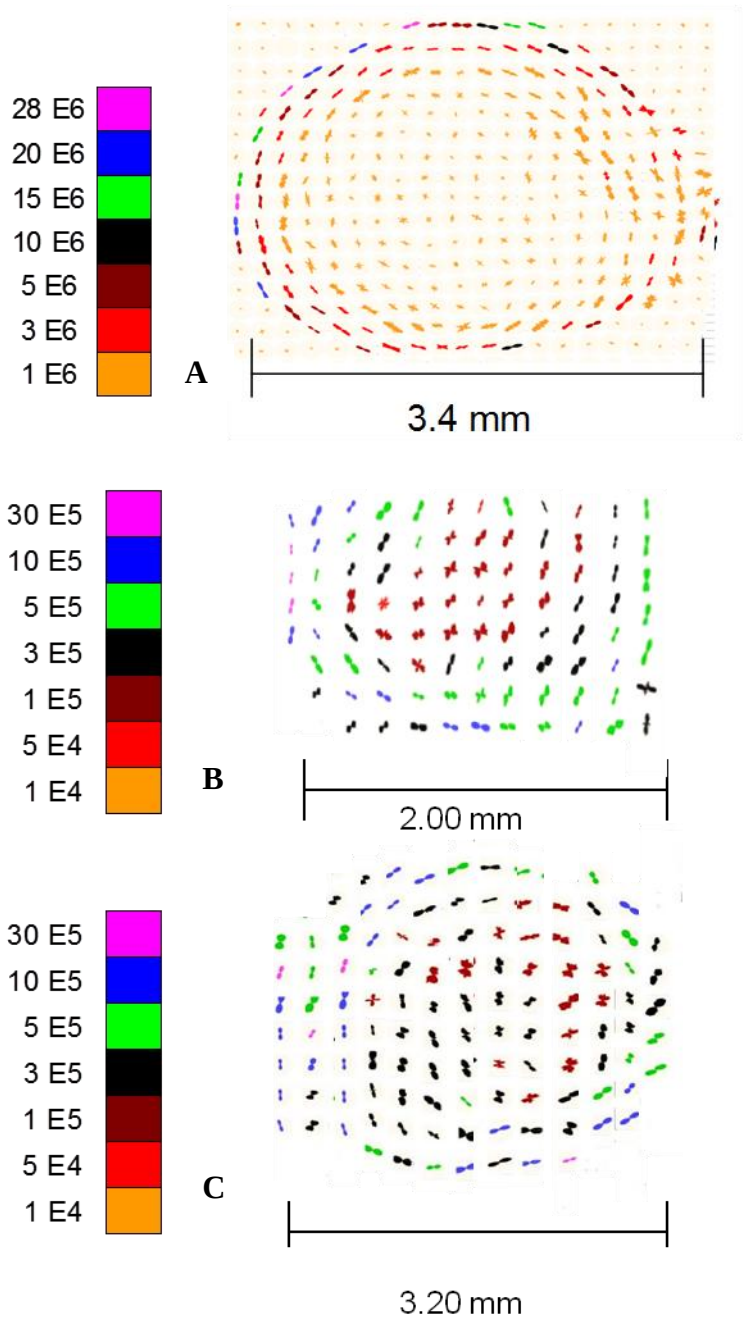

Figure 3.10: Collagen orientation maps for CBA wildtype (A), small eye Pax77+(B), and large eye Pax77+ (C) . Both the small and large eye PAX77+ demonstrate oblique collagen organisation in the central cornea however it is not as unilateral as the orientation in the first study but more than in the wild-type (A). There is also a clear annulus of higher intensity collagen present in both of the samples. The total amount of scatter indicates higher levels of scatter along the periphery. Colours represent scale down factors ranging from orange (least scaling) to pink (greatest scaling) measured in arbitrary units (AU).

3.5 Discussion

3.5.1 General Corneal Development

In the corneal development of the chick there is an acelluar matrix of collagen forming a 'primary stroma' which is later populated with cells forming a secondary stroma. Haustein (1983) noted that in the mouse this does not occur, and the stroma develops singularly. The mouse cornea develops with the presence of single collagen fibrils and a sub-epithelium which later thickens. It is posthulated that in this way the mouse cornea is similar to that of the primates (Haustein,1983).

It is also thought that the stoma of the mouse could not be derived from the epithelium as it lacks the mechanisms for protein synthesis and the mouse epithelium does not contain enough mitochondria to promote the differentiation of the new structure. It is thought that in the mouse at E16, larger collagen fibrils begin to be produced independently by fibroblasts which are derived from the mesenchyme and attach to the Bowman's membrane (Haustein, 1993).

Morishige et al. (2007) performed non-invasive *in vivo* SHG microscopy on mice and rabbits to determine the collagen ultra-structure of the corneas. They determined that in both the rabbits and mice there were two distinct collagen layers; the anterior layer was comprised of collagen which was interwoven and the posterior stroma demonstrated collagen in an orthogonal pattern (with collagen at right angles). Zieske et al. (2004) noted that during embryogenesis of the cornea the neural crest cells migrate in either one or two cascades depending on the species. It was found that reptiles, birds and primates have two waves of cell migrations whilst rodents only have one (Clinton et al., 1983).

The Pax 6+/- and Pax77+ eyes observed in these studies followed the phenotypic morphological trends described in the literature. These included an overall reduction in eye size as a trend in the genotypic small-eye mouse corneas. The eyes analysed appeared to be similar in both male and female individuals with no apparent differences due to sex. The presentation of the disorder was not always bilateral so left and right eyes were not always equally affected. The morphological defects (e.g.

loss of ocular structures) were not always noted in the same combinations within each phenotype grouping; there was evidence of lens defects (in Pax 77+), under development of cilary bodies, and anirida observed upon dissection of our samples, however, these traits were also not always isolated to one group (Grindley et al.,1995). They are also expressed in various combinations within each group as indicated by Dora et al. (2006).

The samples analysed to date indicated a trend where the Pax 6+/- and Pax 77+ mutants and the respective 'wildtype' specimens demonstrated similar collagen scatter and organisation patterns within groups but differing from one another in all cases studied. If the two mutant species (and their wild-type counterparts) were of similar genetic strains, it would be assumed that they would demonstrate similar results to each other. This was not the case. There were clear and consistent differences between all three groups.

It should be noted, however, that although the general trend for small-phenotype matched the small-eye genotype, there were significant instances where this was not always true (Dora et al., 2009). As there were instances where genotype and phenotype did not match it cannot be assumed that this is a purely genotypic study. The sample number was too low to determine this and further investigation would be required. The eyes initially chosen for the study were based on phenotype and then the genotype was later tested. In a small percentage of instances, there was a mis-match in genotype vs. phenotype. This could be an indication that the phenotype changes which occur to the corneas may not be based entirely in genotype but may develop later on due to environmental stimuli.

Manuel et al. (2008) noted that the over-expression of Pax 6 in the form of Pax77+ (from the addition of extra Pax 6 genes), causes some similar phenotypic changes to the eye as Pax 6 +/- deficiency (i.e. small eye) but the overall cause for the reduction is not thought to be the result of the same biological cascades and pathways. Although the final results look similar (i.e. a smaller than normal eye), the process through which the abnormal structural changes are thought to develop is entirely different. The changes which occur during the Pax77+ deficiency occur later in development E12-14 (dependent on study) after the eye already has undergone a

degree of differentiation from the neural crest and the structures are present (albeit not entirely developed or *in situ*). The Pax 6+/- (sey) occurs in the earliest stages of development as the lack of Pax 6 is thought to stunt overall development and it is thought to be due to a defect in the initial biochemical cascades (including the differentiation of the lens capsule) (Manuel et al., 2008).

a. Collagen Ultrastructure

The orientation of the collagen in the second set of corneas studied in the present investigation was unusual when compared to the first. Figure 3.11 compares the collagen organisation from the second set of Pax77+ corneas with those from the first set (Study 1). The Cardiff University CBA wild-type sample appeared to have collagen which was evenly distributed out towards the periphery with a clear collagen annulus (figure 3.11A). This is what would be expected in this strain of normal mouse cornea (NB: in some strains it has been indicated that the central cornea appears to be thicker than the periphery). The Pax77+ corneas demonstrated similar collagen organisation to each other for both the large and small eye, however between the two studies there was a striking change of the collagen from a uni-directional to a more randomised oblique arrangement with the formation of a true collagen annulus. One possible reason for this change in collagen orientation may be due to the age of the individual mice. The second group of mice were slightly older than the first and this could have an impact as Pax77+ is thought to be a regressive disorder. There could be a trend where the majority of the collagen in the earlier stages is highly aligned and then is gradually remodelled with age to appear more like the wild-type corneas. As an auto-regulation there could be a possible decrease in Pax expression in the later stages leading to the orthogonal orientation characteristic of the posterior stroma (Morishige et al., 2007). However there was an overlapping age range in some samples so this may not be the case.

The Pax 77+ corneas demonstrated a high degree of alignment in both the small and large eyes at the younger time-point (figure 3.12 B and D) than in the large and small eyes (figure 3.12 C and E) which appeared to have an annulus and resembled the CBA wildtype in some respects. At the later time-point the percentage alignment was decreased as the collagen became less uni-directional although it remained in the

oblique orientation especially in the centre region). This new arrangement appeared to be somewhere between the CBA wild-type and the younger Pax77+ samples suggesting some developmental influence.

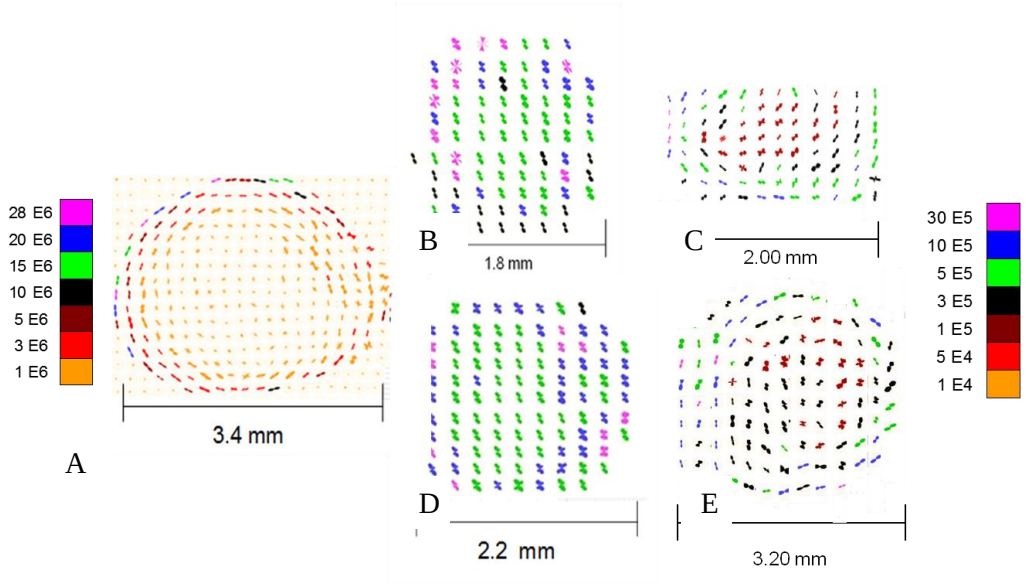

Figure 3.11: Collagen organisation of CBA wildtype (A), small eye Pax77+ first study (B) and second study (C), and large eye Pax77+ first study (D) and second study (E) corneas. The Pax77+ in the first study both demonstrated oblique collagen organisation. The two second study specimens also both demonstrated oblique collagen arrangements however they were not as uni-directional as in the other mice. There was a higher intensity ring of collagen in E suggesting a circumferential annulus. Colours represent scale: down factors ranging from orange(least scaling) to pink (greatest scaling).

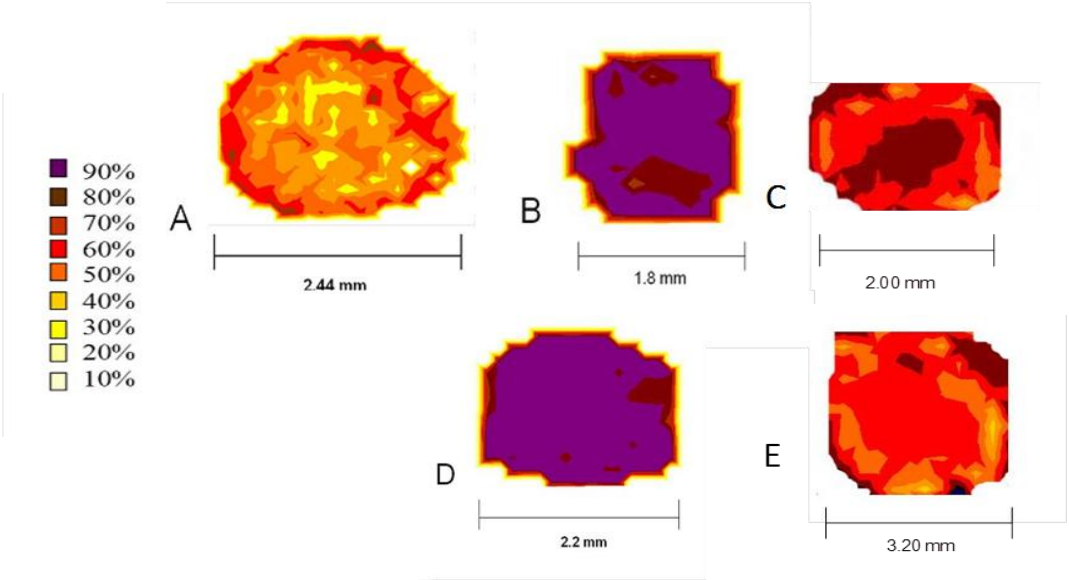

Figure 3.12: Percentage collagen alignment of CBA wildtype (A), small eye Pax77+ first study (B) and second study (C), and large eye Pax77+ first study (D) and second study (E) corneas. The collagen in the first study presents a very high degree of order, more than in the second study (but both were still higher than in the CBA). The collagen in C is similar to the developing mouse cornea. In E the percentage of collagen alignment is approaching that of the wildtype, however there remains areas of high organisation along the peripheral regions.

Sheppard et al. (2010) performed WAXS on the normal developing mouse cornea and noted that the annulus in not present at birth but appears shortly after eye opening. In their study, they noted through orientation maps that the annulus began to organise gradually post-natally with eye opening being a driving factor (Figures 3.13 and 3.14).

In our study, some of the adult Pax 6+/- mutant corneas (Figure 3.7) retained small areas of organised collagen which resembled these early developmental stages of an annulus as seen in the normal embryological mouse. This partial annulus was surrounded by seemingly disorganised collagen. In the adult Pax 6+/- small eye mouse, there appeared to be strong similarities with the developing embryological wild-type mouse in this respect. The collagen orientation of the adult mutant strongly resembles the early post-natal development pre-eye opening and then halts. Where the normal mouse would have a complete circumferential limbus present by D28, our mice small eye Pax 6+/- mutant mice demonstrated the arrested development of the limbus fully into maturity. This may be due to an abnormal development and differentiation of neural crest derived keratocyte cells which would have a knock-on effect for normal stromal development/organisation. Another cause may be that due to the small eye size and squint the normal biomechanics associated with eye-opening do not occur.

Sheppard et al., (2010) also found that in the very early stages following eye opening the collagen presented a relatively homogeneous degree of order. This is supported by other research which indicates that in the days just before eye opening there is an increase in corneal collagen, proteoglycans, and other matrix materials which are switftly re-modelled upon eye opening. The high degree of collagen order in the normal mouse cornea presents itself as a high degree of homogeneity in the distribution and alignment of collagen. In our study there was also a very homogeneous degree of alignment in the Pax 77+ corneas, however our results demonstrated that the percentage alignment was much greater (Sheppard et al., 2010).

In the normal mouse, by the four month age point the corneas should have fully developed and reorganised to a normal adult morphology; our samples did not demonstrate this trend.

In the first Pax77+ experiment, there was a collagen organisation that appeared to be in a unidirectional oblique orientation. Sheppard et al. (2010) noted that at D11 the corneal collagen organisation in a number of the corneas they observed was in the horizontal or oblique which then changed in maturity to a an arrangement with a clear circumferential collagen annulus. The changes observed by Sheppard et al. (2010) occurred in the later adolescence stages with collagen organisation returning to a normal morphology in the mature adult. In our study, all of the adult mice

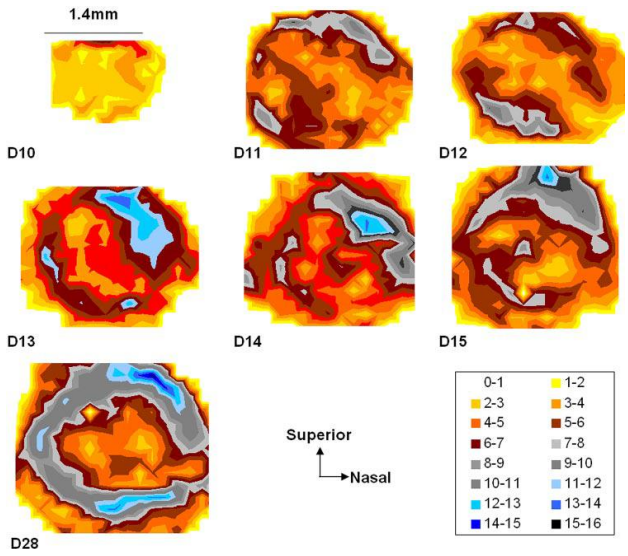

Figure 3.13: Collagen alignment maps of WAXS scans of the developing mouse cornea (from Sheppard et al 2010). In the first experiment, the small eye Pax77+ corneas appeared to resemble the eyes at D10 with a high degree of aligned collagen (especially in the central cornea) and absence of annulus. The adult larger eye Pax77+ maps resemble maps D11 – D13 with areas of partial collagen alignment along the periphery.

initially studied in the Pax77+ group (including both small-eye and larger eye 'wildtype') demonstrated this oblique pattern of highly aligned collagen. The larger eyes did contain a trace of increased collagen along the periphery which could be attributed to an annulus.

In the second batch of Pax 77+ corneas studied (generally older animals) the collagen remained oblique but appeared to reorganise into a less of a uni-directional alignment with the presence of the annulus. This could be indicative of a delay in development (e.g. as in the normal developing eye changing from a unidirectional to annular arrangement with age). In the case of the Pax77+, this change could be occurring at a later time-point. The thickening along the periphery was also more evident in the earlier stages.

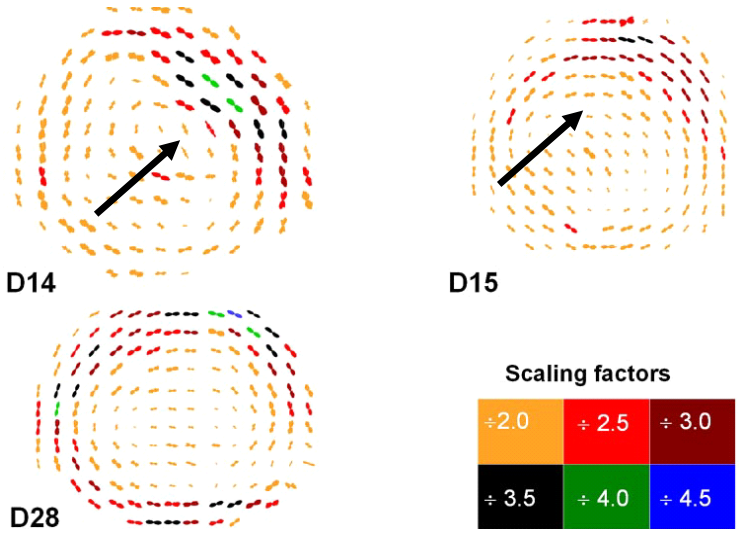

Figure 3.14: Collagen orientation maps of mouse WAXS scans of the developing mouse cornea (from Sheppard et al 2010). The first batch of small eye adult Pax 6+/- corneas appear to resemble the eyes at D14-D15 with small areas of annular collagen developing but not completely formed into a ring (as indicated by the black arrows). Colours represent scale: down factors ranging from orange(least scaling) to blue (greatest scaling).

In the second study of Pax77+ corneas, the smaller eyes demonstrated strikingly similar patterns to those observed in early development at D10 as indicated in the Sheppard study (figure 3.13). The percentage of collagen alignment is higher, however the distribution of the aligned and preferentially aligned collagen is similar. The overall size of the eyes are also similar to the developing mouse. There were however marked differences in the orientation and the distribution of collagen (i.e. the unique oblique arrangement of collagen with the clear annulus). As Pax77+ is a degenerative disorder, it could be possible the smaller eye is an indication of the further progression of the disorder leading to a degeneration of the eye as the annulus is not as strong as in the larger eye. This could be a stage of developmental

regression. It would be of interest to study more mice and additional time-points to determine if this is, in fact, a ontogenological regression at set time-points.

b Collagen Amount

The WAXS results have demonstrated a clear difference between the Cardiff University CBA wildtype, Pax77+, and the Pax 6+/- corneas. The Pax 6+/- and Pax77+ corneas both demonstrated an overall decrease in collagen amount when compared to the Cardiff University wildtypes. The larger eye phenotypes of both groups also demonstrated an annulus which was absent in the small eye phenotypes, where there only appears to be small areas of aligned collagen. The presence of the annulus has been flagged as an indicator of biomechanical stability in the eye which maintains its curvature (Newton and Meek, 1998). In the Pax77+ first study the larger eye, there was observed a peripheral band of thicker collagen but this did not entirely resemble a true annulus in terms of orientation. The Pax77+ large eye remained flattened both *in situ* and following dissection which is further indication of the absence of the true annulus. In the second study the larger eye demonstrated a clear collagen annulus.

The Pax 6+/- corneas most notably demonstrated a reduction in collagen amount across the entire cornea along with a degree of localised disorder. The reduction in total scatter/collagen amount was observed in both the small-eye and large-eye phenotypes. The way in which the thinner collagen was distributed across the cornea was also of interest as there were regions of decreased scatter and decreased collagen alignment, most notably in the small-eye. This could be an indication that the keratocytes have not fully differentiated to form a normal stroma.

Mort et al. (2011) performed TEM studies on wildtype, Pax 6+/- , and Pax77+ corneas to further determine information regarding the collagen ultrastructure. Previous studies did not demonstrate any major differences in the stromal collagen architecture of both the Pax 6+/- mutants with most of the changes present found in the epithelium (Dora et al., 2009). The only observations were that the Pax 6+/- corneas appeared to have a hyper-cellular stroma in some individuals but not in all (Ramesh et al., 2003). The corneas otherwise did not appear to demonstrate any significant ultra-structural differences when compared to wild-type corneas. The Mort

et al., (2011) study focused on the regions of stromal collagen located around the keratocytes in both the Pax 6 +/- and Pax77+ increased models and discovered vacuoles in the tissue (figure 3.15).

The Pax 6 +/- knockout models presented large vacuoleated areas within and around the keratocytes. The vacuoles were acellular and devoid of collagen and other matrix materials (Mort et al., 2011). In our study, we discovered that the Pax 6+/- mice retained on average a 100 fold decrease in total scatter when compared to the Cardiff CBA wildtype and a ten-fold decrease when compared to Pax77+. It could be possible that in the adult small eye Pax 6+/- mutant corneas, these vacuoles could contribute to the reduction of total collagen scatter. This would differ from the amount of collagen in the developing mouse, however it has been established that corneal keratocytes which are driven through differentiation and migration by Pax 6, could be damaged or may not produce adequate amounts of collagen.

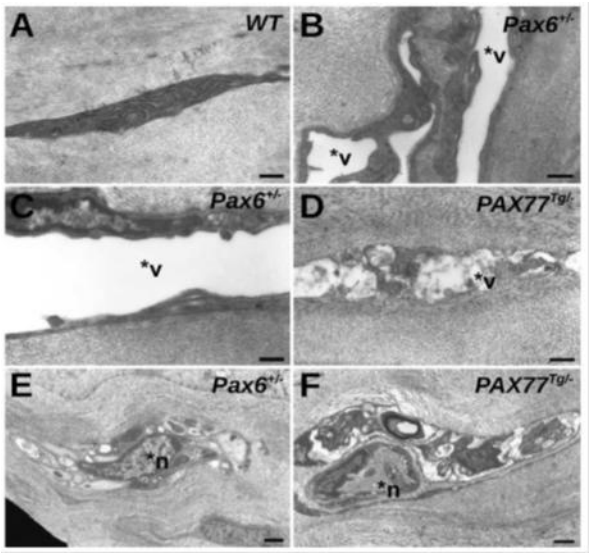

Figure 3.15: Electron microscopy of corneal stroma. TEM micrographs of (A) WT corneal stroma showing normal keratocyte morphology with no vacuoles; (B,C) Pax6+/- corneal stroma showing keratocytes with very large vacuoles; (D) PAX77 corneal stroma showing keratocyte with small vacuoles; (E) Pax6+/-corneal stroma showing nerve cell; (F) PAX77corneal stroma showing nerve cell. Abbreviations: *v, vacuole; *n, nerve cell. Scale bars = 500 nm in A–D and 1 mm in E and F. From Mort et al 2011

Another theory with the overlarge vacuoles in the Pax 6+/- mouse is that they resemble the ‘corneal lakes’ described in Chapter 1. Swelling of the cornea can lead

to spacing difference between the collagen fibrils leading to changes in light scattering and the observation of a corneal haze. The corneal lakes result from abnormal spacing between the collagen layers, and are also believed to contribute to changes in refraction. These lakes are similar to the collagen devoid regions which appear with Pax 6 +/- corneas. In other corneal studies these lakes have been observed to lead to a loss of corneal transparency. This may be another contributing factor to the overall pathology as Pax 6+/- often presents a cloudy cornea in a number of clinical cases where other Pax defects do not.

These large vacuole regions appear similar to some of the changes described in stages of the normal developing cornea (Quantock and Young, 2008; Sheppard et al., 2010). These collagen-devoid regions may also contribute to the lower degrees of total collagen scatter amount present in the mutant models. Comparatively large vacuoles have been observed during the later embryological and early post-natal stages across species (Quantock and Young, 2008**;** Sheppard et al., 2010) and in these mutants the development may be arrested in this stage of collagen re-modelling. They may also be indicative of damaged corneal keratocytes which do not produce the normal collagen and matrix materials necessary for maintaining homeostasis.

As noted earlier in this chapter, during normal cornea development, it is though that the stromal collagen increases rapidly immediately before eye opening. It is also thought that the total collagen amount does not change after eye opening but instead there is a reorganisation of the collagen and matrix which is already present in the stroma. This collagen is then remodelled and redistributed (Sheppard et al., 2010). During this process, large acellular and collagen-devoid regions are present in the corneas which eventually become organised through maturity and the formation of the ordered collagen annulus (Sheppard et al., 2010). The modulation of the corneal collagen in the early stages appears similar to the Pax 6+/- small eye mice. This could indicate that in the Pax 6+/- adult the cornea resembles that of the developing juvenile and does not reach a fully mature adult state.

Mort et al., (2011) also found that Pax77+ corneas there also retained smaller vacuoles in and around the keratocytes but to a much lesser degree. These vacuoles were significantly smaller in size and overall volume than in the Pax 6+/- corneas.

Both tissues types differed from the normal corneal tissue which demonstrated no vacuole regions. As with the total collagen amount in the Pax 6+/-, this may also be the reason for the 10x average reduction in total collagen scatter found in the Pax77+.

Moller-Pedersen et al., (1995) noted that in the normal cornea, keratocytes make up roughly 10% bulk of the stromal bulk. The loss of collagen around the keratocytes may contribute to the reduction in total collagen. It is also of interest that in both Pax mutants the changes which were observed are linked to the keratocytes and would be a path for further research.

3.5.2 Biomechanics and Development

The highly oblique pattern of collagen in the Pax77+ samples at the younger ages may be due to mechanical forces present on the tissue due to the reduction of ocular chamber size, however the orientation of collagen was observed in both small and 'wildtype' individuals so may be more indicative of an overall strain difference. That noted, the Pax77+ large eye did appear to retain some variation on a collagen annulus. The highly orthogonal collagen observed in the older Pax77+ corneas is also an indication that the differences may be due to strain and more likely be developmental, but possibly not due to the biomechanical strains of the reduced ocular chamber. In the older Pax77+ mice there was also present a variation on the annulus which was not present in the small eye. At both time points, this presence or absence of the annulus appears to be the most commonly observed factor.

One observation regarding the Pax 6 +/- and Pax77+ small eyes is that in many cases the eyes remain closed or in a squint. If the act of eye opening postnatal at day 11 or 12 is thought to be the stimulus for the cascade of genetic and biochemical events which lead to a fully functioning and biomechanically sound cornea, this may be a reason behind the lack of further development. This would be most likely the cause for the failure of the collagen annulus to form. Norman et al. (2004) confirmed with serial analysis of gene expression studies (SAGE) that there is an increase in gene expression at the time of eye opening in murine development (Norman et al., 2004).

Huble and Wiesel (1969) preformed experiments on the eye closure of developing kittens. They surmised that there was a feedback system for the full developing of vision and if eye opening did not occur. They found that in crucial windows of development, a closed eye for up to six days could result in a decrease in cortical cell production (Huble and Wiesel, 1969). In the case of the small eye mouse, the mal-functioning of the eye-lid and visual feedback system may arrest the development of the eye. This system can be random which would explain why the 'small eye' does not appear in all of the individuals or even bi-laterally. This may also explain why the 'small eye' and 'large eyes' often, but now always, match the associated genotypes. In humans with Pax 6 deficiencies (anophthalmia and microphthalmia) there is also a rage of morphological changes which follow a trend but are not always easily or reliably predicted in the individual.

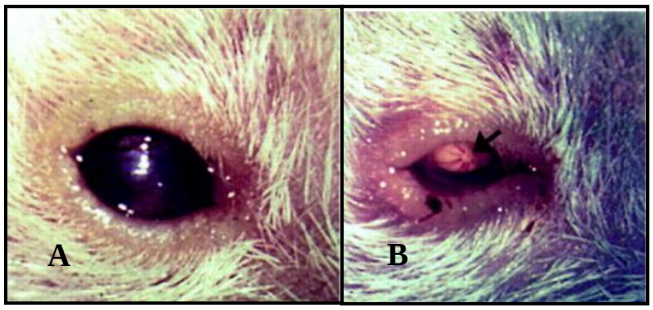

Figure 3.16: Normal (A) and small eye Pax 6+/- (B) mouse eyes. The severely reduced eye size can also resemble a squint with eyes that appear to be unopened in the adult (Image from Schedl et al., 1996)

Another factor may be that when the amount of Pax is altered (either through an increase or a decrease in dose), the signals sent to keratocyte cells are also altered which may have a direct negative impact on cell division and migration (Fumderburgh et al., 2006). This, in turn, would have a direct impact on the synthesis of collagen and extra cellular matrix (ECM) products in the stroma. In the case of the Pax deficiency, the cells may not be able to function normally from the early stages when differentiating from the neural crest. The tissue is, therefore, underdeveloped (Funderburgh et al., 2006).

Funderburgh et al., (2006) also noted that there remained Pax 6 expression in the keratocyte which is thought to be differentiated from the neural crest cells. There was

enough expression in the keratocytes that it could be reliably used as a cell marker. The damage caused during embryogenesis caused by a decrease in Pax 6 expression may lead to a degree of disorder in collagen production and subsequent organisation. Pax 6 is thought to be key in both the differentiation and migration of the neural crest cells. The lack of Pax 6 may lead to failure in the collagen organisation and amount due to the production and migration of the cells. Although Ramaesh (2009) found that there were additional keratocytes found in some of the Pax 6 +/- corneas, the cells may be abnormal and not be functional like normal keratocytes.

3.5.3 Genetic Strain

There is the substantial possibility that the differences observed between the mice are due to genetic strain. Our findings found similar trends between the Pax 6+/- large and small eyes (as a group) vs. the Pax77+ large and small eyes as a group. Chanas et al. (2009) studied the same strains of mice as were used in this study (wildtype CBA and Pax77+) and found that the larger eye genotype-phenotype Pax77+ had a wet weight which was approximately 20% lower than a normal wildtype eye. Our larger eye Pax77+ also demonstrated a slightly reduced corneal diameter when compared to the wildtype. This may also be due to individual variations so should be taken with a caveat. This does raise the question, however, of whether genetic strain has an impact on the collagen ultrastructure results.

Other strains of Pax77+ mice which have been studied (e.g. CD1-Pax77+) demonstrated structural changes which differed from both the Pax77+ used in this study and wildtype CBA strain. Of the three Pax77+ strains observed in the Chanas study, the Pax77+ strain fell at the mean on the overall spectrum for reduction in eye size (60% reduction in size vs. 20% and 90% in other strains). It is for this reason that the Pax77+ are used as a general representative for the additional Pax changes (Chanas et al., 2009).

Most of the Pax 6+/- corneas demonstrated a thinner central cornea rather than in the periphery. This is not normally found in most murine models but was also found in the CBA mouse strain which where there is an increase in collagen thickness along the periphery. Henrikssion et al. (2009) reviewed corneal thickness (stromal and

epithelial) in three strains of mice (129/SVJ, C57BL/6, and BALB/c) and found that the central cornea was significantly thicker than the periphery than all three strains. They also noted differences in the collagen ultra-structure when compared to human corneal collagen (namely in the direction of the collagen lamellae at the Bowman's interface). They raise a caveat in that some mouse strains may differ in collagen architecture and may not be readily compared to humans. It therefore could be a possibility that some of the changes found in the Pax 6 +/- may be due to strain difference between the Pax mutants provided by our research collaborators at the University of Edinburgh.

The Use of Oral Mucosal Fibroblasts as a Novel Treatment for Increasing Transparency and Flap Strength in LASIK Wounded Sheep Cornea

4.1 Introduction

The biological changes which occur following corneal injury/surgery were discussed in detail in Chapter 1. Following injury, the cornea undergoes a series of inflammatory and proliferative stages which ultimately result in phenotypic changes to the corneal fibroblasts and the formation of new corneal collagen and matrix components. The collagen and matrix produced following wound healing possesses a different phenotype and overall organisation from the native tissue (Wilson et al., 2000). The collagen produced is less ordered due to the need to quickly close the wound to prevent invasion from foreign bodies and possible infection. The disordered collagen transmits light less effectively than the native tissue leading to a loss of best vision (Farrell and McCally, 2000).

In addition, there are thought to be phenotypic changes in the fibroblast following TGF-B activation where they are thought to become reflective and scatter light (Moller-Pedersen et al., 2000). This can contribute to a 'corneal haze' which also negatively impacts on vision. In many cases, more superficial corneal wounds return to homeostasis in six months to a year due to the re-modelling of the newly laid collagen and cells are thought to undergo either apoptosis or return to quiescence of fibroblasts (Moller-Pedersen et al., 1998). In a substantial number of cases, a complete return to homeostasis never truly occurs and scars and loss of vision persevere (this will be discussed in detail in Chapter 5). In extreme cases where scarring remains along the visual axis corneal transplant (and all of the associated complications), may be the only option available (Al-Towerki et al., 2004; Arentsen, 1983;Vail et al.,1997).

In some surgeries (e.g. LASIK and PK), there also remains the complication of the wound margin only partially healing without complete tissue re-integration along the flap bed. The flaps created are thought to only retain approximately 2% -28% of the original tensile strength of the un-injured eye (Schmack et al., 2005; Randelman et al.,

2008). The upper limit found is usually found in wounds over 10 years old which remains only a fraction of the original strength. For a decade or more following the surgery, patients have reported that the flaps have undergone accidental dehiscence following eye trauma (Melki et al., 2000; Geggel and Coday, 2001). Post-LASIK flap dehiscence is a common problem for a number of patients; it is rare but significant to the affected patient (Tumbocon et al., 2003). Whilst most surgeries do not present traumatic dehiscence, there are enough case studies to cause concern amongst patients.

One of the ultimate goals of eye research is to increase corneal transparency whist increasing the biomechanical strength of the LASIK flap. This would positively impact on millions annually world-wide. Research into this field has focused on topical treatments such as various signal inhibitors or cell/matrix based therapies (Mi et al.; 2010; Kamma-Lorger, 2007; Muller et al., 2005, Littlechild et al., 2011). It has also been suggested that stem cells could be used for treatments for ocular defects; the theory behind using stem cells originates with past research indicating that a good supply of autologous limbal stem cells results in corneal wound healing. An absence of these cells can result in non-healing ocular wounds. Other studies have indicated that stem cells from an embryological or adult source can be 'coaxed' into transforming into other tissue types based on environmental factors (Du et al., 2005).

In the cornea, these cells could theoretically be transformed to produce a collagen type and organisation more similar to that of native collagen formed during embryogenesis. The stem cells are not 'adult' or of a fully differentiated phenotype and could have unlimited reparation potential (N.B. some studies have also categorised quiescent keratocytes as not fully adult and remaining in the G0 phase due to their ability to transform following wounding, this will be addressed later) (Faragher et al., 1997). There are a number of drawbacks to both embryological and adult stem cell treatments, ranging from practical issues (i.e. a ready supply and creating the correct cell phenotype) to the ethical issues of using embryological cell sources; it is for these reasons other repair sources have been sought (Shi and Garry, 2006). A new breakthrough in these treatment studies are induced pluripotent stem cells (IPS) for corneal repair (Funderburgh Group, 2012).

Forman et al., 2006 previously established an *in vitro* organ culture model for the study of wound healing of enucleated corneas. Kamma-Lorger, 2007 and Mi et al., 2010 utilised this organ culture model to assess various cytokines, growth factors, and cell-based treatments to determine their effects on corneal wound healing of LASIK type flaps, most notably regarding transparency and flap strength. Mi et al., 2010 concluded that of the various treatments, riboflavin and ultra-violet corneal cross-linking retained the transparency of the cornea and increased flap strength. The study also found that corneal fibroblasts (cultured keratocytes treated with TGF-B) led to increased flap strength however there was a decrease in corneal transparency as quantified through visual assessment.

Whilst the UV cross-linking results appear promising, the technique is relatively new and further long term studies are required. The crossed linked results also demonstrated a very strong flap in the first weeks following UV/riboflavin treatments, however, the flap strength decreased sharply in subsequent time points. Another potential drawback is how truly transparent the cornea following cross-linking treatments. Some studies have noted hyper-reflective keratocytes and the presence of reflective spheres remaining in the tissue possibly as the result of keratocyte apoptosis. Apoptosis can also lead to a decrease in collagen producing cells and may also have a negative impact on wound healing.

In the current work, it is postulated that oral mucosal fibroblast cells could be used as an autologous cell source which is similar to neural crest derived stem cells. These cells could be applied to the flap bed of LASIK-type surgeries, PK, PRK, non-healing corneal ulcers, and other corneal defects and injuries with the aim of increasing wound healing. In the case of LASIK, it is hoped that these cells will produce a stronger flap, as do conventional corneal keratocytes, but also will result in the production of a collagen phenotype which remains transparent due to advanced preferential wound healing properties.

4.1.2 Oral Mucosal Fibroblasts

The unique wound healing properties of oral mucosal fibroblasts were discussed in the general introduction chapter. Oral mucosal fibroblasts are thought to retain foetal-

type wound healing properties and a degree of ‘stem-ness’ which is not normally observed in adult somatic cells (Stephens et al., 2001; Enoch et al., 2008 and 2009; Mosley et al. Davies et al., 2010) (Table 4.1). Following wounding, the inflammatory stages that have occurred and the type of collagen produced, should result in wounds which appear ‘scarless’ and tissue which has a phenotype more like neighbouring native tissue (Goss, 1977). In the oral environment which requires a rapid cell turnover due to mastication and high risk from exogenic injury factors, this specialised wound healing is important for maintaining homeostasis and provides a healthy supply of tissue (Wertz et al., 1993).

The use of oral tissue in ocular treatments has an established clinical history. From the mid-twentieth century, surgical operations like osteo-odonto-keratoprosthesis (OOKP) have used autologous oral epithelium to partially restore vision (Hull et al., 2000). More recently, research has focused on autologous and allograph oral epithelial sheets and cells *in lieu* of traditional corneal replacement in patients with bilateral eye injuries where a limbal stem cell source is lacking (Lindberg et al., 1997; Pelegrini et al.; Nishida et al., 2004). Whilst both of these operations have been able to restore a degree of vision, there are substantial drawbacks (mainly extensive and pervasive angiogenesis) (Nishida et al., 2004; Sekiyama et al., 2006). The oral mucosal fibroblasts differ from the superficial oral epithelium as their role is to synthesise collagen and extracellular matrix components without producing excessive amounts of a-sma which is associated with myofibroblast phenotype formation and is thought to be a possible inhibitor of fibroblast cells returning to homeostasis (Wilson et al. 2000).

Oral mucosal wound healing :

Tissue Type	Foetal	Oral Mucosa	Skin Wounds
Microphages	decreased	decreased	increased
IL-10 presence	decreased	increased	increased
Inflammatory cell infiltration	decreased	decreased	increased
Wound angiogenesis	decreased	decreased	increased
Wound contraction	decreased	decreased	increased
myofibroblast presence in scar	None in small scarless wounds but low levels in larger wounds	Low to high range dependent on individual and wound size	increased
Cell senescence	later	later	earlier
Active Telomeraise	Present	None	None
Migration and Cell repopulation	rapid	rapid	Slower
Activated Myofibroblasts	Apoptosis following initial response	Apoptosis of myofibroblasts	Apoptosis to some extent but may cause fibrosis
Fibrosis formation	None in mid gestation	Scarring rare	Scar formation re-modelling occurs
Strength of wound area	Strong resembling neighbouring tissue	Strong resembling neighbouring tissue	Tension is weak along the scar due to the orientation of fibres 2%-30% of original tissue depending on scar
Collagen type	Highly varied	Type I	Type I
Hyaulnaron	Increased	Increased	Decreased
TGF-B1	Down regulated	Down regulated	Up-regulated
Inflammatory Response	Low, rapid, transient	Rapid and transient	Longer inflammatory response
Hayflick number doubling populations	high	High- 80-115	Low 45-60
Cell differentiation	Low rates	Low rates	High rates
Collagen organisation	Reticular	Reticular	Parallel or highly disordered fibrils

Table 4.1: Comparison between foetal, oral mucosal and adult skin tissue and cells. The foetal and oral mucosal demonstrate preferential wound healing with the oral mucosal sitting at the middle of the spectrum. Stephens et al., 2001 a ;Stephens et al., 2001 b; Enoch et al., 2009; Colwell et al., 2003;

4.1.3 Ultra-structure of Oral Mucosal Collagen

Research into the ultrastructure of the oral mucosa is important for understanding both the biomechanical function of the tissue and the type/organisation of the collagen and the associated matrix. The oral mucosa is comprised of three layers (epithelium, basement membrane and lamina propia). The lamina propia is a connective tissue which is divided into a papillary layer and a reticular layer (Squire et al., 1971). The lamina layers are rich in cells (fibroblast and mast cells), collagen fibrils, elastin fibrils and sub-types, proteoglycans, and ground substances. The layers are also vascular rich (Squire et al., 1971).

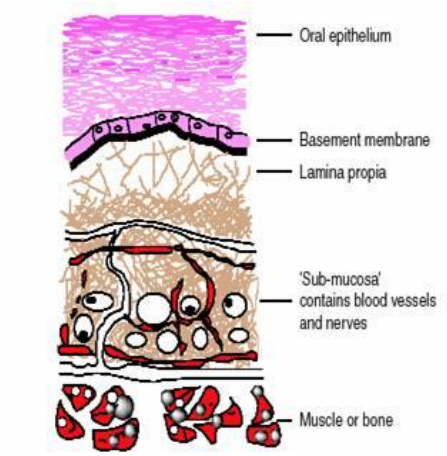

Figure 4.1: Schematic of oral mucosa www.pharmainfo.net/reviews/current-status-buccal-drug-delivery-system accessed 2011

The lamina is comprised by a number of different collagen types, but the bulk of the collagen is type I (Chatterjea, 1991) (figure 4.1). It is thought that this collagen provides biomechanical strength to the tissue during the biomechanical stresses involved in the stretching of the tissue during chewing and swallowing. As in the cornea, there is also laminar collagen types located in the basement membranes. Unlike in the cornea, the type III collagen present surrounds the blood vessels (Orban and Bashkar, 1991). It is though that the upper lamina is comprised of loose collagen of thinner diameters, elastin, and proteoglycans. The collagen nearer the bone and ligature is comprised of longer fibrils with larger diameters (Squire, 1971).

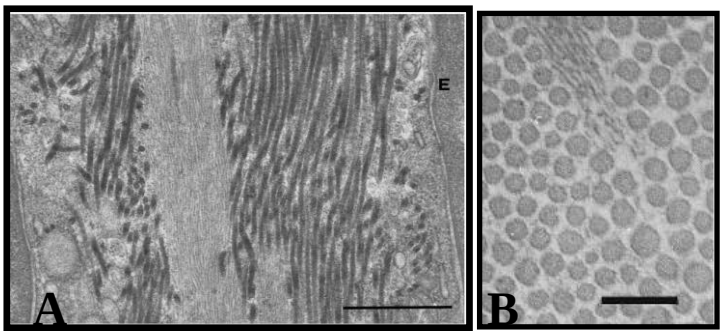

Figure 4.2: A). Free buccal gingiva stained with tannic acid. In the core of the connective tissue of the papilla, between the epithelial cells (E), an oxytalan fibre runs parallel to the collagen fibres. Bar, 1 lm. B) Cross-sectioned collagen fibrils and an oxytalan fibre. Bar, 250 nm. In B the order of the fibrils is evident. Ottani et al., 1998

There have been few studies of the fibril arrangement and spacings of oral mucosal collagen (figure 4.2). In both the soft tissues, it is thought that the upper layers of collagen are loosely packed and have diameters ranging from 38-51 nm. In the deeper layers where the mechanical force is greater it is thought that the diameters are between 70-72 nm (Ottani et al., 1998). It is thought that in these deeper layers the collagen is looped around in long sheets to provide strong collagenous bands (Squire, 1971).

Ottani et al., 1998 performed one of the few TEM studies of primate (rhesus monkey) oral mucosal collagen and found that the collagen is generally ordered in stacked lamellae which is inter-dispersed with fibroblasts and elastin (oxytalan fibrils). It is thought the human oral mucosa is similar in fibril arrangement.

Structure	**Collagen Type**	**Function**
Fibrilar collagen	I	Forming oral mucosa
	III	Reticular fibrils e.g. around vessels
	VII	Basement membrane anchoring

Table 4.2: Main collagen types found in the oral mucosa. These are similar to the collagen types found in the cornea (see General Introduction Chapter 1). After Squire et al 2011

Davies et al. 2010 recently discovered that within the lamina propria there has been found a potential source of multi-potent neural crest derived progenitor cell population. These cells are not thought to be immunologically distinct and have

potential for non-autologous transplantation. This is of interest as the corneal keratocytes are also thought to be derived from the neural crest (Jester et al., 2009; Funderburgh et al., 2006).

4.1.4 Other Molecular Differences of the Oral Mucosa

Oral mucosal cells have been found to have increases in some fatty acids on the cellular membranes which provide higher levels of ATP turnover when compared to regular skin keranocytes (Kuroki et al., 2009). Oral mucosal cells have also been found to produce increased levels of the lower weight dimmer of MMP-2 which is vital in the remodelling of collagen following fibrotic scar formation. It should be noted that MMPs 2 and 9 are both instrumental in corneal wound healing. There are also differences in the amount of tissue inhibitors (TIMPS) in matrix synthesised by the oral mucosa (Stephens et al., 2003).

The GAG hyaluronan (HA) is found in connective tissue was discussed in Chapter 1 in its role in proteoglycan synthesis (Hascall, 1977). It has also been found to regulate TGF-B1 and fibroblast behaviour; increases in HA is thought to promote TGF-B activation (Samuel et al., 1993). Oral mucosal fibroblasts have been found to be on the most part resistant to activation by TGF-B and the resulting scar formation. It is thought that oral mucosal cells uptake HA differently from other somatic cells with a decrease of HA coating the cells and therefore do not promote TGF-B1 activation (Meran et al., 2007).

4.1.5 Differences in Wound Healing Between Oral Mucosal and Somatic Tissue

Since the unique and privileged wound healing properties of the oral mucosa were identified, the cells have been used in a range of wound healing research. Szpaderska et al., 2003 and Wong et al., 2009 demonstrated preferential wound healing of in vivo porcine epidermis tissue when treated with oral mucosal fibroblasts. Chen et al., 2010 demonstrated healing of a murine model.

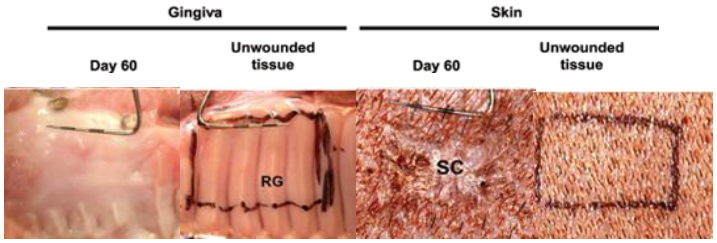

Figure 4.3: Pictures of preferential wound healing of the oral mucosa v skin in a porcine model. Larjava et al., 2011

All of the studies indicated a statistically significant preferential wound healing in the oral mucosal tissue and oral fibroblasts treated models. This confirmed both the advanced wound healing properties of the oral fibroblast and in the case of the transplanted cells, the intrinsic properties on the cellular level. This was further confirmation that the wound healing occurs due to the genotypic and phenotypic properties of the cell and not the moist environment of the oral cavity (Stephens et al., 2001).

It has been thought that in first and second trimester foetal wounds like oral mucosal wounds collagen in not laid down in a fibrotic clot or mass but rather is laid down in a more ordered reticular or "net like" phenotype. This allows the tissue to maintain its biomechanical strength and more closely match the native tissue (figure 4.3). It is thought that this type of ECM deposition is due to the unique balance between the cells themselves which produce a collagen type which is more akin to embryogenesis, the altered balance of MMPs and TIMPs and collagenases and possibly apoptosis which is thought to occur after day 14 where there is generally a marked decrease in the presence of a-sma myofibroblasts preventing scarring further down the line (Funato et al., 1999).

4.2 Experimental Aims

In Chapter 1 the existing clinical and research uses of the oral mucosa in ocular surgery and surface repair were discussed. The oral epithelium and tissue engineered oral epithelial sheets for use in corneal replacement and repair were also discussed; these existing studies have demonstrated autologous oral mucosal donor tissue to be a viable repair tool in the restoration of sight. Studies have also indicated the

similarities between the oral mucosal fibroblast cell and adult stem cells (e.g. of limbal origin). Early stage research has used oral mucosal stem cells as an aide for ocular repair both clinically and *in vitro*. Combining these streams of thought, it was hypothesised that using oral mucosal fibroblasts for corneal injury could present an autologous model for wound healing.

The aim of this experiment was to establish a novel wound healing treatment of LASIK type incisions using applied oral mucosal fibroblasts in an *in vitro* organ culture model in order to increase transparency and flap strength at one, two, and three week time-points. The transparency of the cultured corneas was quantified using spectrophotometry and the flap strength was measured using an extensionmeter. Preliminary small angle X-ray scattering was performed at the one week time-point. The tissue was also processed for histological analysis and cell counts were performed on the tissue to establish the presence or absence of a-sma in the incision and type of collagen produced.

4.3 Methods

4.3.1 Tissue Collection and Preparation

Sheep eyes were obtained from the local abattoir within hours of slaughter and stored on ice. The muscles, fat and connective tissue was removed from the eyes and the cleaned eyes were transferred to a 500 ml beaker, covered and stored at 4°C until required.

A 5% solution of the skin disinfectant Betadine® (Purdue Products) in dH_2O was prepared in advanced and poured over the eyes for five minutes to sterilise the tissue. The eyes were transferred to a class II cabinet for enucleating and the creation of the LASIK type flap using the surgical microkeratome (Bausch and Lomb, Germany).

4.3.2 Microkeratome

The Bausch and Lomb Hansatome Microkeratome is a specialised surgical instrument used to create corneal stromal flaps for refractive surgery procedures. The microkeratome is basically comprised of:

1) A motor and oscillating blade: used to create the flap through an incision.

2) A vacuum pump and metal suction ring: used to create pressure on the surface of the cornea and the motor and blade in place. The vacuum also collects any fluids or detritus materials which arise during surgery.

The power source for the motor and the vacuum are operated by a series of foot pedals allowing for the hands to be free to perform the operation (figure 4.4).

Figure 4.4: Image of a microkeratome. www.centreforsight.com accessed 2012

4.3.2.a Operation of Microkeratome

The microkeratome was assembled as per manufacture's instruction. The vacuum pump was attached to the metal vacuum guide ring and a series of tests were performed on a supplied prop to standardise the vacuum pressure. If the pressure was too high or low, the motor stopped half-way through the procedure when used clinically for the safety of the patient and to ensure the proper cut.

Before being introduced to the class II tissue culture cabinet, the microkeratome hardware was autoclaved. The motor, cables, and vacuum pump were all thoroughly sprayed with 70% ethanol in dH_2O to prevent contamination.

The cleaned and sterilised eye (see general methods section for complete process) was placed on a piece of blue towel soaked in 70% ethanol with the cornea facing upwards. The sterile metal vacuum ring of 8.5 mm was placed in slightly offset from the centre of the cornea and the vacuum pump was activated. The microkeratome motor and oscillating blade were attached to the guide ring and the incision was created. No additional corneal bed ablation was performed.

4.3.3 Cell Origins and Preparations

Oral mucosal fibroblasts were provided by Cardiff University School of Dentistry in compliance with regulations outlined in the Human Tissue Act. The cells came from an established cell line from patients #4 and #5. The cells originated from an oral mucosal buccal biopsy from the inside surface of the patient's cheek. The oral epithelium of the sample was removed, and the dermal layer was cultured in an Eagle's DMEM (Invitrogen, UK) preparation at 37^0C and 5% CO_2 to expand the cell population The cells were stored in 10% DMSO DMEM (Invitrogen, UK) media preparation, rapid frozen, and stored at -80^0C.

4.3.4 Seeding and Passage of the Cells

Three weeks prior to the experiment, defrosted cells were cultured in T75 culture flasks (manufacture) at a density of 1.5×10^5 cells per ml.
The 500 ml Eagle's DMEM solution (Gibco, Invitrogen 21969) was used with the following properties:
+ 4.5 g/L dextrose
+1.1 g/L sodium pyruvate
-L glutamate
The DMEM was fortified with other agents to prevent infection of the sample. 10% foetal calf serum (Sigma, USA) and 1% penicillin streptomycin solution (10,000 units/ml penicillin G, 10ug/ml streptomycin sulphate, and 25 g amphotercin) were

added to the stock mix. In addition, 1% non essential amino acids 100x (Gibco, Invitrogen 111-40) and 5% Fungizone (Invitrogen, UK) was also added to the mix to prevent fungal growth.
In addition to the DMEM solution made with foetal bovine serum (used for activating the fibroblast cells), 250 ml of the preparation without serum was created for cell washes and application of the fibroblasts.

4.3.5 Cell Trypinisation

Fibroblast cells formed a mono-layer at the base of the T75 flask. The cells were passaged and expanded to allow the cells to grow with more room. As previously noted the cells were seeded at 1.5×10^5 ml. The flask was then filled with 50 ml of the DMEM foetal bovine mix. Once the DMEM solution was removed cultures were washed with PBS solution.

To detach the cells from the base of the flask, Trypsin was applied to the cell monolayer (TryplE, Invitrogen). 2 ml of Trypsin was introduced to the flask. The flask was placed in an incubator at 37^0C and 5% CO_2 for up to ten minutes. A Leica light microscope (Leica, Germany) with a specialised stage to accommodate culture flasks at 40x magnification was used to periodically monitor the cells to make sure that the cells detached but were not damaged due to toxic necrosis.

When the cells were detached, 10 ml of the DMEM solution (containing 10% FBS) was added to the flask and the flask was gently rocked to wash the cells with the solution. The cells and media solution was transferred to a sterile 50 ml centrifuge tube. The tube was spun in a centrifuge set at 4^0C and 1500 RPM for four minutes to form a cell pellet. The excess media was then removed from the tube leaving the pellet.

10 ml of the DMEM solution (without FBS) was added to the tube. The cells were then spun as before and the above step was repeated. The final spin and wash of the cells was performed using 1 ml of DMEM without FBS. The pellet was pipette mixed until the cells were in suspension.

4.3.6 Counting the Cells

Using a sterilised pipette, 10 µl of the cell suspension solution was transferred to a C Chip Haemocytometer cell counting slide. The slide contains a central grid of 5 x 5 squares of 1/25 sq mm and smaller 4 x4 squares of 1/400 mm. The cells were counted at a 40 x magnification using a Leica light microscope (Leica, Germany).

This cell count figure obtained was based upon the number of cells in 10ul. This figure was then multiplied up by 100 to calculate the total amount of cells in 1 ml. Media was then added to dilute the cell population used to bring cells to a density of 1.5×10^5/ml. Once calculated the cells can be divided in DMEM for further passages, freezing, or applying to the corneas in accordance with the ARVO Statement for the Use of Animals in Ophthalmic and Vision Research.

4.3.7 Organ Culture

The methodology for the organ culture (as outlined by Forman et al., 2006) was introduced in the general methods chapter. The experiment was carried out in accordance with the ARVO Statement for the Use of Animals in Ophthalmic and Vision Research and the Human Tissue Act.

4.3.8 Application the Oral Mucosal cells

10ul of the cell suspension solution was added beneath each flap. Care was taken not to scratch or damage the stroma. The flap was then carefully repositioned using a pipette tip. Dishes were transferred to the incubator set at 37^0C with 5% CO_2. Several drops of DMEM media were applied twice daily to prevent drying. The media was changed every five days.

4.3.9 Returning Corneas to Homeostasis Following Culture

The artificial environment of the organ culture can lead to observable swelling of the corneas. As the cultured corneas are not exposed to the hydrodynamic and mechanical forces found *in vivo* (e.g. blink, tear, and waste mechanisms) and culture

media may cause swelling, it was necessary to devise a non-toxic and clinically acceptable method for returning the eyes to homeostasis. In this experiment, the corneas were placed in a 8% Dextran in DMEM (Invitrogen, UK) solution in a 37^0C water bath for three hours. The clarity of both the cell treated and control corneas improved.

4.3.10 Corneal Pachymetry

A pachymeter is a device which measures corneal thickness in a clinical or *in vitro* setting using a contact ultrasound method. In this experiment, it was important to measure the corneal thickness in order to determine how near the cornea was to a homeostasis. *In vitro*, the cornea is placed in a dish epithelium down and the ultrasonic transducer wand was placed perpendicularly in the centre of the cornea. In the optimisation of the experiment, readings were attempted but were unsuccessful. Due to the swelling of the corneas in the optimisation culture, pachymetery measurements were not able to be taken as the thickness of the corneas exceeded the equipment's limit of 1000 nm. In the final experiment, these difficulties were overcome by the treatment with dextran and drying on the bench for a short period before analysis.

In this experiment, the corneas were removed from the dextran solution and placed on the bench to dry for twenty minutes to further decrease excessive swelling. Three readings were taken using a DGH ultra-sonic Pacchette 2 pachymeter on or near the same area and the results were recorded. Dextran has been used in clinical studies of the cornea, so the use of dextran in human or animal models would be an acceptable practice.

4.3.1 Spectrophotometry

As previously noted, the transparent qualities of the cornea are based in the arrangement of collagen, proteoglycans, and stromal cells along with the maintenance of homeostasis in the fluid regulation of the structure. A change to any of these components would lead to a quantifiable change in the light scattering properties of

the cornea (Freund et al. 1991). For this reason, corneas were measured before and after scarring and at various wound repair time points using a spectrophotometer.

A spectrophotometer is a device which measures the absorbance of light by a substance (in this instance the cornea in a silicon oil suspension to prevent reflection) (figure 4.5). When a light beam is sent through the cornea, as there is no absorbance in the visible range, the instrument measures just the light scatter. In this experiment the beam of white light was passed through a series of filters to produce monochromatic light at 10 nm intervals between 400 nm and 700 nm (the visible spectrum).

Figure 4.5: Pye Unicam Spectrophotometer which was used for experimentations.

The intensity of light (I_0) is measured as it is passed through a blank (i.e. silicon oil). The reason for using a blank is to quantify the scattering of light evident in the measurement cell. It was also important to keep the cell in the same position for each measurement taken in order to standardise cell path length. In the second instance the intensity of light passing through the sample (I) is measured.

The transmittance (T) and scattering (S) factors are then calculated by the following formulae:

$$T = I / I_0 \quad \text{and} \quad S = -\log 10T$$

(Gore, 2000)

A Pye Unicam SP8-100 spectrophotometer was prepared by introducing a 1mm gate to the light source to decrease the width of the beam. A purpose built cornea chamber

(figure 4.6) with two flat machine polished glass openings was filled with silicon oil (Dow Corning 200/5cS,Midland MI USA) (which has a refractive index similar to that of the cornea) and placed into the spectrophotometer 1.5 cm from the gated light source. The chamber was elevated and centred so that the beam passed through the centre of the chamber (figure 4.6).

To obtain a blank measurement, the machine was calibrated to 400 nm and set to a concentration of 100. The wavelength was then increased by intervals of 10 nm until the upper limit of 700 nm was achieved. The concentration was recorded at each interval.

To obtain the measurement, the corneas were removed from culture and rinsed in PBS. The corneas were then introduced to the chamber (see diagram) and the chamber was filled with silicon oil using a syringe. A 5mm valve stopper was placed in the top of the posterior valve and a cap was screwed on. The needle was then injected into the valve and more oil was added. This was to maintain intraocular pressure. Care was taken to entirely fill the chamber and to avoid the introduction of air bubbles which could affect the final results.

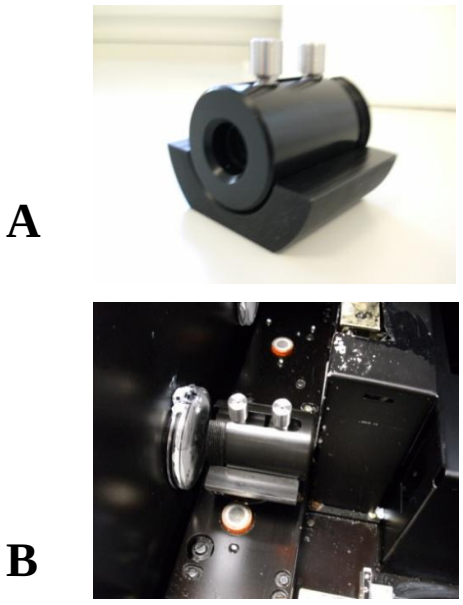

Figure 4.6 : (A) Image of custom design chamber cell used for spectrophotometry. (B) Image of chamber in situ. Chamber design Cardiff University.

The sample/chamber was re-introduced into the calibrated spectrophotometer and the chamber was centred so that the beam passed through the central area of the cornea. For LASIK flap wounds, the height of the chamber was adjusted with glass slides of 1mm thickness so that the light beam enters through the centre of the scar area, 3mm and 5 mm. Eyes which were too small to fit the chamber or where otherwise damaged (e.g. tears along the limbal interface) were not tested in the spectrophotometer however were used for the other forms of analysis.

The interval readings were repeated three times for each sample and recorded in an Excel spreadsheet. The readings were plotted against the wavelength from 400-700 nm. The data was normalised by dividing the blank reading into the sample and multiplying by 100. This provides the percentage transmission of light across the wavelengths.

4.3.12 Extensometer

In this experiment, the force needed to detach the LASIK type flaps was recorded for both the control and oral mucosal samples over the three time-points. An extensometer is a precision instrument used here to measure the tensile strength of the corneal flap at pull-to-break mode (figure 4.7). The extensometer slowly pulls on the substance at a set rate and force measuring the stress and strain on the flap. When the integrity of the flap was compromised, there was a drop in this level of force. The extensometer has been successfully used to evaluate flap strength in cultured tissue in prior experiments (Mi et al., 2010).

In this experiment, the flap strength was measured using a Lloyd Instruments Ltd. extensiometer which was controlled by a computer operated user interface Nexygen 4.1 software package (Lloyd Instruments, Bognor Regis, UK).

Figure 4.7: Lloyd Instruments Ltd. Extensiometer used in the experiment (Mi et al., 2010).

The extensometer was set up with a piece of card with a folded lip which was clamped into the apparatus chuck. The chuck was covered in sandpaper to provide traction. The corneas were removed from culture, gently rinsed in PBS and placed on the bench until the surface appeared matte.

The cornea was attached to the top of the card lip with superglue (Loctite, Ohio, USA) by centralising and resting the posterior upon a cardboard prop. The cornea was gently pressed so that the cornea remained in place. The anterior side of the cornea was attached from above with another piece of card in the same manner. Care was taken to centralise the cardboard lip in the middle of the flap so the seal did not affect the flap edges. The upper arm of the machine was lowered and the card was clamped into the chuck. It has been noted in prior experiments that the superglue does not damage the tissue (figure 4.8).

Figure 4.8: Orientation of cornea onto extensometer. The sample was placed on a card platform and another card arm was attached from above using superglue adhesive.

Corneas which were damaged at the limbus were not used in this experiment as the biomechanics would have been additionally compromised.

The extensometer was activated using the computer interface and the first point of breakage was recorded for each sample tested. Both the stress (MPa) and the force (N) were measured against time. The force reading was normalised by subtracting the reading at time zero. The results were entered into an Excel spread sheet and statistical analysis was performed. Following the experiment, the eyes tested were returned to PFA for further analysis including histology.

4.3.13 Histological Analysis

4.3.13 a) Wax Imbedding Protocol

Following flap tension testing, the sheep corneas were fixed for three weeks in a 10% solution of neutral buffered formalin (Sigma). The corneas were stored at 4ºC. The corneas were removed from the solution and placed in a glass dish. A stitch was used to determine the location of the flap and the corneas were divided into halves using a razor. Once divided, the tissue was transferred to glass jars for dehydration.
The tissue was initially covered in a solution of 50% IMS alcohol (volume/volume with distilled water) and left covered for 30 minutes. The alcohol was removed with a disposable pipette and placed in a 70% IMS alcohol prepared as above for 1 hour. Finally, the alcohol was removed and the eyes were immersed in 90% IMS alcohol overnight. To prevent evaporation of the alcohol, the glass pots were covered and wrapped in ParaFilm™ (Pechiney, UK).

On the second day, the corneas were treated in 100% IMS alcohol for 1 hour, changed, and then treated again at the same concentration for 30 minutes. The alcohol was decanted and in a fume hood the tissue was treated with a 50% volume/volume mixture absolute alcohol/chloroform for 30 minutes. The samples were then treated with 100% chloroform for 30 minutes changed and for another 30

minutes. The chloroform was then poured off and warmed for 10 minutes by placing it atop a warm oven. The tissue was blotted on filter paper and placed into clean wax pots in wax oven. The samples were left for 1 hour to remove the chloroform.

The samples were then transferred to clean wax pots and left for 30 minutes to ensure wax had impregnated all of the tissue. The wax blocks were then hardened on a refrigerated base for 30 minutes and then transferred to refrigeration overnight to further set.

The tissue blocks were sectioned at a thickness of 7 μm using a Lecia microtome (Lecia, Germany) and transferred to Histabond® slides in a tepid water bath. The tissue sections were dried in a 35 ºC oven overnight. The slides were then processed by immersion in Xylene for 2x 5 minutes to remove the wax and placed in decreased concentrations of IPS alcohol for 3 minutes each to re-hydrate the tissue. At 50% hydration the tissue was placed in PBS (Sigma,UK). The tissue was then H&E stained and observed under the Lecia 6000 light microscope (Lecia, Germany) to identify the flap. Once the sections presenting the flap were identified, further slides were prepared with neighbouring tissue for immunohistochemistry.

4.3.14 Immunohistochemistry a-sma

The protocol for processing the tissue for a-sma immunostaining has been outlined in detail in Chapter 2 general methods.

4.3.15 Cell Counting

Cell counting protocol and statistical analysis has been outlined in Chapter 2 general methods.

4.3.16 Small Angle X-ray Scattering

In order to examine the corneas at the ultra-structural level, small angle x-ray scattering analysis were performed on one week oral musocal treated LASIK-type

wounded and control LASIK-type wounded corneas. This was to determine the spacing and diameter of the collagen within the samples (namely at the wound interface). The samples were analysed on Station 102 at the synchrotron at Diamond Light Source (Didcot, England). The samples were scanned from limbus to limbus. The methodology for the scanning of the cornea and analysis were outlined in Chapter 2 of the general methods chapter.

4.4 Results

4.4.1 Corneas Analysed

The corneas were cultured over the three week time points. Due to the nature of the organ culture process, not all of the eyes survived for experimentation. Below is a table indicating which samples were used for each portion of the experiment.

Spectrophotometry	**Oral Mucosal Treated**	**Control**
One Week	N=5	N=4
Two Week	N=7	N=5
Three Week	N=3	N=5
Flap Strength		
One Week	N=5	N=4
Two Week	N=7	N=5
Three Week	N=4	N=4
Average Corneal Thickness		
One Week	N=5	N=4
Two Week	N=7	N=5
Three Week	N=4	N=5
Histology		
One Week	N=2	N=2
Two Week	N=2	N=2
Three Week	N=2	N=2

Table 4.3: Total number of corneas used in each part of the study

4.4.2 Corneal Thickness

The average corneal thickness with standard error for each of the time points is as follows:

Avg. Corneal Thickness	Oral Mucosal Treated	Control
One Week	733.0 µm ± 13.7	747.8 µm ± 50.8
Two Week	703.0 µm ±56.3	745.2 µm ±87.1
Three Week	805.5 µm ±47.4	767.4 µm ±65.1

Table 4. 4: Average thickness and standard error of oral mucosal cell treated and control corneas used in this study at one, two, and three week time-points. Whilst the difference in average thickness was not significant, there was much less variation in the oral mucosal treated tissue.

The overall average corneal thickness between the oral mucosal treated and control corneas did not demonstrate statistical significance. Two tailed t test results demonstrated a p value of 0.76 at the one week time point; p value of 0.571 (two weeks); and a p value of 0.623 (three weeks). The differences in the results were therefore not statistically significant (table 4.4 and figure 4.9).

The most marked difference between the two groups appeared to be the differences in standard error between the two. The control corneas demonstrated a higher degree of deviation when compared to the treated corneas. Between weeks one and three there was no significant difference in the thickness of the control corneas. However, there was a clear trend by the three week time-point of increased corneal thickness for all of the oral mucosal-treated corneas when compared to the one week time point.

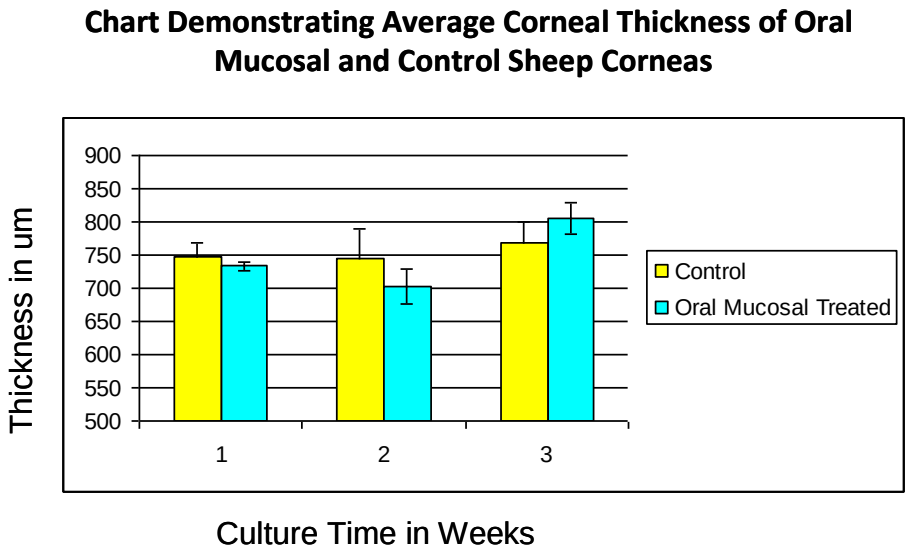

Figure 4.9: Average thickness of corneas (nm) used in the study over three week time period. There was not a significant difference in thickness between groups at each time point.

4.4.3 Transparency

The cell-treated corneas demonstrated greater transparency than the control samples (Figure 4.10) at all three time points. The increase in transparency of the oral mucosal treated when matched to the controls was approximately 10% each culture week. By the three week time-point, the transparency of the cell-treated corneas was similar to that of the controls at one week. In both the cell-treated and control samples, the transparency progressively decreased with time at a rate of approximately 10% with

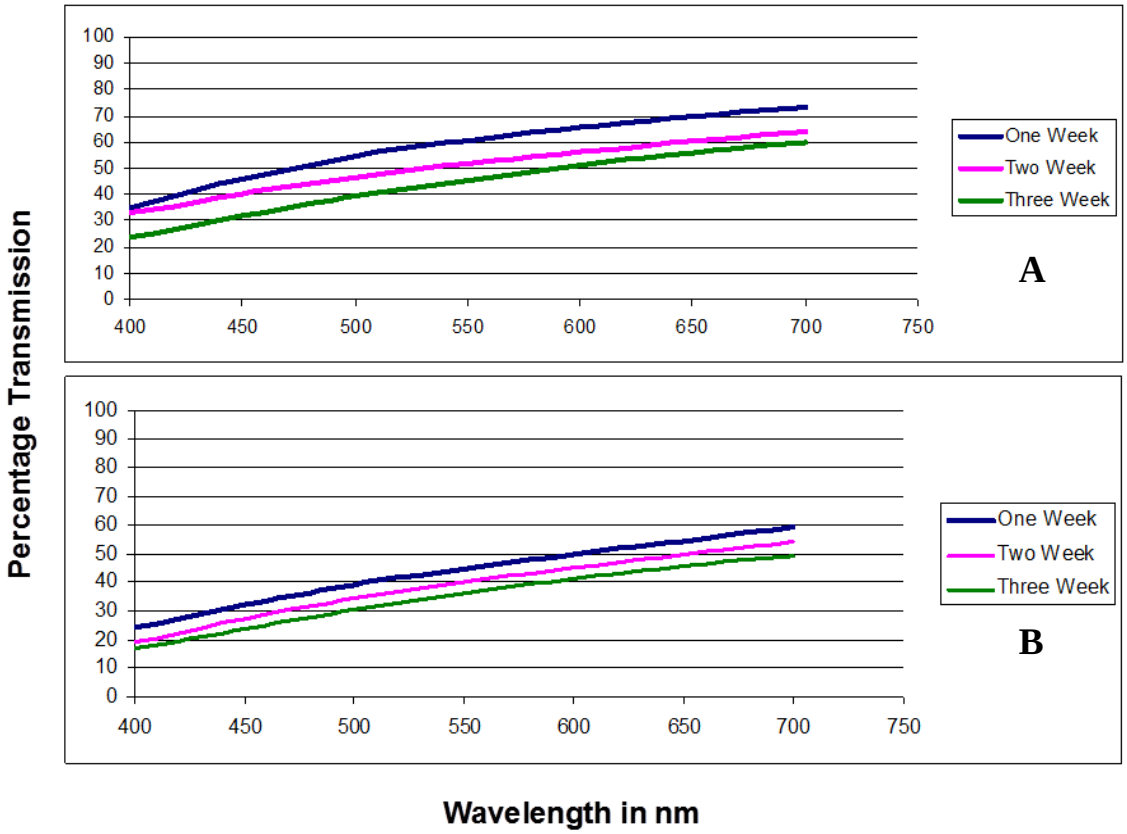

Figure 4.10: Transparency of A) oral mucosal treated and B) control corneas. Within each group there was an approximately 10% decrease in transparency at each culture time point, however the oral mucosal treated corneas demonstrated a higher degree of transparency at each time-point.

each culture week time-point. This trend was observed in both the cell-treated and control corneas and therefore is not thought to impact on the comparative overall results.

At the three week time point, the oral mucosal treated samples demonstrated a significant increase in transparency when compared to the control corneas. At the three week time-point, the thickness of the oral mucosal corneas was also greater than that of the control through the central wound region. Factoring in the greater corneal thickness, the transparency could be assumed to be significantly greater; this could indicate an even better transparency result for the oral mucosal treated corneas at the three week time-points.

The percent transmission measurements were collected at three positions: through the central region of the cornea, at 3mm from the centre and at 5mm from the centre near the peripheral cornea. In the treated corneas, the 3mm and 5mm measurements were

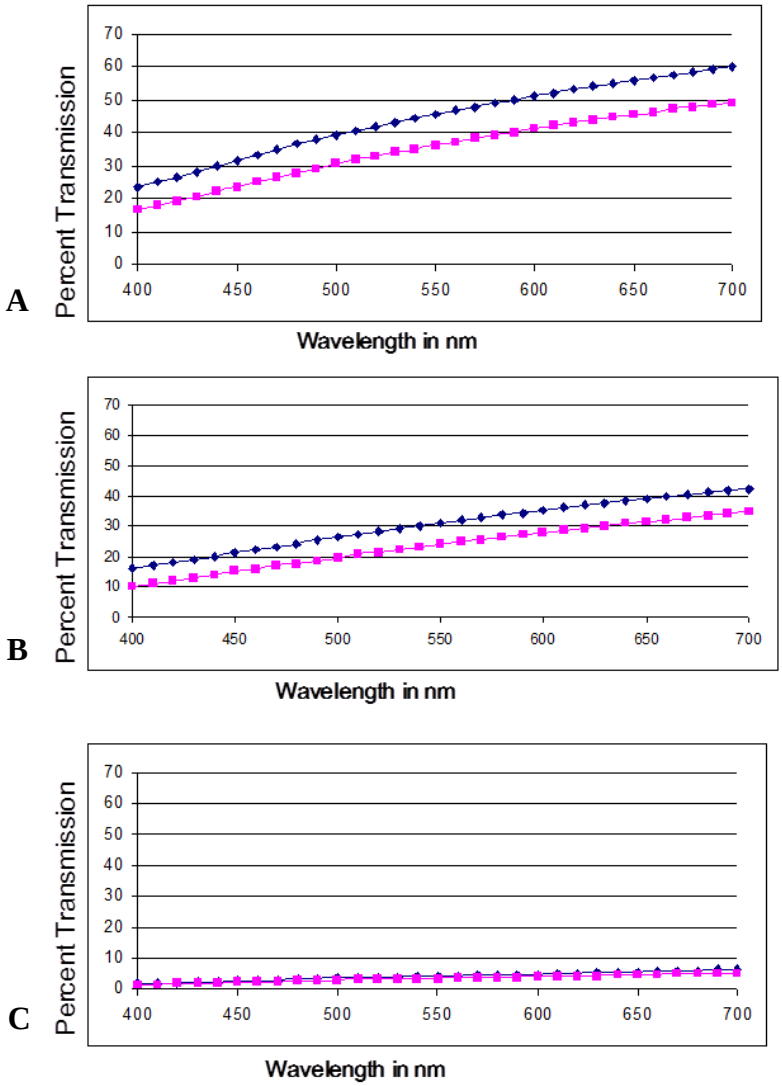

Figure 4.11: 3 week oral mucosal (blue diamonds) and control (pink squares) at centre (A), 3mm (B) and 5 mm (C) as the cornea thickens towards the periphery the percentage of light transmission decreases. The oral mucosal treated corneas also demonstrated clarity over the control corneas outside the wound margin n=3.

outside the flap. The measurements were taken in this manner for two reasons. In previous studies, it had been noted that transparency decreases as tissue thickness increases towards the periphery. In this experiment readings towards the periphery were performed to confirm that any changes noted in the treated corneas outside the wound were not due to this thickness increase. As the transparency readings were performed from the central cornea to the periphery, the transparency decreased for all of the corneas (treated and control) at all time-points (figure 4.11).

The other reason why measurements taken outside the LASIK flap are of importance is due to the possible beneficial effects a treatment may have on the surrounding tissue outside the immediate wound region. The application of an anti-inflammatory agent could result in a down-regulation of inflammation in the entire wound region (and not just be localised to the wound margin or bed). In these cases it would be of interest to note if any beneficial knock-on effects from the cell treated area was evident in neighbouring tissue. At the three week oral mucosal treated time-point, there was an increase in transparency in both the central cornea and 3mm outside the wound when compared to the respective controls. Beyond this region (i.e. 5 mm) the results were similar in both the cell treated and control. This would be expected as in this region both tissues would appear similar to native unwounded tissue (figure 4.11).

The three week cell-treated corneas demonstrated an increase in transparency which could be attributed to the degree of preferential wound healing associated with the oral mucosa (e.g. less inflammation). Outside the initial wound area this trend of increased and preferential wound healing was observed in all of the cell-treated corneas at three week culture point. This could be an indication that the products created by the oral fibroblasts at the three week time-point may reduce the overall inflammatory response. This trend was also observed slightly at two weeks but the difference between the oral mucosal and control corneas were most marked in the three week samples. The increase in wound healing outside the immediate wound region will need to be investigated in further studies to determine if it continues or if the wound area and surrounding region lose transparency.

4.4.4 Flap Strength

The oral mucosal and control corneas demonstrated an increase in mean in flap strengths at the one week time point (figure 4.12). Vertical break points are evident in both the oral mucosal-treated and control corneas. The corneas often demonstrated a series of breaks. The first of these is due to the initial detachment of the flap. Other breaks are indicative of the remainder of the flap separating from the flap bed. In all cases, the first break was used to determine flap strength. The mean flap strength for the one week control corneas was 0.3 N where the oral mucosal treated flaps were detaching at 0.8 N (figure 4.13). This follows the trend established by Mi et al.

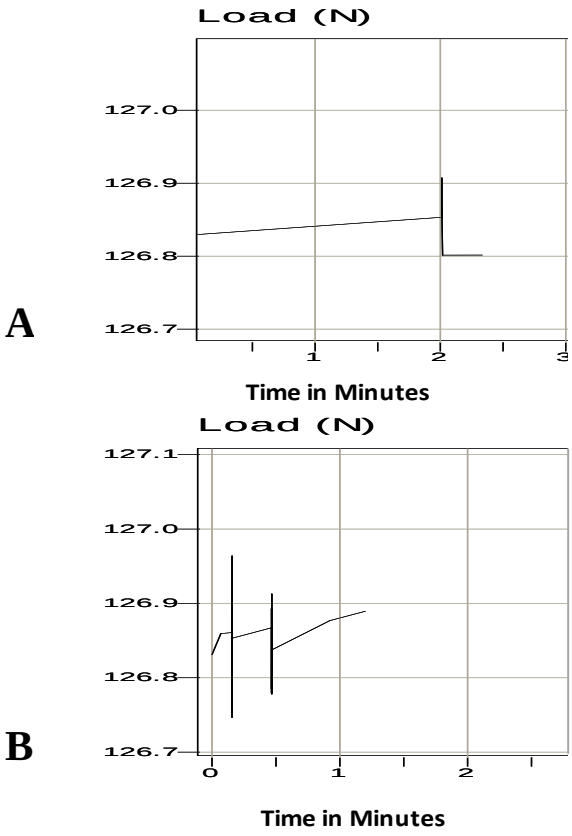

Figure 4.12 : Output graphs from NexGen software. One week extensometer graphs for A) oral fibroblast treated and B) control corneas. The oral mucosal treated flaps demonstrated both cleaner breaks and longer time before first point of breakage (vertical line). Control corneas also demonstrated a more rapid cycle of multiple breaks.

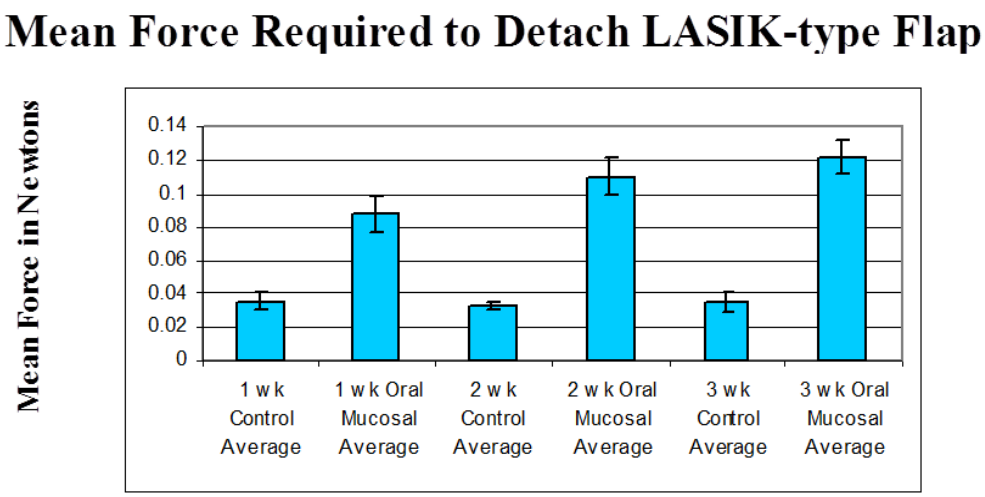

Figure 4. 13: Mean force required to detach LASIK-type flaps in cultured sheep corneas over three week time-points. There is a progressive and significant increase in required flap strength in the cell treated corneas. There is also a higher variation in standard error in the oral mucosal treated tissue.

(2010) and Kamma Lorger (2007) using the same experimental rig. At the two week time point, the oral mucosal-treated flaps were significantly stronger (0.11 N). At three weeks, the oral mucosal-treated flap strength increased, significantly to 0.12 N. This demonstrated a clear trend in flap strength between the oral mucosal treated and control corneas. t-tests (two tailed un-paired) were performed with highly significant p values of p=0.0089 at one week; p=0.0006 at two weeks; and p=0.0003.

There was a higher variability in the flap detachment force in the oral mucosal-treated corneas than the controls. The control corneas all appeared to have a smaller standard deviation and standard error when compared to the oral mucosal treated corneas. This variability could be due to the culture method, the adhesive properties of the cells themselves or it could be attributed to the possible matrix collagen/proteoglycan products synthesised by the oral fibroblasts in the corneal environment. Kamma-Lorger (2007) noted that in the control corneas an epithelial plug forms at the flap interface and that there did not appear to be epithelial infiltration in the organ culture model used. It therefore thought that the existing

The parameters of the extensometer rig did not allow Young's Modulus (Stress/Strain) to be measured in this experiment; that noted, the increase in time to detach the flap could provide information on the physical properties of the flap. The average time to detach the flap was significantly different between the oral mucosal treated and controls (figure 4.14). At all three time-points there was an increase in time for the detachment of the oral mucosal-treated flaps when compared to the control.

Whilst the standard error for the flap detachment times for oral mucosal-treated tissue at the one and two weeks was at the mid to upper threshold of the control, by the three week time-point the increase in time to detach the flap was highly significant (even taking standard error into consideration) (figure 4.14).

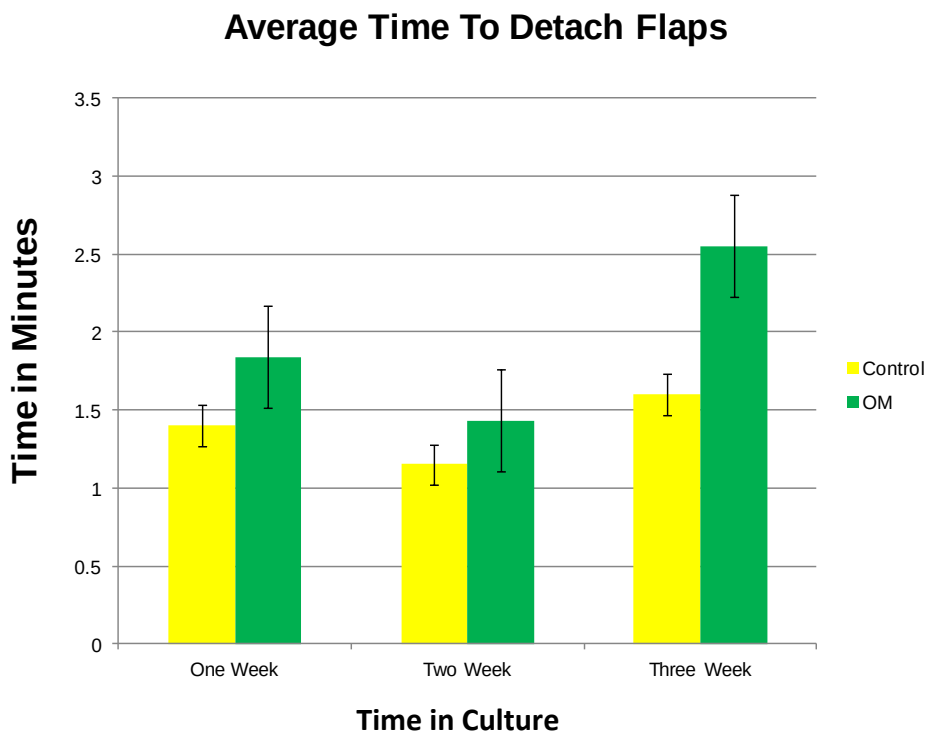

Figure 4.14 : Average time to detach flap. At all three time-points there was an increase in time for the oral mucosal cell treated corneas.

4.4.5 Histology

The H&E staining of the corneas demonstrated the general architecture of the cornea and the location of the flap. There were a few corneal lakes present at the later culture time points, but this may be due to an organ culture or processing artefact. The collagen in the wound bed of the control corneas demonstrated a collagen phenotype of a less fibrotic tissue type in an evenly distributed layer (staining similar to the native surrounding collagen) whilst the collagen bed of the oral mucosal-treated corneas demonstrated less collagen in the wound bed and a more stable sectioned flap.

The immunohistochemistry (a-sma) and Hoechst staining indicated a marked increase in the number of cells present in the cell treated corneas compared to the controls at all three time points. Cell number increased in both the oral mucosal and controls between week one and two. At week three, there appeared to be a significant decrease in cell number in the treated corneas, however it was still higher than the baseline readings at one week. This could possibly be attributed to apoptosis, however TUNEL analysis would be required to confirm this programmed cell death.

Sample	AvgTotal Cells 20x	% Activated Cells
One Week		
Oral Mucosal	**66**	**26.63%±0.024**
Control	**51**	**49.84%±0.134**
Two Weeks		
Oral Mucosal	**148**	**17.10%±0.047**
Control	**64**	**49.11%±3.06**
Three Weeks		
Oral Mucosal	**84**	**21.62%±0.039**
Control	**67**	**41.65%±0.029**

Table 4.16 : Percentage of a-sma activated cells at each time point for oral mucosal and cell treated corneas. There was an overall increase in total cell number in the oral fibroblasts. The treated demonstrated a down regulation in cell activation.

Oral mucosal cells are not thought to stain for a-sma in high percentages (Middelkoop, 2005). Meran et al., (2007) noted that oral mucosal fibroblasts appeared to retain some degree of resistance to TGF-B1. In this study, a-sma was present across the immediate wound bed/margin of the oral mucosal treated tissue but not to the same extent as the controls (figure 4.16). The control corneas demonstrated a high degree of activation along the wound margin and deeper into the wound bed. In the oral mucosal tissue there did not appear to be as much a-sma activation deeper into the tissue (when compared to the control) and the percentage of activation appeared to be consistent at the three time-points without substantial increases.

The oral mucosal activated cells that were located along the epithelium and lower flap bed could actually be the native keratocyte population which had become activated. Another possibility is that the cells are oral fibroblast that have been transformed due to the inflammatory wound healing products created by the damaged corneal epithelium and activated native keratocytes along the wound margin. This could mean that the cells are changed to a more ‘corneal’ phenotype. Whether the cells

activated were the native keratocytes or oral-fibroblasts which have changed phenotype will require further staining using specific oral mucosal/stem cell markers. Overall, the total percentage of activated cells was decreased in the oral mucosal treated corneas, most likely indicating that the oral fibroblast retained their intrinsic preferential wound healing properties.

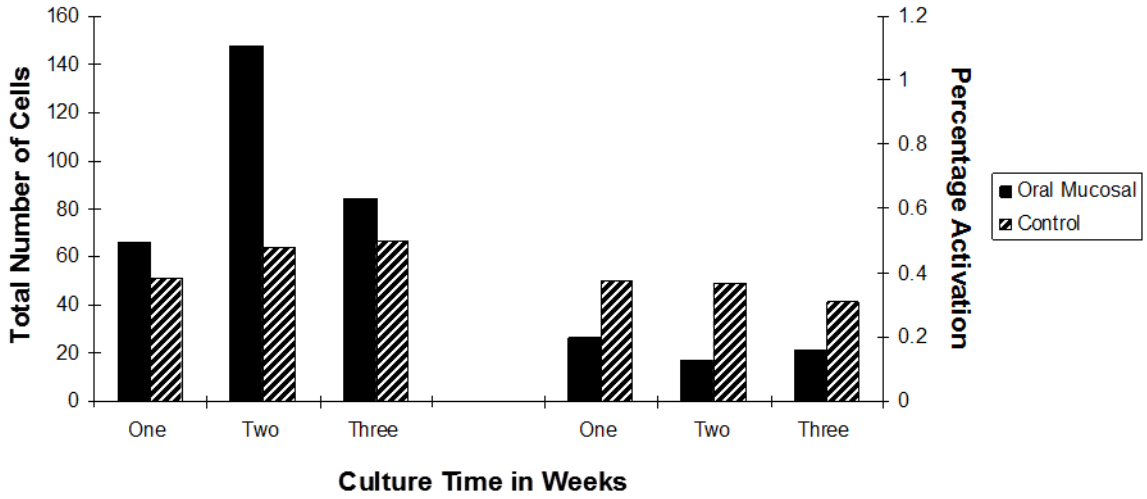

Figure 4.15: Average cell counts and percentage of activated cells. The cell counts for the control remained relatively low. The cell treated corneas demonstrated an increase in total cell number as wound be expected. There appeared to be an increase in the cell population in the oral fibroblasts treated corneas at two weeks which may be due to cell proliferation. There was a decrease in cell number in both samples at three weeks which is most likely due to apoptosis.

In the control corneas, there were very clear thin a-sma filaments of about 10-30 nm evident in the ECM at all of the time points observed but with a marked increase at each time-point (figures 4.16). In Mi et al., (2010), the corneas seeded with activated bovine fibroblasts also demonstrated a high frequency of a-sma filaments in the ECM (note Mi paper in annex). A-sma was present in the cells themselves in both the oral mucosal and control, but it was only in the control that the filaments were detected in the surrounding tissue area including both the wound margin and the wound bed. These filaments were different from the general background staining. To ensure that this is not due to cell death, further studies will require a specific or global apoptosis marker (e.g. TUNEL).

The presence of a-sma filaments in the surrounding tissue of the control samples (but not in the oral mucosal tissue) may be of importance as it demonstrates that the surrounding oral mucosal-treated tissue did not appear to become activated in the same manner as the non-treated tissue. This could support the transparency findings as the oral mucosal tissue was more transparent at all three time-points; there is an established relationship between the presence of a-sma activation and loss of transparency (Mi et al., 2010).

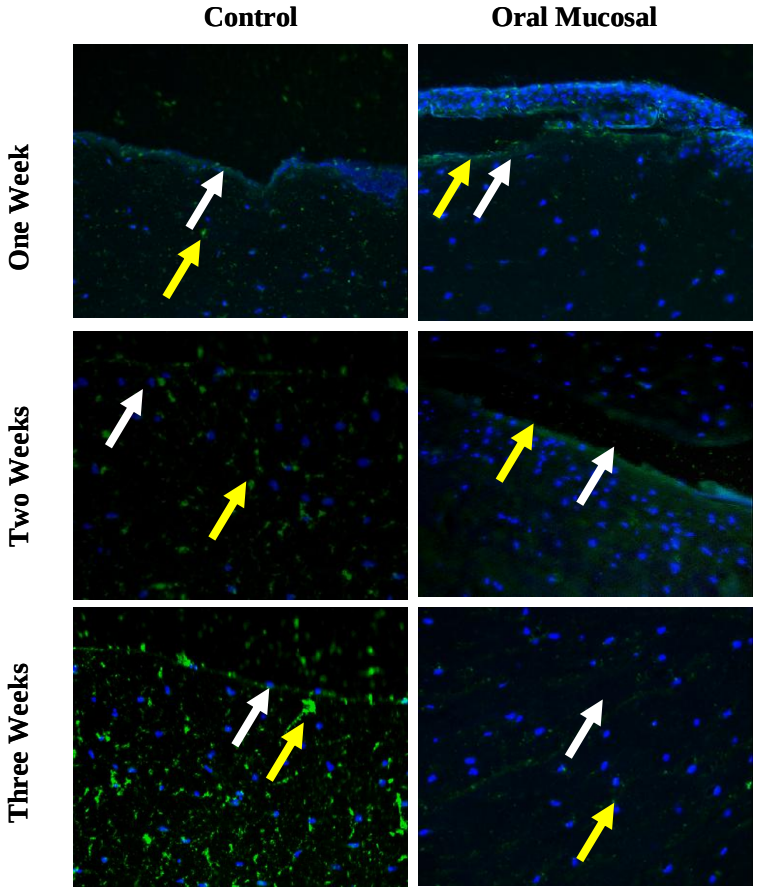

Figure 4.16: Series of images at x 20 magnification of the flap bed of a-sma stained control and oral mucosal treated corneas at each time point. The white arrow indicates the flap bed region. The yellow arrow indicates activation of a-sma in the tissue. In the oral mucosal-treated tissue, the expression of a-sma was low and generally restricted to the flap region. In the control the expression was increased with the presence of a-sma in the cells and as filaments in the matrix.

The overall cell counts were higher in the oral mucosal treated samples due to the initial seeding of cells. At the two week time-point there appeared to be a marked increase in total cell number in the oral mucosal treated samples. This cell number

decreased slightly at the three week time point. This increase in cell number at the two week oral mucosal treated time point may be due to the rapid proliferation which is a characteristic of the oral mucosa. The cells would then normally undergo apoptosis. The control corneas demonstrated a small but steady increase at each time-point.

4.5.6 X-ray Scattering Results

Preliminary small angle x-ray scattering (SAXS) was performed on an oral mucosal treated and a control LASIK-type wounded sheep cultured cornea at the one week (n=1) time-point to determine if there were any ultra-structural changes to the collagen fibril spacing or diameter following one week of wound healing in a culture model. The intention was to repeat the analysis on two and three week culture time-points, but this was not possible due to beam-time limitations so will need to be carried out in the near future.

The small angle analysis was carried out at station I22 Diamond Light Source. The corneas were frozen at -80 °C immediately following culture and stored on dry ice for transport. There is potential for an increase swelling due to the organ culture model. As the corneas scanned were from an earlier test batch, the corneas were not placed in dextran before the analysis.

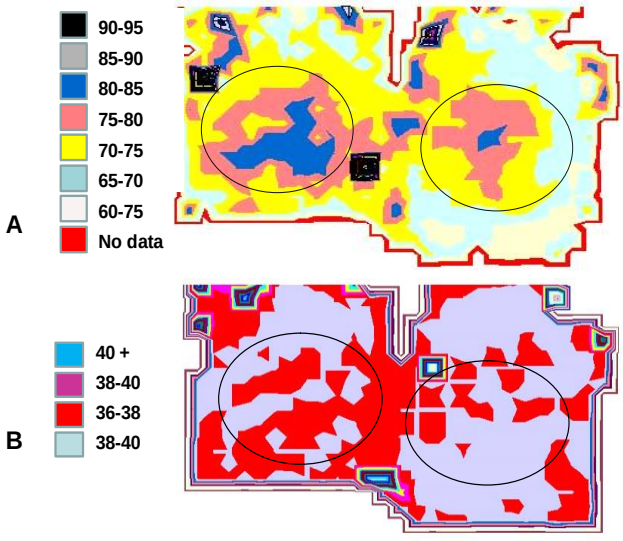

Figure 4.17: Interfibrillar spacing (A) and fibril diameter (B) measured in nm from control (left) and oral mucosal-treated (right) corneas. Oval indicates approximate wound area Average sheep interfibrillar spacing 67.7 ± 5.6 Gyi, Meek et al 1988; Average sheep fibril diameter 37.0 ± 1.8 Meek and Leonard 1993

The cornea treated with fibroblasts (one week culture) had an average interfibriliar Bragg's spacing of 71.49 ±5.9 nm in the wound region and immediately surrounding tissue (figure 4.20). In the untreated cornea the Bragg's spacing was 74.01 ±8 nm evaluating a similar region. The surrounding tissue of the cell treated cornea was is the normal range (as indicated by Gyi and Meek, 1998; Leonard and Meek 1993), however the control cornea demonstrated an increase in spacing out to the periphery. There was a marginally significant difference between the diameter of collagen between the two samples (untreated 35.93 ±2 nm / treated 35.9 ±1). Although small, the treated eye demonstrated consistently lower spacing.

The results at the one week time-point appeared to demonstrate the initial trend of preferential wound healing in the oral mucosal treated samples when compared to untreated samples. Due to resource allocation and beam-time, samples at two and three week time-points were not able to be scanned and evaluated; there are future plans to scan pair matched corneas at further time-points. It would also be advantageous to pre-treat the corneas with dextran to de-swell them towards homeostasis, as was done in the percent transmission studies.

4.6 Discussion

4.5.1 Corneal Thickness

In Figure 4.9 a significant increase in corneal thickness was observed in the oral mucosal-treated corneas between the one- and three-week time points. This could be due to either increased tissue deposition or to tissue swelling due to changes to the proteoglycans produced.

Oral mucosal fibroblasts are thought to produce a collagen/ECM product more similar to that formed during embryogenesis than normal adult fibrotic collagen. Within the oral cavity, this is thought to be due to the high cell/tissue turn-over required due to biomechanical forces from mastication. As discussed in the introduction, these intrinsic cell properties which lead to preferential healing could be the products formed by the cells at the three week time-point and may differ from normal post-wound keratocyte collagen which is normally produced in the cornea. This would

need to be tested with either immunostaining for Type I collagen or determining the wet weight/dry weight of the samples. This will be performed in future studies.

The thickness increase in the flap bed may be due to the additional number of cells which are applied, where a higher volume of cells may indicate more ECM and wound healing products produced if activated. Oral fibroblast populations are thought to have a rapid turn-over time and the increased thickness may be due to additional collagen and proteoglycans which have been laid down in the region.

Whilst the Foreman et al. (2006) organ culture model used in this experiment contains an air/media interface (which is similar to *in vivo*) the model has been demonstrated to produce swelling. In this experiment dextran was used to decrease the overall swelling of the corneas (Borderie et al., 1997) but the hydration may still have been above normal.

One of the three week cell treated corneas appeared to have an increase in thickness as the cornea was drying on the bench. This swelling affect did not appear to adversely affect the transparency (when evaluated by eye) and was swiftly reversed following a brief immersion in physiological salts (PBS). Similar studies using keratocyte derived stem cells in the same organ culture model also demonstrated an increase flap bed thickness in cell treated corneas (Morgan et al., 2012 unpublished). In the Morgan study the corneas also returned to homeostasis when immersed in PBS. This could be a possible indication that there are changes to the proteoglycans in the tissue at the three week time-point. This will require further investigation using TEM, Western Blot, immunostaining, and possibly qPCR to determine changes to the PG content, distribution, and amount. Until PG studies are performed on the wounded tissue, the exact cause of the increased thickness can only be speculated upon.

4.5.2 Mean Force Required to Detach Flap

The wound healing process of the control corneas has been established and there is a known cascade of events. The healing is isolated to the flap margin where keratocytes are activated by damaged epithelial cells (Wilson et al., 2000) with only

rudimentary collagen laid down along the wound bed. This process has individual variations based on endo/exogenic factors; however it remains rather consistent.

Previous in vivo studies on New Zealand white rabbits indicated a range of flap strengths of 2.05 N (converted from gram-force) to 4.0 N to detach the flaps depending on the methodology for flap creation (Knorz and Vossmerbaeumer, 2008). In this in vitro study, the overall flap strength was much lower, but increased in the oral mucosal fibroblast treated samples at the one, two, and three week time-points when compared to the control corneas. The differences between the oral mucosal

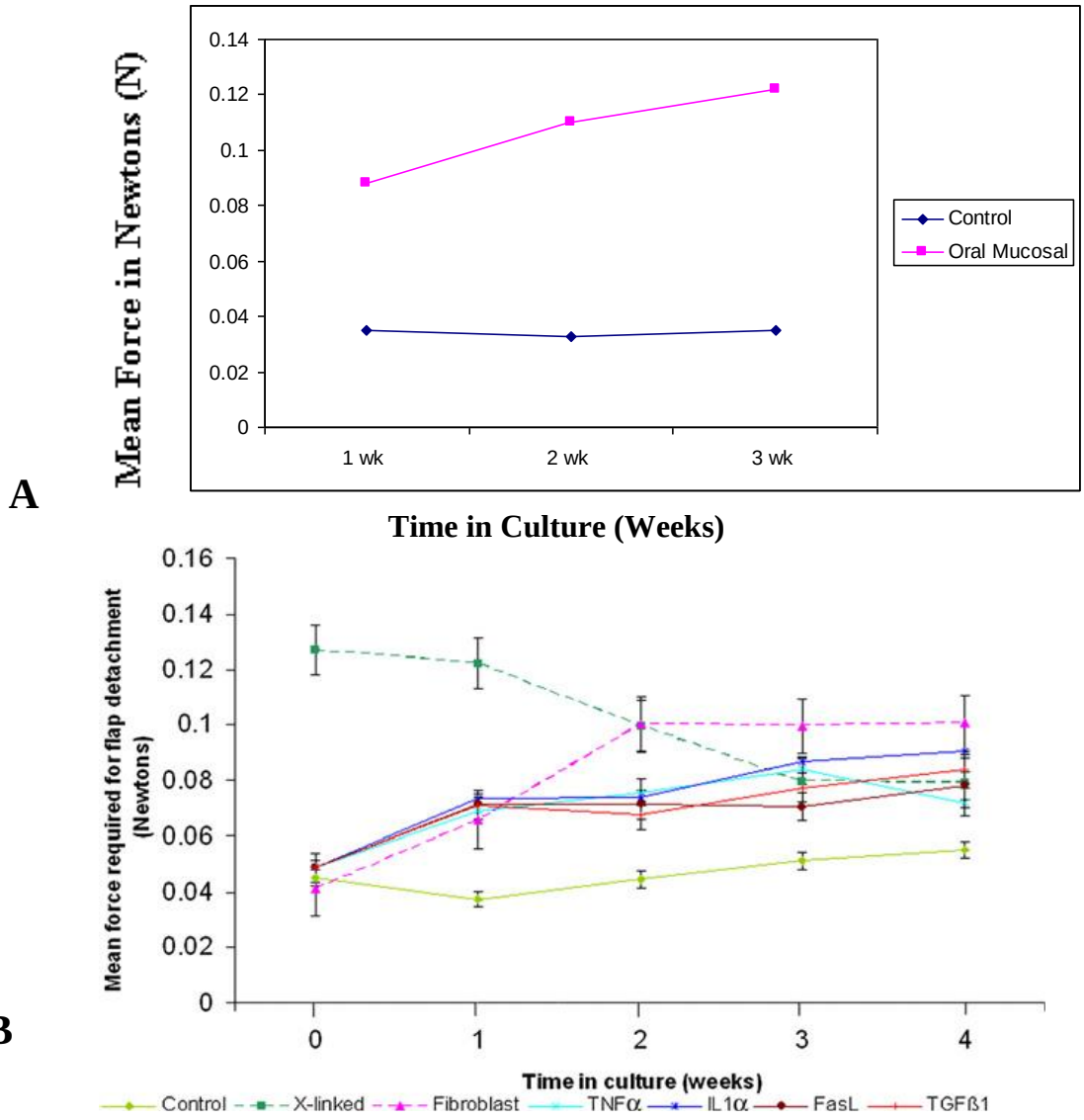

Figure 4.18: A) Representation of mean force required to detach LASIK-type flaps in oral mucosal treated (pink) and untreated (blue) cultured sheep corneas. The control force increased slightly but remained relatively constant. The cell treated flaps required more force to remove the flap and force increased at each time-point. The final flap strength of the flap treated corneas were similar to the keratocyte treated corneas (B) observed in Mi et al 2010

treated and control were highly significant at all time-points however there was a progressive increase in the flap strength of the oral mucosal treated corneas with highly significant results at the three week time-point. When compared to our previous studies (Mi et al 2010, Kamma-Lorger, 2007) the flap strength results for the oral mucosal fibroblasts demonstrated the strongest overall flap adhesion (figure 4.18). In the Mi study, the cultured keratocytes also fibroblasts, but with an 'adult' differentiated phenotype demonstrated the strongest flap results within the experimental set which were similar in value to the results found in this study, however this study demonstrated an even greater flap strength.

It is thought that through applying an increased number of fibroblasts at the wound bed/margin would increase the amount of product synthesised along the wound margin and in the flap bed. With an increase in keratocytes,which are known to produce fibrotic collagen, there is an increased chance of scar formation and a decrease in transparency. This was noted in a number of previous studies (Mi et al., 2010; Kratchmer et al., 2005).

The Mi study also noted that although the overall flap strength increased with traditional activated corneal fibroblasts, there was a visible decrease in the transparency of the tissue. In the general introduction (Chapter 1) it was noted that TGF-B activated cells can produce a-sma which is thought to transform the keratocytes and lead to haze and scar formation (Wilson et al., 2000). In this study, the oral mucosal collagen formed did not appear to produce fibrotic tissue. This is in line with the findings of a number of previous studies performed on oral mucosa, skin, and artificial constructs which have been tested both *in vivo* and *in vitro* (Meran et al., 2007).

The increased flap strength along with the apparent retention of transparency may be due to the unique intrinsic properties of the oral mucosal cells and their products during the wound healing process. This is thought to be more reticular with a high degree of re-modelling. Due to the reticular nature of the collagen, the biomechanical properties are thought to be evenly distributed as opposed to the parallel arrangement of collagen along the wound interface. The oral mucosal fibroblasts appear to

synthesise ECM at similar levels and strengths as activated adult keratocytes (N.B. the similar detachment times) but the products produced appeared to be more transparent when visually assessed.

4.5.3 Time Required to Detach Flap

In the current study it was thought that observing the time taken to detach the flap would provide additional information regarding the physical properties of the collagen and matrix materials produced and their biomechanical properties. Whist the force to detach the flap provides information about the mean flap-strength, the time to detach the flap can provide some additional information regarding the biomechanics of the flap. From a clinical stand-point determining the time taken to detach the flap is of interest for two reasons.

1) As noted earlier in the chapter, traumatic flap dehiscence is common and often serious complication of LASIK and PK procedures

2) The time taken for the flap to detach in the in vitro model may provide information regarding the type of collagen and matrix materials produced (namely the elasticity of the collagen).

The results of the average time to detach the flap demonstrated that there was a significant increase detachment time in the flaps of the oral mucosal treated corneas when compared to the control corneas over each subsequent culture week. The increase in time is clearly evident by the third week. Whilst we did not perform traditional deformation studies on the flaps (stress/stain curves), the increase in time to detach the flap does suggest an increase in elastic properties of the collagen produced. As all elastic materials (especially organic biomaterials) do not deform in the same way, the results also indicate that there is high variability in the time taken to detach the flap in the oral mucosal group than in the control group. This could be due to the suspected higher elasticity of the oral mucosal matrix.

One theory proposed is that the products produced by the oral mucosal cells may be of a more elastic phenotype than normal fibrotic corneal collagen. This could explain

the additional time required to detach the flap rather than a strong clean break which would normally be indicative of a less compliant material. As with the mean force to detach the flaps, there was also a higher degree of variability within the oral mucosal group when compared to the control. This may also be the result of the alternative collagen/proteoglycans synthesised by the oral mucosal fibroblasts.

The increased flap strength in the oral mucosal LASIK injured corneas indicates that there may be an increase in collagen production along the flap bed and wound edge or there may be an increase in strength due to the cells sticking to the surrounding ECM. As noted in Mi et al 2010, fibroblast (corneal keratocyte) treated corneas produced similarly increased flap strength (.11-.12 Newton) (figure 4.14). Overall, however, the oral mucosal treated flaps appeared to be less fragile when compared to the controls.

Randleman and Dawson (2008) measured the tissue elasticity based on Young's modulus by cutting LASIK treated corneal strips and loading the strips along their long axis. Whilst determining elastic deformation in this way provides some information regarding the mechanical strength of the tissue (and the total force required to deform the tissue or detach the flap), the cornea is a viseo-elastic material and events such as flap dehiscence rarely, if ever occurs along the x and y axis. Most flap dehiscence would occur with more of a sheer motion or a compressive motion with a degree of torque. Randleman and Dawson note this in their paper as well and suggest that further experimental designs may be required to better match *in vivo* injuries (Randleman and Dawson, 2008).

The most common flap dehiscence injuries usually occur following eye injury, rubbing, or injury from sport, namely martial arts or other contact sport. In the future, it would be of advantage to measure the sheer forces applied to the flap as this would indicate a result similar to *in vivo*. For this experiment we did not have the access to equipment to test for sheer so measurements were taken along the y axis, similar to Randleman and Dawson, however their study used strips of tissue and not the whole cornea/flap.

The mechanical testing equipment used in this experiment was able to capture stress, however strain was not recorded because the extensometer was not set up for this measurement. For this reason only force in N (or stress in MPa) over time was measured. With the greater force needed to detach the flap along with greater time, there is an initial indication that the attachment is more elastic in the cell treated corneas. If the results do indicate a strong but more elastic tissue type (which is also associated with more reticular tissue and younger tissue e.g. foetal tissue), then there is the possibility that this tissue may withstand sheer forces by displacing and evenly distributing the mechanical forces (Squire and Kremer, 2001).

In the introduction, it was noted that the oral mucosal fibroblasts produce small elastin fibrils (oxytalan) which are randomly dispersed within the loose collagen layers and present in a more orderly configuration in the lower levels of the lamina. This may explain why the collagen produced in this study appeared to be more elastic than the collagen produced naturally by the corneal keratocytes (Roodenburg, et al., 2000). This may also indicate why the elasticity of the tissue appeared to increase over the three week period with the increased production of the collagen and matrix products over time.

Further studies would be required to better understand the exact type of matrix which is produced. This could be done using immunohistochemistry to stain for elastin and oxytalan products in the wound bed of cell treated and normal corneas. Determining the expression of matrix components could also be performed using gene assays. In addition, a new method of measuring stress/strain could be developed to more conclusively provide information on the elastic properties of the tissues.

4.5.4 Transparency

The results obtained from spectrophotometry followed several established trends some which have been noted in other corneal transmittance studies. The two main trends are:

1) An overall trend of the oral mucosal treated wounded cornea to transmit more light across the visible spectrum than the untreated control corneas

2) An observed decrease in transmittance as the thickness of the corneas increased from the central cornea through the periphery.

Quantifying the thickness of the tissue studied is an important factor in determining the transparency of the tissue (Farrell and Hart, 1969; Cox et al., 1970; Doutch et al., 2008). Spectrophotometry performed as standard in eye banks has measured corneal transmittance hours to days after death and has indicated that corneas begin to swell and present a reduction in transmittance levels over this period (Ventura et al., 2002).

Taking into account the increased thickness of the oral mucosal treated corneas in this experiment, the transparency of the treated corneas were still greater than that of the controls, which was unexpected in view of the inverse relationship between thickness and transparency.

Although some degree of swelling may be attributed to the culture process (e.g. the gradual slowing of endothelial metabolism in the enucleated cornea), this could not be related to the observed transparency changes in the oral mucosal-treated corneas particularly at three weeks because these remain very clear. This trend was also observed in human stem cell treated corneas tested by the group (Morgan, 2012 unpublished). An alternative hypothesis is that the components of the newly deposited matrix possess highly transparent properties, which holds enormous potential for future tissue engineering and regenerative medicine applications.

There was also a trend in all of the corneas that the transparency gradually decreased from centre to periphery. Doutch et al., (2008) noted that as transmission readings are collected over the visible spectrum from centre to the periphery the amount of light transmission gradually decreases. Our findings confirm this; across both the cell treated and control corneas there as a decrease in light transmission from centre out to 5 mm. It should be noted, however that, compared to the controls, there is an increase in light transmittance especially at the three week time point immediately outside the wound (at the 3mm position). This improved healing noted in the central wound region was observed outside the wound area in the three week oral mucosal treated corneas. Part of the reason for this may be the overall down regulation of TGF-B induced cell activation or a decrease in the apoptosis process (due to traumatic cell

death), which would extend beyond the flap incision. It may also be due to an alteration in matrix components or a change in other biochemical signal cascades activated during the wound healing process.

4.5.5 SAXS Data Mean Spacing and Diameter: Treated vs. Untreated Corneas

Cornea treated with oral mucosal fibroblasts at the one week culture had a Bragg's spacing of 71.49 ±5.9 nm. In the untreated cornea the Braggs spacing was 74.01 ±8 nm. The Bragg's spacing for normal un-injured sheep cornea has been noted to be around 67-68 nm. Kamma Lorger et al. (2007) noted in similar wound healing studies on bovine corneas (LASIK and PRK) where there was an increase in Bragg spacing following wound healing. This increase is thought to be due to the original mechanical disruption of the tissue, inflammatory responses of the tissue, and changes in tissue hydration during the wound healing process. Whilst both the control and wounded corneas demonstrated an increase in spacing from normal, the oral mucosal treated tissue presented spacing nearer to homeostasis. Further studies would need to be performed on a higher number of samples as well as additional time-points. It would be of interest if this wound healing trend continues in the subsequent time-points.

There was little difference between the diameter of collagen between the two samples (untreated 35.93 ±2 nm / treated 35.9 ±1). Although small, the treated eye demonstrated consistently lower diameter in the wound region. This was closer to the normal diameter proposed for sheep of 34 to 35 nm. Although the difference was almost negligible, it was less in the treated eye. Meek and Leonard (1997) noted in wound healing studies of rabbits that there was a change in collagen spacing following injury, but collagen diameter appeared to remain unaltered. This is consistent with their findings where the spacing was altered but the diameter did not appear to change. It is thought that the diameter of the native collagen would remain unchanged with the exception of mechanical injury. Fibroblasts are not fully activated and motile until the one week time period; it would be of benefit of perform studies on two and three week time-points to determine if there was an increase in fibril diameter due to the laying down of new collagen.

4. 5.6 Histology

Meran et al. (2007) performed analysis on the oral mucosa when compared to skin. The study noted that the skin fibroblasts demonstrated an increase in a-sma activation when exposed to TGF-B. Mi et al., (2010) and Kamma-Lorger, (2007) demonstrated that the corneal keratocytes (fibroblasts) also produced a high degree of a-sma when activated and placed in a wound healing model. In the event that the oral mucosal fibroblasts demonstrated a high degree of resistance to the TGF-B induced differentiation and was able to proliferate using a different bio-chemical pathway. If the oral mucosal fibroblasts are not activated in the same way, the collagen and matrix products would differ from a-sma up-regulated tissue.

The overall cell count numbers demonstrated an increase in total cell numbers in the oral mucosal treated samples at all time-points when compared to the controls. This would be expected given the cell volume which was applied to the flap beds at the initial time of the experiment. This was also found to be true in the Mi et al., 2010 study. Both the oral mucosal treated and control corneas demonstrated a slight increase in total cell number at each time point. This is most likely due to the proliferation and migration of the cells during the wound healing process. Oral mucosal cells are known for rapid proliferation as a high cell turn-over is necessary for maintaining the oral surfaces due to the biomechanic and hydrodynamic forces of mastication and digestion (Cutright and Bower, 2005).

The percentages of cell activation of the control corneas were consistent with the literature (Mi et al., 2010). The percentages of cell activation of the oral mucosal corneas were overall much lower than the controls (about half). It was originally thought that the oral mucosal cells would not present any a-sma activation around one week based on other *in vitro* studies (Wong et al., 2009). It was surprising that in this study the one week fibroblast treated cells appeared to demonstrate a degree of activation of a-sma in both the suspected native fibroblasts along the flap bed lining and wound margin, but also small amounts in the central portion of the flap bed at one week.

Whilst the a-sma expression in the oral mucosal treated corneas was much less than in the control corneas where there were definite bright strands of a-sma detected within the cells and neighbouring tissue, a limited amount of activation was still present at the first week time-point of the oral tissue. The a-sma in the oral treated tissue all but disappeared at the two and three week time-points. These findings are consistent with Funato et al., 1999 where there was noted a rapid a-sma expression in days 2-10 in wounded oral mucosal tissue that sharply decreased from day 14. The group also noted high levels of apoptosis in their study.

In this study, TUNEL analysis and detection of caspase activity (specifically caspases 9,3,12) were not performed on oral fibroblasts and control corneas. These studies would need to be carried out on the tissue to determine the suspected end fate of the oral mucosal cells (Darzynkiewicz et al., 2008; Ti et al., 2003). There will also be scope for additional fluro-labelling to determine which cells are being affected. There appeared to remain very high levels of oral mucosal cells in the flap at all three stages of the study. It would be of interest to carry out the experiment to establish that the cells are in fact oral mucosal cells and to determine if, when and how these cells undergo apoptosis.

4.5.8 Overall Observations for Variation

With all organ culture studies, there is a high level of individual variability in wound healing process, tissue and cell quality. Whilst this could present an impact on the final results, a high population number and proper culture model can provide results appropriate for early stage wound healing research. The tissue used in this experiment was collected on the day of slaughter however there was a high degree of variability of the quality of the tissue. Care was taken to select individual healthy corneas of standardised size.

In some of the corneas evaluated for this experiment, especially in the early stages of optimising the protocol, there was a degree of fungal contamination which was evident in some samples. These were discarded and not included in the analysis. The experiment had to be repeated to ensure that the cultured corneas were of the highest quality. It is hoped that in the future study including *in vivo* animal models that these

difficulties will be overcome and the only variation will be in the wound healing of the individual. The in vivo study will also be of benefit as the treated and untreated left and right eyes of the individual animal can be evaluated as a matched pair.

The initial Mi et al. (2010) and Kamma-Lorger (2007) studies were performed on bovine corneas. In this study, ovine tissue was used as it is of similar size and overall thickness to human tissue and would fit more appropriately in the experimental rig for the spectrophotometer. One drawback to ovine tissue, is that it is known to swell more in organ culture when compared to bovine, human, and porcine tissue. This can lead to variation in the overall thickness and quality of the cultured tissue. Between the first series of cultures and the final study, it was decided that the corneas would be placed in a dextran solution to decrease the amount of swelling in the cornea. As previously discussed, this swelling may be due to the organ culture model. If there remains swelling in the *in vivo* study, then dextran has been used clinically as a topical agent in other ocular procedures (e.g. cross linking studies). In theory this stage could be applied to the *in vivo* model.

Some of the cell treated corneas appeared to be a bit more swollen and thicker in the central flap bed especially at the two week point. It is currently not known if this increased swelling is due to an individual variation, is an artefact of the culture model, or may have a biomolecular cause. In spite of this observed thickness, the central corneas of the cell treated samples remained more transparent than the controls. This is generally counter-intuitive to the thickness/transparency light transmission rule so if this may be due to increased clarity of the extra collagen produced by the oral mucosal fibroblasts mitigating the changes due to swelling. Even where the pachymeter results were normal or near normal, the tissue appeared to be a bit different from the one and three week tissue with a much clearer central flap region.

The division of cells and their Hayflick numbers were discussed earlier in the general introduction. Researchers at Cardiff University school of Dentistry determined that oral mucosal cells undergo a longer culture life than adult somatic cells. Whilst they are able to survive for longer, the cells do eventually slow and proliferation generally decreases. In the initial study we found that the cells began to slow down around passage week 10-12. It is therefore important to utilise the cells within the appropriate

window. Using cells of different ages could produce a high degree of error in the transparency (maybe some cells were more activated that the others). In future studies, it will be of interest to see if different cell passage time points lead to increased or decreased wound healing.

Evaluation of Corneal Scar Tissue Following a Twelve Year Post-operative Penetrating Keratoplasty for the Treatment of Keratoconus

5.1 Introduction

Keratoconus (KC) is a progressive disorder of the cornea where the cornea steepens into a 'cone like' shape which adversely affects vision. In advanced cases corneal replacement surgery (penetrating keratoplasty) may be required. Following surgery, a scar is formed along the border of the graft altering the collagen orientation, distribution, fibril diameter, and spacing (Kirkness et al., 1990; Brierly et al., 2000). It is also thought that following corneal surgeries such as PK the normal biomechanics of the cornea may be disrupted resulting in loss of corneal curvature, reduction of IOP and an increase in corneal ectasia (Alio et al., 2002; Pramanik et al., 2006; Simmons et al., 1989).

The structural changes associated with keratoconus are found in the central 2/3 of the cornea and result in a high degree of visual impairment due to changes in refraction (Wilson et al., 1991). The disorder is also characterised by corneal thinning, protrusion and scarring. This results from the formation of ulcerations due to biomechanical induced abrasions from the eyelid rubbing against the corneal surface. In some patients abnormalities of the tear film are found and these may contribute to the discomfort (Smith et al., 2001; Dogru et al., 2003).

The first course of treatment is generally the prescription of soft progressing to rigid contact lenses. Due to the changes in corneal shape and the progressive nature of the disorder the required lenses tend to be ill fitting and can lead to corneal ulcers. This has additional impacts on corneal health as recurring ulcers can lead to permanent corneal damage (Dana et al. 1992; Hartstein and Becker, 1970). Even when at best corrected vision, patients with KC regularly complain of visual disturbances (Dana et al., 1992).

It is thought that KC affects between one in two thousand to three thousand individuals in the general population. There has been much debate as to the exact incidence of KC due to variation in classification (e.g. some ophthalmologists include

other conditions such as extreme astigmatism and pellucid marginal degeneration under the wider umbrella of KC) (Rabinowitz, 1998). Despite the discrepancies in numbers, KC remains one of the most common ocular disorders. KC was originally thought to be a universal disorder not attributed to any geographical, ethnic, social or cultural groups, however some studies indicate a male bias (although this is contested). The disorder is also generally diagnosed during or slightly after the onset of puberty into early adulthood and gradually progresses over time. The corneal changes which occur may present bilaterally, or in individual eyes. The disorder can gradually develop over one or two decades and then stabilise, however each patient is different (Krachmer et al., 1984).

There have been suggestions that there is both a genetic and environmental component to KC. Some researchers have suggested that excessive contact lens wear, eye rubbing, dry eye or allergy may also be contributing factors. It is thought that there could be a combination of factors with those being predisposed genetically increasing in risk due to behavioural or environmental factors. Other studies have noted an increase in frequency in patients with underlying Ehlers Danlos and Leber's disorders (Krachmer et al., 1984; Rabinowitz, 1998).

5.1.2 Biological and Physiological Changes Associated with KC

Although KC is classified as a non-inflammatory disease which results in the thinning of the cornea's stroma, recent molecular research has indicated that there are a number of underlying abnormal biological factors which may contribute to the disorder. The molecular biology of the KC cornea is presently poorly understood (Rabinowitz, 1998). A number of theories have been suggested that it is caused by a degeneration of the anterior cornea. There are thought to be varying degrees of pathology especially to the epithelium, Bowman's and stroma (Kenny et al., 1997; Scroggs and Proia, 1992).

KC corneas have also been known to have a reduction in tear break up times which are known to have a knock-on effect on epithelial health and homeostasis. As the symptoms of KC progress the tear film becomes more pathological. This can cause a damaging cycle where the epithelium degenerates and then causes further problems to

the tear function. Epithelium degeneration has also been associated with damage to the unmyelinated nerves which can lead to further anterior eye complications (Krachmer et al., 1984; Brookes et al., 2003).

Some studies found a reduction in a-1 proteinase and a-2 macro-gloublin which normally act as proteinase inhibitors in the corneal epithelium and stroma (Sawaguchi et al.,1990). There is also thought to be an up-regulation in enzymes which target and degrade extracellular matrix (ECM) proteins. These enzymes could lead to the progressive abnormal degeneration and thinning of the tissue (Sporel et al., 2004; Abalain et al., 2000).

Keratocytes in the keratoconic individual have been noted to express four times the amount of Interleukin 1 (IL-1) cell surface receptors which promote an inflammatory cascade (note Chapter 1). An increase in IL-1 uptake can lead to apoptosis and programmed cell death in cells within the activation zone. A loss of keratocyte cells can lead to abnormalities in the production of collagen and matrix (Wooj et al., 1999). Within the KC affected stroma there are thought to be abnormal numbers of keratocytes; in some cases the existing keratocytes appear to be hyper-reflective indicating previous cell activation without evidence of direct prior injury. Wilson et al. (1997) noted that in some viral and inflammatory diseases keratocytes may undergo apoptosis causing thinning of the corneal stroma. This could be a similar to what occurs during KC apoptosis. TUNEL studies have indicated that the majority (60%) of the central portions of the keratoconic corneas presented indicators of programmed cell death (Kim et al., 1999).

The bio-molecular pathways associated with apoptosis (Fas-L, cytochrome c, ER stress, increased caspase activity) are also highly inflammatory cellular responses which may be associated with keratoconic changes on the cellular level. There are also thought to be abnormalities in the overall levels of free radicals present in the KC corneal tissue. It is thought that an increase in free radicals along with an increase in cell stress exasperated by the overproduction of aldehydes and degenerative enzymes as previously discussed, could lead to irreversible keratocyte activation (Kenney et al., 2000).

More recent research has explored the genetic causes behind keratoconus. There has been some clinical evidence which associates the disorder with other collagen/connective tissue disorders such as Ehlers Danos and Marfan's Syndrome and other genetic disorders like Down Syndrome (Krachmer et al., 1984). In a minority of subjects there is thought to be an inherited component to the disorder, however the majority of cases are not thought to be hereditary. The unclear pattern of inheritance, along with the complexities of the various ocular components associated with the disorder, has made it difficult to determine the exact molecular cause. At present, many genetic studies have been performed to rule out different coding genes for collagen in the hope to narrow the field down and thereby hit upon the true gene(s) responsible (Edwards et al., 2001).

Eye rubbing has been put forward as a major contributing factor to the disorder and is also thought to run in families (either through genetic predisposition or through learned behaviour). Eye rubbing may be linked to the dry eyes, tear film deficiencies, or environmental factors (e.g. dry, arid, and high altitude) (Karseras and Ruben, 1976). It is thought that those pre-disposed to excessive and pressurised eye rubbing may undergo increased levels of apoptosis in the corneal epithelium. The inflammatory products released following cell death may lead to a release of epithelial cytokines associated with wound healing and inflammation. There is also a proposed link between eye rubbing and a localised increase in IOP (McMonnies, 2007).

Excessive eye rubbing is also thought to promote changes to the un-myelinated nerves which feed through the stroma to the epithelium. There is thought to be a decrease in the total number of nerves and an abnormal thickening of the individual nerve fibres near the anterior stroma and epithelium (Mannion et al., 2007). Damage to the neural feedback system could affect tears, cell migration and proliferation, communication between epithelium and stroma, and loss of overall sensations. This loss of sensation could contribute to further increased eye rubbing pressure promoting the cycle (Kenny and Brown, 2003).

It should be remembered that not all of these symptoms are found bilaterally or in every individual. As the disease presents itself differently over the progress of many years, it is also thought that some or all of the symptoms may be time dependent with

processes such as increased cell death occurring during specific time windows. This high level of individual variation is a main contributing factor to the diagnosis, treatment and management of the disorder (Scroggs and Proia, 1992).

5.1.3 Biomechanical and Ultra-structural Changes

Patients with KC present a number of clinical difficulties and visual aberrations. The alteration of the cornea's shape changes the refractive index of the eye resulting in blurred and double vision. Keratoconus involves marked changes to the cornea's morphology and biomechnical strength (Andressen et al., 1980). The central cornea thins and steepens whilst the peripheral collagen is thought to increase in thickness and collagen bulk. One theory proposed is that the existing collagen lamellae begin to slip, shift, and possibly unravel (Meek et al., 2005). This may be due to a degeneration of the complex extracellular matrix as discussed previously in the chapter.

The changes associated with the corneal collagen are at the lamellar level; the interfibrilar spacing between the collagen and the diameters of the individual collagen fibrils remain unaltered so the cornea itself retains transparency (Fullwood et al., 1992). In some keratoconic patients there may be some complex associated pathologies which result in a clouded cornea, however overall it is thought that in uncomplicated KC the results is a misshapen albeit transparent cornea. As the lamellae in the anterior stroma are thought to become thin and disordered (with a shift of collagen bulk to the periphery), the apex of the progressively developing cone tends to be orientated in the central nasal position. It is at this point where the collagen is at its thinnest. This partial thinning directly impacts on the visual axis leading to a change in refraction (Meek et al., 2005).

In the normal cornea collagen is ordered along horizontal and vertical meridians with a more orthogonal arrangement in the centre of the cornea. The collagen at the periphery then changes direction to create the annular ring (note Chapter 1) (Wang, 2009). In the KC cornea the angle of the collagen shifts to around 20°-160° in the affected portion of the cornea. Most of the changes to collagen orientation are thought to occur at the apex of the cone with much less alteration at the base. The

orientation of the collagen in the periphery of the keratoconic (KC) cornea remained a puzzle as in vitro studies focused on the button removed from the central portion of the cornea (Daxer and Fratzl, 1997).

There have been a number of recent ultra-structural studies of the KC cornea using SAXS and WAXS analysis (Meek et al.; 2005; Daxer and Fratzl, 1997; Hayes et al., 2007) as well as second harmonic generation confocal microscopy (Morishige et al., 2007). Studies have included TEM and X-ray scatter analysis of collagen orientation and distribution. These studies found a marked decrease in the total amount and total alignment of the collagen. The orientation of the collagen in the central portion of the cornea has been found to present regional areas of collagen disorder across the cornea (figure 1). The previous drawback has been that studies were performed on the post-operative trephined button of keratoconus tissue removed during penetrating keratoplasty surgery. This is generally preformed in advanced cases and is limited to the central 9 mm of the cornea. There are also a number of changes which occur in the limbus/annulus of the KC cornea which will be discussed in further detail in the following chapter (Chapter 6). At present, the changes which occur in the periphery of the native keratoconus tissue are presently poorly understood.

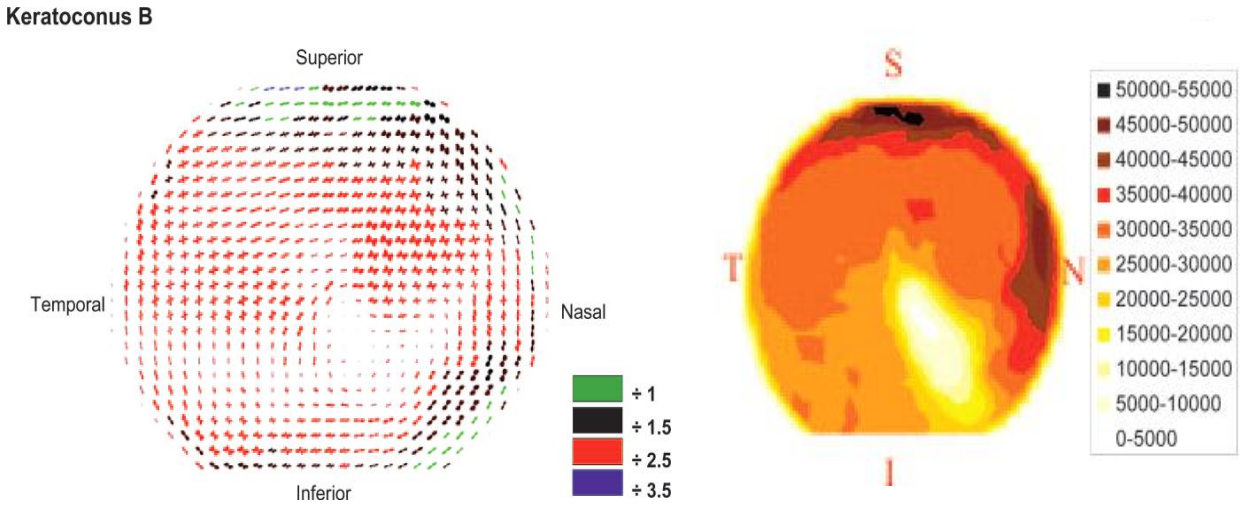

Figure 5.1: Left image collagen orientation map of the trephined centre portion of an advanced KC cornea. Nasally, the central/inferior collagen is very thin and the surrounding collagen is disordered. The collagen along the periphery is of a higher intensity and more ordered as would be expected. The right image shows the distribution of total collagen (arbitrary units) in the same cornea. In this figure the loss of collagen at the KC peak is clearly evident along with the increasing alignment out towards the periphery. Meek et al., 2005

The exact nature of how the ultrastructure of collagen in the KC cornea begins to change is presently unknown. Earlier in this introduction the theorised molecular degeneration of the cornea was discussed. It is thought that the enzymatic or free-radical damage to the cornea could lead to a breakdown in the ECM 'glue' which bonds cornea lamellae and allows them to slip (Hayes et al., 2006). The other theory is that there is a degeneration to the collagen or damage to the collagen producing keratocytes which leads to a loss of collagen. It has also been proposed that there is a progressive 'unravelling' of the collagen lamellae with a detachment of the collagen from the Bowman's layer (figure 5.2) (Meek et al., 2005; Bron et al., 2010).

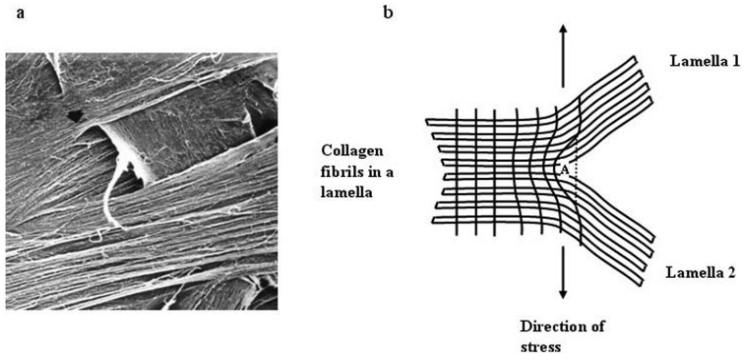

Figure 5.2: a) Collagen lamellae demonstrating the different stacking layers. b) schematic demonstrating the possible changes which may occur during KC progression. The collagen layers may 'un-zip" from each other leading to instability. Meek et al., 2005

Another biomechanical change which may occur during keratoconus is the rupturing, stretching, and thinning of the laminar Bowman's. As discussed in the general introduction (Chapter 1) the Bowman's plays a role in corneal biomechanics aiding in curvature maintenance as well as adhering the epithelial cells to the stroma. It provides a barrier between the epithelium and the stroma maintaining separate environments which is vital to corneal homeostasis (Wilson et al., 2003). It also acts as a barrier between the biochemical signalling of the cells in the two layers. With the thinning of the collagen and distortion of the cornea the Bowman's can stretch and break in places (figure 2). In some advanced KC cases the Bowman's along the limbus may begin to rupture causing small epithelial bleeds leading to iron deposits creating what is known as a Fleischer's ring (Iwamato and DeVoe, 1976). In some cases the laminar collagen of the disrupted Bowman's may regenerate causing

infiltrations into the stroma, but it is never thought to return to its normal state (Bron, 1998).

Figure 5. 3: H&E stained human KC cornea demonstrating an intact and ruptured Bowman's Image Heidelberg Engineering, 2005

5.1.4 PK Surgery

In Chapter 1 of the general introduction, corneal transplant surgery was discussed. In advanced keratoconus, penetrating keratoplasty (PK) surgery has been the standard procedure utilised to restore best vision to the individual. The procedure consists of replacement of a trephined button of healthy donor tissue situated over a similar trephined region of cornea removed from the host (figures 4 and 5). The cornea is then attached with either individual or running stitches which will be required to stay *in situ* for six months to a year and a half (Thompson et al., 2003). The overall success rate of the PK procedure is variable, but rejection is thought to be 11-18% with bilateral rejections to be more common (Musch and Meyer, 1989; Kirkness et al., 1990). It is thought that the bilateral rejection may be due to an abnormal immune response. Some complications of PK surgery include partial graft dehiscence, total rejection (graft failure), keratectasia due to the weakening of the corneal collagen from incision, or a progressive return of astigmatism in the new implant (McNeill et al., 1989; Mader et al., 1993). In some patients a change of prescription is required for months to years following surgery until the symptoms settle down. In most patients some form of corrective lens is required for life (Lim et al., 2000).

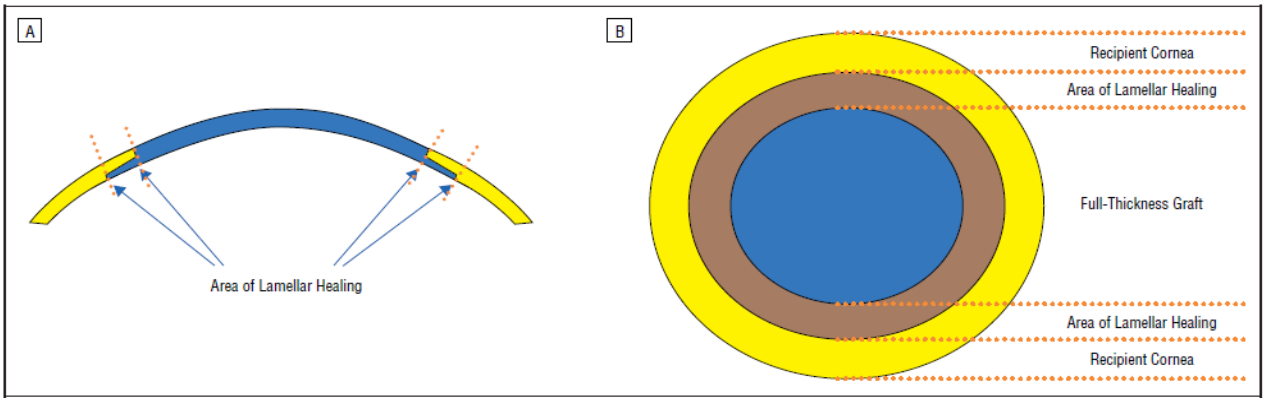

Figure 5.4: Schematic views of PK surgery and wound healing interfaces from Busin 2003

Healing can take from six months up to a year or more depending on the individual. Following the surgery, the graft appears to be swollen and may remain so for the life of the graft although in some patients there is a return close to homeostasis. More modern studies have indicated no discernible differences in thickness. Following the implant surgery the patient will require some topical steroids for several weeks to months. Some studies note that the lifetime of the grafts may only last for about 10 years, however most patients keep their grafts for several decades or for life. There is also evidence that nerves never completely return to homeostasis even thirty years following the procedure (Patel et al., 2007). As discussed previously, proper innervation contributes to overall eye health and ocular sensations. It is also thought that the nerves contribute to tear film production and epithelial cell signalling.

5.1.5 PK Wound Healing

The corneal wound healing process following the formation of scars was discussed in detail in the general methods chapter (Chapter 1). Following the initial incision, growth factors from the epithelium activate the corneal keratocytes into a myo-fibroblast phenotype resulting in the production of collagen and matrix materials. It has also been noted that along the limbus, there is an increase in epithelial wound healing due to the presence of limbal stem cells. It has been documented that there is an initial loss of keratocytes through injury and apoptosis at the wound interface of both the donor and host tissue; this a-cellular zone may impede initial wound healing and collagen production due to a reduction in corneal keratocytes (Ohno et al.,2002).

Kato et al. (2000) preformed PK procedures on rabbits to better understand the extracellular matrix alterations (namely collagens I, III, IV and proteoglycans) which may occur following the surgery. The group noted that within the first three days following surgery there began the re-development of laminar type IV collagen along the wound interface. At the one week time-point type III collagen and proteoglycans (C-6-S) being to populate the wound margin during wound repair. Re-epithelisation of the wound took a month and the Descemet's took three months to fully repair. Other studies have noted that complete re-integration of the whole wound appears to occur at the six month time-point (Wu et al., 1991; Kato et al., 2000) Prior to this, there is the risk of wound slippage and graft dehiscence especially following accidental injury (Farley and Pettit, 1987; Tseng et al., 1999).

Schmitz et al. (2006) repeated a similar experiment in rabbits with trephine and laser wounds at time points at three and six weeks and six months. The group found that the mechanical damage caused to the host tissue by the laser was minimal and the incisions appeared clean. This is supported by other laser based surgical procedures such as LASIK (Stonecipher et al., 2006). At the three and six week time-points both groups demonstrated expected trends in wound healing and matrix synthesis. At the six month time-point the wounds appeared to be entirely healed with collagen organisation at the wound margin running in a strict parallel orientation. In some younger patients there were found to be an increase in keratocyte population in the posterior with no changes in the anterior from normal. This may be due to the suspected gradual decrease in keratocyte populations in the aging KC cornea. It would indicate that younger patients may undergo a more comprehensive degree of wound healing.

Earlier in the general introduction chapter (Chapter 1) the biomechanical changes which occur following corneal surgery was briefly outlined. Following an incision to the cornea, it is thought that the collagen fibrils could be damaged, incised and weakened. With healing only occurring superficially, even over many years, there are a number of complications which can arise following surgery. In addition to graft dehiscence (figure 5), there remains the threat of ectasia or the flattening of the cornea. This keratectasia is associated with keratoconus (as well as surgery) and is

thought to be due to the thinning of the stroma following the procedure (Tuft and Gregory, 2005).

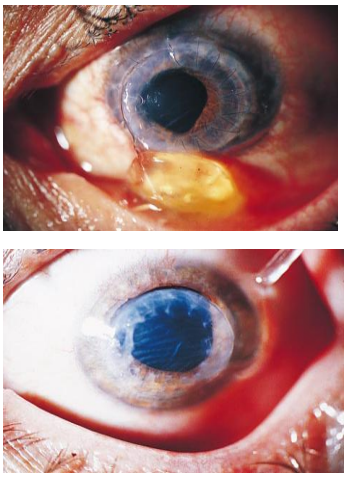

Figure 5.5: Full (above) and partial (below) PK flap dehiscence
Rehany et al., 2000

In earlier corneal transplants, the cornea was stitched using isolated stitches at 12, 3, 6, and 9 o'clock. This, however, was found to cause specific areas of tension causing distortion to both the donor and host tissues (McNeill and Wessels,1989; Busin, 2003). In KC there are already thought to be underlying abnormal biological factors to the tissues, and this distortion could cause additional complications. To remedy this, more recent surgeries have incorporated running stitching around the periphery of the graft reinforcing the graft and distributing the strain on the host tissue.

Clinically, the changes in biomechanics can be measured using ocular response analysers ORA. There have been studies comparing the biomechanical properties of PK vs. deep anterior lamellar keratoplasty (DALK) with no statistically significant differences (Jafarinasab et al., 2011). The average normal IOP is between 15 and 16 mmHg with both graft procedures indicating an IOP of 9 – 10 mm Hg. Following LASIK studies have found that there was an initial decrease in IOP with 14 mm Hg immediately postoperatively dropping to 8 mm Hg a few weeks following surgery. The readings would gradually increase with healing but never reach normal corneal biomechanics. There is however a marked improvement from the untreated KC however (Hsu et al., 2005).

5.1.6 Wound Healing in KC Corneas

Earlier in the introduction, some of the unique biomolecular traits of keratoconus were discussed. In wound healing studies of keratoconus it is important to put the 'normal' wound healing process in the context of an underlying disorder which is thought to impact on the keratocytes and matrix. It is thought that the pre-existing condition of KC would result in a more abnormal would healing process (Kenney and Brown, 2003). One study found an increase in tenascin (which tends to be present in embryological tissue) and an up-regulation in inflammatory growth factors and cytokines. Excessive vascularisation of the wound area or limbal stem cell defects could contribute to abnormal wound healing in more complicated cases of KC, but it is thought that these are not exclusively due to uncomplicated kerataconus (Dua et al., 2000; Solomon et al., 2002).

Limbal defects or deficiency adversely affects the wound healing and in some cases a partial limbal transplant is also performed with the PK procedure (Dua et al., 2000; Solomon et al., 2002). In some patients with PK there is excessive vascularisation at the wound edge. Success of the wound is variable by patient and sometimes several small factors in combination leads to the rejection or problems with the grafts. It was found that other disorders such as lattice corneal dystrophy (LCD), which is a rare condition associated with TGF-B, or systemic cancers had a greater negative effect on post-PK epithelial wound healing than keratoconus (Kawamoto et al., 2006)

5.2 Aims

In this experiment we used X-ray scattering techniques (wide and small angle) to analyse corneal tissue from the left eye of a deceased patient with advanced keratoconus who underwent penetrating keratoplasty (PK) twelve years prior, with the aim to better understand the biomechanical and ultra-structural changes to collagen which occur during scar re-modelling in a patient with this disorder. It is hoped that through researching this unique sample more information regarding keratoconic collagen organisation and distribution along the wound edge and periphery (native host) could be determined. It is also key to understand if there are any biomechanical changes which occur to the implant over the twelve year post-operative period.

5.3 Methods

5.3.1 Wide and Small Angle X-ray Scattering

The cornea and surrounding sclera from the right eye of a male who developed advanced KC which was treated for a penetrating keratoplasty (PK) procedure twelve years previously was obtained from the Danish Eye Bank (Aarhus, Denmark). The patient was a male (age of death 79 years) and had also undergone a similar surgery for KC in his right eye twenty-eight years previously; the SAX results from this pair matched cornea will be discussed in the next chapter (Chapter 6). The specimen was wrapped in clingfilm and stored at -80° C until the X-ray experiments. Following the SAXS experiment the cornea was stored in in Optisol (Bausch and Lomb, Germany). The entire sample was evaluated using small and wide angle X-ray scattering at synchrotron stations I22 and I02 at the Diamond Light Source, Didcot. The methodology for the experiment was discussed in full detail in the General Methods (Chapter 2). The cornea was wrapped in cling film to prevent dehydration and placed in a purpose built Perspex and Mylar chamber on the beam-line. The sample was scanned at 0.25 mm intervals (wide angle) and 0.5mm intervals (small angle). The cornea was orientated based on a suture at the 12 o'clock position which was added by the eye-bank. Later slit-lamp analysis on the cornea revealed that this suture was put in the wrong place (i.e. at the 4 o'clock position). The data was then analysed for collagen fibril diameter and spacing using Statistica™ and total collagen and orientation using Optimas ™ and Microsoft Excel.

5.4 Results

The cornea was imaged under a Leica 6000 light microscope at 5 x magnification (Figure 5.6). The wound margin was clearly visible around the entire implant border as a 0.5 to 1 mm border of increased light scatter. The donor graft button appeared clear and undamaged. The host corneal tissue also appeared clear and unremarkable when compared to normal human corneal tissue, except that at the nasal margin there was a crescent shaped corneal opacity extending from the limbus (Figure 5.7, orange arrow).

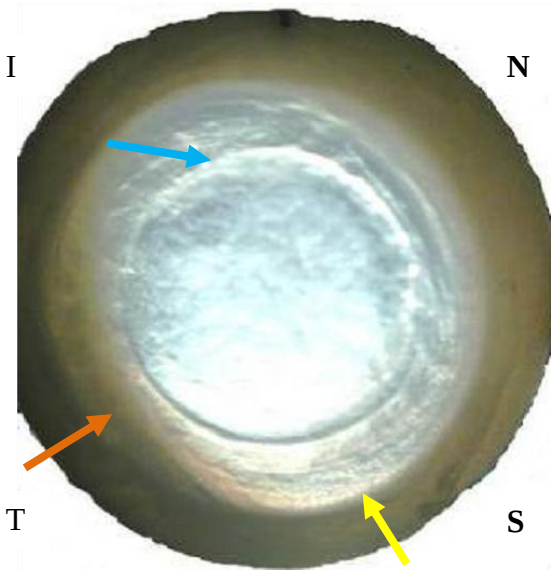

Figure 5.6. Photograph of right twelve year post-operative keratoconic cornea sample. The yellow arrow indicates the area along the limbal/scleral border. The blue arrow indicates the wound edge and the orange arrow indicates a corneal opacity.

5.4.1 Wide Angle X-ray Scattering

b. Collagen Orientation

The central region of the cornea was dominated by the PK graft button and surrounding wound margin. The collagen in the donor graft presents the highly orthogonal collagen orientation which is indicative of a normal human cornea (as indicated by the red crosses in the centre of figure 5.7). Interestingly, in this case the orientation of the cross-shaped plots within the donor cornea matches those in the peripheral host button, implying that the graft was orientated with lamellae aligned with those in the host. Furthermore, the donor lamellae retained the 'normal' orthogonal collagen pattern rather than the disordered collagen phenotype which is generally found in KC corneas even after a period of over a decade. Along the circumference of the donor cornea there was a border of re-modelled highly aligned tangential collagen forming an opaque scar (brown arrow).

From the scar region out towards the peripheral cornea, the orientation of the tissue

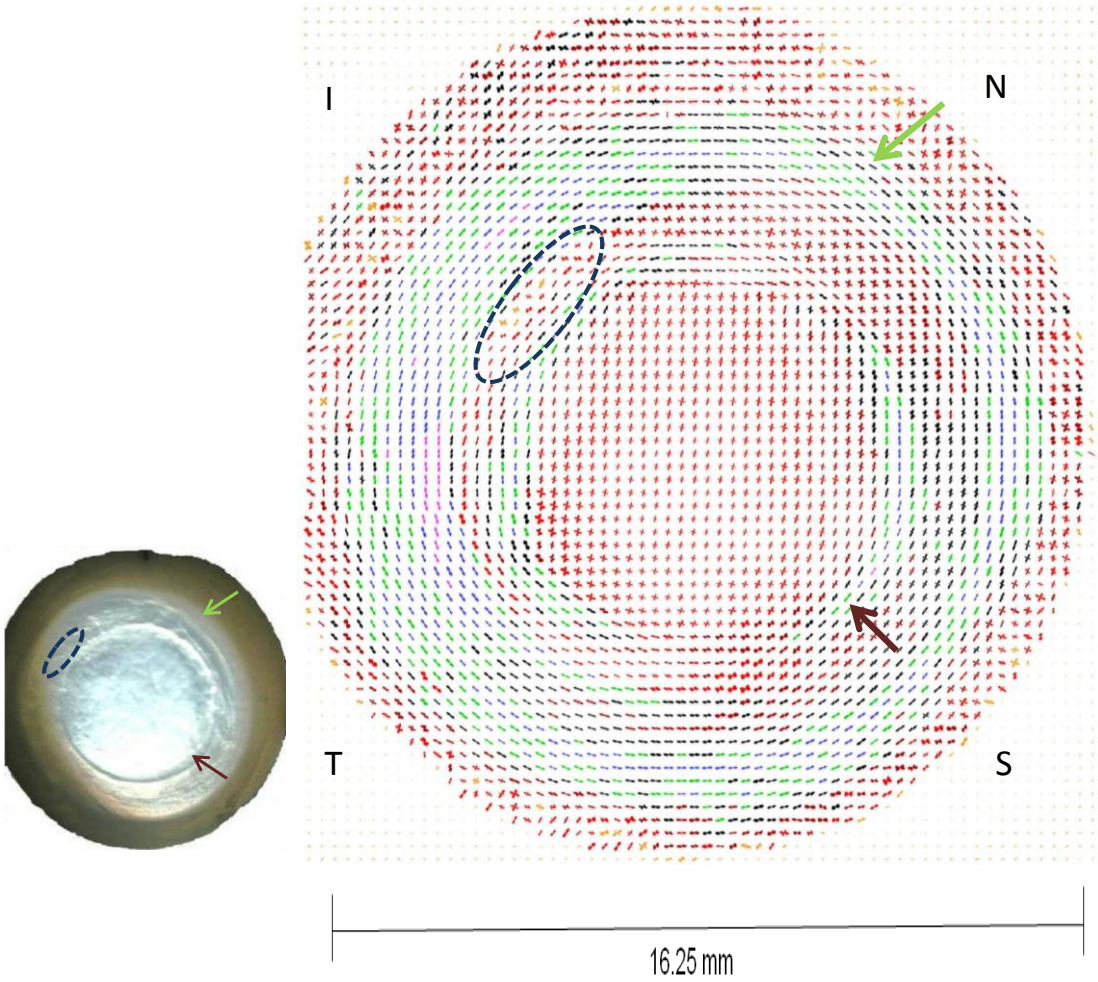

Figure 5.7: Wide angle polar plot map of the KC graft. Each file represents 0.25 mm. Navy circle represents collagen disorder outside the graft. The brown arrow indicates areas along the wound edge which appears highly aligned tangentially. The limbal annulus (green arrow) also appears to have highly aligned collagen. Scale down factors: orange (1), red (2), black (4), green (6), blue (8), purple (12).

was very variable. Some regions looked normal, showing cross-shaped plots whereas others, such as the region circled, appear to be highly disrupted. On the temporal side of the host peripheral cornea, the collagen was highly aligned so that there was no clear distinction between the wound margin and the limbal annulus. This zone corresponded to the corneal opacity in the peripheral host cornea (see inset). The limbal region demonstrated the normal circumferential annulus of high intensity collagen running around the native host cornea (green arrow). The periphery of the tissue (sclera) demonstrated collagen disorder with scattering in a number of different directions.

b. Total Collagen

The total collagen scatter produced in the different regions of the cornea has been established as an indicator of the different corneal architecture (Meek and Boote, 2009). In the normal human cornea the amount of total collagen gradually increases from centre to periphery with an increase in thickness at the annular limbus; this sample demonstrated an overall similar trend, however there was an increase in total scatter circumferentially at the wound margin (figure 5.8, brown arrow) and a decrease in the host corneal tissue which may be due to keratoconic changes in the peripheral cornea (figure 5.8, blue ring). It has been reported that in KC corneas, there is thought to be a shift in collagen amount from the centre to the periphery of the cornea (Meek et al., 2005). In this instance, there did appear to be some regions of higher intensity in the periphery, however this may just be an individual variation and would need to be taken with a caveat.

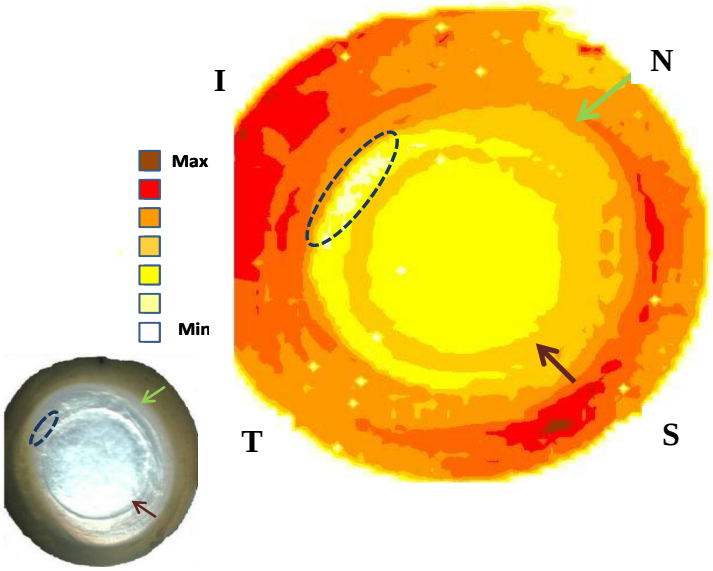

Figure 5.8. Surface map demonstrating the total amount of collagen (AU) based on the intensity of total scatter. There is increased scatter along the wound margin (brown arrow). Outside the inferior wound margin there is a significant decrease in collagen amount (blue ring). There also appears to be a significant increase in scatter along the margin of the graft implant in the superior region (green arrow).

c. Preferentially Aligned Collagen

Aligned collagen surface maps were created to demonstrate the distribution and amount of preferentially aligned collagen in the cornea. The delineation between preferentially aligned and isotropic collagen scatter was described in detail in Chapter 2 (General Methods). In the normal human cornea, there is a greater alignment of collagen when moving from centre to periphery. In the total scatter map, the central cornea generally demonstrates a circular pattern of lower scatter intensity. In the normal aligned map the circular pattern is replaced with a more rhomboid or diamond shape.

This 'diamond' shape is seen in all normal human corneas. As noted in the general introduction chapter (Chapter 1) it is thought that long anchoring collagen fibrils run from limbal/sclera to limbal/sclera to create this shape (Agamohammadzadeh et al., 2003). The aligned collagen maps of this sample followed what would be expected in that the donor button retained the diamond shape (central white/yellow region in figure 5.9). There was observed a high degree of collagen alignment all along the wound margin but to different degrees. Along the temporal/inferior wound margin, there was a great increase in localised collagen alignment along the wound edge near the limbal border (figure 5.9, black arrow). Along the limbus there was a high degree of aligned collagen corresponding to the annulus seen in all normal human corneas. When compared to normal (non KC) corneas, the collagen alignment in the peripheral keratoconic cornea did not appear to be remarkable.

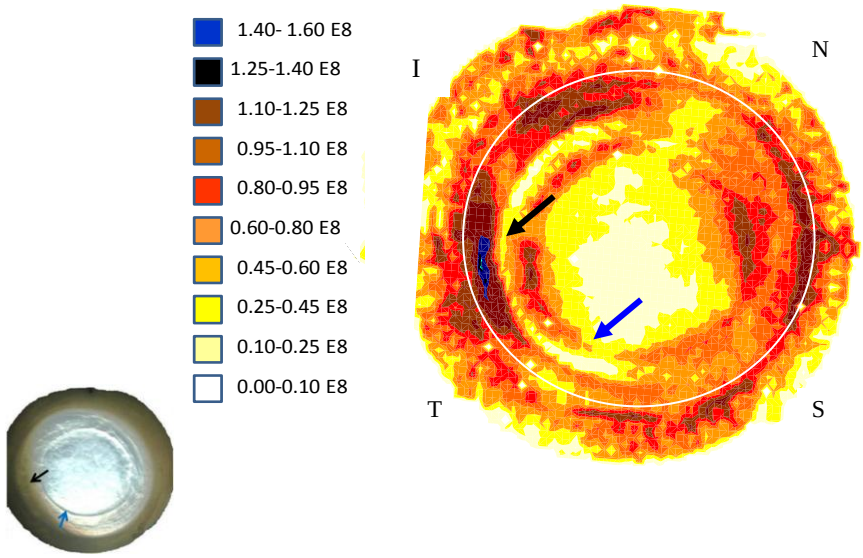

Figure 5.9: Surface map of KC cornea demonstrating the aligned collagen (AU). The limbus is indicated by a white circle. The black arrow indicates a region where the peripheral keratoconic corneal lamellae are highly aligned. This corresponds to a region of corneal opacity. The blue arrow indicates the wound margin where the collagen is also highly aligned.

d. Percentage Aligned Collagen

The percentage of aligned collagen (Beta Maps) was determined by dividing the aligned collagen by total collagen (this is discussed in further detail in Chapter 2). In the normal human cornea, the percentage of collagen alignment tends to be around 40% to 50% mostly evenly distributed across the cornea. In the normal cornea the central region would have a low degree of percentage alignment which would gradually increase out towards the periphery (never exceeding 50%). The surface maps created for this sample (figure 5.10) demonstrated striking differences when compared to normal cornea as described in the literature. In the KC sample, the host and native tissue demonstrated the trend of 40%-50% collagen alignment as would be expected when compared to normal with the central cornea demonstrating moderate collagen alignment. The most striking difference in the KC sample was that there was a high degree of collagen alignment present along the scar margin (with localised regions at 70% -90%).

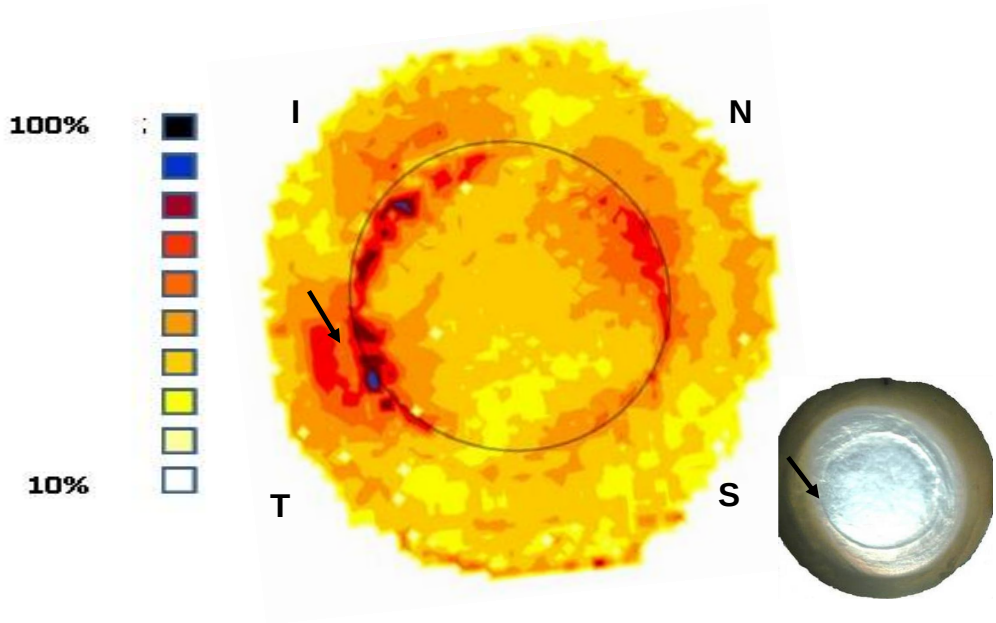

Figure 5.10: The percentage of aligned collagen calculated by dividing the aligned collagen by the total collagen. The area with the highest proportion of aligned collagen is along the wound edge (black arrow). Whilst the entire wound edge is evident there seems to be a higher proportion of aligned collagen near the temporal region.

5.4.2 Small Angle Results

a. Diameter

In this study, the entire cornea was scanned at 0.5 mm intervals. The files were analysed as described in Chapter 2 (General Methods). In the donor cornea the average spacing was 34.0 ±1 nm. If the donor, scar and peripheral host cornea are averaged, this figure increased to 35.7±0.2 nm. The fibril diameter increased in the limbal/sclera (Table 5.1).

Location	Average Spacing/nm	Average Diameter/nm
Central	47.6±0.4	35.7±0.2
Limbal/Sclera	100.9±2.6*	56.4±0.6

Table 5.1 Table indicating the average collagen spacing and diameter of corneal collagen for the twelve year post-operative KC cornea. Both the collagen spacing and diameter increase from centre to periphery. *The figure is an average of two interfibrillar peaks at ~80 nm and 120 nm. This will be discussed in more detail in the following chapter.

The overall diameter of collagen in the scar region was up to 2nm higher in some regions (figure 5.11, green arrow), but did not appear to show a statistically significant trend around the entire circumference of the cornea There was a slight variation in the right cornea which will be discussed in further detail in the following chapter (Chapter 6). Another region where there appeared to be a small increase in the diameter was in the regions of corneal opacity (figure 5.11, blue arrow).

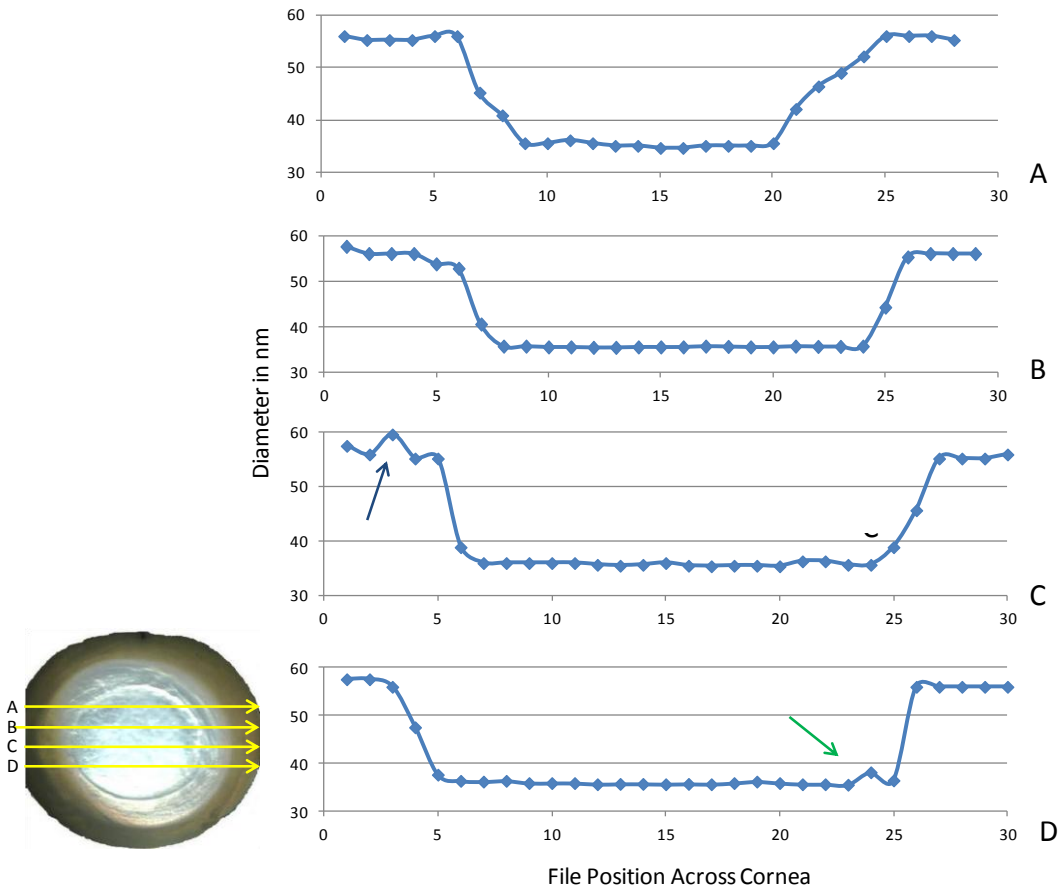

Figure 5.11. Scatter plot transects of the cornea in four scans (yellow arrows inset) demonstrating fibril diameter in a cross section of KC cornea. Central file is at position 15. The diameter of the collagen appeared normal with only slight variation. Green arrow indicates a slight increase in the scar region and blue arrow indicates the slight increase believed to correspond with the corneal opacity.

b. Interfibrilar Spacings

The cornea was also analysed for the interfibril spacings as described in Chapter 2 (General Methods). The results (Table 5.1) indicate that the average interfibril spacing in the central cornea (host and donor portion) was 47.6±0.4 nm.

Figure 5.12 shows the interfibrillar spacing measured several different horizontal transects. As noted with the diameter of the collagen fibrils of the KC cornea, there was a slight increase in the scar region (± 1-2 nm) but this increase was not found around the entire circumference of the wound margin. The increase was more evident where the graft was situated closer to the corneal opacity. The increase was however generally localised to the wound region indicating that this was a result of either the scar tissue or the actual wound margin. As the region of the increase also corresponded with the gradual increase in spacing which occurs towards the limbus (periphery) the results may appear slightly exaggerated.

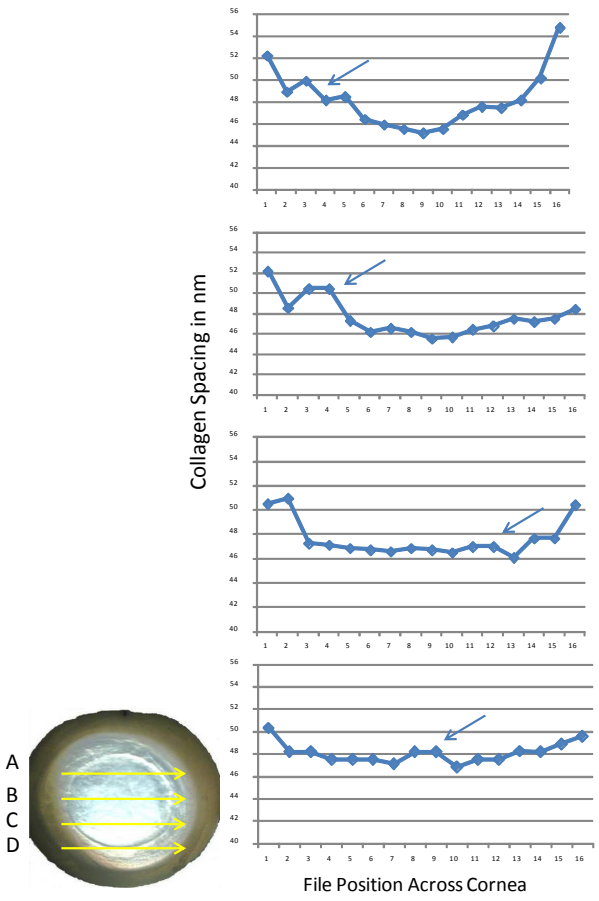

Figure 5.12: Small angle interfibrillar spacings for cross sections of KC cornea. Scans plotted limbus to limbus with file 9 as the central meridian of the cornea. Plots are from the regions shown in the inset. The arrows indicate the scar region.

c. Degree of Order

Following the analysis of the Bragg spacing and diameter of collagen across the entire scanned left KC cornea, X-ray intensity profiles from individual regions (e.g. the host sclera, limbus, peripheral host cornea) were observed in series from periphery towards centre (figure 5.13). The purpose of this was to determine if there were any changes in the packing order of the collagen fibrils. The equatorial Bragg peak was not observed in the sclera or outer limbus (figure 5.13 A and B), and was just evident as a double peak in the limbus (figure 5.13 C). It was clearly evident in the peripheral host cornea (figures 5.13 D-F).

Determining the degree of order using SAXS analysis was outlined in Chapter 2 (General Methods). The overall height of the spacing peak is divided by the width of the peak at half the height to determine the overall peak morphology and hence the order in the fibril packing. In the normal cornea, there is generally a trend of a high degree of order in the central cornea which decreases sharply out towards the periphery (limbus). Under normal circumstances there should be an inverse relationship between the fibril spacing and the degree of packing order.

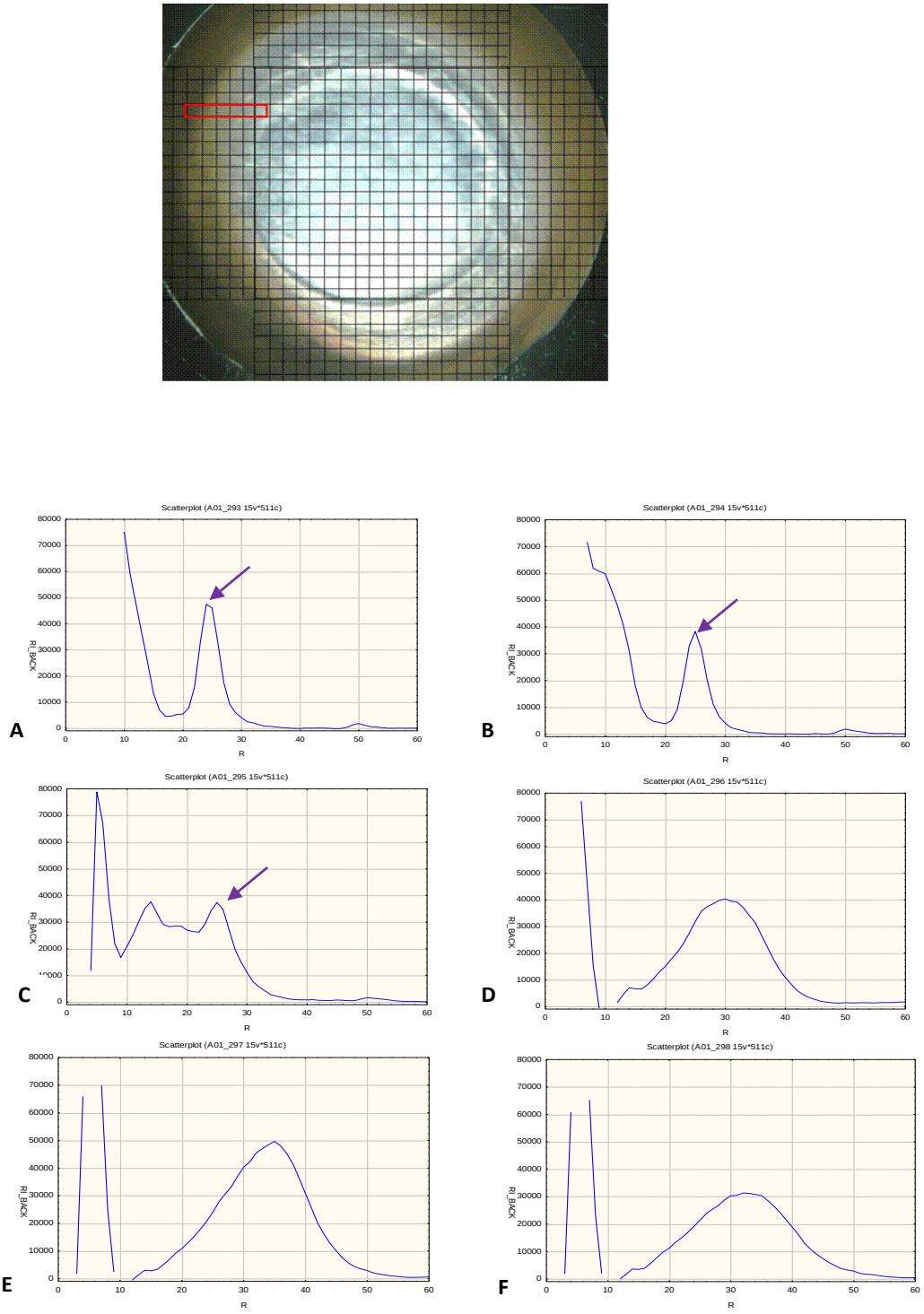

Figure 5.13: Graphs of small angle X-ray scatter for Bragg spacings plotted as Intensity in arbitrary units (I) vs Position in pixels (R). (A, B) from the sclera; (C) from the limbus; (D-E) from peripheral cornea; (F) from outer edge of scar region The sclera demonstrates a single sharp meridional peak (arrow) characteristic of that tissue. The limbus demonstrates a double equatorial peak pattern which will be discussed in the next chapter.

In the KC cornea there was found to be significant differences in the degree of order of the collagen spacing along the wound margin. The data collected over the wound margin indicates a dip in the collagen order at the scar (figure 5.14). The overall order dips at the limbal border as the spacing increases. This is what would be expected.

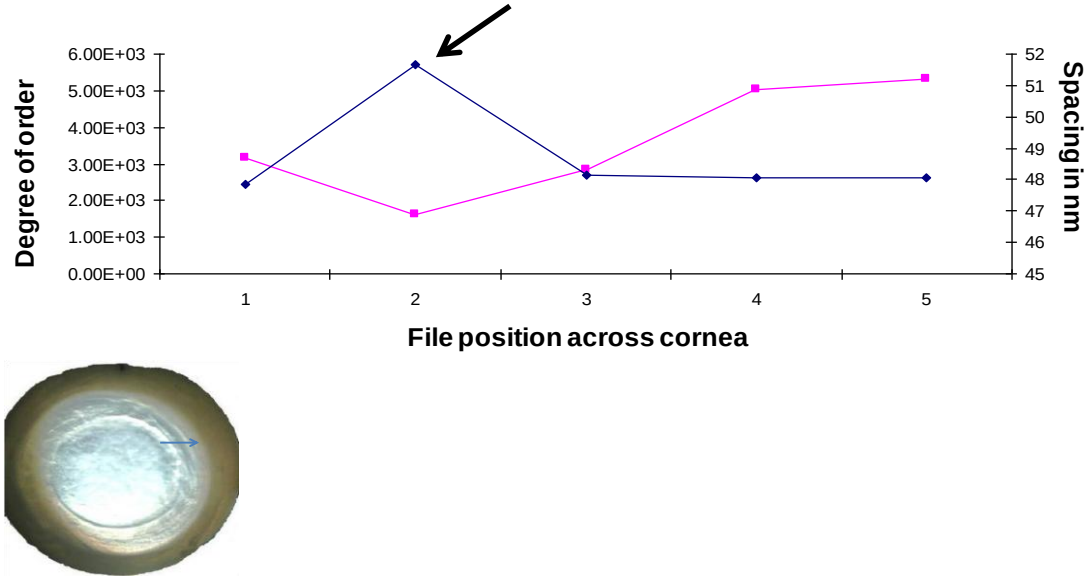

Figure 5.14: Degree of order (pink diamonds) and the Bragg fibril spacing (blue diamonds) from the inside edge of the wound to the periphery of the host cornea. File one is from the donor cornea. Black arrow indicates suspected scar region where there is variation in the degree of order. The degree of order drops off significantly near the peripheral host cornea. The overall spacing is only slightly increased in the scar region (±2 nm), however there is a rapid increase at the periphery. Inset blue arrow indicates region of scan

5.6 Discussion

This sample presented a unique opportunity to study peripheral changes in the keratoconic cornea, together with long term wound healing and matrix remodelling following PK surgery. The progressive changes which occur to the keratoconic cornea are thought to compromise the general health and wound healing process to some extent but there appears to be a large individual variation. There are also thought to be temporal changes which may occur randomly in different individuals (and not always bilaterally in the same individual). Some of these changes are thought to be low level 'inflammatory' type changes associated with shared wound healing pathways. Symptoms similar to those of wound healing pathways include an imbalance of collagenases, TIMPs and MMPs; an overall increase in the production

of heat-shock proteins associated with apoptosis/programmed cell death; and general keratocyte pathology which may impact on collagen production. For this reason, the pathology associated with KC and general wound healing are thought to be interlinked.

5.6.1 The Donor Button

As this sample provided a unique opportunity to study the ultra-structure of a cornea which has undergone PK surgery, the ultra-structural biomechanics of original KC host and normal donor as analysed with WAXS and SAXS had never been analysed to date. If keratoconus is an exclusively biomechanical disorder, it would be expected that a trephine button of normal implanted donor tissue could be re-modelled over time to resemble KC tissue with anterior thinning and collagen slippage. However, a striking finding in this study has been the lack of 'keratoconic' type alignment in the donor tissue; the collagen in the central button appeared to retain the orthogonal collagen orientation after many years in situ. The total amount of collagen did not appear to be different from the surrounding host tissue with the exception of the wound edge. In the aligned collagen map, there is the distinct diamond shape evident in the donor cornea which once again appeared to be unaltered after many years within the host. In normal corneas, this diamond is thought to be the result of anchoring collagen lamellae that run from limbal/sclera to limbal/sclera, but these are not normally observed in keratoconic tissue (Hayes et al., 2007). Finally, with the exception of the wound margin, the interfibrillar spacings and fibril diameters were unremarkable in the donor button.

The lack of any structural changes in the donor button could be an indication that the donor button retains its physiological and bio-physical properties despite being placed in the KC environment. There was no evidence of recurrence of keratoconus. In this condition, recurrence is rare, possibly because most donor corneas are from elderly patients whose corneas are naturally crosslinked. The fact that the lamella organisation within the button was unchanged after so many years could be due to newly deposited collagen being laid down to exactly replicate the tissue it replaced. However, it is more likely to reflect the extremely slow rates of collagen turnover in the quiescent stroma (Smelser et al.,1965).

5.5.2 PK wound healing

In addition to the underlying issue of KC in the sample studied, there was also an opportunity provided to analyse a large post-operative scar which was re-modelled over a twelve-year period. For this reason, the case study also presents an opportunity to better understand wound healing in vivo, changes to the collagen ultrastructure, and loss of transparency.

Along the wound margin there was evidence of healing in the formation of a fibrotic scar. The collagen within this scar appeared to run in parallel bundles and demonstrated a high degree of overall alignment, this was consistent with the finding of Schmitz et al. (2006) who noted that the scar tissue which runs along the PK wound margin is highly aligned and runs parallel to the graft (Schmitz et al., 2006). However, the Schmitz study was based on histology and was therefore qualitative. Our study is the first quantitative study of collagen organisation in a fibrotic corneal scar. We showed that at some positions around the scar as much as 90% of the newly deposited collagen was parallel to the wound edge (figure 5.10). The resulting circumferential arrangement of collagen is likely to be of significance in terms of graft integrity. Specifically, a relative lack of radial lamellae spanning the graft margin might be reasonably expected to encourage a wound under tension to reopen (figure 5.16). With this in mind, it is relevant to note that traumatic wound dehiscence has been reported up to 19 years after PK (Farley and Pettit,1987; Pettinelli et al., 2005), while stress analysis experiments have indicated that the graft-host interface remains weak even after the tissue appears fully healed (Calkins et al.; 1981).

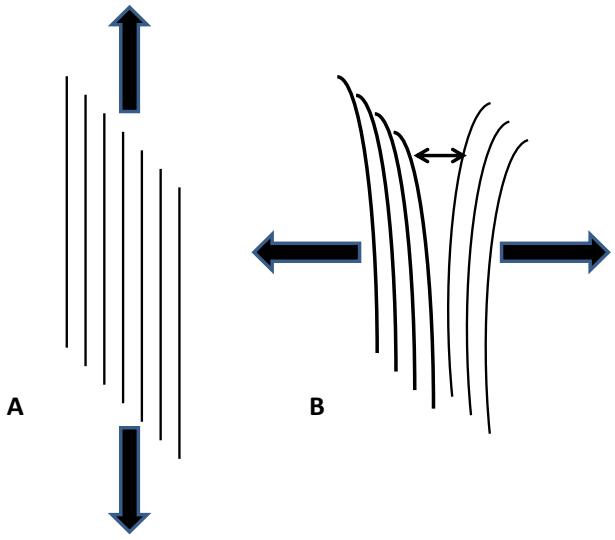

Figure 5.15 Schematic demonstrating force on collagen fibrils (vertical lines) laid tangentially to the scar. (A) Along its fibril axis the collagen retains its tensile strength. (B) At right angles to the fibril axis, the fibrils are easily pulled apart.

As a general rule, the wound border of LASIK and PK wounds are not thought to fully heal through the full depth of collagen, but with a small degree of new collagen deposited along the wound margin and a higher degree of general re-epithelialisation. Whilst the tensile strength of the wound is greatly reduced and dehiscence is always possible (years after surgery), dehiscence and graft rejection due to poor collagen integration are rare (Kim et al., 2010). It is possible that, in the case of this cornea, the proper alignment of the donor button to the host tissue and the comprehensive wound healing around the circumference of the button contributed to success of the graft however this cannot be conclusively determined.

It is generally thought that the pre-existing condition of KC would result in a more abnormal wound healing process leading to either a general lack of wound healing or an increase in keratocyte death along the wound edge (Kenney and Brown, 2003). Studies have found an increase in tenascin in some KC wounds (which also tends to be present in embryological tissue) and an up-regulation in pro-inflammatory growth factors and cytokines especially in the IL-1 family. IL-1 is a pro-inflammatory cytokine instrumental in the early wound healing cascade (especially in the activation of epithelial growth factor (EGF) and TGF-B (Wilson et al., 2000).

There have been a number of experiments involving SAXS scanning of normal human corneas. These studies (along with TEM micrograph analysis) have established the mean fibril diameter of corneal collagen between 31nm and 34nm increasing with age (Meek and Leonard, 1993; Daxer and Fratzl, 1997; Boote et al., 2003). Based on previous SAXS wound healing studies, it was expected that there would be a marked increase in fibril diameter and spacing along the wound margin due to the re-modelling of scar tissue (Cintron et al., 1973; Kamma-Lorger et al., 2009; Connon and Meek, 2003). This was not entirely observed in the KC sample. Whilst in some localised regions there was found to be a slight increase in spacing and diameter (~ +2 nm) the increase was not as marked as expected and may just be attributed to the normal variation in the tissue. To determine if these slight increases were due to the observed fibrotic appearing tissue in the scar region, the degree of order was analysed.

Meek et al.(2004), Meek and Leonard et al.(1994) and Connon and Meek (2003) noted that TEM analysis of wounded rabbit corneas demonstrated re-modelling of the collagen on the fibril level in both deep and superficial wounds (figures 5.16 and 5.17). Whilst the diameter of the collagen fibrils appeared to be slightly affected, the spacing between the fibrils was found to be increased and disturbed for a limited period where it later becomes resolved. SAXS analysis of the KC corneal scar tissue also supports these findings as the diameters of the tissue were not found to be increased however the spacing was marginally increased and the shape of the peaks produced were distorted.

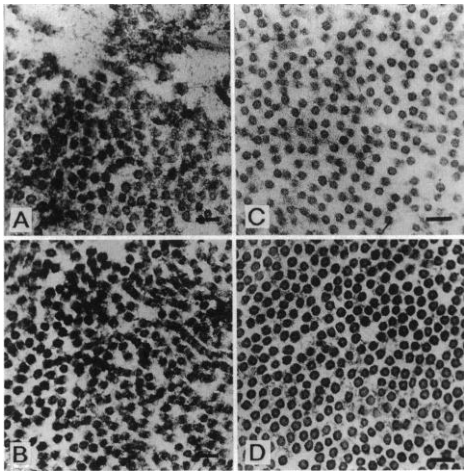

Figure 5.16 Cross-sections of collagen fibrils in rabbit penetrating scar tissues (A, B, C) and normal rabbit (D). The ages of the scars were: (A) 3 weeks, (B) 7 months, (C) 14 months. (Bar = 100 nm). Tissue shows a progressive re-ordering of the fibril (Rawe et al., 1994)

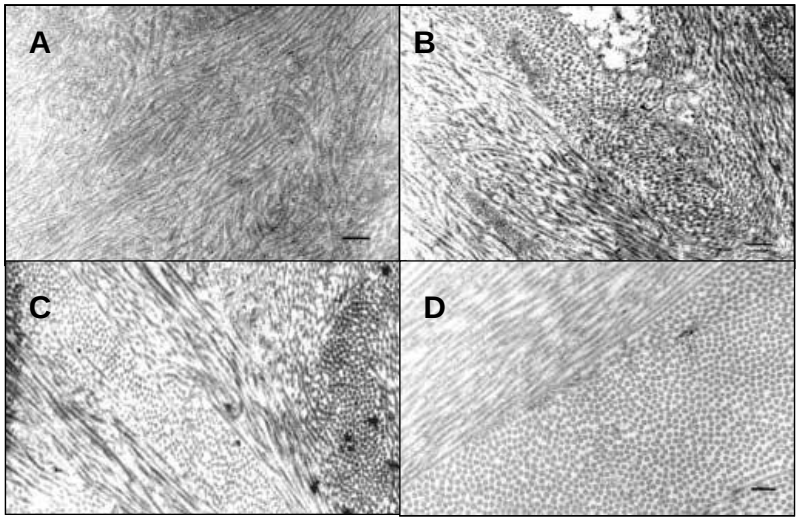

Figure 5.17 TEM micrographs of mid-stromal depth superficial wounds in rabbit corneas (in vivo study) at A) five months B) ten months C) sixteen months D) Normal cornea bar=200 nm Tissue again shows the progressive re-ordering of the tissue. Connon and Meek, 2003

In this sample the intermolecular peak morphology, did differ between the wounded and unwounded tissue. The peaks in the unwounded tissue (both native and KC peripheral cornea) appeared to be sharp and clear with an average Bragg's spacing of 46 nm. The scar had a similar Bragg spacing (in some regions +2 nm), however the peak was shorter, broader, and more irregular. This is more consistent with a more disordered fibril packing arrangement in the scar region. Like in a previous in vitro rabbit study (Rawe et al., 1994), in this sample the wound margin appeared not to

return to homeostasis after several years but continued to demonstrate the degree of disorder.

5.5.3 KC changes in the peripheral cornea

To our knowledge, this paper presents the first documented investigation of keratoconic stromal ultrastructure outside the central 8mm of the cornea. Three major observations were made:

- Localised alterations in the normal preferential alignment of collagen fibrils, along with a corresponding reduction in collagen mass.
- A distinct corneal opacity which gave the appearance of the limbus moving towards the central cornea.
- The appearance of an extra equatorial reflection in the SAXS patterns.

The collagen organisation map demonstrated a small region in the inferior peripheral cornea which appeared to have a disorder of the type associated with keratoconus, along with a corresponding reduction in collagen mass. A possible explanation for this may be the location of a suture in the region. With the underlying pathologies of KC, it has been known that collagen around the area of high tension created by a suture may lead to collagen becoming slack. This is region dependent.

Astigmatism is associated with post-PK and can occur early or late in the graft history (Nobel and Ball, 2004). Pesudovs et al., (2003) noted that severe astigmatism and corneal thinning in the host cornea can occur more than 10 years following PK procedures. Patients with a mean age of 41.2 years who underwent PK at a mean age of 28 years demonstrated progressive keratoconic changes in the host cornea which presented itself as a large astigmatism (Pesudovs et al., 2003). In this sample there appeared to be a reduction in total collagen scatter beyond the inferior wound edge. This could be attributed to corneal thinning and astigmatic changes that occurred following the graft procedure. Valldeperas et al., (2010) described a patient who underwent a bilateral case of keraectasia following PK surgery 34 years previously. They noted that the graft appeared clear and unremarkable however outside the graft

thinning of the cornea (mid-peripheral thinning) and bowing developed. These resulted in corneal changes. It was thought that this was due to late keratoconus presentation.

However, it is more likely that these are keratoconic changes, given that they occur on the inferior (i.e. cone) side of the cornea and, moreover, that previous WAXS studies of the central keratoconic cornea using keratoplasty buttons have shown similar changes extending well beyond the cone and, in some cases, all the way to the button edge (Hayes et al. 2007; Meek et al., 2005). Furthermore, tissue thinning in keratoconus has also been previously demonstrated as far as 5.6mm from the corneal centre inferiorly (Sen et al., 1969). Taken together, these previous and current findings suggest that, in some patients, keratoconic changes in the alignment and distribution of collagen lamellae likely extend beyond the region normally grafted.

The observation of a corneal opacity in the periphery where the collagen was highly aligned (figure 5.10) and of an extra SAXS reflection will be discussed in the next chapter, where data from the pair matched grafted keratoconus sample was studied.

Evaluation of Limbus in a Twelve Year and Twenty-eight Year Post-operative Keratoconic Corneas

6.1 Introduction:

In Chapter Five, the collagen ultra-structure of the left enucleated cornea of a patient who underwent penetrating keratoplasty (PK) for keratoconus twelve years prior was analysed. The sample was scanned using both wide and small angle X-ray scattering techniques to determine collagen organisation, distribution, diameter, degree of order, Bragg interfibril spacings. In this chapter, the collagen ultra-structure and biomechanics of both the normal limbus and the keratoconic limbus of both the left eye and right eyes (the latter of which was grafted some 28 years prior to death) will be discussed in detail, with an emphasis on the changes to fibril packing along the limbal border.

6.1.1 Anatomy and Physiology of the Limbus

The normal corneal limbus presents a unique morphology and ultra-structure when compared to the neighbouring corneal and sclera tissue. The limbus is the transitional region between the two ocular tissues, and as such is thought to retain properties of both neighbouring tissues to create a smooth transitional zone between the transparent corneal stroma and scleral stroma (Bron, 2001). The collagen organisation of both the anterior and posterior limbus is unique when compared to both neighbouring tissue (this will be discussed in greater detail later in the chapter).

The limbus serves several ocular functions and has some unique physiological roles/morphology including:

- Maintenance of corneal curvature and normal corneal biomechanics
- Provision of nourishment to the cornea as a vascular rich tissue
- The believed location of stem cells/progenitor cells which are thought to be stored in specialised environmentally controlled niches and differentiate for regeneration and wound repair of the anterior ocular surface.

- The location of channels for transport of differentiated epithelium cells to assist in wound healing and corneal regeneration
- Maintenance of proper corneal hydration levels in the anterior eye providing channels which ocular fluid can be exchanged.

(as indicated by Hogan et al.,1971; Saltzmann, 1912; Krachmer et al.,1997; Potten, 1996)

The anatomical limbus is thought to be approximately 1 mm wide and is circumferential (Hamilton and Boyd, 1956). The limbus is comprised of three main cellular layers and two membranes (epithelium, anterior laminar layer, stroma, posterior laminar layer, specialised endothelium) (Larke, 1997); in this way it is similar to the cornea. At the posterior of the limbus is located the Schwalbe's ring which is the ridge that demarcates the end of the normal central corneal endothelial layer from that of the limbus although the line may be an optical effect based on the different thickness of the tissue (Larke, 1997; Meek and Boote, 2009).

In some animals with darker eye pigmentation (e.g. ovine), the limbal ring is visible along the border of the cornea and sclera as a dark band. In some individuals the limbal region appears slightly less transparent than the central cornea; this is attributed to the changes in peripheral corneal collagen which will be discussed in more detail later in this chapter (Barraquer, 1964).

a) Anterior Limbus

The anterior portion of the limbus is highly vascularised and is believed to be vital to stem cell production and corneal epithelial regeneration (Pottin, 1996). The tissue at the limbus has unique properties which differ in architecture from the adjoining central cornea and sclera. The overall morphology of the anterior limbus is described as having a thicker more irregular epithelial layer with an increase in wing cells (ten layers of cells on average as opposed to six or seven in the corneal epithelium) (Hogan et al., 1971). In the limbal Bowman's there appear to be a series projection-like basal cell processes which are punctuated between shafts or 'pegs' of stromal matrix, this differs from the smooth unbroken Bowman's noted in the cornea (Gipson,

1989). It is also thought to be the location of the channels of Vogt which radiate from the periphery of the scleral rim and are thought to be fundamental to differentiated epithelial cell transportation. These channels are not found in all mammalian species and are most evident in human tissue (Gipson, 1989).

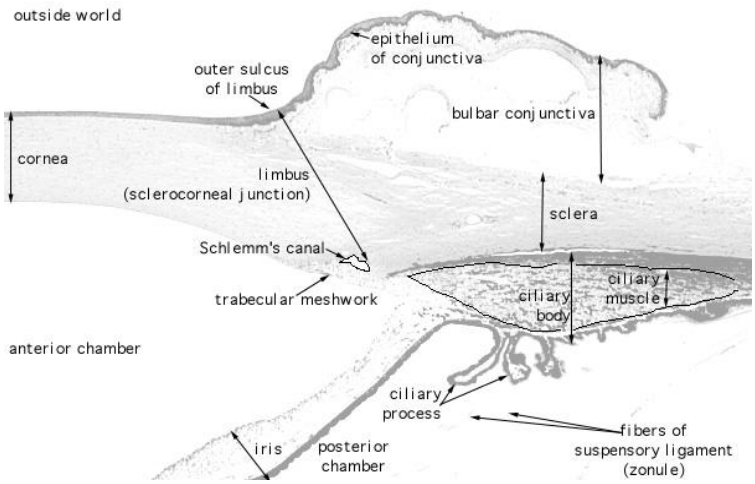

Figure 6.1: Illustration of the interface between the cornea, limbus, and sclera. This demonstrates the complexity of the limbal region. Copyright Boston University http://www.bu.edu/histology/p/08005loa.htm accessed December, 2011

As in the central cornea, the Bowman's layer of the limbus provides adhesion points for collagen and a degree of biomechanical stability. Unlike in the central cornea, it is thought that the laminar collagen in the limbal Bowman's may not be distributed as smoothly and evenly as in the central cornea; this irregular collagen arrangement is thought to accommodate for the other anterior limbal structures (e.g. palisades, vessels, and stem cell niches). It is also thought that the stromal collagen attachment foci at the limbus are set at different angles when attaching the limbal Bowman's as compared to the central cornea (Bron, 2001; Meek and Boote, 2004). This anterior collagen attachment is thought to contribute to some of the unique biomechanical properties of the limbus, however much of the biomechanical strength is attributed to the posterior limbus (Meek and Boote, 2009).

b) Posterior Limbus

The posterior limbus is thought to be an area of transition between the stromal layers of the cornea and the sclera. It is in this region where the ordered collagen of the corneal annulus is merged with the more randomised collagen on the sclera. The

posterior limbus (posterior 2/3rd) is thought to contribute to the biomechanical strength of the cornea and provides a structurally sound transition zone between the cornea and scleral stromas (Ross and Pawlina, 2006).

6.1.2 General Ultrastructure of the Limbus

Until recently, there were relatively few studies of the ultra-structure of the limbus performed. The initial studies focused on electron microscopy and general histology of the region. Sheilds et al. (1977) studied the ultra-structural properties of healthy and glaucoma limbal tissue. The tissue chosen was directly over the trabecule region at the base of the cornea. In the normal samples, it was found that the fibril diameter was different in the anterior and posterior regions. The collagen diameter in the healthy corneas measured 99.89 nm in the inner layer and 122.15 nm in the outer layer (Shields et al., 1977). The study, however was not as interested in the spacing of the collagen fibrils it only touched upon the finding that the 'compactness' of the fibrils which seemed to be similar in the inner and outer limbal regions. It could then be surmised that if the compactness of the tissue was similar that the interfibril spacing in each of the layers was in relative proportion to the fibril diameter. This could indicate a slightly higher or generally different spacing in the outer layer (Shields et al., 1977).

From the late 19th century to the present there have been a number of studies regarding the physical properties of limbal collagen (Ischreyt, 1899; Fischer, 1933; Maurice, 1969). Kokott (1938) postulated that in the collagen annulus there are circumferential fibrils which are located in the posterior region of the limbus. He proposed that in this posterior region the collagen was of a different orientation to the anterior limbus which is super-imposed on top. This was also postulated to contribute to the bio-mechanical strength of the cornea. Laminar section studies of the anterior and posterior of the cornea have indicated that there are marked difference between the regions at different depths and these differences are thought to contribute to the overall biomechanical stability of the tissue (Meek et al., 1987; Abahussin et al., 2009; Petsche et al., 2012). More recently it has been confirmed that the

circumferential collagen in located in the posterior 1/3 of the limbus providing strength and stability (Kamma-Lorger et al., 2011).

There was initial speculation as to whether the circumferential collagen in the annulus was an entirely separate structure from the rest of the cornea (with central corneal collagen just attaching to the ring) or if it was a region where the central lamellae changed direction to become circumferential. SHG and histological studies could not determine where the lamellar collagen sheets begin or end and it was thought that this provided evidence for an integrated collagen system across the cornea but with the possibility of collagen lamellae bifurcating and combining with collagen leading from other directions possibly from both the cornea and sclera (Meek and Boote, 2009; Newton and Meek, 1998). If this is the case, it would explain why the interface between the limbus and adjoining tissue demonstrates a decreased degree of strength when compared to the central cornea or sclera. This weakness along the limbus has been noted in a number of mechanical strength studies (note Chapter 4 and the organ culture model).

6.1.3 Biomechanics of the Normal and KC Limbus

Battaglioli and Kamm (1984) performed mechanical studies on the limbal sclera and found it to have an elastic modulus for circumferential tangential stress was 100 x higher than the elastic modulus for perpendicular/ compressive stress (Hanna et al., 1989). Maurice (1969) proposed that the limbus evolved to resist similar circumferential tangential stress, but not radial stress. It is thought that where the collagen attaches to the limbus there is an inherent weakness. This demonstrates that whilst the limbus retains a degree of strength in one direction, there are inherent weaknesses in the other.

Overall, the limbus plays an important role in the normal cornea for maintaining biomechanics and hence correct refractive properties. Any aberration to these functions (e.g. due to a pathology such as keratoconus), could lead to abnormal tissue architecture and overall function. Our hypothesis, therefore, is that in keratoconus structural changes may occur in the limbal region. This bilateral case study has given

us a unique opportunity to study the keratoconic limbus, and in particular to investigate the spacing and organisation of the limbal collagen fibrils.

6.2 Aims

The aims of this chapter are to use both keratoconic grafted eyes:

- To further investigate the opacities observed in the peripheral cornea
- To further investigate the doubling of the limbal interfibrillar spacing.

6.3 Methods

Details of the left cornea are given in the previous chapter. The right eye underwent PK for keratoconus 28 years prior to death. No further information was available. Four post-mortem corneo-scleral buttons from donors aged 71yrs (Control 1), 47yrs (Control 2), 88yrs (Control 3) and 71yrs (Control 4), with no history of keratoconus or refractive surgery, were obtained from Bristol Eye Hospital (Bristol, UK). The specimens were wrapped in clingfilm, frozen and stored at -80°C until the time of x-ray experiments. All corneas were evaluated using small angle X-ray scattering analysis at synchrotron station I22 Diamond Light Source, Didcot. The corneas were analysed at different sessions; however they were treated in the same manner. The cornea was placed in a purpose built Perspex and Mylar chamber on the beam line. The left eye was scanned at 0.5 mm intervals in a 29 x 29 mm grid (figures 6.2).

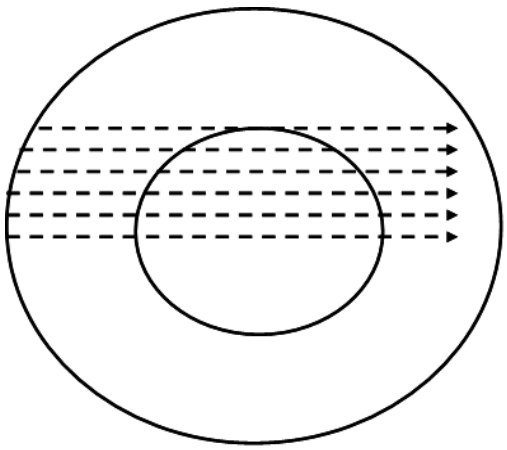

Figure 6.2: Schematic representing the collection of X-ray scans of the left post-PK keratoconus cornea. The entire cornea was scanned in 0.5 mm intervals. The normal human corneas were scanned at 0.5 mm in horizontal and vertical cross sections sclera to sclera.

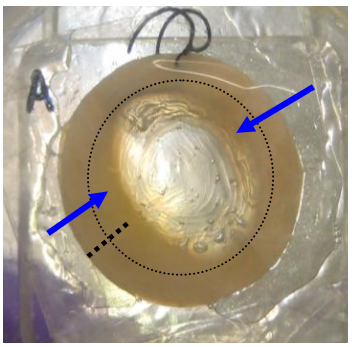

Figure 6.3: Anterior photograph of right cornea. There are two defined translucent corneal opacities in the cornea (blue arrows). Dashed line indicates the superior orientation.

The paired matched keratoconus grafted cornea (right eye)(figure 6.3) was scanned in four cross corneal sections (figure 6.4). The scans were created at 0.25 mm intervals to increase the resolution and thus discern more details about the changes in the peripheral cornea and limbus.

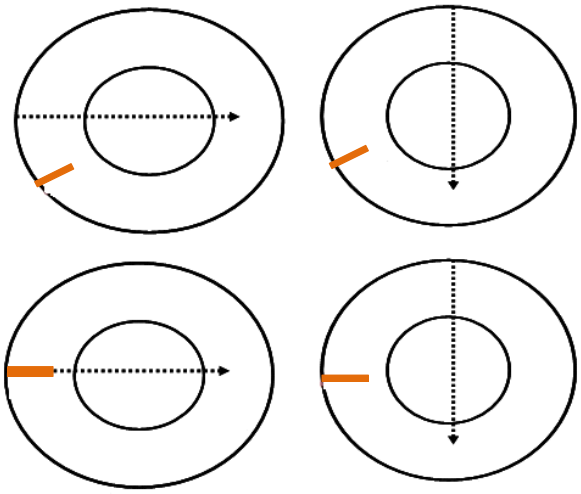

Figure 6.4: Schematic representing the scanning positions for right eye post operative PK keratoconus cornea. Dotted line represents scan and orange tag indicates superior position.

The collected data was then analysed for collagen fibril diameter and spacing using Statsitca ™ (StatSoft, UK) and Fit2D imaging software (ESRF, Grenoble, France). Graphs were created using Microsoft Excel 2007. A more in-depth overview of the methodology and analysis can be found in the General Methods (chapter 2).

6.4 Results:

6.4.1 Left Eye

When the left KC cornea was analysed using wide angle X-ray scattering, a feature not noted in the previous chapter was a clear doubling of the limbal annulus in the aligned collagen maps. This is, perhaps, more evident when the contour plot is displayed in Excel 2010 (figure 6.5). This doubling was observed in the region where there was a corneal opacity, so it was unclear if this opacity was being caused by scleral-like tissue in the peripheral cornea, or by some inward movement of the limbus.

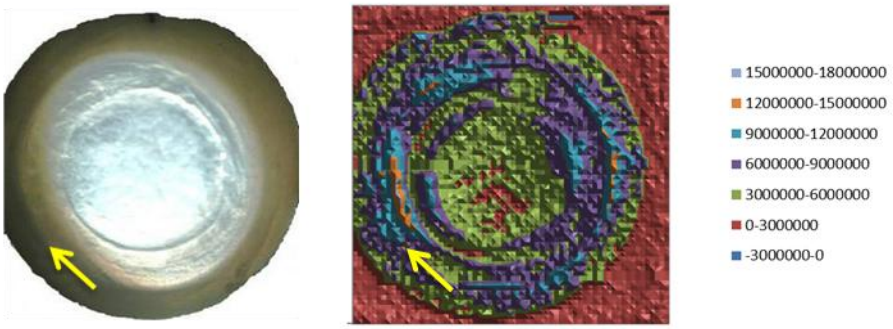

Figure 6.5: 3D aligned collagen map demonstrating the highly aligned doubling pattern in the limbal region (yellow arrow) which corresponds to the opaque region in the peripheral keratoconus cornea. This unusual pattern observed at the limbus had not been observed in any previous normal samples. As this pattern was unique, it was thought that exploration of the ultra-structure of the sample (and the matched pair) may also show some unusual changes.

a. Diameter

The diameter of the collagen at the corneo-scleral junction (as discussed in Chapter 5) demonstrated occasional increases in the region of the corneal opacity (figure 5.12C). Other diameter changes kept in line with those normally observed (Boote et al., 2003).

b. Spacing

During the initial analysis of the sample carried out in the last chapter, the presence of an unusual equatorial peak present in the inter-fibril spacing transform along the limbal/scleral region was also discovered (figure 5.14). This distinct double peak

corresponded to spacings of ~80-90 nm and ~100-120 nm and was not found in the host sclera, scar region or donor cornea. The normal expected spacing found in the extreme periphery of the limbal scleral region is ~80-90 nm (Boote et al, 2003; 2011). Therefore, the peak at ~100-120 nm presented an unexpected anomaly. It was thought that this required further investigation on the ultra-structural level so the SAXS patterns from the entire cornea were analysed.

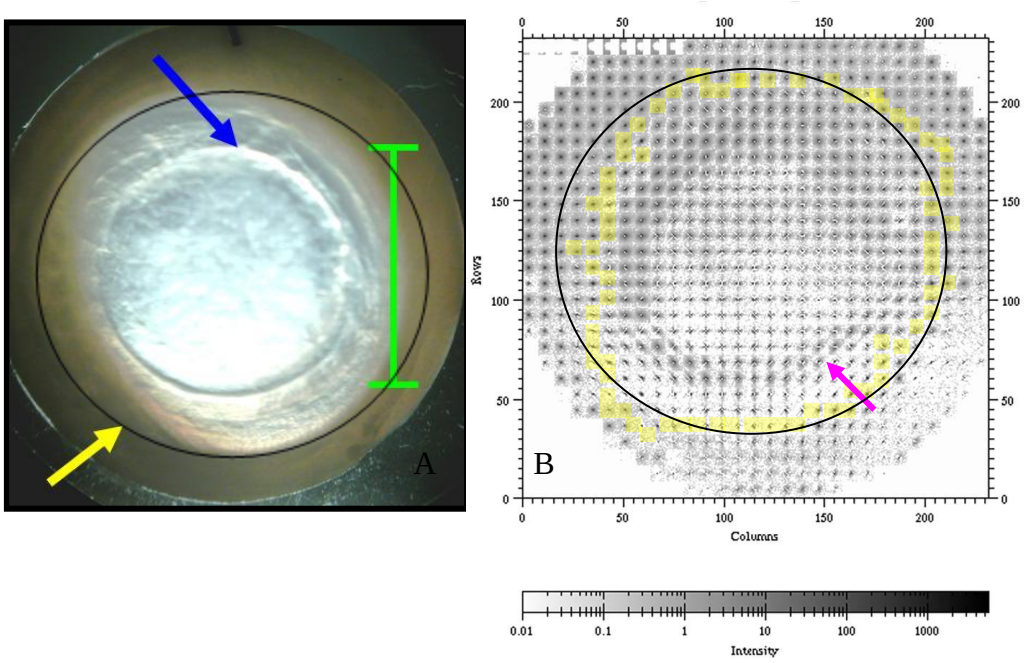

Figure 6.6: A) photograph of left post-PK keratoconus cornea. Yellow arrow indicates limbus and blue arrow indicates wound edge. Green bar = 8.5 mm B) Small angle X-ray montage of individual files. There is a higher intensity ring around the wound edge (pink arrow). The files that demonstrated a double peak are highlighted in yellow and the approximate position of the limbus is described by the black circle.

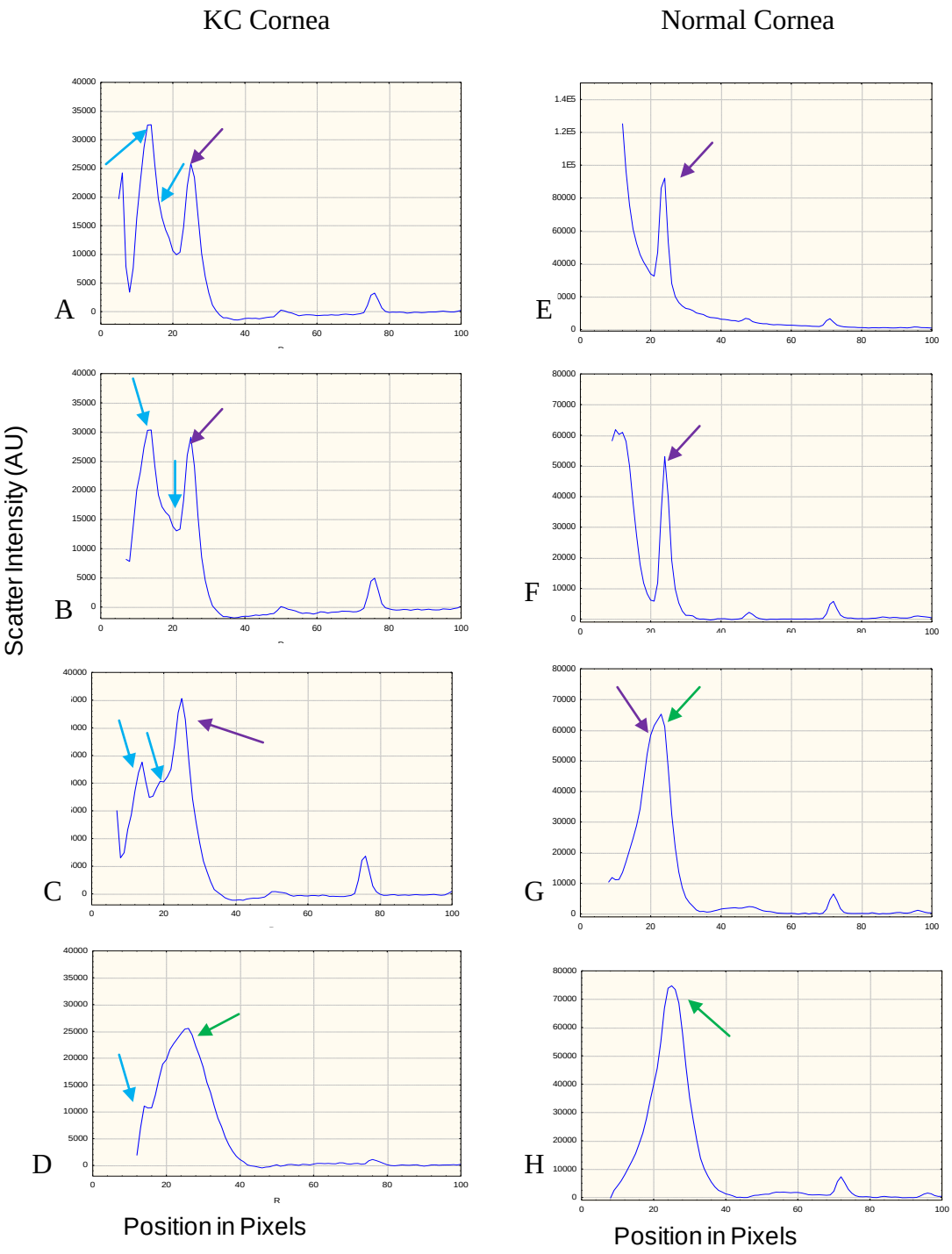

Figure 6.7: Demonstration of double peak (blue arrows) in the limbal/scleral region of a 12 year post-operative PK cornea (A-D). The position of the peak gradually moves until it merges with the equatorial spacing peak (green arrow). The purple arrows indicate the meridional peaks. In the normal human cornea (E-H) there is no double peak present. In G the equatorial peak begins to merge with the meridional peak before demonstrating a pure equatorial pattern.

A

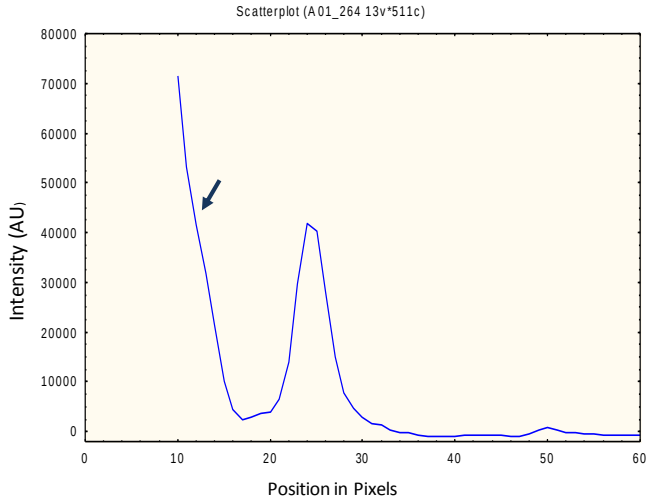

B

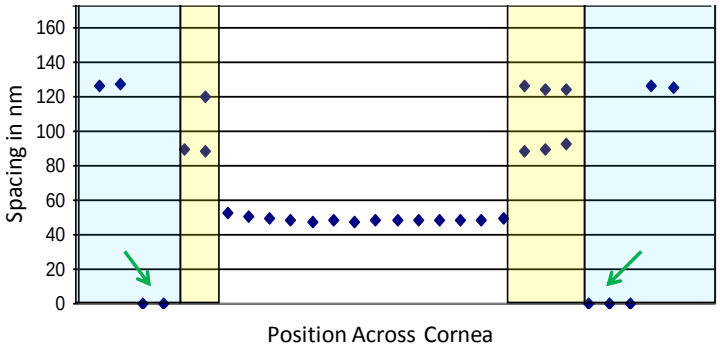

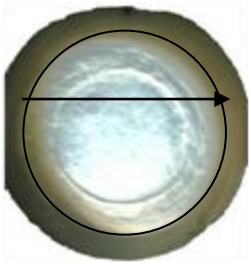

Figure 6.8: A) Increase in scatter found outside the double peak region which prevented measurement of the interfibrillar spacing. B) X-ray spacings in a transect across the KC cornea in nm (left eye). White section is the central cornea, yellow sections are the peripheral cornea and the blue section is the limbal/sclera. The doubling of reflections at the corneo-scleral junction is clearly evident. Interfibrillar spacings along the limbal/scleral border (green arrows) could not be quantified (represented by 0 in figure B). This was observed as a mostly circumferential ring outside the double peak. Inset demonstrates region of scan.

The double peak region was approximately 0.5-1.0 mm (one to two files) thick around the corneal/limbal join (figure 6.6). As the file position moved from periphery to centre the definition of the peaks first increased from the sclera and then gradually decreased until merging with the spacing peak associated with the central corneal tissue forming a shoulder. This was seen in figure 5.14 and can also be seen in figure 6.7 D, which was taken from a different region across the limbus where the double peak was more pronounced. In normal tissue the double peak was not present in any of the normal corneas studied in any of the corneal regions.

In addition to the 'double peak', in many regions there was an unusual area of increased background scatter found immediately beyond the zone where the double peak occurred. This area of increased scatter was so high that no peaks could be clearly quantified using the analysis tools (figure 6.8A). As this effect also occurs in the normal sclera, this increased scattering may be associated with scleral collagen in both normal and KC cornea. Figure 6.8B demonstrates the typical pattern of spacings in nm in a transect. The green arrows indicate the region of high scatter which precedes the region of the peripheral cornea where the double peaks are present (yellow bands).

6.4.2 Right Eye

The right eye (figure 6.3) was from the same patient, however there were several key differences noted between the left and right corneas:

The PK performed on the right eye was twenty to twenty-eight years prior. This presents a series of possible differences in the surgical/trephine method of removing the corneal button and re-alignment of the graft tissue. There also may have been differences in the type of stitches which were used in the procedure.
The right eye was suspected to have more progressed keratoconus (hence the earlier operation when compared to the left eye). There were two opposing corneal opacities (figure 6.3 blue arrows) that which were clearly visible more so than in the left cornea.

The scar was clearly visible in this sample, as it was in the other sample.

The graft appeared not to be orientated in the correct position (especially when compared to the later graft of the left eye shown in the previous chapter). In the small angle analysis, the SAXS patterns found in the right-eye appeared to be rotated several degrees (figure 6.9).

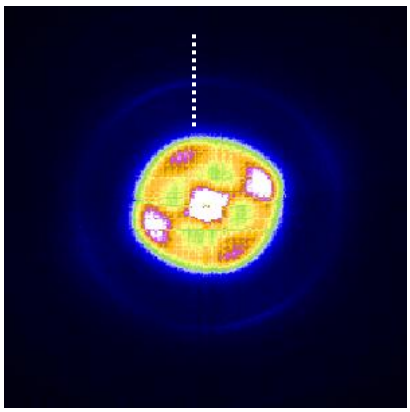

Figure 6.9: Central corneal scatter pattern from right-eye indicating the rotation of the samples. In a normal cornea the lobes would be orientated from a 12 o'clock position (white dotted line).

a. Diameter

There was a trend where, in the region corresponding to the corneal opacity, there was a statistically significant increase in the diameter (in some isolated regions +3 nm) (figure 6.10A). This increase in diameter was only observed in the regions of the corneal opacity. When the scan went through non-opaque regions of the tissue, an increase in diameter was not observed and the diameter appeared to be similar to normal corneal tissue as indicated by Boote et al. (2003) (figure 6.10 B).

b. Spacings

Figure 6.11 shows a series of transects across the whole specimen. In all four of the scans analysed, there was found the double peak at ~80 and ~120 nm in the peripheral corneal regions. This was observed bilaterally in each scan. In addition to these double peaks, there was also present an additional peak at ~140 nm found exclusively

in the regions of corneal opacity. This additional peak was not observed in the non-opaque tissue regions which were similar in appearance to the left KC cornea.

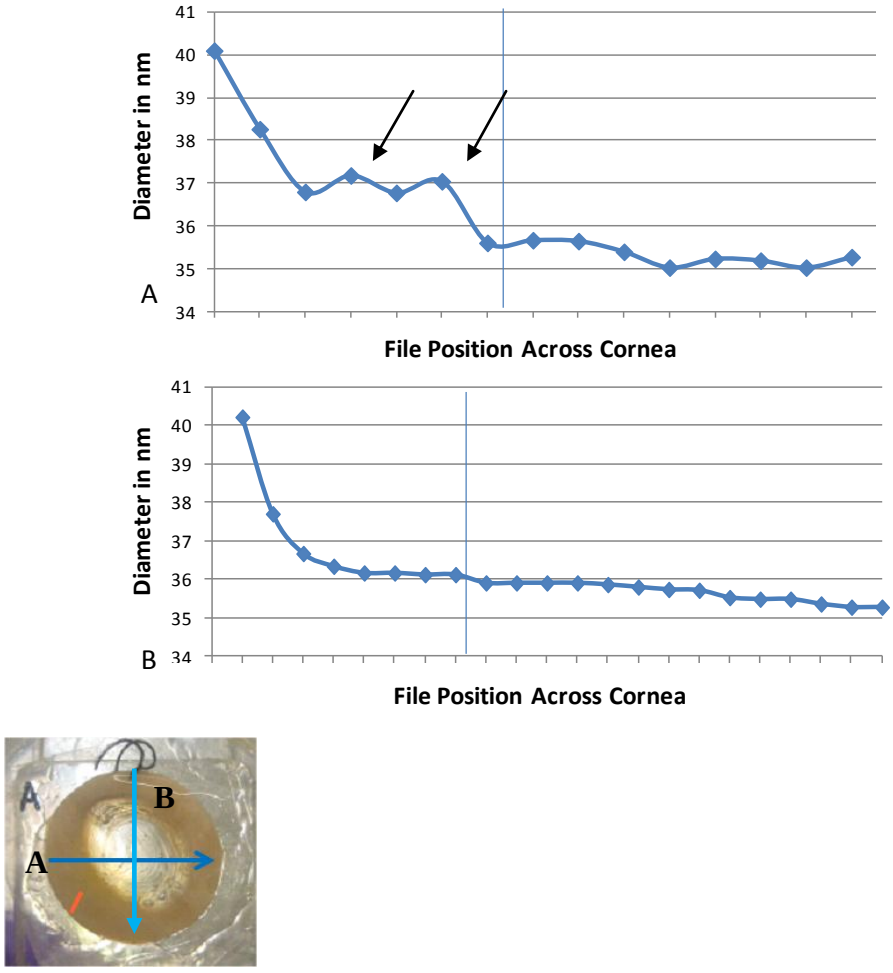

Figure 6.10: Fibril diameter for scan of KC cornea at 0.25 mm intervals. Central cornea is end of data series. There is a gradual decrease in spacing from periphery to centre as would be expected. Inset image of right eye indicating the scans (blue arrows) and the surperior position (orange tag).

However, the interesting observation was that there was a rapid increase in spacing corresponding to the observed opacity in the peripheral host cornea and limbus. In this region, there was the appearance of multiple interfibrillar spacings, similar to the doubling seen in the left eye. In addition to the spacings found at ~80 to ~120 nm, there were also present large spacings of ~140 to 160 nm in the same region (figure 6.11A and B). This additional set of peaks was not observed in the 'younger' graft, and may be an indication of a more advanced KC.

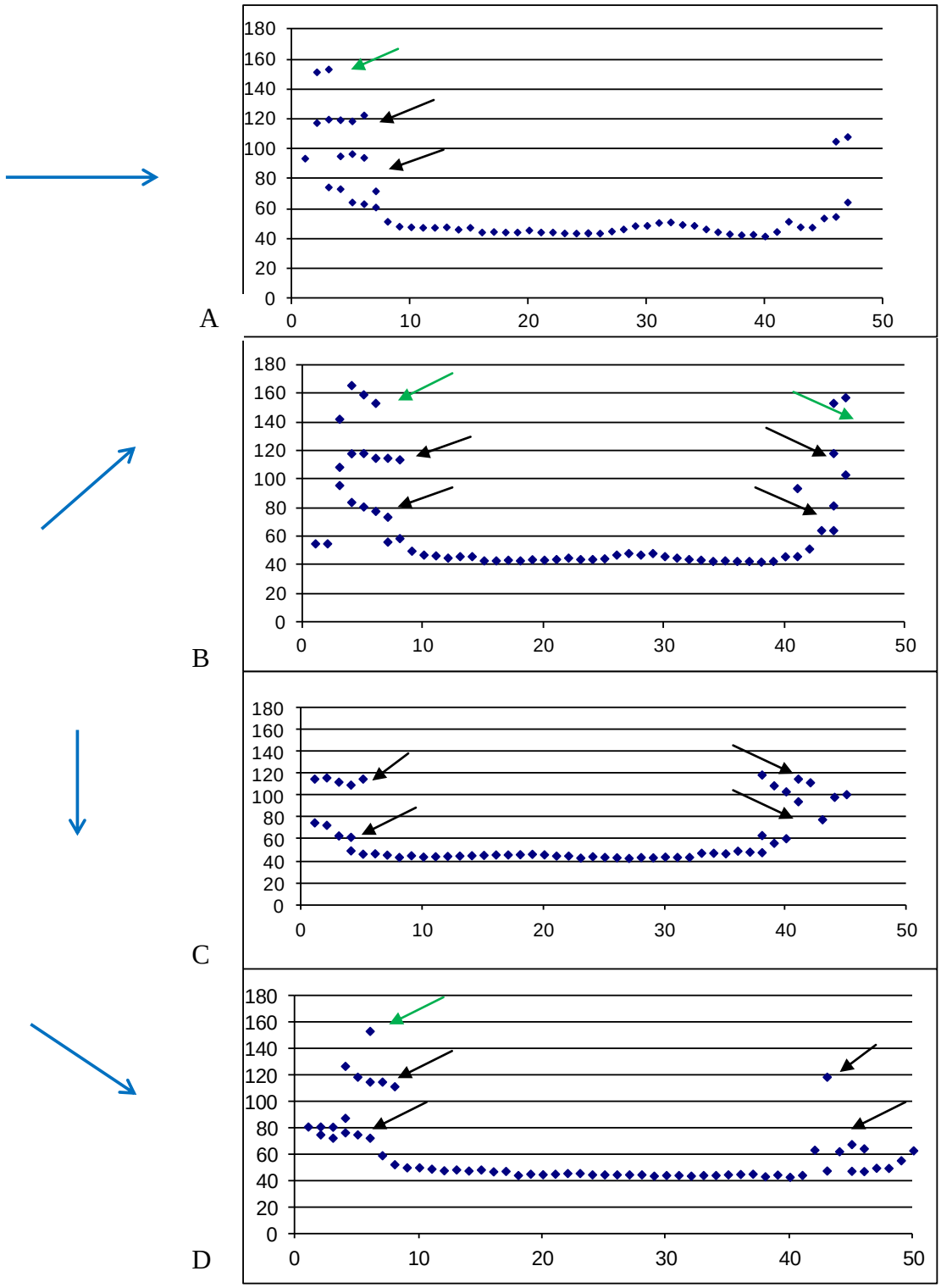

Figure 6.11: Transects of right cornea as indicated by the blue arrows in the inset. Black arrows indicate the double peak present at ~80 nm and ~120nm also observed in the left eye. The green arrow indicates an additional population of large spacings which appears to correspond to the corneal opacity.

There was a double peak present along the limbal borders in all of the cross sections, however in this sample there was more variation in the overall peak spacings (including additional peaks). The peaks at 120 nm and 80 nm remained however (figure 6.11).

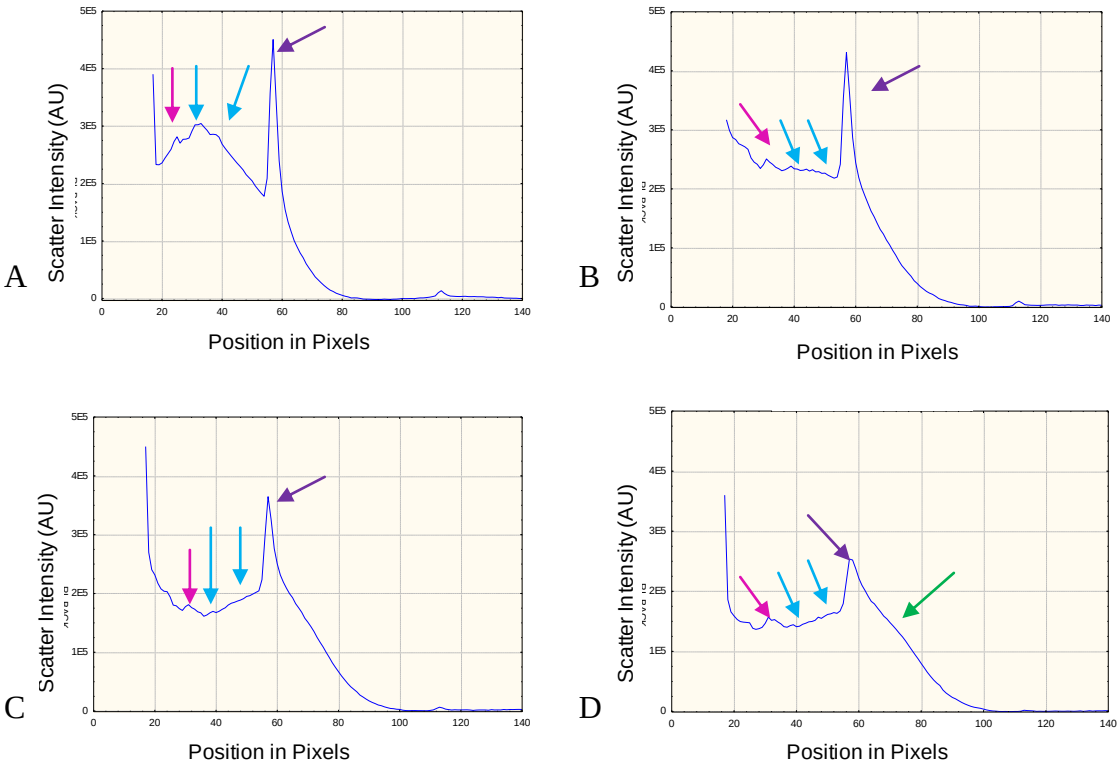

Figure 6.12: X-ray scatter from the right eye, from limbus into the cornea (periphery to centre A-D) demonstrating a high degree of disorder in the spacing peaks. The double peak was present at 89-90 nm and ~120 nm (blue arrows), but there were also additional high intensity peaks present (pink arrows). The disorder and extra peak corresponded with the region of corneal opacity. Purple arrow indicates the meridonal peak; green arrow indicates corneal equatorial peak.

6.5 Discussion

Novel discoveries were made regarding ultra-structural changes to the peripheral cornea and limbal/sclera of both the KC affected corneas. These include:

1) An apparent break-up and splitting of the limbal annulus as observed by WAXS.
2) A double spacing equatorial peak which was observed in the peripheral cornea in both the left and right eyes using SAXS. As the entire left eye was scanned,

this double peak was present circumferentially around the entire cornea. In the right eye, the double peak was present bi-laterally in the peripheral region of the scan. In both corneas the double peak was not observed in scleral or donor tissue.

3) The regions of corneal opacity demonstrated an increase in fibril diameter, an additional equatorial spacing at ~140 nm. These changes were not observed in either the scleral or donor tissue.

6.5.1 Left KC Cornea

The wide angle aligned collagen map of the left eye (as presented in figure 6.5) demonstrated structural changes in the peripherial cornea/limbal region. This was even more evident in the pair matched right eye (Gardner, 2012 unpublished). There appeared to be an annular splitting in the region of the corneal opacity which is not normally observed in the cornea. One possible explanation for this may be that the collagen in these regions is slipping or moving. The rings appear to be moving towards the central cornea.

The wide angle orientation map of the left eye in Chapter 5 (figure 5.8) also demonstrated a region of highly aligned collagen along the peripheral cornea which appears to correspond with the region of limbal splitting and the corneal opacity. One possible cause for the highly aligned opaque appearing tissue in this region may be due to a slippage of larger fibrils infiltrating the central cornea and possibly shifting the location of the limbal edge towards the central cornea. Upon visual inspection, this opaque region resembled scleral tissue. It was therefore thought that the results may be indicative of the congenital disorder sclerocornea.

Histological tests on the opaque tissue region from the right eye (Gardner 2012 unpublished) did not demonstrate the tell-tale signs of classic sclerocornea (i.e. an stromal architecture indicated by two distinct collagen populations with larger randomly arrayed collagen fibrils anterior and normal corneal stroma posterior. The histology also indicated that the limbus as illustrated in figure 6.1 was in the expected orientation and did not appear to migrate towards the central cornea. In terms of histology, the results for whether there is a population of larger diameter fibrils in this

region is inconclusive and would require TEM analysis in that region to better understand the ultra-structure.

Small angle analysis of this left KC cornea demonstrated a clear and unique circumferential ring presenting the double peak morphology in the interfibril spacing transform. These unique patterns were not detected in the limbal regions of the normal corneas analysed. The right cornea demonstrated the same doubling in the interfibril spacing indicating that this is either an individual condition or an indication of changes which may occur in the peripheral cornea during KC. This was different from the scatter patterns noted in the pre-pupiliary host and cornea graft tissue. The patterns observed also differed from the collagen noted in the scar tissue.

6.5.2 Right KC Cornea

In the general introduction chapter (Chapter 1) and Chapter 5 the orientation of donor corneal button following PK was discussed. In the past two decades, research has indicated that the proper harvesting of the corneal button and orientation to the host tissue is important in terms of improved wound healing, maintaining corneal biomechanics, and a reduced incidence of graft rejection. Wide angle analysis of the right eye (unpublished) indicated that the graft was not orientated correctly in the host cornea (Figure 6.9). This mis-alignment, the more advanced state of KC, and the increased age of the PK graft in the right eye may account for some of the more unusual results when compared to the left eye and normal tissue.

These results included:

- An increase in the collagen fibril diameter corresponding to the corneal opacity.
- Regions with additional x-ray peaks at 140nm in addition to the ~80 and ~120 nm peaks. These increases in spacing were again localised to the peripheral keratoconus tissue and corresponded to the regions of corneal opacity.

The x-ray data from the normal corneas examined in this study followed the same trend as outlined by Boote et al., (2003) where x-ray patterns change markedly and

rapidly from a limbal/scleral type to a corneal type (figure 6.10 B) of one large smooth peak and then back again on the other border. There was not observed any transitional regions as observed in the KC cornea.

6.5.3 Biomechanical implications

Whilst there were fundamental differences between the two eyes, both the left and right eye demonstrated the unique double peak at ~80 and ~120 nm. In this respect it may be relevant that there is normally found a ~120 nm in the peripheral scleral tissue in the trabecular meshwork. However, the presence of multiple spacings presents evidence for a potentially keratoconus related causation be it bio-chemical, biomechanical, or a combination of the two. This said, it is important to bear in mind that this is a single case study, so there is the possibility that the changes observed are individual variation, however as none the normal corneas demonstrated this double peak, the findings do fit into more of a keratoconus model.

As this effect has not been noted in any previously analysed corneas, in order to better understand what is occurring in the KC sample it is necessary to look at other similar SAXS studies on collagen and other biological tissues. There are few SAXS studies in the literature which have demonstrated doubling of collagen equatorial X-ray reflections. The few studies available for comparison have either indicated double peaks in the meridional collagen transform and/or have been based on the degradation of tissue/collagen in fibrotic diseases.

Weidermann et al. (2007) looked at non-ischemic fibrosis of cardiac tissue and found that SAXS scattering produced a distinct double peak which was equatorial (Weidermann et al., 2007). Kennedy et al. (2004) also noted a double peak evident in their SAXS analysis of Type I collagen (parchment) once treated with lasers of certain damaging frequencies, however these peaks were meridional (Kennedy et al., 2004). These two scenarios could both be possible explanations for the double peak which might indicate a pathological destruction of the fibrils of that region due to the underlying bio-molecular changes namely an underlying bio-molecular tissue pathology which leads to degradation when put under destructive forces. Another

theory is that there is an actual mechanical separation of the collagen layers of the limbus. These theories will be discussed in greater detail.

6.5.4 Double spacing in the limbus

Earlier in Chapter five, the observed phenomena of an equatorial 'double spacing' at ~ 80-90 nm and ~100-120 nm was briefly introduced. The observation of this unusual spacing was limited to outer edge of the transparent keratoconic cornea. In some positions, this effect was adjacent to a small area (approximately 0.25 mm) of intensely high scatter on the limbal/scleral side. Neither of these was observed in the normal human peripheral cornea or limbus.

Prior SAXS analysis of normal and pathological corneas focused on scans from limbus to limbus. It was thought that the scleral tissue outside these regions in the sclera consistently produced too high a scatter pattern similar to the Type I collagen of the rat tail tendon. In these extreme peripheral regions, the first collagen order appears to gradually disappear. A complete analysis of the limbal/scleral tissue of this KC sample is the first of its kind, and there have been no other known studies or publications to date focusing on this research (Hayes et al., 2010).

There has been much speculation regarding the processes which occur along the limbus with the progression of KC. There are known structural changes which occur in the anterior portion of the cornea (e.g. the fracturing of the Bowman's which is thought to lead to vascular ruptures and a decrease in corneal innervations). There are also a number of structural changes which at the moment are poorly understood. Theories have been proposed for several different models including the slippage and "unravelling" of collagen along the limbus as well as a pulling on the collagen. As was noted earlier in the introduction chapter, it is thought that collagen lamella change orientation along the limbus and it may be an area of structural weakness (Meek and Boote, 2004). However, Edmund (2009) performed a study analysing the diameter of the approximated corneal/ limbal ring in both normal and keratoconic patients and found that there were no significant differences in the size and shape of the corneal limbal ring leading to the belief that the changes associated with KC on the

biomechanical level are most likely isolated to the central and pre-pupillary cornea (Edmund, 2009).

I propose to present a number of theories to attempt an explanation for the 'double peak' phenomenon found in the peripheral KC corneal tissue.

6.5.5 Stress and Strain

Both organic and inorganic materials undergo structural changes when placed under a degree of biomechanical force (e.g. stress, strain , sheer, or compression). When materials are faced with a pulling force along the x/y axis, they have a degree of elasticity or 'give' before reaching plastic deformation and then a breaking point. Forces may also be applied with a degree of rotational motion (sheer forces) which may cause distortion to the material. Viscoelastic materials may also undergo deformation on the structural level after forces are repeatedly applied before tissue failure.

Analysis tools such as TEM/SEM and other microscopy have been useful to better understand the structural changes which occur on the molecular and fibril levels of tissue however these changes are observed at set time points (e.g. stress/time). Whilst X-ray scattering techniques could provide invaluable information regarding the ultra-structural changes which occur in tissue, applying the technique on tissue as it is undergoing stress or strain has been difficult.

Non-destructive techniques such as XRD can be used to observe ultra-structural changes in real-time. There has been, one recent study where Type I rat tail tendon collagen has been analysed using SAXS whilst under stress. The study discovered that under stress, changes in the spacing between the collagen molecules led to a meridonal double peak from the D-periodicity of the collagen (figure 6.13).

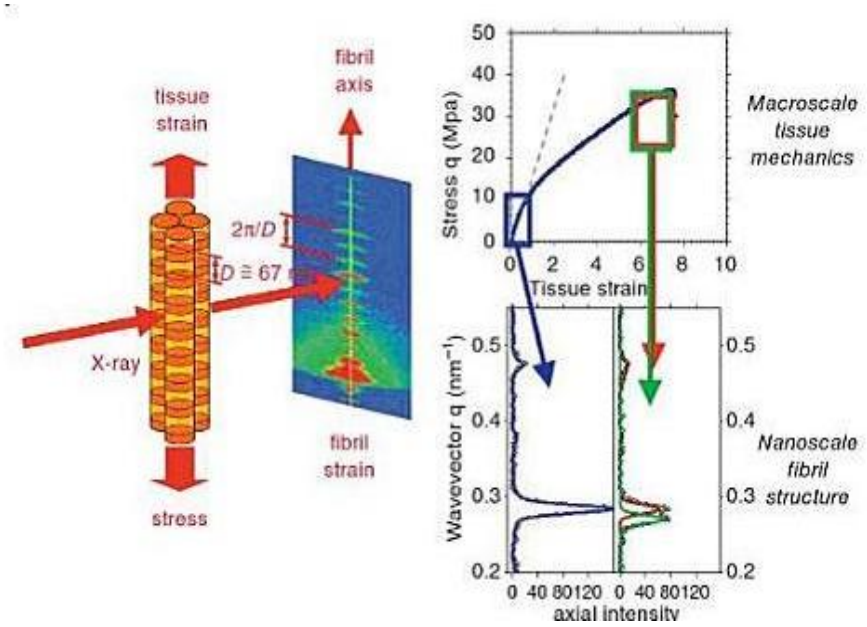

Figure 6.13: Schematic representing the SAXS double spacing of collagen fibrils which can occur when the tissue is under direct stress. Kumar (2010)

Kennedy et al., (2004) and Wess et al. (2004, unpublished) noted that there was a meridional double peak produced in parchment collagen following laser cleaning at certain light wavelengths (figure 6.14). The double peak was not found in the control samples nor was it found in samples which were cleaned at the less destructive wavelengths. The group surmised that damage was caused to the collagen long range order and caused a double spacing. Whilst that study focused on meridional scatter patterns, the principle behind the scattering is the same and the double peak in our KC specimens may be the result of damage or degradation of collagen.

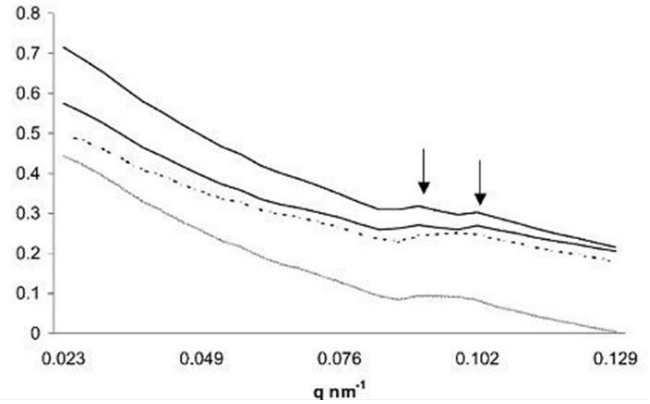

Figure 6.14: Demonstrating a meridional double peak which occurred in parchment following damage from a laser used for surface cleaning. It is thought that the damage to collagen may cause such a peak. CJ Kennedy et al., 2004

Applied to the KC corneal model, it could be possible that the tissue along the limbus is put under a high degree of pressure and strain with the advancement of the KC tissue as the pressures increase, the elasticity of the material may decrease. As noted previously if the KC tissue has underlying bio-mechanical deficiencies (especially along the limbus) the strain which is put on the periphery of the cornea could lead to the collagen being pulled apart or frayed resulting in the collagen spacing to be altered. Whilst the normal cornea possesses elastic properties to accommodate this compressive pressure, in the KC cornea there may be underlying biological weaknesses and the stresses may be too great; the tissue may not return back to near normal physiology, even after the PK surgery. This could only be a partial explanation as the changes observed in the previous study using rat tail tendon was observed in the meridional peak and not in the equatorial packing of the collagen.

6.5.6 Separation of the Limbal Collagen Layers

The most plausible explanation for the double spacing based on the limited literature available may be due to differences between the anterior and posterior collagen layers in the limbus. Sheilds et al. (1973) noted that the normal limbus is made up of two distinct collagen layers with two distinct fibril diameters. In their study, they

Table I. Ultrastructure of human limbal collagen

	Average fibril diameter (nm.)		*Fibril concentration, avg. & (range) (percent of area)*	
	Inner portion	*Outer portion*	*Inner portion*	*Outer portion*
Glaucoma cases:				
1	96.51	96.51	54 (55-71)	66 (61-73)
2	113.10	124.74	61 (58-66)	64 (57-71)
3	94.67	109.22	63 (52-67)	65 (62-64)
4	103.01	103.69	67 (59-77)	68 (65-70)
Average	101.82	108.50	64 (56-70)	66 (61-71)
Nonglaucoma cases:				
5	89.34	102.34	69 (63-74)	71 (65-76)
6	78.76	84.49	68 (67-69)	68 (65-73)
7	116.98	134.73	66 (62-71)	65 (61-73)
8	114.46	167.03	64 (61-67)	61 (59-62)
Average	99.89	122.15	67 (63-70)	66 (63-71)

Figure 6.15: Chart demonstrating the variation in collagen fibril parameters between anterior and posterior limbus of normal and glaucoma patients (Sheilds et al. (1973)).

were concerned with the differences between glaucoma and healthy eyes. There was also a focus on how the pressure of glaucoma affected the fibril diameters and collagen packing (figures 6.15 and 6.16). Applicable to the current study, they obtained TEM images of the two collagen segments to determine average fibril diameter and packing. In the normal eye, the two layers are atop each other. If the two layers were sheared, the spacing within either or both layers could change, resulting in two separately spaced populations of fibrils such as we have observed.

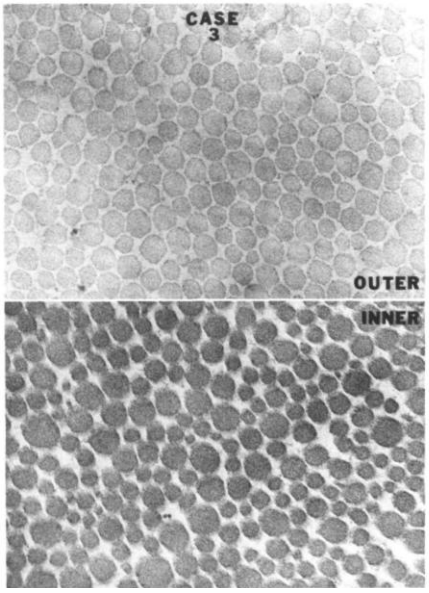

Figure 6.16: Electron micrograph of collagen fibrils from the inner and outer portions of the limbal collagen. X56,0000 (Shields et al., 1977)

The KC data also demonstrated that as the tissue was analysed closer to the central cornea and the donor tissue, the additional peak gradually disappeared until it merged with the first order of collagen. This could be an indication that the limbus is facing more strain out towards the periphery and the effect is not as pronounced towards the central cornea. This may also be an indication that the strain is located in the area of greater weakness which would be the join between the limbal and corneal stromas (figure 6.17).

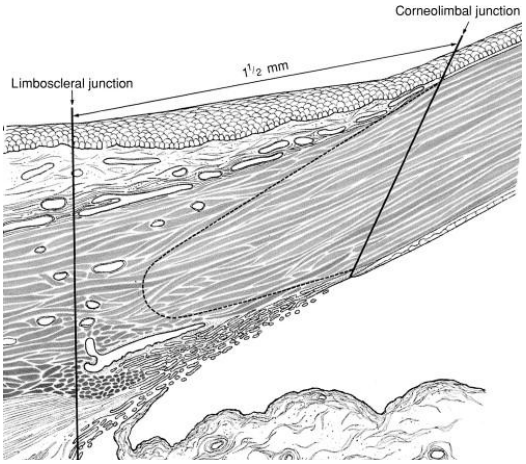

Figure 6.17: Schematic of the limbal/scleral/corneal join. This may be the region where the limbus begins to separate. Ehlers and Hjortal 2005

6.5.8 Sclerocornea

In the congenital disorder sclerocornea, there is a transitional region between the limbus and the cornea which appears translucent to opaque (note chapter 5). In both samples studied, there was found a partial arcus of sclerocornea type tissue (although it is not known if the patient was officially diagnosed as having the disorder). As previously noted, the disorder presents a double layer of collagen in the limbal stroma (one layer scleral in phenotype and one normal corneal/limbal) with an increase in fibril diameter in the region. Our findings did note a possible 'double population' of collagen with an increase in diameter especially in the regions where the transparency was most decreased. This may indicate that the unique double spacing may not be attributed to KC but to sclerocornea.

To date, there has never been X-ray analysis of sclerocornea so further investigation may be required to conclusively rule it out. This may be difficult as one of the markers used to diagnose the disorder is a ruptured or interrupted Bowman's layer (which is also a common symptom of KC. Although the presence of the sclerocornea may be the underlying cause of the double-peak found, as it was observed in selected regions and not circumfrentially around the limbus, it could possibly be ruled out.

7. General Discussion

In this wound healing study, a range of different pathological and acutely injured mammalian corneas (human, sheep, and mouse) were evaluated using a range of quantitative techniques. These techniques encompass small and wide angle X-ray scattering, histological analysis, immunofluroescence, confocal microscopy and second harmonic imaging, spectrophotometry, UV/Riboflavin cross-linking and cell/organ culture model.

The aims of this thesis were:

1) To use X-ray scattering techniques to investigate the role of Pax 6 on the ultrastructure of murine corneas
2) To investigate the use of oral mucosal fibroblasts in corneal wound healing treatment of LASIK injured ovine corneas
3) To use X-ray scattering techniques to investigate the healing response in a 12-year post-operative penetrating keratoplasty for keratoconus
4) To use small-angle X-ray scattering to investigate limbal collagen ultrastructure of keratoconic and normal human tissue**.**

7.1 The Use of X-Ray Scattering to Determine Collagen Organisation in Pax Mutant Microphthalmic Mouse Corneas

Given the results to date, there does not appear to be a conclusive answer as to whether the morphological changes associated with the microphthalmic pheynotype is directly or indirectly caused by an alteration in collagen amount, alignment, and orientation and what external factors (e.g. eye opening) or endogenic factors (e.g. genetic strain or the natural aging process) may have on the overall organisation of collagen. As similar results are observed in both the small eye mutant and the large eye ‘wildtype’ specimens, it cannot yet be ascertained if the differences between groups are due to genetic strain or due to the actual Pax dosage. Some of the

differences which were noted between the Cardiff University wildtype eye and the Edinburgh eyes (e.g. total collagen amount) may also be due to the separate XRD analysis or to the specific genetic strain of mouse. Further analysis would be required at both similar and different time-points to determine if the differences can be substantiated.

The differences between the Pax +/- and the PAX77+ specimens (with their associated 'wildtypes') did present a repeatable, albeit unexpected, result. As both mutations were bred into the same genetic strain background, it would be assumed that they would resemble each other in the large eye genotype/phenotype. This was clearly not the case. In all individuals within the groups, the proposed collagen amount (scatter), alignment, and orientation were similar but differed between the groups of reduced Pax and increased Pax expression. Further analysis would be required to determine if this is a real result based upon the desired mutations or if it is evident strain differences.

As the Pax gene family is highly evolutionarily conserved, there is an established global pathway of activated genes and biological cascades. Alterations to these pathways carry a high level of individual variability as they are interlinked with other developmental genes (e.g. Sox) and a number of down-stream growth factors. Whilst there is an overall trend of phenotypic changes in both Pax 6 +/- and Pax 6 over-expression (as outlined by Dora et al., 2006), this individual variation makes it difficult to conclusively note differences and an increase in specimen numbers would be required. There is also the added complication of the possible developmental dependency on the results and a further study similar to the Sheppard study (Sheppard et al., 2010) may be of benefit for each of the mutant strains at various developmental time-points. This would provide conclusive evidence as to whether the differences observed are also developmental and more importantly (in the case of Pax77+) regressive.

Although the results are at present inconclusive, there could be a possible link between individual eye opening, the visual feedback system spurring post-natal development, and the incidence of the small-eye phenotype. This could be a possible explanation as to why there are genotypic small eye mouse which present a large eye

phenotype and vice versa. This could be an indication that the cause lays more with the biomechanical changes which occur preceding and following eye-opening and not necessarily the dose of Pax.

In addition, if the ultra-structural changes noted in the samples are liked to development (both pre and post-natal) then the results would be age dependent. In this study there were marked differences between the two groups studied at different age points. It would be of interest to perform an age-dependent study of the mice to determine if the age of the animal does in fact impact on the collagen organisation and distribution.

7.2 The Use of Oral Mucosal Fibroblasts as a Novel Treatment for Increasing Transparency and Flap Strength in LASIK Wounded Sheep Cornea

The overall results from this preliminary study have indicated a potentially useful autologous cellular treatment for increasing transparency and overall flap strength for LASIK-type corneal wounds. The results demonstrated that cultured corneas treated with oral mucosal fibroblasts produce a flap which is more transparent and stronger than naturally healing flaps. There were clear increases in flap transparency in the oral mucosal treated corneas at the one, two and three week time-points along with increasing flap strength. There also appeared to be an overall down-regulation of a-sma in the oral mucosal treated flaps which would be consistent with an increase in overall transparency and a decrease in haze/scatter however this will require further exploration. It was also noted that there was an increase in the time required to detach the flap so the elastic properties of the oral mucosal collagen may affect flap dehiscence. This would require further biomechanical analysis.

The possibility of immunological rejection has not been explored with this study. The human cells appeared to promote wound healing, and it would be of interest when performing in vivo studies if there is a degree of rejection. Also if any swelling or inflammatory response found in this study may be due to an immunological response. The oral fibroblasts are adult differentiated cells from a base population of oral progenitor cells. Recent studies have indicated that oral progenitor cells are immunosuppressive in a dose dependent manner (Davies et al., 2011). There is the

possibility that is the oral fibroblast population there remain a certain number of the un-differentiated oral progenitor cells. These latent cell populations may provide immunosuppressant properties. This will also require further study.

7.3 Evaluation of Corneal Scar Tissue Following a Twelve Year Post-operative Penetrating Keratoplasty for the Treatment of Keratoconus

The unique 12 year post-operative KC cornea presented a range of results which were both expected and unique. Overall, it was surprising that after 12 years the wound margin was clearly visible with a clearly defined ring of circumferential fibrotic collagen. It was also surprising that the supposed KC related changes were isolated outside the graft margin in the host tissue and that the donor tissue remained bio-mechanically unchanged. This leads to the conclusion that the changes which occur to the KC cornea are most likely a combination of both the underlying tissue and the biomechanical forces and are not exclusive of each other. In the event that KC was caused entirely by biomechanical changes then the central tissue would have been affected to resemble pre-operative KC buttons.

Below is a summary of key pull-out points regarding the first part (left eye) of this study.

1) The donor tissue did not change collagen orientation, spacing, or distribution nor was it re-modelled in any obvious way. This could be the result of the biomechanical uncoupling of the donor and host following the surgical incision or of the slow tissue turnover in the donor tissue.

2) Although the scar region along the wound margin remained visible to the naked eye and under the light microscope, the alterations of the collagen ultra-structure were not as marked as expected. The collagen spacing and diameter of the wound appeared to be similar to the surrounding tissue (bar the degree of disorder of the peak). At the lamellar level there remained collagen which appeared to run parallel to the wound around the entire margin. This is consistent with the overall appearance to the scar apparent along the graft.

3) The host tissue along the peripheral cornea and limbus demonstrated small localised regions of lamella disorder, however most of the tissue appeared normal. This is supported by the literature where it is noted that most of the KC based changes are located in the central/nasal button. There was an increase in collagen along the limbal/sclera which would be expected, but the peripheral cornea did not appear thicker than normal.

4) Overall, the differences between the peripheral cornea of the host and the donor tissue did not demonstrate many clear differences when analysed using SAXS. This was generally consistent with the findings of Daxer and Fratzl, (2007) and Fullwood et al., (1993). The SAXS analysis of the limbus did demonstrate 'double peaks' in the interfibril spacing transform which followed the border of the limbus/corneal opacity. This will be discussed in full detail later.

7.4 Evaluation of Limbus in a Twelve Year and Twenty-eight Year Post-operative Keratoconic Corneas

There were clear and evident changes in the corneal collagen ultra-structure of the limbus as discovered using small angle x-ray diffraction. The unique small angle scatter patterns observed in the periphery of the cornea (limbal/sclera region) will require further investigation. This will include and comparison to healthy tissue.

The exact causes of the 'double peak' can only be hypothesised at present. The most plausible reasons appear to be either a shear induced separation of corneal layers containing collagen of different spacing and packing density which may be attributed to the distortion of the cornea. Another possible explanation may be the fraying or separating of the collagen fibrils which could create a separate peak during tissue stress and strain. The final explanation may be the presence of another substance along the peripheral cornea/limbus which may be causing additional scattering.

The bio-mechanical hypothesis of collagen ultra-structural changes resulting from keratoconus is thought to be based on alterations to both the anterior and posterior

cornea. In the anterior cornea is hypothesised that the collagen detaches from the Bowman's where in the posterior cornea it is thought that the lamellae detaches from the limbus. This could result in an increase in collagen length and a lateral re-arrangement of the collagen (Meek et al., 2005). The overall effect is a slippage between the lamellar collagen and a reduction of cohesive strength at the apex of the cone where the stroma is the thinnest (Smolek, 1993). Keratocytes are thought to add to biomechanical strength and a loss or damage to keratocytes may lead to a loss in overall stromal stability. This could be a contributory factor to the structural changes associated with KC (Snyder et al., 1998). It is not inconceivable, and indeed may be highly likely, that these changes could also occur in the peripheral keratoconic cornea.

In the unique keratoconic tissue, there was found to be a 0.5 -1.5 mm circumferential ring of collagen following the limbus with a clear double spacing at 80-90 nm and 120 nm. Whilst the spacings indicate the possibility of two populations of collagen with different packing, the diameter of the collagen in this region was consistent with neighbouring collagen. There were slight increases from centre to periphery, however this was not aberrant from what would be expected from previous studies of collagen diameter across the cornea (Boote et al., 2003). The shape of the fibril diameter transform in this region demonstrated a slight degree of disorder, but not significant when compared to other areas of the tissue. It is for this region that it is thought that effect of the shearing of the two distinct limbal collagen populations leads to measurable changes in their respective interfibrillar spacings, but the shearing has little or no effect on their respective diameters.

Whist there have been studies of the meridonal peaks produced by collagen SAXS scanned under tension, there have not been any studies to date of the equatorial peaks produced. As the equatorial peaks would indicate the packing order and spacing of the tissue through the depth, it would also be necessary to perform similar experiments to determine if a double peak is created in similar circumstances. It should also be noted that as KC involves a degree of ECM degradation, the effect produced in normal tissue may be different from the diseased tissue. The experiment could be repeated using corneas which have undergone some type of collagen digestion which may be akin to the ECM changes associated with KC.

7.3 Future Studies

The research presented in this thesis raised a number of questions which will require further investigation at a later point. As this thesis was focused on X-ray scatter techniques, further information may be uncovered using alternative research methods including in-depth immunohistochemistry, TEM, and molecular biology techniques. In the following section, some of these are outlined:

7.3.1 The Use of X-Ray Scattering to Determine Collagen Organisation in Pax Mutant Microphthalmic Mouse Corneas

- Microcorena tends to result in a more flattened cornea phenotype in humans, it would be of interest to measure the curvature of the PAX77+ corneas using photo-keratoscopy. It would also be interesting to see if there are any refractive aberrations in the Pax 6+/- corneas due to the abnormal distribution of cornea.

- It would be of interest to perform a count of the total number of fibroblasts in the stroma using H&E stain. This would confirm or refute the theory that there are less fibroblasts in *Pax 6* deficient eyes or that the fibroblasts are somehow damaged.

- Small angle X-ray scattering has been performed on samples and would need to be analysed in the future. Preliminary analysis has indicated differences between the three strains. This will give us more information about the collagen fibril size and spacing. This would be of particular interest in the Pax 6+/- corneas which sometimes appear to have a clouded phenotype.

- It was noted that PAX77+ mice had a high incidence of congenital cataracts. The lenses of these mice could be analysed in the future using X-ray scattering

7.2.2 The Use of Oral Mucosal Fibroblasts as a Novel Treatment for Increasing Transparency and Flap Strength in LASIK Wounded Sheep Cornea

- Future experiments could be performed *in vitro* with species/autologous matched oral mucosal fibroblasts. In our experiment we used human cells on a sheep model. A species match may produce even better results and provide information regarding the immunosuppressive properties of the cells.

- TEM images could be taken of the newly deposited matrix to see how the new oral mucosal collagen compares to the native collagen when viewed in the flap bed.

- Cells could be fluorescent labelled/tagged to see if they migrate and how many stay on the wound. It may be necessary to create a contact type bandage, collagen gel, or other transport vehicle to see if the results could be improved.

- In vivo studies on species such as rabbits could be performed. In these cases the tissue could be autologous mucosal samples and the wound healing time-frame could be extended to six months or more. This would allow for the tissue to be re-modelled naturally and better match a natural human model.

- Further X-ray scattering could be performed at other time-points

- PCR or wound healing gene assays could be performed on the tissue to see if the oral mucosal cells retained their ‘oral mucosal-ness’ or have been transformed in tissue with more of a corneal genotype.

- Western Blot and immunohistochemistry can be performed to determine if the treated cells undergo apoptosis.

- Cross linking studies could be performed to observe cell death over time.

- Ultimately, it is hoped that the study can be applied to human research subjects with autologous cell treatments. If animal trials are successful, there may be scope to explore oral mucosal cells as a treatment following surgery or injury.

- Repeating the test using other types of OM cells (e.g. oral progenitor cells) which may have even more 'stem-like' properties.

- TUNEL or apoptosis analysis could be performed to indicate whether the increased flap strength is due to the cells or if it is due to the newly deposited matrix

7.3.3 Evaluation of Corneal Scar Tissue Following a Twelve Year Post-operative Penetrating Keratoplasty for the Treatment of Keratoconus KC Cornea

- Preliminary TEM has been performed on the thicker scar region along the by a colleague (results to be published). It would be of interest to obtain TEM results from the KC corneal host tissue and the donor tissue to compare the ultra-structure with the scattering results.

- A series of histological analysis could be performed on the samples including H&E staining, TUNEL analysis to detect keratocyte apoptosis and immunohistochemistry for a-sma to detect any long term activation of the keratocytes and types of collagen deposited.

- Second harmonic generation of the host, donor, and scar tissue to observe the collagen arrangement in the anterior and posterior cornea.

- Studies of the Bowman's along the wound edge and limbus to determine collagen changes.

7.3.4 Evaluation of Limbus in a Twelve Year and Twenty-eight Year Post-operative Keratoconic Corneas

- In order to determine if the stretching of the cornea results in the formation of a double peak, SAXS analysis could be performed on corneas which are under tension to determine if the tissue deformation results in a double peak. In addition to normal corneas under tension, it would be of interest to digest some corneas in a-amalyse before stretching to replicate the believed changes which occur on the bio-molecular level in KC disorders.

- Histological analysis along the limbus of the KC and normal corneas to determine if there are micrograph evidence of a double spacing in the collagen along the limbus or if the tissue is in fact sclerocornea.

References

Aghamohammadzadeh, H., Newton, Richard H & Meek, Keith M, 2004a. X-Ray Scattering Used to Map the Preferred Collagen Orientation in the Human Cornea and Limbus. , 12, pp.249–256..

Alió, J. et al., 2002. Intracorneal rings to correct corneal ectasia after laser in situ keratomileusis. *Journal of cataract and refractive surgery*, 28(9), pp.1568–74. Available

Alió, J.L. et al., 2005. Corneal modeling of keratoconus by conductive keratoplasty. *Journal of cataract and refractive surgery*, 31(1), pp.190–7.

Almer, J.D. & Stock, S.R., 2005. Internal strains and stresses measured in cortical bone via high-energy X-ray diffraction. *Journal of structural biology*, 152(1), pp.14–27.

Ambrose and Wilson 2003 LASEK vs PKR *Seminars in Ophthalmology* Volume 18 no 1 pp 2-10.

Andreassen, T.T. et al., 1980. Biomeehanieal Properties of Keratoeonus and Normal Corneas Institute of Anatomy C , University of Aarhus , and Department of Ophthalmology . pp.435–441.

Arentsen, J.J., 1983. Corneal transplant allograft reaction: possible predisposing factors. *Transactions of the American Ophthalmological Society*, 81, pp.361–402.

Ashery-Padan, R. & Gruss, P., 2001. Pax6 lights-up the way for eye development. *Current opinion in cell biology*, 13(6), pp.706–14.

August, R., 1965. Persistence of D o n o r Collagen in Corneal Transplants * Department of Opthahnology , Col , umbia University Col &’ gc of l) hysicians and. , 26.

Battaglioli, J.L. & Kamm, R.D., 1984. Measurements of the compressive properties of scleral tissue. *Investigative ophthalmology & visual science*, 25(1), pp.59–65.

Boote, C., 2003. Collagen Fibrils Appear More Closely Packed in the Prepupillary Cornea: Optical and Biomechanical Implications. *Investigative Ophthalmology & Visual Science*, 44(7), pp.2941–2948.

Boote, Craig et al., 2006. Mapping collagen organization in the human cornea: left and right eyes are structurally distinct. *Investigative ophthalmology & visual science*, 47(3), pp.901–8.

Boote, Craig et al., 2011. Quantification of collagen organization in the peripheral human cornea at micron-scale resolution. *Biophysical journal*, 101(1), pp.33–42.

Bourges, J. et al., 2010. Greffe de cornée automatisée assistée par laser femtoseconde optimisé en longueur d ' onde. , pp.1–201.

Boza, Y. et al., 2010. Single Exposure of Human Oral Mucosa Fibroblasts to Ultraviolet B Radiation Reduces Proliferation and Induces COX-2 Expression and Activation. , pp.123–127.

Bron, A J., 1998 Keratoconus *Cornea* Volume 7 Issue 3.

Bron, A J., 2001. The architecture of the corneal stroma. *The British journal of ophthalmology*, 85(4), pp.379–81.

Brookes, N.H. et al., 2003. Involvement of corneal nerves in the progression of keratoconus. *Experimental Eye Research*, 77(4), pp.515–524.

Busin, M., 2003. A new lamellar wound configuration for penetrating keratoplasty surgery. *Archives of ophthalmology*, 121(2), pp.260–5.

Calkins, J.L., Hochheimer, B.F. & Stark, W.J., 1981. stress-test analysis M , pp.322–334.

Carvalho, L.A. et al., 2009. Keratoconus prediction using a finite element model of the cornea with local biomechanical properties. *Arquivos brasileiros de oftalmologia*, 72(2), pp.139–45.

Cavanagh, H Dwight, Petroll, W Matthew & Jester, James V, 2000. Instability and Haze Development after. , 6420(00), pp.1235–1245.

Cejka, C. et al., 2010. The influence of various toxic effects on the cornea and changes in corneal light transmission. *Graefe's archive for clinical and experimental ophthalmology = Albrecht von Graefes Archiv für klinische und experimentelle Ophthalmologie*, 248(12), pp.1749–56.

Chanas, S. a et al., 2009. Effects of elevated Pax6 expression and genetic background on mouse eye development. *Investigative ophthalmology & visual science*, 50(9), pp.4045–59.

City, I., 1986. The Lipid Composition of Oral Porcine. , 31(Ii), pp.741–747.

Collier, S.A., 2001. Review Article Is the corneal degradation in keratoconus caused by. , pp.340–344.

Connon, C J et al., 2010. The variation in transparency of amniotic membrane used in ocular surface regeneration. *The British journal of ophthalmology*, 94(8), pp.1057–61.

Connon, Che J & Meek, Keith M, 2003. Organization of corneal collagen fibrils during the healing of trephined wounds in rabbits. *Wound repair and regeneration : official publication of the Wound Healing Society [and] the European Tissue Repair Society*, 11(1), pp.71–8.

Content, C., Computing for Bioinformatics Core II Module 1 . (2) Statistical Applications in Bioinformatics , Genetics and Epidemiology. , (1), pp.1–9.

Cristodor, P., 2008. Microbial and Fungal Contamination of Keratinocyte and Fibroblasts Cell Cultures. , (3), pp.123–128.

Darley, R., 1994. Gene Transfer I Why Gene Transfer ? , pp.1–29.

Darzynkiewicz, Z., Galkowski, D. & Zhao, H., 2008. Analysis of apoptosis by cytometry using TUNEL assay. *Methods (San Diego, Calif.)*, 44(3), pp.250–4.

Davies, L.C. et al., 2012. Oral Mucosal Progenitor Cells Are Potently Immunosuppressive in a Dose-Independent Manner. *Stem cells and development*, 21(9), pp.1478–1487.

Davis, J. et al., 2003. Requirement for Pax6 in corneal morphogenesis: a role in adhesion. *Journal of cell science*, 116(Pt 11), pp.2157–67.

Dawson, D.G. et al., 2008. Corneal ectasia after excimer laser keratorefractive surgery: histopathology, ultrastructure, and pathophysiology. *Ophthalmology*, 115(12), pp.2181–2191.e1.

Daxer, a & Fratzl, P, 1997. Collagen fibril orientation in the human corneal stroma and its implication in keratoconus. *Investigative ophthalmology & visual science*, 38(1), pp.121–9.

Dogru, M. et al., 2003. Tear function and ocular surface changes in keratoconus. *Ophthalmology*, 110(6), pp.1110–8.

Dorà, N. et al., 2008. PAX6 dosage effects on corneal development, growth, and wound healing. *Developmental dynamics : an official publication of the American Association of Anatomists*, 237(5), pp.1295–306.

Dorà, N. et al., 2009. UKPMC Funders Group Wound Healing. , 237(5), pp.1295–1306.

Doutch, James et al., 2008. Light transmission in the human cornea as a function of position across the ocular surface: theoretical and experimental aspects. *Biophysical journal*, 95(11), pp.5092–9.

Du, Y. et al., 2007. Secretion and organization of a cornea-like tissue in vitro by stem cells from human corneal stroma. *Investigative ophthalmology & visual science*, 48(11), pp.5038–45.

Dua, H.S. et al., 2003. Stem cell differentiation and the effects of deficiency. *Eye (London, England)*, 17(8), pp.877–85.

Edelhauser, Henry F, The Balance between Corneal Transparency and Edema The Proctor Lecture. , pp.1755–1767.

Editor, D., Raphson, N.- & Software, B.S., 1995. Letter to the Editor. , (June), pp.419–420.

Enoch, S et al., 2009. Increased oral fibroblast lifespan is telomerase-independent. *Journal of dental research*, 88(10), pp.916–21.

Enoch, S et al., The oral mucosa : a model of wound healing with reduced scarring.

Eyre et al., 1984 Quantisation of Hydroxy Cross-links in Collagen by Hyper-performance Lipid Chromatography Analytical Biochemistry Volume: 137 Issue: 2 pp 380-388

Fagerholm et al.; 2009 Corneal Regeneration Following Implantation of a Biometric Tissue Engineered Substitute *Clinical and Translational Science* Volume 2 Issue 2 162-164

Faragher, R.G. et al., 1997. Aging and the cornea. *The British journal of ophthalmology*, 81(10), pp.814–7.

Foreman, D.M. et al., 1996. A simple organ culture model for assessing the effects of growth factors on corneal re-epithelialization. *Experimental eye research*, 62(5), pp.555–64.

Fratzl, P & Daxer, a, 1993. Structural transformation of collagen fibrils in corneal stroma during drying. An x-ray scattering study. *Biophysical journal*, 64(4), pp.1210–4.

Fratzl, Peter & Daxer, A., 1993. Structural transformation of collagen fibrils in corneal stroma during drying. , 64(April).

Frcophth, M.E. et al., 2001. Review Article The genetics of keratoconus. , pp.345–351.

Freund, D E et al., 1995. Ultrastructure in anterior and posterior stroma of perfused human and rabbit corneas. Relation to transparency. *Investigative ophthalmology & visual science*, 36(8), pp.1508–23.

Freund, I., Deutsch, M. & Sprecher, a, 1986. Connective tissue polarity. Optical second-harmonic microscopy, crossed-beam summation, and small-angle scattering in rat-tail tendon. *Biophysical journal*, 50(4), pp.693–712.

Fullwood, N J et al., 1992. Synchrotron x-ray diffraction studies of keratoconus corneal stroma. *Investigative ophthalmology & visual science*, 33(5), pp.1734–41.

Funari, S.S., 2002. Small Angle X-Rays Scattering Studies of Biomolecules. , 101(5), pp.647–658.

Funato, N. et al., 1999. Evidence for Apoptosis Induction in Myofibroblasts during Palatal Mucoperiosteal Repair. *Journal of Dental Research*, 78(9), pp.1511–1517.

Gallin P., 2002 *Paediatric Ophthalmology* Thermal Medical Publishers

Gatlin, J. et al., 2003. In vivo fluorescent labeling of corneal wound healing fibroblasts. *Experimental Eye Research*, 76(3), pp.361–371.

Geggel, H.S. & Coday, M.P., 2001. Late-onset Traumatic Laser in Situ. , pp.505–506.

Gipson, I.K., 1989. The epithelial basement membrane zone of the limbus. *Eye (London, England)*, 3 (Pt 2), pp.132–40.

Grindley, J.C., Davidson, D.R. & Hill, R E, 1995. The role of Pax-6 in eye and nasal development. *Development (Cambridge, England)*, 121(5), pp.1433–42.

Grøn, B. et al., 2002. Oral fibroblasts produce more HGF and KGF than skin fibroblasts in response to co-culture with keratinocytes. *APMIS : acta pathologica, microbiologica, et immunologica Scandinavica*, 110(12), pp.892–8.

Gupta, H.S. et al., 2006. Cooperative deformation of mineral and collagen in bone at the nanoscale. *Proceedings of the National Academy of Sciences of the United States of America*, 103(47), pp.17741–6.

Gyi, T.J., Meek, Keith M. & Elliott, G.F., 1988. Collagen interfibrillar distances in corneal stroma using synchrotron X-ray diffraction: a species study. *International Journal of Biological Macromolecules*, 10(5), pp.265–269.

Hart, R.W. & Farrell, R.A., 1969a. Light Scattering in the Cornea. *Journal of the Optical Society of America*, 59(6), p.766.

Hart, R.W. & Farrell, R.A., 1969b. Light Scattering in the Cornea. *Journal of the Optical Society of America*, 59(6), p.766.

Hashimoto, S. et al., 1998. Linkage of chondrocyte apoptosis and cartilage degradation in human osteoarthritis. *Arthritis and rheumatism*, 41(9), pp.1632–8.

Hassell et al., 1993 Proteoglycan Changes During Restoration of Transparency in Corneal Scars *Archives of Biochemistry and Biophysics* Volume: 222 Issue: 2 pp 362-369

Hayashida, Y. et al., 2005. Ocular surface reconstruction using autologous rabbit oral mucosal epithelial sheets fabricated ex vivo on a temperature-responsive culture surface. *Investigative ophthalmology & visual science*, 46(5), pp.1632–9.

Hayes, S et al., 2010. A structural investigation of corneal graft failure in suspected recurrent keratoconus. *Eye (London, England)*, 24(4), pp.728–34.

Hayes, Sally et al., 2007. A study of corneal thickness, shape and collagen organisation in keratoconus using videokeratography and X-ray scattering techniques. *Experimental eye research*, 84(3), pp.423–34.

Hayes, Sally et al., 2008. Effect of complete epithelial debridement before riboflavin-ultraviolet-A corneal collagen crosslinking therapy. *Journal of cataract and refractive surgery*, 34(4), pp.657–61.

Henriksson, J.T., McDermott, A.M. & Bergmanson, J.P.G., 2009. Dimensions and morphology of the cornea in three strains of mice. *Investigative ophthalmology & visual science*, 50(8), pp.3648–54.

Hero, I., Farjah, M. & Scholtz, C.L., 1991. The prenatal development of the optic fissure in colobomatous microphthalmia. *Investigative ophthalmology & visual science*, 32(9), pp.2622–35.

Hollande , 2005 *Cornea* 2nd Edition Ohio USA

Hotta, T. et al., 2007. Clinical and histopathological analysis of healing process of intraoral reconstruction with ex vivo produced oral mucosa equivalent. *The Kobe journal of medical sciences*, 53(1-2), pp.1–14.

Howell, S.J. & Doane, K.J., 1998. Type VI collagen increases cell survival and prevents anti-beta 1 integrin-mediated apoptosis. *Experimental cell research*, 241(1), pp.230–41.

Iaizzo, P. a et al., 2012. Wound healing during hibernation by black bears (Ursus americanus) in the wild: elicitation of reduced scar formation. *Integrative zoology*, 7(1), pp.48–60.

Isnard, N. et al., 2005. Studies on corneal wound healing. Effect of fucose on iodine vapor-burnt rabbit corneas. *Ophthalmologica. Journal international d'ophtalmologie. International journal of ophthalmology. Zeitschrift für Augenheilkunde*, 219(6), pp.324–33.

Ivarsen, A. & Laurberg, T., 2003. Characterisation of corneal fibrotic wound repair at the. , pp.1272–1279.

Jafarinasab, M.R. et al., 2011. Graft biomechanical properties after penetrating keratoplasty versus deep anterior lamellar keratoplasty. *Current eye research*, 36(5), pp.417–21.

Jaycock, P.D. et al., 2005. Interferometric technique to measure biomechanical changes in the cornea induced by refractive surgery. *Journal of cataract and refractive surgery*, 31(1), pp.175–84.

Jean, D., Ewan, K. & Gruss, P., 1998. Molecular regulators involved in vertebrate eye development. *Mechanisms of development*, 76(1-2), pp.3–18.

Kamma-Lorger, C.S. et al., 2010. Collagen and mature elastic fibre organisation as a function of depth in the human cornea and limbus. *Journal of structural biology*, 169(3), pp.424–30.

Kamma-Lorger, C.S. et al., 2009. Collagen ultrastructural changes during stromal wound healing in organ cultured bovine corneas. *Experimental eye research*, 88(5), pp.953–9.

Kamma-lorger, C.S. et al., 2009. Effects on collagen orientation in the cornea after trephine injury. , (August 2008), pp.378–385.

Kamma-lorger, C.S. et al., 2007. The Healing of LASIK Flaps Doctoral Thesis Cardiff University, (2007)

Kanda, T. et al., 2003. Evidence for fibroblast growth factor receptors in myofibroblasts during palatal mucoperiosteal repair. *Archives of Oral Biology*, 48(3), pp.213–221.

Kato, N. et al., 2008. Five-year outcome of LASIK for myopia. *Ophthalmology*, 115(5), pp.839–844.

Kato, T., Nakayasu, K. & Kanai, a, 2000. Corneal wound healing: Immunohistological features of extracellular matrix following penetrating keratoplasty in rabbits. *Japanese journal of ophthalmology*, 44(4), pp.334–41.

Kawamoto, K. et al., 2001. Keratoplasty in Individuals With. , pp.173–174.

Kennedy, C.J. et al., 2004. Laser cleaning of parchment: structural, thermal and biochemical studies into the effect of wavelength and fluence. *Applied Surface Science*, 227(1-4), pp.151–163.

Kim, W.J. et al., 1999. Keratocyte apoptosis associated with keratoconus. *Experimental eye research*, 69(5), pp.475–81.

Kirkness, C.M. et al., 1990. The success of penetrating keratoplasty for keratoconus. *Eye (London, England)*, 4 (Pt 5), pp.673–88. Available at:

Knorz, M.C. & Vossmerbaeumer, U., 2008. Using the Amadeus Microkeratome and Rabbits. , 24(November), pp.875–878.

Koomer et al. 1994 *JOSA* Volume 39 Issue 5 pp 370-372

Krachmer, J.H., Feder, R.S. & Belin, M.W., 1984. Keratoconus and related noninflammatory corneal thinning disorders. *Survey of ophthalmology*, 28(4), pp.293–322.

Kuroki, S. et al., 2009. Epithelialization in oral mucous wound healing in terms of energy metabolism. *The Kobe journal of medical sciences*, 55(1), pp.E5–E15.

Lam, F.C., Rahman, M.Q. & Ramaesh, K, 2007. Traumatic wound dehiscence after penetrating keratoplasty-a cause for concern. *Eye (London, England)*, 21(9), pp.1146–50.

Langham, M.E., 1970b. (Received 23. , pp.601–616.

Larjava, H. et al., 2011. Exploring scarless healing of oral soft tissues. *Journal (Canadian Dental Association)*, 77(C), p.b18.

Lee, Y.G. et al., 2001. Corneal haze after photorefractive keratectomy using different epithelial removal techniques: mechanical debridement versus laser scrape. *Ophthalmology*, 108(1), pp.112–20.

Leonard, D.W. & Meek, K M, 1997. Refractive indices of the collagen fibrils and extrafibrillar material of the corneal stroma. *Biophysical journal*, 72(3), pp.1382–7.

Lippincott 2008 Manual of Ocular Diagnosis and Therapy 6th Additon: Wilkins and Wilkins Philadelphia USA

Littlechild, S.L. et al., 2012. Fibrinogen, riboflavin, and UVA to immobilize a corneal flap--conditions for tissue adhesion. *Investigative ophthalmology & visual science*, 53(7), pp.4011–20.

Mak, K. et al., 2009. Scarless healing of oral mucosa is characterized by faster resolution of inflammation and control of myofibroblast action compared to skin wounds in the red Duroc pig model. *Journal of dermatological science*, 56(3), pp.168–80.

Mannis and Hollande 2002 Ocular Surface Disease: Medical and Surgical Management Springer: New York

Manuel, M. et al., 2008. Overexpression of Pax6 results in microphthalmia, retinal dysplasia and defective retinal ganglion cell axon guidance. *BMC developmental biology*, 8, p.59.

Martin, P., 1997. Wound Healing--Aiming for Perfect Skin Regeneration. *Science*, 276(5309), pp.75–81.

Mazzotta, C. et al., 2007. Stromal haze after combined riboflavin-UVA corneal collagen cross-linking in keratoconus: in vivo confocal microscopic evaluation. *Clinical & experimental ophthalmology*, 35(6), pp.580–2.

McCally, R L & Farrell, R. a, 1976. The depth dependence of light scattering from the normal rabbit cornea. *Experimental eye research*, 23(1), pp.69–81.

McCally, Russell L et al., 2007. Light-scattering and ultrastructure of healed penetrating corneal wounds. *Investigative ophthalmology & visual science*, 48(1), pp.157–65.

McCulley, J.P., 1989. The circulation of fluid at the limbus (flow and diffusion at the limbus). *Eye (London, England)*, 3 (Pt 2), pp.114–20.

Mccally, R.L., Johns, T. & Spring, S., 1973. Maryland 20910,. , pp.589–612.

Meek, K M et al., 2003. Transparency, swelling and scarring in the corneal stroma. *Eye (London, England)*, 17(8), pp.927–36.

Meek, K M & Leonard, D.W., 1993. Ultrastructure of the corneal stroma: a comparative study. *Biophysical journal*, 64(1), pp.273–80.

Meek, K.M & Fullwood, N.J, 2001. Corneal and scleral collagens—a microscopist's perspective. *Micron*, 32(3), pp.261–272.

Meek, Keith M et al., 2005. Changes in collagen orientation and distribution in keratoconus corneas. *Investigative ophthalmology & visual science*, 46(6), pp.1948–56.

Meek, Keith M & Boote, Craig, 2009. The use of X-ray scattering techniques to quantify the orientation and distribution of collagen in the corneal stroma. *Progress in retinal and eye research*, 28(5), pp.369–92.

Meek, Keith M. & Boote, Craig, 2004. The organization of collagen in the corneal stroma. *Experimental Eye Research*, 78(3), pp.503–512.

Melki, S. a et al., 2000. Late traumatic dislocation of laser in situ keratomileusis corneal flaps. *Ophthalmology*, 107(12), pp.2136–9.

Meran, S. et al., 2008. Hyaluronan facilitates transforming growth factor-beta1-mediated fibroblast proliferation. *The Journal of biological chemistry*, 283(10), pp.6530–45.

Meran, S. & Steadman, R., 2011. Fibroblasts and myofibroblasts in renal fibrosis. *International journal of experimental pathology*, 92(3), pp.158–67.

Meyer, R.F., 1986. Corneal allograft rejection in bilateral penetrating keratoplasty: clinical and laboratory studies. *Transactions of the American Ophthalmological Society*, 84(1), pp.664–742.

Michael, A., 1945. Wednesday 19 th September Thursday 20 th September. , pp.14–17.

Mort, R.L. et al., 2011. Effects of aberrant Pax6 gene dosage on mouse corneal pathophysiology and corneal epithelial homeostasis. Che John Connon, ed. *PloS one*, 6(12), p.e28895.

Møller-Pedersen, T. & Ehlers, N., 1995. A three-dimensional study of the human corneal keratocyte density. *Current eye research*, 14(6), pp.459–64.

Nader, H.B. et al., 1987. Heparin sequences in the heparan sulfate chains of an endothelial cell proteoglycan. *Proceedings of the National Academy of Sciences of the United States of America*, 84(11), pp.3565–9.

Nakayasuk 1996 Distribution of Types I,II,IV and V Collagen in Normal and Keratoconus Corneas *Ophthalmic Res* 18:1-10.

Newton, R H & Meek, K M, 1998a. Circumcorneal annulus of collagen fibrils in the human limbus. *Investigative ophthalmology & visual science*, 39(7), pp.1125–34.

Newton, R H & Meek, K M, 1998b. The integration of the corneal and limbal fibrils in the human eye. *Biophysical journal*, 75(5), pp.2508–12.

Nishi, H. et al., 2010. Wound healing effects of gingival fibroblasts cultured in animal-free medium. *Oral diseases*, 16(5), pp.438–44.

Nishida, K. et al., 2004a. Corneal reconstruction with tissue-engineered cell sheets composed of autologous oral mucosal epithelium. *The New England journal of medicine*, 351(12),

Noble, B. a, 2004. Late onset post-keratoplasty astigmatism in patients with keratoconus. *British Journal of Ophthalmology*, 88(3), pp.317–317.

Norman, B., 2004. Postnatal Gene Expression in the Normal Mouse Cornea by SAGE. *Investigative Ophthalmology & Visual Science*, 45(2), pp.429–440.

Olsen, T., 1982. Light scattering from the human cornea. *Investigative ophthalmology & visual science*, 23(1), pp.81–6.

Opencourseware, M.I.T., 2008a. 5.069 Crystal Structure Analysis.

Opencourseware, M.I.T., 2008b. X-Rays and Matter.

Ottani, V. et al., 1998. Collagen fibril arrangement and size distribution in monkey oral mucosa. *Journal of anatomy*, 192 (Pt 3, pp.321–8.

Ottani, V. et al., 2002. Hierarchical structures in fibrillar collagens. *Micron (Oxford, England : 1993)*, 33(7-8), pp.587–96.

Patel, S.V. et al., 2007. Keratocyte and subbasal nerve density after penetrating keratoplasty. *Transactions of the American Ophthalmological Society*, 105, pp.180–9; discussion 189–90.

Patel, S.V. et al., 2008. Scattered light and visual function in a randomized trial of deep lamellar endothelial keratoplasty and penetrating keratoplasty. *American journal of ophthalmology*, 145(1), pp.97–105.

Pei, Y., Sherry, D.M. & McDermott, A.M., 2004. Thy-1 distinguishes human corneal fibroblasts and myofibroblasts from keratocytes. *Experimental eye research*, 79(5), pp.705–12.

Pei and Rhodin 1970, The Prenatal Development of the Mouse Eye Volume: 168, Issue 1, pp 105-125

Petsche, S.J. et al., 2012. Depth-dependent transverse shear properties of the human corneal stroma. *Investigative ophthalmology & visual science*, 53(2), pp.873–80.

Pogrel, M.A., Low, M.A. & Stern, Robert, 2003. Hyaluronan (hyaluronic acid) and its regulation in human saliva by hyaluronidase and its inhibitors. *Journal of oral science*, 45(2), pp.85–91.

Porter, S., 2007. The role of the fibroblast in wound contraction and healing. , 3(1).

Pramanik, S. et al., 2006. Extended long-term outcomes of penetrating keratoplasty for keratoconus. *Ophthalmology*, 113(9), pp.1633–8.

Quantock, A.J. & Young, R.D., 2008. Development of the corneal stroma, and the collagen-proteoglycan associations that help define its structure and function. *Developmental dynamics : an official publication of the American Association of Anatomists*, 237(10), pp.2607–21.

Ramaesh, T. et al., 2009. Histopathological characterisation of effects of the mouse Pax6(Leca4) missense mutation on eye development. *Experimental eye research*, 89(2), pp.263–73.

Ramaesh, T. et al., 2006. Increased apoptosis and abnormal wound-healing responses in the heterozygous Pax6+/- mouse cornea. *Investigative ophthalmology & visual science*, 47(5), pp.1911–7.

Rawe, I.M. et al., 1994. Structure of corneal scar tissue: an X-ray diffraction study. *Biophysical journal*, 67(4), pp.1743–8.

Res, B., Foundation, R. & Albino, M., 1973. Corned Scar Formation. , pp.251–259.

Sanchis-Gimeno et al.; 2005 Reduced Corneal Thickness Values in Post Menopausal Women With Dry Eye *Cornea* January 2005 Volume: 24 Issue: 1, pp 39-44.

Segment, A., 2008. Controversies in Cross-linking Treatment for Keratoconus. , pp.64–68.

Sekiyama, E. et al., 2006. Different expression of angiogenesis-related factors between human cultivated corneal and oral epithelial sheets. *Experimental eye research*, 83(4), pp.741–6.

Shannon, D.B. et al., 2006. Phenotypic differences between oral and skin fibroblasts in wound contraction and growth factor expression. *Wound repair and*

regeneration: official publication of the Wound Healing Society [and] the European Tissue Repair Society, 14(2), pp.172–8.

Sheppard et al. 2010. Changes in Corneal Collagen Architecture during Mouse Postnatal Development ***IOVS***. 51(06), pp.2936–2942.

Shi, X. & Garry, D.J., 2006. Muscle stem cells in development, regeneration, and disease. *Genes & development*, 20(13), pp.1692–708.

Silver, J. & Hughes, a F., 1974. The relationship between morphogenetic cell death and the development of congenital anophthalmia. *The Journal of comparative neurology*, 157(3), pp.281–301.

Smelser, G.K., 1962. Corneal hydration. Comparative physiology of fish and mammals. *Investigative ophthalmology*, 1, pp.11–32.

Snell and Lamp 1998, Clinical Anatomy of the Eye 2nd Edition Blackwell Science: London

Sohajda, Z. et al., 2006. Microcornea associated with myopia. *Graefe's archive for clinical and experimental ophthalmology = Albrecht von Graefes Archiv für klinische und experimentelle Ophthalmologie*, 244(9), pp.1211–3.

Spoerl, Eberhard, Wollensak, Gregor & Seiler, Theo, 2004. Increased resistance of crosslinked cornea against enzymatic digestion. *Current eye research*, 29(1), pp.35–40.

Stephens, P, Hiscox, S., et al., 2001. Phenotypic variation in the production of bioactive hepatocyte growth factor/scatter factor by oral mucosal and skin fibroblasts. *Wound repair and regeneration : official publication of the Wound Healing Society [and] the European Tissue Repair Society*, 9(1), pp.34–43.

Stephens, P, Davies, K.J., et al., 2001a. Skin and oral fibroblasts exhibit phenotypic differences in extracellular matrix reorganization and matrix metalloproteinase activity. *The British journal of dermatology*, 144(2), pp.229–37.

Stephens, P, Davies, K.J., et al., 2001b. Skin and oral fibroblasts exhibit phenotypic differences in extracellular matrix reorganization and matrix metalloproteinase activity. *The British journal of dermatology*, 144(2), pp.229–37.

Stocum 2006 Regenerative Biology and Medicine Oxford Press Elseiver: London

Svergun, D.I. & Koch, M.H.J., 2003. Small-angle scattering studies of biological macromolecules in solution. *Reports on Progress in Physics*, 66(10), pp.1735–1782.

Tada, T. & Reidy, M. a, 1987. Endothelial regeneration. IX. Arterial injury followed by rapid endothelial repair induces smooth-muscle-cell proliferation but not intimal thickening. *The American journal of pathology*, 129(3), pp.429–33.

Takahashi, N. et al., 2009. Structures of the corneal limbus detected by laser-scanning confocal biomicroscopy as related to the palisades of Vogt detected by slit-lamp microscopy. *Japanese journal of ophthalmology*, 53(3), pp.199–203.

Textbook of Veterinary Ophthalmology 1981 ISBN 0-8121-0886-5788 pp xiv

Tseng, S.C., Smuckler, D. & Stern, R, 1982. Comparison of collagen types in adult and fetal bovine corneas. *The Journal of biological chemistry*, 257(5), pp.2627–33.

Vail, A. et al., 1997. Conclusions of the corneal transplant follow up study. , (Table 1), pp.631–636.

Valldeperas, X. et al., 2010. Bilateral Keratectasia 34 Years after Corneal Transplant. *Case reports in ophthalmology*, 1(1), pp.24–29.

de Veld, D.C.G. et al., 2004. Effects of individual characteristics on healthy oral mucosa autofluorescence spectra. *Oral oncology*, 40(8), pp.815–23.

Ventura, L. et al., 2005. Portable light transmission measuring system for preserved corneas. *Biomedical engineering online*, 4, p.70.

Watson, S.L., Tuft, Stephen J & Dart, J.K.G., 2006. Patterns of rejection after deep lamellar keratoplasty. *Ophthalmology*, 113(4), pp.556–60.

Wiesel, T.N., 1970. Medical School, Boston, Massachusetts 02115, U.S.A. , pp.419–436.

Wollensak, G et al., 2004. Keratocyte cytotoxicity of riboflavin/UVA-treatment in vitro. *Eye (London, England)*, 18(7), pp.718–22.

Wollensak, Gregor, Spoerl, Eberhard & Seiler, Theo, 2003. Riboflavin/ultraviolet-a–induced collagen crosslinking for the treatment of keratoconus. *American Journal of Ophthalmology*, 135(5), pp.620–627.

Wong, J.W. et al., Wound healing in oral mucosa results in reduced scar formation as compared with skin: evidence from the red Duroc pig model and humans. *Wound repair and regeneration: official publication of the Wound Healing Society [and] the European Tissue Repair Society*, 17(5), pp.717–29.

Yue, B.J.T. et al., 1990. Alpha-l Proteinase Inhibitor Levels in Keratoconus. , pp.549–554.

Zhao, B. et al., 2006. Development of a three-dimensional organ culture model for corneal wound healing and corneal transplantation. *Investigative ophthalmology & visual science*, 47(7), pp.2840–6.

Appendix I

Buffers and Solutions

Agar/Gelatine Corneal Support

200 ml of Agar/Gelatine Solution*

20 ml 10x Eagle's Minimum Essential Medium (MEM)

10 ml 7.4% $NaHCO_3$ Solution (dissolved in ddH_2O)

2 ml Stock Antibiotic Solution**

1 ml Fungizone™ Fungiside

Solution Prep: Agar/Gelatine mixture is heated in the microwave on medium/low power until molten. The remaining solutions are filtered into the molten mixture using a 0.2µm filter (in sterile conditions) and hand shaken until thoroughly mixed.

*Agar/Gelatine Solution

2 g Agar

2 g Gelatin

200ml ddH_2O

Solution Prep: Agar and Gelatin are added to distilled water in a 250-300 ml bottle (with metal lid) and mixed until dissolved and autoclaved at 120°C for 15-20 minutes (depending on autoclave cycle). The solution is transferred to a sterile cabinet where the metal lid is exchanged for a sterile plastic lid.

**Stock Anti-biotic solution

500 mg Sigma Streptomycin Sulfate

500 mg Kanamyecin

300 mg Penicillin G

730 mg L-Glutamine

50 ml ddH_2O

Solution Prep: Solution prepared and filtered into 10 ml aliquots using a 0.2µm filter in sterile conditions.

Betadine™ Solution 25% (volume/volume)

100 ml Betadine™ (Povidone-iodine (PVP-I))

400 ml ddH_2O

Solution prep: After combining, solution should be mixed well. Solution can be re-used several times before disposal.

Appendix II

Published Papers